

DISSERTATION

COMBINING FUNDAMENTAL STUDIES WITH ADVANCED CHARACTERIZATION
FOR ANALYZING NITRIC OXIDE POLYMER SYSTEMS

Submitted by

Jessica Marie Joslin

Department of Chemistry

In partial fulfillment of the requirements

For the Degree of Doctor of Philosophy

Colorado State University

Fort Collins, Colorado

Spring 2014

Doctoral Committee:

Advisor: Melissa M. Reynolds

Branka M. Ladanyi

Amber T. Krummel

Christopher J. Ackerson

John D. Williams

Copyright by Jessica Marie Joslin 2014

All Rights Reserved

ABSTRACT

COMBINING FUNDAMENTAL STUDIES WITH ADVANCED CHARACTERIZATION FOR ANALYZING NITRIC OXIDE POLYMER SYSTEMS

Nitric oxide (NO) releasing materials have been investigated over the past couple of decades as potential biomaterials. A multitude of NO releasing platforms have been reported with different NO release properties indicating use in various bioapplications. Despite the positive implications associated with these materials, the field is currently limited by a couple of major issues. First, the reservoirs of NO stored in current systems do not allow the prolonged and controllable release necessary for long-term usage. Additionally, the field has experienced a lack of complete characterization of both the NO loading and release processes associated with these systems. To develop NO releasing platforms with enhanced NO reservoirs and controllable NO release profiles, fundamental studies are required to probe the physical processes that occur in these polymers.

To enhance NO reservoirs in polymer systems, it is critical to probe the efficiency of the NO loading process. Systematic studies are presented where the efficiency and nature of *S*-nitrosothiol NO donor formation is investigated in a polymer environment. The nitrosating agent and polymer presence have a significant impact on the kinetics of *S*-nitrosation. Also, due to the versatile nature of nitrosation, NO byproducts that form competitively with *S*-nitrosothiols are characterized. By tuning the polymer functional groups, competitive nitrosation products can be eliminated and NO recoveries enhanced. Another critical obstacle towards understanding NO materials involves probing NO donor behavior in conjunction with NO release. For model

polymers containing covalently linked *S*-nitrosothiol moieties, spectroscopy is coupled to direct NO detection to fully characterize the NO loading and release stages. Decomposition of the *S*-nitrosothiol moiety is directly correlated to NO release. *S*-nitrosothiol blended films are also investigated to determine the spatial distribution of NO release, which is critical to ensure a localized NO effect at the material surface. Finally, NO releasing polymer substrates are exposed to water plasma processing conditions. Surface wettability is significantly enhanced, while the NO release kinetics are maintained, suggesting that these materials can withstand processing towards tunable surface properties. Overall, fundamental and systematic studies of model NO releasing materials are presented that have not been formerly considered. Only by characterizing these materials completely can this class of biomaterial be better understood towards the ability to control the therapeutic and surface properties.

ACKNOWLEDGEMENTS

During my time at Colorado State University, I have had an absolutely amazing support team. Thank you to my incredible parents, Sam and Crissy, for instilling my love of learning and to my sweet sister, Sarah, for her encouragement and beautiful smile. My loving husband, Scott, perhaps deserves the greatest recognition for his constant support; coming home to him each night has been an unbelievable blessing and relief. Thank you to my research group, especially Sarah Lantvit, Dr. Vinod Damodaran and Dr. Dori Pegalajar-Jurado, for scientific and emotional support. Finally, a huge thank you to my advisor, Melissa, who has given me endless opportunities during my time in her group to explore, investigate and develop myself as a scientist.

TABLE OF CONTENTS

ABSTRACT.....	ii
ACKNOWLEDGEMENTS.....	iv
CHAPTER 1: INTRODUCTION	
1.1 Nitric oxide releasing materials.....	1
1.1.1 Nitric oxide: A natural therapeutic agent.....	1
1.1.2 Nitric oxide donors.....	4
1.1.3 Nitric oxide incorporation into materials.....	6
1.1.4 Nitric oxide materials for improved blood compatibility.....	7
1.1.5 Methods for quantifying nitric oxide.....	15
1.1.6 UV-visible spectroscopy to probe NO donors.....	18
1.2 Current limitations & research goals.....	27
1.3.1 Current limitations of nitric oxide materials and methods.....	27
1.3.2 Project goals.....	30
CHAPTER 1 REFERENCES.....	34
CHAPTER 2: SYSTEMATIC EVALUATION OF <i>S</i> -NITROSATION KINETICS IN AQUEOUS POLYMER SOLUTION	
2.1 Preface.....	58
2.2 Introduction.....	59
2.3 Experimental section.....	61
2.3.1 Materials.....	61
2.3.2 Methods.....	62
2.3.3 Statistical analysis.....	65
2.4 Results & discussion.....	65
2.4.1 Model system.....	65
2.4.2 Nitrosation under aqueous conditions.....	66
2.4.3 Nitrosation in the presence of dextran polymer solution.....	80
2.4.4 A comparison of HNO ₂ and <i>t</i> -butyl nitrite reagents.....	87
2.5 Conclusions.....	94
CHAPTER 2 REFERENCES.....	95
CHAPTER 3: CHARACTERIZATION OF MAJOR NITROSATION PRODUCTS FOR THIOLATED POLYMERS AND ACHIEVING SELECTIVE <i>S</i> -NITROSATION	
3.1 Preface.....	101
3.2 Introduction.....	102
3.3 Experimental section.....	107
3.3.1 Materials.....	107
3.3.2 Polymer synthesis.....	107
3.3.3 Ellman's assay for thiol quantification.....	110
3.3.4 Nitric oxide loading.....	111

3.3.5 Nitric oxide donor, byproduct and NO characterization.....	111
3.4 Results & discussion.....	113
3.4.1 Dextran derivatives prepared by reductive amination.....	113
3.4.2 Dextran derivatives prepared by carboxymethyl intermediate.....	124
3.4.3 Impact of NO moiety formation on NO loading and release.....	127
3.5 Conclusions.....	130
CHAPTER 3 REFERENCES.....	132

CHAPTER 4: COMPLETE CHARACTERIZATION OF NITRIC OXIDE LOADING AND RELEASE PROPERTIES FOR *S*-NITROSATED BIODEGRADABLE POLYMER DERIVATIVES

4.1 Preface.....	137
4.2 Introduction.....	139
4.3 Experimental section.....	142
4.3.1 Materials.....	142
4.3.2 Preparation of <i>S</i> -nitrosated PLGH copolymers.....	143
4.3.3 Characterization of PLGH derivatives.....	144
4.3.4 Characterization of PLGH derivatives for bioapplications.....	146
4.3.5 Nitric oxide analysis.....	147
4.4 Results & discussion.....	147
4.4.1 Influence of thiol incorporation on polymer properties.....	147
4.4.2 NO storage and delivery as a function of thiol structure.....	150
4.4.3 Feasibility for biomaterial applications.....	161
4.5 Conclusions.....	162
CHAPTER 4 REFERENCES.....	163

CHAPTER 5: CORRELATING *S*-NITROSOTHIOL DECOMPOSITION WITH NITRIC OXIDE RELEASE FOR POLYMER FILMS

5.1 Preface.....	168
5.2 Introduction.....	168
5.3 Experimental section.....	170
5.3.1 Materials.....	170
5.3.2 Methods.....	171
5.4 Results & discussion.....	172
5.4.1 Analysis under thermal, oxygenated conditions.....	172
5.4.2 Analysis under thermal, deoxygenated conditions.....	173
5.4.3 Analysis under deoxygenated buffer soak conditions.....	176
5.4.4 Analysis under deoxygenated exposure to UV light.....	177
5.5 Conclusions.....	179
CHAPTER 5 REFERENCES.....	180

CHAPTER 6: STUDIES IN DONOR LEACHING AND LOCALIZED NITRIC OXIDE RELEASE FOR DONOR-BLENDED POLYMER FILMS

6.1 Preface.....	182
6.2 Introduction.....	183
6.3 Experimental section.....	187

6.3.1 Materials.....	187
6.3.2 Methods	188
6.3.3 Statistical analysis	194
6.4 Results & discussion.....	195
6.4.1 Small molecule <i>S</i> -nitrosoglutathione characterization.....	195
6.4.2 GSNO-blended Tygon films	204
6.4.3 GSNO leaching studies	209
6.4.4 Total thiol content in soaking solution.....	211
6.4.5 Monitoring surface sulfur content.....	216
6.4.6 Varying donor concentration in the film.....	220
6.4.7 Surface properties pre- and post-soak.....	224
6.5 Conclusions.....	227
CHAPTER 6 REFERENCES	229

CHAPTER 7: EFFECT OF WATER PLASMA TREATMENT ON NITRIC OXIDE RELEASE AND SURFACE PROPERTIES OF *S*-NITROSATED POLYMER FILMS

7.1 Preface.....	236
7.2 Introduction.....	237
7.3 Experimental section.....	242
7.3.1 Materials.....	242
7.3.2 Preparation of <i>S</i> -nitrosated PLGH-cysteine films.....	242
7.3.3 Plasma treatment of polymer films	244
7.3.4 <i>S</i> -nitrosothiol characterization	244
7.3.5 NO release analysis.....	245
7.3.6 Water contact angle analysis.....	245
7.3.7 Surface composition analysis: XPS and SEM-EDS	245
7.3.8 Surface morphology analysis: SEM and optical profilometry.....	246
7.3.9 Bulk composition analysis: IR.....	247
7.4 Results & discussion.....	247
7.4.1 Effect of plasma treatment on RSNO content and NO release.....	247
7.4.2 Effect of plasma treatment on surface wettability	252
7.4.3 Effect of plasma treatment on surface composition.....	254
7.4.4 Effect of prolonged treatment time on surface composition.....	264
7.4.5 Effect of plasma treatment on surface morphology.....	267
7.4.6 Stability of the plasma treatment	269
7.5 Conclusions.....	271
CHAPTER 7 REFERENCES	273

CHAPTER 8: SUMMARY AND FUTURE DIRECTIONS: A BRIGHT FUTURE FOR NITRIC OXIDE MATERIALS

8.1 Summary.....	281
8.1.1 Controlled preparation and advanced analysis.....	281
8.1.2 Summarizing remarks.....	283
APPENDIX 1: BIOMATERIALS LITERATURE REVIEW.....	285
APPENDIX 1 REFERENCES.....	301

CHAPTER 1:
INTRODUCTION

1.1 NITRIC OXIDE RELEASING MATERIALS

1.1.1 Nitric oxide: A natural therapeutic agent.

In the 1980s, the revolutionary discovery was made that nitric oxide (NO) is the endothelium-derived relaxing factor and is responsible for vasodilation.¹ The importance of NO in the cardiovascular system was realized and the 1998 Nobel Prize in Physiology or Medicine was awarded to Furchgott, Ignarro and Murad for their contributions to this discovery. After this critical finding, research was directed at understanding the other physiological roles of NO. To date, the biological roles of NO have been found to reach from the cardiovascular system to neurotransmission, wound-healing, angiogenesis and even anti-bacterial and anti-tumor applications (see Figure 1.1).²

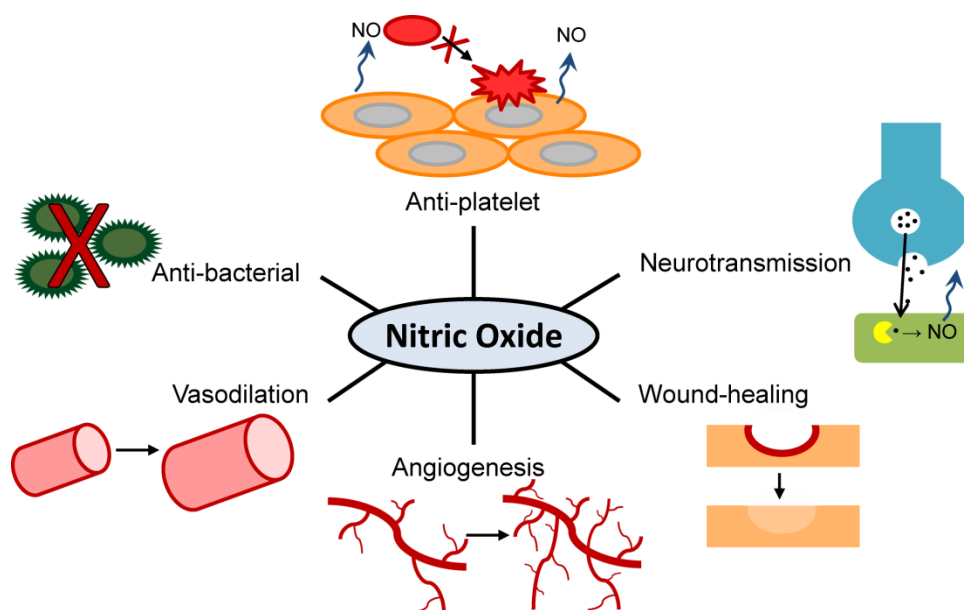


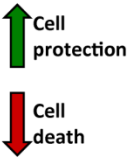
Figure 1.1 A schematic representation of the physiological roles of nitric oxide.

Physiological production and action of NO. Nitric oxide is produced *in vivo* through an L-arginine pathway via nitric oxide synthase (NOS). Three major forms of NOS exist: endothelial (eNOS), inducible (iNOS) and neuronal (nNOS).³ Generation of NO via eNOS occurs in the endothelial cells that line the inner vasculature and is responsible for inducing vascular tone⁴ and angiogenesis.⁵ Nitric oxide produced from the endothelium is also responsible for regulating platelet activity by inhibiting platelet activation and adhesion, critical to the blood clotting process.^{6, 7} iNOS generates NO in macrophages, resulting in immune system function to defend against parasites, bacteria and tumor growth,⁸ as well as to modulate inflammation.⁹ Generation of NO via nNOS occurs in neurons and functions as a neurotransmitter in the central¹⁰ and peripheral¹¹ nervous systems for cell signaling processes.¹² From a clinical perspective, there is still much to be learned about the diverse range of functions that NO serves, while it is clear that NO plays many important roles in maintaining homeostasis.

Concentration dependence on biological action. With the many functions of NO beginning to come to light, it is important to recognize that different concentrations of NO in the body result in various physiological effects. In fact, there is a very delicate balance between lower concentrations of NO inducing protective and proliferative effects, while slightly higher concentrations of NO induce harmful effects (Table 1.1).¹³ Lower NO ranges (1-30 nM) result in vasodilation and angiogenesis in the cardiovascular system. Intermediate ranges result in anti-oxidant effects to protect against cell apoptosis (30-60 nM) as well as anti-inflammatory and wound-healing responses to protect and repair injured tissues (100 nM). Overall, NO concentrations ranging from 1-100 nM result in cell protective and proliferative effects. Increasing NO concentrations to 400 nM will result in cell apoptosis. From a harmful

perspective, these higher NO concentrations will result in cell damage, yielding destructive physiological effects. However, cell death effects can be harnessed toward applications in anti-bacterial and cancer cell treatments. A further increase in NO concentration ($>1 \mu\text{M}$) will result in full cell cycle arrest, where fully toxic results will arise. Overall, the fine balance in the amount of NO that imparts significantly different biological effects requires fine control over NO delivery and regulation in biological systems.

Table 1.1 The concentration ranges of NO and corresponding biological functions.

[Nitric Oxide]	Physiological Results	
1-30 nM	Proliferative and protective effects (vasodilation, angiogenic effects)	
30-60 nM	Apoptosis protection (anti-oxidant)	
100 nM	Tissue injury protection (anti-inflammatory, wound-healing)	
400 nM	Induces apoptosis (antibacterial & anticancer function)	
$> 1 \mu\text{M}$	Full cell cycle arrest (toxic function, tumor cells)	

Nitric oxide therapies. The involvement of NO in cardiovascular, neurological and immune response functions has led to a variety of NO therapies associated with cardiovascular disease, cancer, wound-healing, infection and prevention of device biofouling.¹⁴ Other applications are directed toward bone and connective tissues.¹⁵ From a regulatory perspective, if the amounts of NO produced naturally are not at the appropriate concentration, many negative effects are demonstrated. In such cases as circulation and cardiovascular applications, NO therapies are administered to maintain homeostasis. In other cases, NO therapies are administered to induce proliferative effects (*i.e.* angiogenesis, wound-healing) or apoptosis (*i.e.* tumor therapy, antibiotics). In other preventative applications, such as NO release in the case of device implantation, NO can serve to regulate platelet and clotting functions. Each of these applications

requires different amounts of NO, thus the amount of NO delivered from a drug system to a patient must be strictly regulated to ensure that the desired biological responses are imparted.

1.1.2 Nitric oxide donors.

As a result of the short half-life and high reactivity of NO, it is not possible to store NO directly within materials. Instead, general classes of molecules exhibiting NO-containing functionalities can be used. Depending upon the decomposition pathway, the NO moiety decomposition can be triggered, resulting in NO release. One of the first known NO donors to be used medically was nitroglycerine, which was prescribed for high blood pressure and angina pectoris as early as over a century ago.¹⁶ Since the realization of the therapeutic potential for NO, many different small molecules with the ability to deliver NO have been investigated, including organic nitrates and nitrites, metal nitrosyls, oximes, hydroxylamines and hydroxyurea.¹⁷ By far, the two most popular NO donors that are being investigated for pro-drug and materials applications are *S*-nitrosothiols^{18, 19} and *N*-diazoniumdiolates,²⁰ which are shown in Figure 1.2.

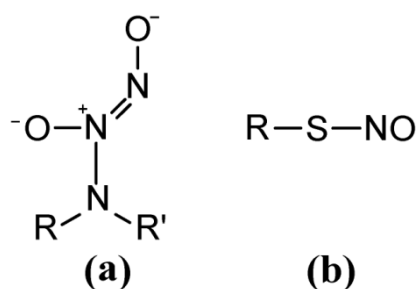


Figure 1.2 General structures for (a) *N*-diazoniumdiolate and (b) *S*-nitrosothiol NO donors.

N-diazoniumdiolates. *N*-diazoniumdiolates have the general structure shown in Figure 1.2(a) and are formed when a parent amine is exposed to a high pressure (80 psi) of NO.^{21, 22} *N*-

diazeniumdiolates are good candidates for NO release under physiological conditions where 2 moles of NO are produced for every 1 mole of moiety. Decomposition occurs in solution at physiological pH (7.4) and temperature (37 °C) due to proton^{23, 24} and heat initiated²⁵ pathways, respectively, and follow first order kinetics.^{23, 24, 26-30} Depending upon the structure of the parent amine, the half-life associated with *N*-diazeniumdiolate decomposition can range from the order of seconds to days. The synthesis of *N*-diazeniumdiolates has been known since the seminal work performed by Drago in the early 1960s,²¹ and, following the discovery of NO's many therapeutic potentials in the 1980-1990s, *N*-diazeniumdiolate donors have been heavily investigated as pro-drugs for clinical applications.^{27, 31}

S-nitrosothiols. *S*-nitrosothiols (RSNOs) have the general structure shown in Figure 1.2(b) and are formed when a parent thiol reacts with a nitrosating agent.³² Common nitrosation conditions include nitrous acid^{33, 34} or alkyl nitrite^{35, 36} nitrosating agents, or exposure to NO gas.³⁷⁻³⁹ *S*-nitrosothiol decomposition is initiated due to exposure to ascorbic acid,⁴⁰⁻⁴² light,⁴²⁻⁴⁴ copper metal ion,^{41, 42, 45-49} or heat^{45, 50, 51} and results in the liberation of 1 mole of NO per mole of moiety, where disulfide is formed according to equations 1.1-1.3.



The literature also demonstrates that pH will affect the decomposition of RSNOs,⁴⁶ as will the presence of oxygen,⁵¹ thiol,^{42, 49} thiolate,⁴⁸ superoxide,⁵² nitrosonium,⁵³ and neutrophils.⁵⁴ Additionally, the ability for transnitrosation processes to occur (exchange of the NO moiety

between an RSNO and another RSH species) has been investigated as an NO releasing pathway.^{55, 56}

An advantage to using *S*-nitrosothiols is that small molecule *S*-nitrosothiols and *S*-nitroso proteins are endogenous NO carriers in the blood.⁵⁷⁻⁵⁹ Additionally, a wide array of thiol precursors are available that, upon nitrosation, yield RSNOs with significantly variable stabilities and NO releasing properties.³⁵ For the research presented in this dissertation, *S*-nitrosothiols will be the predominant NO donor of interest, where specific chemical properties of *S*-nitrosothiols will be presented within the relevant chapters.

1.1.3 Nitric oxide incorporation into materials.

In 1996, shortly after the discovery of the many critical biological roles of NO, the seminal paper by Smith *et al.* was published that described the ability to store NO within polymers.⁶⁰ Influenced by the previously developed NO small molecule donors that were being investigated for pro-drug therapies, this work described the incorporation of *N*-diazoniumdiolate donors into material matrices. The main goal of this work was to modulate “the time course of NO release in a controllable way,” as well as limit the “NO exposure to selected sites within the body.” Essentially, the goal was to use a polymer matrix to help control the kinetics of donor decomposition as well as ensure localized NO release.

Three major approaches were defined toward NO donor incorporation (Figure 1.3): (a) a blended incorporation of pre-formed small molecule donors within the material matrix, (b) covalent attachment of donor moieties directly to sites on the polymer backbone, or (c) covalent attachment of donor moieties onto groups pendant to the polymer backbone. In each case, under physiologically triggered settings, these materials released their NO payloads and demonstrated

antiplatelet behavior for a vascular graft in a baboon model, as well as prevented proliferation of smooth muscle cells to prevent scarring and overgrowth. These results ultimately suggested to Smith *et al.* that polymers capable of storing and releasing NO “may hold considerable promise for a variety of biomedical applications in which local delivery of NO is desired.”

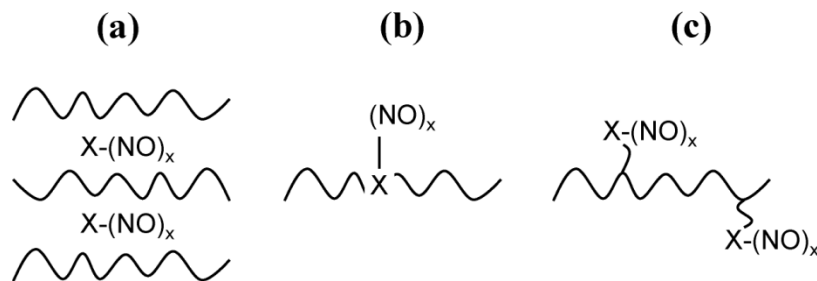


Figure 1.3 NO donor incorporation into a polymer matrix accomplished by (a) small molecule donor blends, or the covalent attachment of NO moieties (b) directly onto the polymer backbone or (c) onto polymer pendant sites. (For *N*-diazoniumdiolates, X=N and x=2; for *S*-nitrosothiols, X=S and x=1.)

1.1.4 Nitric oxide materials for improved blood compatibility.

Since the publication of the seminal NO materials paper in 1996, there have been a multitude of NO releasing material platforms that have been investigated, where several comprehensive reviews are available on the subject.⁶¹ These materials are intended as coatings for existing biomedical devices to prevent thrombosis and infection, while promoting integration of the implant. In other cases, biodegradable NO releasing materials are of interest for temporary device applications, or as macromolecular pro-drug scaffolds. The general idea of an NO releasing surface mimicking the natural endothelium to prevent biofouling is demonstrated in Figure 1.4.

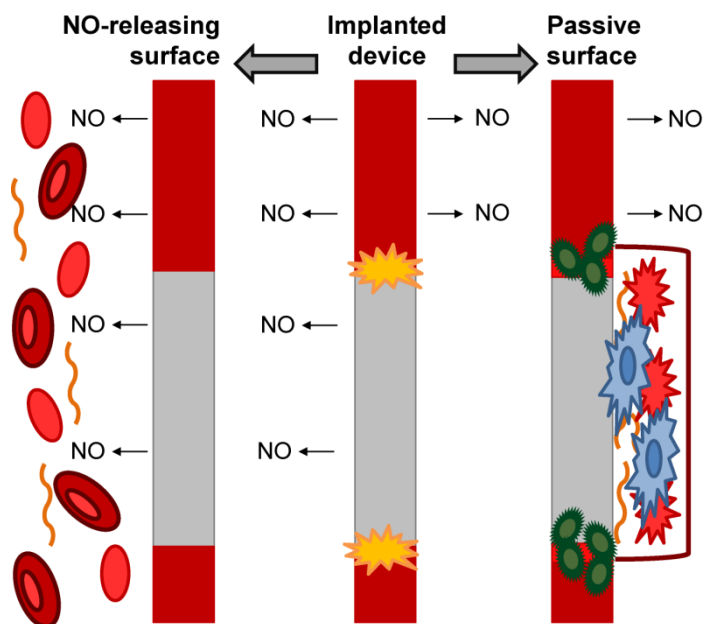


Figure 1.4 A general diagram of an NO releasing coating that serves to mimic the natural endothelium compared to a passive surface.

N-diazoniumdiolate materials. The majority of NO releasing materials that were initially investigated involved the incorporation of *N*-diazoniumdiolate donors, where donors have been blended into polyurethane (PU),⁶²⁻⁶⁵ poly(vinyl chloride),⁶²⁻⁶⁹ dextran,⁷⁰ silicone rubber (SR),⁷¹ and PU-SR copolymers.⁷² *N*-diazoniumdiolate blended materials have been used to prevent biofouling of electrochemical sensors,^{62, 71} demonstrating reduced platelet activation and adhesion,^{63, 68, 69, 73} as well as an overall reduction in thrombus formation for coated devices implanted in animal models.^{66, 67} In 2000, diffusion studies demonstrated significant leaching of blended hydrophilic donors, which is problematic for developing localized NO therapies.⁶³ In an attempt to overcome leaching issues, more lipophilic *N*-diazoniumdiolates were investigated.⁶⁶ *N*-diazoniumdiolate blended material approaches have also been combined with surface immobilization of heparin and are expected to result in an anti-thrombogenic surface via two different complementary mechanisms.^{64, 72} Systems involving NO release from *N*-

diazeniumdiolate donors have also been investigated in the presence of liposomes and micelles,³⁰ while donors have been incorporated into electrospun nanofiber networks⁶⁵ and into polysaccharide microspheres for transdermal delivery.⁷⁰ Some *N*-diazeniumdiolate donors are rather unstable, so their long-term NO release is limited; therefore, protecting groups have been investigated to help stabilize the moiety to slow down the release kinetics.⁷⁴ Despite these donor-blended *N*-diazeniumdiolate materials exhibiting promising biocompatibility, these systems are notorious for donor leaching. For these amine-containing small molecules, toxicity issues of the amine as well as amine byproducts are of concern; therefore, in the mid-to-late 2000s, there was a shift in the material development strategy toward covalently attached donor systems.

A variety of synthetic strategies have been employed to incorporate secondary (2°) amine sites within polymers, where covalently attached *N*-diazeniumdiolate groups can be formed upon exposure to NO. Material platforms have included poly(ethylene glycol) hydrogels⁷⁵ and xerogels,⁷⁶⁻⁷⁸ polymethacrylate,^{64, 79, 80} silicone rubbers,²⁵ poly(vinyl alcohol) hydrogels,⁸¹ sol-gels,⁸²⁻⁸⁶ silica particles⁸⁷⁻⁹¹ and nanorods,⁹² acrylonitrile,⁹³ polyurethanes,⁹⁴⁻⁹⁶ gold nanoparticles,⁹⁷ polyethylenimine,⁹⁸ dendrimers,^{99, 100} polyethers,¹⁰¹ and poly(diols citrate) elastomers.¹⁰² Silica nanoparticles have also been synthesized with combined *N*-diazeniumdiolate functionality and quaternary ammonium sites for dual antimicrobial action.¹⁰³ These materials represent an advancement in the field since the donor will remain fixed within the polymer to yield a truly localized NO release. Biocompatibility studies have demonstrated that these covalently attached *N*-diazeniumdiolate donor systems result in reduced platelet activation and adhesion,^{25, 75, 82, 85, 94} minimized thrombus formation,⁸⁷ reduced smooth muscle cell proliferation,^{75, 94} enhanced endothelial cell growth,⁹⁴ improved wound-healing,⁸¹ and exhibited antibacterial effects.^{77, 78, 83, 86, 89, 92, 100}

S-nitrosothiol materials. The investigation of early NO releasing materials in the 1990s and early 2000s predominantly utilized *N*-diazeniumdiolate donors. However, due to their natural role in the body, there was a transition toward exploring *S*-nitrosothiol donors within materials for biomedical applications that would minimize toxicity issues associated with amine sites. Several RSNO-blended polymer systems have been reported, where small molecule RSNO donors have been incorporated into hydrogels,¹⁰⁴⁻¹⁰⁶ poly(vinyl alcohol)¹⁰⁷ and poly(vinyl pyrrolidone) films,^{108, 109} poly(ethylene glycol),^{110, 111} as well as contained within lipid vesicles that are doped into a silica matrix.¹¹² These NO releasing systems have been utilized for topical applications to increase blood flow¹⁰⁵ and promote wound-healing.¹⁰⁶ RSNO-blended materials have demonstrated significant donor leaching when exposed to soaking solutions, where half-lives on the order of minutes were demonstrated for a water soluble donor blended into hydrophilic polymer films.^{108, 109} Since these particular materials were being used for transdermal NO delivery applications, a lower extent of hydration was expected for a polymer exposed to moisture in the skin compared to an aqueous solution; therefore, the rate of RSNO diffusion would be slower for dermal applications. It was pointed out, however, that RSNO diffusion from the polymer will still likely occur, and these materials were considered to release both NO and RSNO as therapeutic agents.¹⁰⁹

A variety of material platforms have been synthesized with pendant thiol sites, which undergo nitrosation to form covalently attached RSNO moieties. These materials include fumed silica particles,^{91, 113-116} polyesters,¹¹⁷⁻¹¹⁹ polyurethanes,¹²⁰ hydrogels,^{75, 121, 122} dendrimers,^{123, 124} xerogels,^{125, 126} and polymer blends.^{127, 128} Collectively, these materials have demonstrated reduction in platelet adhesion,^{75, 121-123, 127} reduction in bacterial attachment,^{118, 125, 126} reduction in smooth muscle cell proliferation,^{75, 121, 122} enhanced endothelial cell proliferation,^{121, 122}

prevention of neointima formation,^{121, 122} prevention of arterial wall thickening,¹²² accelerated wound closure,¹²⁸ reduced ischemia/reperfusion injury,¹²⁴ and antibacterial effects.^{116, 119, 126}

Nitric oxide releasing parameters. The predominant goal of any NO material study is to prepare a material platform with the ability to store NO until appropriately triggered to release controllable amounts of NO at the material-biology interface. The total NO reservoir is critical to define the lifetime of the therapeutic release from the material, while the amount and type of donor will control the spatial and temporal NO release parameters. The kinetics of NO release, typically reported as a surface flux, should be of physiological relevance for the intended bioapplication. The general target value is 0.05-0.4 nmol NO cm⁻² min⁻¹, which is the NO flux associated with the natural, non-thrombogenic endothelium.^{7, 129} However, individual material studies have identified specific ranges for different physiological effects. In addition, different amounts of NO are required to promote protective and proliferative effects versus preventing cell overgrowth and eradicating bacteria, thus the NO releasing material must be tailored to exhibit appropriate release kinetics over a necessary duration for an intended application.

The seminal 1996 NO materials paper published by Keefer performed experiments using rat aorta smooth muscle cells and, coupled to NO measurements performed in PBS, estimated an NO release rate of 0.025 nmol NO min⁻¹ mg⁻¹ for 50% inhibition of smooth muscle cell proliferation.⁶⁰ It is important to note that the mol NO min⁻¹ value is normalized by the mass of polymer, rather than by the estimated surface area. Due to discrepancies in the NO measurement reporting across the literature, it can be difficult to compare NO measurements across studies. Additionally, the NO release measurements are typically performed under simplistic deoxygenated buffer conditions, whereas the cell experiments are performed in complex cell

media in the presence of oxygen. Therefore, the NO values that are reported and correlated to a biological event are likely over-reported, since NO scavenging events can occur due to components in media¹³⁰ as well as due to the formation of nitrite under oxygenated conditions. It should be noted that, overall, the NO values reported in the literature may not accurately represent the amount of NO delivered to cells and bacteria within complex biological systems to result in certain physiological responses.

Studies published in the early 2000s reported ranges associated with preventing platelet activation and adhesion toward the ultimate goal of preventing thrombus formation. Films that released NO on the order of $5 \text{ nmol NO cm}^{-2} \text{ min}^{-1}$ over a 10 h period were demonstrated to prevent platelet activation and adhesion, leading to >95% inhibition of thrombus formation for a graft that was implanted for 21 days (the NO release parameters were not reported over the extended 21 day period).⁶⁶ Similar studies further demonstrated that an NO profile exhibiting an initial “burst” of $12 \text{ nmol NO cm}^{-2} \text{ min}^{-1}$, followed by an exponential decay to $<1 \text{ nmol NO cm}^{-2} \text{ min}^{-1}$ after a 21 day period successfully resulted in a 98% reduction in thrombus formation for whole blood studies.⁶⁷ Subsequent studies indicated a minimum flux of $1.37 \text{ nmol NO cm}^{-2} \text{ min}^{-1}$ to completely preserve platelet function and prevent the formation of thrombus for an extracorporeal circuitry model.⁶⁸ However, fluxes as low as $0.23 \text{ nmol NO cm}^{-2} \text{ min}^{-1}$ still demonstrated preserved platelet function with the ability to prevent platelet activation and adhesion. The lowest flux reported to reduce platelet adhesion is $0.024 \text{ nmol NO cm}^{-2} \text{ min}^{-1}$.⁸⁵ Another study varied the amount of donor in a polymer matrix and found a flux of $0.71 \text{ nmol NO cm}^{-2} \text{ min}^{-1}$ to reduce platelet adhesion by nearly 80%, while fluxes as low as $0.09 \text{ nmol NO cm}^{-2} \text{ min}^{-1}$ also inhibited platelet adhesion.⁶⁹ An NO flux range of $1.0\text{-}2.5 \text{ nmol NO cm}^{-2} \text{ min}^{-1}$ was found to minimize platelet activation and adhesion, prevent clot formation, and maintain 90% of

platelet activity for an extracorporeal circuit in a rabbit model,²⁵ while lower fluxes of 0.1-0.5 nmol NO cm⁻² min⁻¹ have also demonstrated minimized platelet adhesion and clot formation.⁸⁷ Overall, there have been a variety of specific NO flux ranges reported to be associated with antiplatelet and antithrombogenic surfaces, where an all-inclusive flux range is represented by 0.024-12 nmol NO cm⁻² min⁻¹. Therefore, the current approach is generally to target a value in the range of these reported values.¹²⁰

Many reports have been published from the Schoenfisch research group toward an understanding of the NO fluxes necessary to prevent bacterial attachment to material surfaces. A flux range of 0.48-3.36 nmol NO cm⁻² min⁻¹ was found to reduce both platelet and bacterial attachment to the material surface, where bacterial attachment represented only <5% of the total surface area.⁸² Additional studies have demonstrated a 50% reduction in *Pseudomonas aeruginosa* (*P. aeruginosa*) bacterial attachment for NO fluxes of 0.06 nmol NO cm⁻² min⁻¹,⁸⁶ where a later study demonstrated a minimum flux requirement of 1.3 nmol NO cm⁻² min⁻¹ to reduce *P. aeruginosa* surface attachment by 65%.⁷⁷ As such, other materials prepared for antibacterial applications aim to at least meet the 1.3 nmol NO cm⁻² min⁻¹ mark, or exceed it.^{118, 125, 126} Other studies have demonstrated NO profiles exhibiting an initial “burst” on the order of 12.0 nmol NO cm⁻² min⁻¹ followed by an exponential decay to 0.8 nmol NO cm⁻² min⁻¹ within 24 h that also prevent bacterial attachment.⁸³ It has been further demonstrated that the NO flux required to reduce bacterial attachment to a material surface is dependent upon the bacterial strain, substrate and the experimental conditions.⁹⁰

In general, the approach is to achieve an NO flux above the threshold ranges that have been reported for preventing platelet and bacterial attachment. However, it is essential to recognize that too high of an NO flux could result in undesirable cytotoxicity effects. More

specifically, while the flux values ranging as high as 5-10 nmol NO cm⁻² min⁻¹ have demonstrated reduction in platelet and bacterial attachment, a flux of 3 nmol NO cm⁻² min⁻¹ was found to result in macrophage cytotoxicity.⁸⁴ Therefore, to prevent cytotoxic effects while still preventing platelet and bacterial attachment, the NO surface flux should range on the order of 0.1-1 nmol NO cm⁻² min⁻¹. Additionally, there are other surface properties exhibited by a biomaterial, in addition to NO release, that will influence cellular and bacterial attachment, thus an NO flux required to achieve physiological results depends upon the specific material.

The NO releasing parameters published across a variety of NO materials are not consistent. In addition to or instead of flux measurements, several parameters may be reported, including the total NO payload as a function of the material surface area (SA) or mass, the total NO release ([NO]_{total}), the point on the NO profile where the maximum amount of NO is released ([NO]_{max}), the half-life associated with the NO release (t_{1/2}), and/or the percentage of the total NO released as a function of time (% NO recovery). Some groups also report the amount of NO released over a fixed time interval that is relevant to a biological study, or they report the duration of time that the NO flux was maintained above a threshold value associated with a biological application. The average NO flux may be reported or the flux profile shown as a function of time. Overall, it is difficult to correlate the NO values associated with different scaffolds to an NO delivery requirement for a given bioapplication. This situation is further compounded by the fact that many NO measurements are made under simplistic conditions that are not representative of the complexity associated with cell or bacteria studies in a variety of media, or the intricacy associated with whole blood studies.

1.1.5 Methods for quantifying nitric oxide.

There are a variety of analytical techniques and instruments that are available for measuring NO. Direct techniques include electrochemical detection,¹³¹ electron paramagnetic resonance spectroscopy,¹³² and fluorescent¹³³ or chemiluminescent detection,¹³⁴ while indirect techniques can assay NO byproducts, such as the Griess assay for nitrite quantification.¹³³ The two most widely reported techniques in the NO materials literature are chemiluminescent detection and the Griess assay.

Direct chemiluminescent detection of NO. The gold standard analytical technique for quantifying NO is the use of a chemiluminescent NO analyzer (NOA). These instruments are commercially available and the method used for NO measurements reported in much of the NO literature. A general schematic of an NOA is shown in Figure 1.5, which highlights the NO releasing sample under deoxygenated (N₂ purged) conditions, where the NO is removed from the sample cell under vacuum and swept into a reaction chamber. In the reaction chamber, NO reacts with ozone to form excited state NO₂ (NO₂^{*}), which, upon relaxation to ground state NO₂, releases a photon of light (see equations 1.4-1.5).



The chemiluminescent emission spectrum exhibits a broad peak in the wavelength range of 600-1200 nm; therefore, a red filter is employed to eliminate chemiluminescent interferences <600 nm. The photons emitted from NO₂^{*} strike a photomultiplier tube (PMT) that is cooled to -12 °C to yield a voltage signal.

The NOAs undergo a daily internal calibration such that the voltage response from the PMT is converted to units of “ppm.” An external calibration procedure involves the reduction of a nitrite to NO, where the ppm response can be converted into units of moles of NO via a calibration constant (units of mol ppb⁻¹ s⁻¹). The NOAs collect the NO data *in situ*, according to a pre-set time interval. The signal that is integrated over the time interval can be converted to a concentration of NO, where the real-time profile indicates the kinetics of NO release as a function of time.

This method is ideal due to its direct and selective detection of NO. The limit of detection associated with this technique is ~10 pmol, which corresponds to a 10⁻⁸ M concentration for a 1 mL sample volume. Gaseous ethylene and sulfur compounds can yield chemiluminescent responses upon reaction with ozone; however, this results in emission below 600 nm, which is effectively eliminated from detection by the red filter. Especially for non-volatile samples, the selectivity toward NO detection is excellent. Despite all of these advantages, this instrument is expensive and single-use for only NO measurements. Additionally, as mentioned previously, the measurement of NO under deoxygenated conditions is not necessarily representative of the NO available within an oxygenated biological system.

Chemiluminescence has been employed extensively for monitoring the real-time NO release profiles for small molecule donors in aqueous solution.^{23, 26, 27, 39, 44, 66, 135} Additionally, NO release profiles upon exposure to buffer have been obtained for a variety of solution-phase materials or solid materials exposed to soaking conditions.^{25, 26, 60, 64, 68-70, 79, 80, 87, 95, 113, 114, 135}

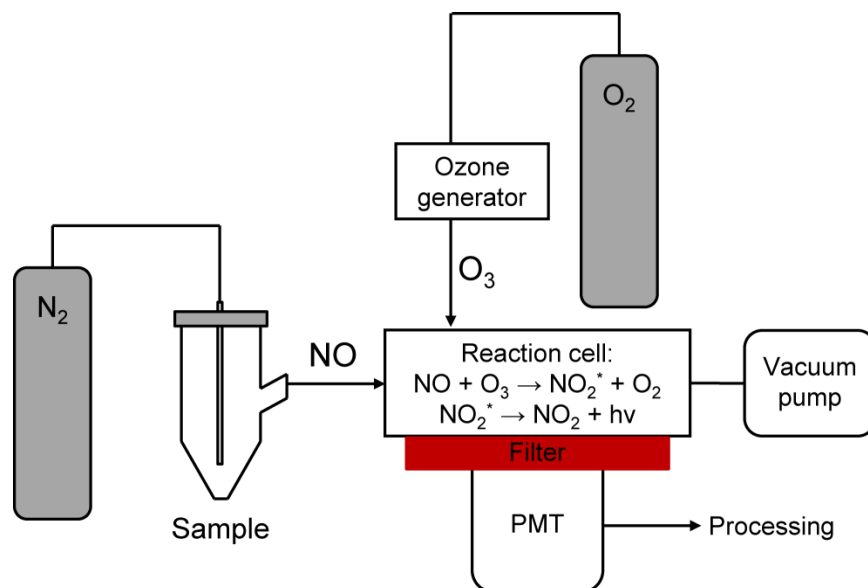


Figure 1.5 A general schematic of a chemiluminescent nitric oxide analyzer (NOA).

Colorimetric assay for the detection of nitrite. The Griess assay is another commonly employed method to measure NO that depends upon the rapid ($k = 8.8 \pm 0.4 \times 10^6 \text{ M}^{-2} \text{ s}^{-1}$) oxidation of NO in aqueous solution to nitrite (NO_2^-), as shown in equation 1.6.¹³⁶



The assay is based upon a two-step diazotization reaction in which nitrite reacts with sulfanilamide and further with *N*-(1-naphthyl) ethylenediamine to result in a product that absorbs strongly at 540 nm.^{133, 137} The nitrite measured by the assay is then directly correlated to the NO that was released into solution. Considering that the synthesis of *S*-nitrosothiols can involve reaction of the parent thiol with inorganic nitrite, some residual nitrite might remain in the material. The detection of this residual nitrite will contribute to the assumed NO release, which is a problem when using an indirect NO detection method. Another problem with the Griess assay involves NO release that occurs before the analysis begins. This prematurely released NO can react in the presence of ambient O_2 and moisture to form nitrite, which will also be detected by

the Griess assay. As a result of this, any NO that is released due to instability within the donor moiety prior to the analysis period could result in a falsely high NO measurement. It is pointed out in *The Chemistry of NO and Redox-Related Species* that “the reaction of O₂ with NO introduces complications to the study of NO chemistry in aqueous solution, since NO₂, N₂O₃ and nitrite can be the source of a variety of side reactions...” Therefore, depending upon the complexity of the NO releasing sample, the ability for NO to be involved in a variety of reactions under oxygenated conditions must be considered when using the Griess assay.¹³⁷

Despite some obvious drawbacks, the Griess assay is still commonly used because it is a quick and inexpensive method that can detect nitrite down to micromolar (μM) concentrations. The Griess assay has been used to quantify nitrite concentration profiles for both *N*-diazoniumdiolate donors^{25, 63, 75, 87, 94, 95, 101, 102} and *S*-nitrosothiol donors^{44, 52, 56, 109, 117, 119} upon exposure to buffer, where the nitrite was correlated directly to NO release.

1.1.6 UV-visible spectroscopy to probe NO donors.

UV-visible (UV-vis) spectroscopy has been employed to characterize both *S*-nitrosothiol and *N*-diazoniumdiolate donors as small molecules and as covalent attachments to polymer backbones. Small molecule *N*-diazoniumdiolates exhibit a characteristic absorbance feature centered at 230-260 nm ($\epsilon_{\text{max}} = 6000\text{-}9000 \text{ M}^{-1} \text{ cm}^{-1}$).^{20, 23} *S*-nitrosothiol small molecule donors exhibit a UV absorbance feature at 330-350 nm ($\epsilon_{\text{max}} = \sim 10^3 \text{ M}^{-1} \text{ cm}^{-1}$) and a visible absorbance feature at 550-600 nm ($\epsilon_{\text{max}} = \sim 20 \text{ M}^{-1} \text{ cm}^{-1}$), which are assigned to $n_{\text{O}} \rightarrow \pi^*$ and $n_{\text{N}} \rightarrow \pi^*$ transitions, respectively.^{18, 138} As described below, the characteristic features associated with the electronic spectra of small molecule NO donors have been applied to polymer systems containing NO donors to confirm functionalization after NO loading.

Spectroscopic analysis of N-diazeniumdiolates. UV-vis methods have been used to characterize *N*-diazeniumdiolates present as small molecule donors in solution,^{22, 23, 26-28, 30, 66, 74, 135} as well as to confirm functionalization of polymers dispersed or dissolved in solution,^{63, 79, 80, 98, 101} functionalization of silica particles in solution,⁸⁷ or functionalization within a thin film.²⁵ One study noted that an increase in amine-containing cross-linkers within polymer films yielded a more intense feature at 250 nm presumably due to an increase in *N*-diazeniumdiolate concentration.⁸²

Decomposition of *N*-diazeniumdiolate small molecule donors^{22-24, 26, 27, 30, 66, 74, 135} has been monitored in conjunction with NO release to ensure that the *N*-diazeniumdiolate moiety is giving rise to NO. However, generally speaking, the polymers containing covalently attached *N*-diazeniumdiolate moieties may undergo initial UV-vis analysis, as mentioned above, to check for the 250 nm absorbance feature; nevertheless, there are several studies involving the incorporation of amine sites followed by NO exposure where UV-vis spectroscopy is not employed to validate the major NO donor.^{60, 75, 76, 81, 83-85, 94, 95} It is very rare to find a study that includes monitoring the decomposition of *N*-diazeniumdiolates that are covalently attached to a polymer; one such study involved water soluble polymeric donors, where the *N*-diazeniumdiolate feature at 250 nm was monitored in buffer at pH 7.4 and 26 °C, where first order decomposition kinetics were determined.⁹⁸ Another study attributed the decay of a 250 nm feature to *N*-diazeniumdiolate decomposition associated with polymethacrylate polymers dissolved in methanol.⁸⁰ In both of these studies, despite a decay in the 250 nm absorbance feature, the kinetics of decomposition were not directly correlated to NO release.

Several studies indicate the formation of *N*-diazeniumdiolate donors within materials, however interferences must be considered. For instance, a 235 nm absorbance band was

demonstrated for NO-loaded silicone rubber films containing amine cross-linkers, where the absorbance feature was initially attributed to *N*-diazoniumdiolate formation.²⁵ However, further studies demonstrated that, upon thickening of the films and thus the pathlength associated with the absorbance measurement, the 250 nm feature grew in intensity and a feature at 355 nm also began to appear.¹³⁹ These spectroscopic features indicated *N*-nitrosamine (RNNO) formation, where RNNOs exhibit characteristic features at 230-235 nm ($\epsilon_{\text{max}} = 7000\text{-}8100 \text{ M}^{-1} \text{ cm}^{-1}$) and 330-350 nm ($\epsilon_{\text{max}} = 100 \text{ M}^{-1} \text{ cm}^{-1}$).¹⁴⁰ *N*-nitrosamines have been demonstrated to form competitively with *N*-diazoniumdiolates during amine exposure to NO.¹⁴¹ Additionally, it has been known since the 1960s that the decomposition of *N*-diazoniumdiolated diethylamine (DEA/NO) in the presence of oxygen will yield the formation of diethylnitrosamine, where the *N*-nitrosamine that forms represents 60% of the starting DEA/NO.¹⁴² The formation of *N*-nitrosamine species due to *N*-diazoniumdiolate decomposition within materials has been confirmed via mass spectrometry and ¹H NMR, where the release of NO under oxygenated conditions forms NO_x species that back react with the parent amine sites.^{63, 79} During the preparation of *N*-diazoniumdiolate materials, due to donor instability, premature decomposition of some donor sites will occur during film curing and storage processes. Under oxygenated conditions, it is possible for *N*-nitrosamine species to form, which could contribute to the UV-vis spectrum of the material during donor analysis. Therefore, the contribution of *N*-nitrosamine species to the electronic spectra of *N*-diazoniumdiolated materials must be considered.

Overall, because there are a variety of NO species that can form, depending upon the synthetic conditions associated with NO donor formation and premature decomposition, UV-vis methods may not be sufficient to characterize major donors. Instead, UV-vis methods should be expanded to be more thorough in terms of tracking the behavior of the donor throughout the NO

releasing period. Further, UV-vis should be combined with other methods, such as infrared (IR) spectroscopy, direct NO detection and stability studies, to ensure characterization of major NO products and to consider competitive byproducts that may form.

Spectroscopic analysis of S-nitrosothiols. Similar to the *N*-diazoniumdiolate materials, UV-vis methods have also been employed to characterize RSNO donors within material matrices. *S*-nitrosothiol formation has been characterized via UV-vis for small molecule donors in solution^{33, 38-41, 52, 56, 58, 59, 143} as well as within liquid hydrogels,¹⁰⁵ polymer solutions,^{110, 117} and films.^{109, 119} Decomposition of *S*-nitrosothiol small molecule donors in solution upon initiation by ascorbate,^{40, 41} copper metal ion,^{41, 59, 74} and light¹¹⁰ has been investigated.

More specifically, the de Oliveira group from UNICAMP in Brazil has published several studies tracking small molecule donors within polymer solutions and polymer films during NO releasing periods. One study followed the formation of *S*-nitroso-*N*-acetylcysteine (SNAC) in aqueous poly(ethylene glycol) (PEG) solution during thiol exposure to NO/O₂ conditions (kinetics were not analyzed).¹¹¹ The decomposition of SNAC was further monitored in aqueous PEG polymer solution at 336 nm, where first order decomposition kinetics were exhibited for thermal or photolytic decomposition. The largest rate constant ($3.4 \pm 0.1 \times 10^{-5} \text{ s}^{-1}$) was determined for SNAC decomposition in aqueous solution (no polymer) and irradiated with light, while the smallest rate constant ($1.7 \pm 0.1 \times 10^{-7} \text{ s}^{-1}$) was found for SNAC decomposition in an aqueous polymer solution in the dark. This slowed rate of donor decomposition in the presence of the polymer indicates donor stabilization via a “cage effect;” this cage effect was attributed to a reduced diffusion of thiyl radical sites formed after NO release to form the disulfide product. The cage effect has also been demonstrated for *S*-nitrosoglutathione (GSNO) and SNAC in

hydrogel, PEG, or poly(vinyl alcohol) (PVA)/poly(vinyl pyrrolidone) (PVP) polymer solutions where either the 545 nm peak^{104, 105, 108, 110} or 336 nm peak¹⁰⁹ was monitored as a function of time depending upon the concentration of donor in the system. Upon further monitoring the donor decomposition in a PVA/PVP polymer solution versus a solid PVA/PVP polymer thin film, the decomposition kinetics were slowed even further for donor trapped within the solid film.¹⁰⁸ Additionally, for the studies involving GSNO blended into PVP and PVA polymers, the rate of donor decomposition was directly impacted by the polymer identity, where the rate constant for GSNO decomposition in solution was $77 \pm 1.6 \times 10^{-2} \text{ h}^{-1}$, and decreased sequentially to 10 ± 0.2 , 9.5 ± 0.4 and $4.7 \pm 0.2 \times 10^{-2} \text{ h}^{-1}$ for GSNO in PVA, PVA/PVP blended, and PVP polymer films, respectively, under dry, thermal (37 °C) conditions.¹⁰⁸ Additionally, changes in the amount of GSNO blended into PVA/PVP films yielded a linear increase in the rate constant (*i.e.* 3.6 wt% yields a GSNO decomposition half-life ($t_{1/2}$) of 8.5 min while 20.4 wt% yields a $t_{1/2}$ of 3.2 min). By changing the identity of the polymer and concentration of donor, different rates of NO release can be achieved. The ability to monitor the behavior of RSNO donor decomposition in polymer solutions and dry solid films is necessary to track the donor during the NO releasing stage; however, the studies mentioned here do not track the donor behavior in conjunction with NO release at different time points but rather assume that the amount of NO that is released is directly correlated to the amount of RSNO that is decomposed. Further, these studies encompass either a dry polymer film or a polymer solution, which is not representative of the actual polymer film exposed to an aqueous soaking environment.

The decomposition of the 335 nm RSNO peak has been correlated to an increase in an absorbance feature at ~250 nm, which has been attributed to the formation of disulfide,¹¹¹ where an isosbestic point is present at ~315 nm.^{108, 109} While the decomposition of the RSNO is first

order under thermal and/or photolytic processes, the formation of the dimer is a second order process due to the diffusion constraints associated with thiyl radical species finding one another within viscous polymer solutions or solid polymer films to result in disulfide formation.¹⁰⁹

In addition to monitoring the donor behavior within a dry polymer film or polymer solution, studies have been performed that monitor the 336 nm absorbance feature for a GSNO-blended PVA/PVP film exposed to soaking buffer.^{108, 109} The donor absorbance within the film decreased significantly, while the soaking solution exhibited an increase in the 336 nm absorbance band, indicating that the donor rapidly diffused from the polymer film and into the soaking solution. One particular study monitored the diffusion of GSNO from a PVA/PVP film and used the Griess assay to indirectly track the release of NO.¹⁰⁹ The GSNO diffusion profile reached a plateau within 12 min, while the NO release profile required 2.5 h to plateau, indicating that the NO released from the system is likely due to a combination of diffused GSNO decomposing in solution and GSNO decomposing within the polymer film; there was no attempt to quantify the NO contribution from donor in the solid versus solution phase. These studies demonstrate that, for donor-blended systems, absorbance studies can be performed to monitor the leaching of RSNOs from polymer matrices into soaking solutions.

The ability to track RSNO within a polymer system can also enable donor stability studies. More specifically, for PVA/PVP films containing 9.3 wt% GSNO, during a 48 h water evaporation film curing stage, only 3.3% of the total GSNO reservoir was lost due to donor decomposition.¹⁰⁸ Further studies demonstrated non-detectable differences in GSNO concentration for PVA/PVP blended films stored for 30 days at 5 °C, or for over 3 months when stored at -20 °C.¹⁰⁹ One of the main benefits of using a donor-blended approach for preparing materials is that the NO reservoir is known based upon the amount of donor that is incorporated

into the matrix; the ability to determine the loss of any donor during film curing and storage stages is critical to ensuring the final concentration of donor available in the material system.

Numerous studies have been reported that involve nitrosation of thiol-containing polymers where no UV-vis data has been provided to demonstrate RSNO formation.^{75, 113, 115, 118, 121, 122} The RSNO formation is assumed after thiol sites in the starting polymer are exposed to nitrosation conditions. Although there is no spectroscopic evidence to support *S*-nitrosation, the quantified NO is claimed to be the initial RSNO concentration, where it is assumed that the RSNO is present and is completely giving rise to the detected NO.

Other studies show characteristic RSNO absorbance features, but do not correlate the behavior of the absorbance feature with NO release, nor do they attempt to characterize the absorbance properties of the material (*i.e.* ϵ_{\max} values).^{120, 123, 125, 126, 128} The λ_{\max} that is claimed to be the $n_o \rightarrow \pi^*$ transition of the RSNO has been reported to be blue shifted to 320 nm, or red shifted to 400 nm for RSNO-bound polymers relative to the 330-350 nm band associated with small molecule RSNOs. Since such extreme variances in the λ_{\max} are reported, it is unclear whether the products are actually RSNO or other nitrosation byproducts or if the systems are exhibiting solvatochromatic behavior. In such cases where an initial UV-vis spectrum suggests *S*-nitrosation, direct NO detection is employed (typically via chemiluminescent detection) to quantify the total amount of NO released from the system until the NO measurement reaches baseline. It is then assumed that this released NO is completely due to RSNO decomposition, and nitrosation efficiencies are determined by comparing the total NO recovery to the amount of available thiol sites as determined by colorimetric assay and/or NMR analysis. In some cases, the disappearance of the characteristic pink color after NO release is used as “a visual indication that all stored NO had indeed been released” and that 100% of the RSNO reservoir has been

effectively depleted.¹²⁵ However, without final UV-vis spectra to confirm this, it is possible that small amounts of RSNO remain in the sample, where the amount of NO release is below the sensitivity of the chemiluminescent response. Additionally, the use of copper ion to reduce RSNOs and result in NO release is extensively reported as a method to quantify all of the RSNO within a polymer system. However, it is possible that other interferences, such as residual nitrite, may also be reduced under these conditions to result in NO release, which will result in a falsely high NO recovery. Use of the Griess assay is also problematic for systems containing residual nitrite as a result of the nitrosation process.

Some studies attempt to use the Ellman's assay to quantify free thiol before and after the nitrosation period, where a decrease in free thiol content is attributed to RSNO formation.^{75, 121, 122} Attempts to correlate a decrease in free thiol content with the formation of RSNO can be problematic primarily because (a) thiols oxidize readily to disulfide under oxygenated conditions,¹⁴⁴ which will result in a decrease in free thiol content and (b) the thiol and disulfide content as well as the solution pH significantly impact the rate of disulfide formation associated with thiol-containing polymers.¹⁴⁵ Additionally, these studies performed the Ellman's assay on the freshly nitrosated polymer, which still required subsequent filtration and photopolymerization steps. The polymerization step will compromise the RSNO concentration due to overlap of the 365 nm light source with the absorbance band associated with the photolytic decomposition of RSNO moieties. Therefore, the final RSNO content associated with the cross-linked polymer film may be significantly lower than initially assumed via free thiol quantification.

One study from the de Oliveira group prepared polyesters containing mercaptosuccinic acid segments along the polymer backbone.¹¹⁷ *S*-nitrosation was monitored by tracking an

increase in the absorbance features at 335 nm and 545 nm during polymer solution exposure to NO/O₂. The decomposition of the 545 nm feature was then tracked for polymer films with a pathlength of 0.01 cm under dry conditions. The absorbance value was converted to concentration of RSNO using a molar extinction coefficient value corresponding to small molecule *S*-nitrosomercaptosuccinic acid in a solution of ethylene glycol, where the decrease in RSNO content was correlated directly to NO release. In this study, NO was not directly measured but assumed to correspond to a concentration of RSNO that was determined based upon a molar extinction coefficient value for a small molecule RSNO. Additionally, based upon the amount of RSNO calculated initially and the molecular weight of the polymer, nitrosation efficiencies were estimated to range from 20-100%. Subsequently, to monitor NO release associated with the *S*-nitrosated films under aqueous soaking conditions, the Griess assay was used to monitor nitrite content as a function of time instead of monitoring the decomposition of the RSNO donor. In later studies, these thiolated polyesters were blended into poly(methyl methacrylate) where nitrosation was monitored as an increase in the absorbance values at 335 and 545 nm as a function of nitrosation time.^{119, 127} In these studies, however, the Griess assay was used to report nitrite formation as a function of material soaking time as a proxy for NO release.

Overall, the use of molecular spectroscopy to probe the NO donor moieties can be a powerful tool for probing the behavior of the NO donor during the NO loading and releasing periods. However, in general there is a consistent lack of comprehensive characterization in the NO materials literature. Initial UV-vis spectra of materials after NO loading may be provided, but usually are not, thus the NO donors that are assumed to be present in the system may not actually be present depending upon the chemistries employed (*i.e.* material properties, nitrosation

conditions). Additionally, for the spectra that are provided, byproducts are not considered that could competitively form and interfere in the same wavelength regions as the NO moiety of interest. If attempts are made to quantify the NO donor, the total amount of NO that is released from the system is related back to concentration of starting donor based on a 1:1 or 1:2 molar stoichiometry of donor-to-NO for *S*-nitrosothiols and *N*-diazoniumdiolates, respectively. However, the possibility for residual species (*i.e.* nitrite) to form during the NO loading process could lead to a falsely high amount of NO being detected, depending upon the donor decomposition pathway and NO quantification method employed. It is of further importance to monitor the decomposition of the donor in conjunction with the liberation of NO to ensure that the kinetics of these processes are the same. By monitoring donor and NO behavior simultaneously, it can be confirmed that the NO donor is truly giving rise to the detected NO. The potential for additional NO moieties to form could have critical implications towards the application of these materials in biological settings due to toxicity and limited NO recovery concerns.

1.2 CURRENT LIMITATIONS & RESEARCH GOALS

1.2.1 Current limitations of nitric oxide materials and methods.

Despite sufficient evidence to suggest that NO materials demonstrate great promise as biomaterials, there are still several limitations to their use in a clinical setting. A recent review of NO materials highlights 5 major limitations to the use of these material platforms for clinical use: (1) the uncertainty associated with NO concentrations that are being delivered *in vivo*, (2) unclear target values for the therapeutic NO doses required for certain applications, (3) variable accuracy associated with common NO detection methods, (4) inconsistency associated with the

reporting of NO measurements and (5) a lack of enhanced NO storage and prolonged delivery for long-term applications.¹⁴⁶ The first two issues are purely analytical, in that advanced measurement systems are required to probe the amount of NO that is being delivered *in vivo* during the NO releasing period. The third and fourth issues can be addressed if researchers within the field will adopt uniform, consistent measurement techniques that enable reproducible and accurate NO measurements associated with these materials. The last issue addresses the fact that advanced material platforms are required that can enhance NO storage and result in efficient NO delivery processes beyond the time frame of days-to-weeks.

Overall, in order to develop NO releasing platforms with enhanced NO reservoirs and controllable NO release profiles, fundamental studies and advanced material analyses are required to probe the physical processes that occur in these polymers. Systematic studies are required to understand the materials properties and external conditions that will result in efficient and selective NO loading. Further, advanced analytical methods are required to probe multiple components within the material system to understand the NO donor behavior in correlation with the NO release kinetics and the fate of NO under simulated physiological conditions. Systematic studies can then be performed to understand which polymer functionalities and experimental conditions will result in tunable NO release parameters. It is additionally important for the application of these materials in biomedical settings that any byproducts formed during the NO loading or releasing period be fully characterized to ensure that no toxic species are being introduced into the system. Another review highlights that the field has experienced a lack of complete characterization of both the NO loading and release processes associated with these systems.¹³ Ideal NO releasing platforms with the ability to deliver therapeutically relevant doses

will not be applied in clinical settings until fundamental studies are performed to characterize these polymer systems towards an understanding of the physical behavior of the system.

Donor-blended materials. Donor leaching issues and toxicity associated with amine sites have limited the use of *N*-diazoniumdiolate blended materials. The use of *S*-nitrosothiol donors is a more attractive approach due to their natural role in NO storage and transport. However, leaching of RSNO donors will still result in downstream NO release rather than the localized therapeutic effect that is necessary at the material-biology interface. Overall, due to issues in small molecule donor leaching, covalently attached NO donor polymers have gained much attention as a strategy. Approaches involving top-coat methods and the use of more lipophilic donors have been attempted to prevent donor leaching and make donor-blended systems a more viable option. However, issues with persistent leaching have effectively halted research involving donor-blended polymers. It must be considered, however, that the donor diffusion properties will be dependent upon the specific donor and material properties and the exposure conditions. Therefore, it is possible that donor-blended polymer formulations could be developed to improve these issues. The benefit of using a donor-blended system is due to the known amount of NO that is incorporated into the material. Rather large NO reservoirs can be incorporated into a coating, where >20 w/w% donor has been blended into polymer films. Subsequently, the donor type and material properties can be tuned to control the NO release kinetics. If significant donor leaching can be eliminated, the use of donor-blended materials will become a much more viable option for biomedical applications, especially for long-term applications that require larger NO reservoirs.

Covalently attached NO donor systems. There are several drawbacks that have arisen as research focus moves toward covalently attached NO donor polymer systems. First, due to synthetic conversion efficiencies, the amount of thiol or amine sites that can be incorporated onto a polymer backbone for subsequent *S*-nitrosation and *N*-diazoniumdiolation is limited, respectively. Next, based upon ratios of NO release to starting thiol content, the nitrosation process is usually <50% efficient. Therefore, the current major limitation associated with NO materials is the finite reservoir of NO, which limits most materials to short-term application due to their ability to release NO on the order of hours to weeks. To move the field towards materials with enhanced NO releasing capabilities, fundamental studies are needed that consider how internal (*i.e.* donor concentration, material type) and external (*i.e.* nitrosation conditions) parameters influence the efficiency of NO loading processes.

1.2.2 Project goals.

It is critical to the progression of the NO materials field that rigorous methods be developed that enable researchers to monitor and quantify all components within the system so that the system can be fully understood. Currently, a general template has emerged for the publications associated with NO releasing materials: (a) a material scaffold is prepared with parent amine or thiol sites, (b) the material is subjected to diazeniumdiolation or nitrosation conditions, respectively, (c) the donor may or may not be characterized initially using UV-vis, (d) the NO release is measured directly (*i.e.* chemiluminescence) or indirectly (*i.e.* Griess assay) and, finally, (e) a biological study may or may not be performed to demonstrate the ability of the material to modulate some biological interaction (*i.e.* platelet adhesion, antibacterial effects). Overall, there is an overwhelming lack of systematic characterization to consider competitive

byproducts that may form during the NO loading and/or releasing stages, especially for nitrosated materials. Primarily, most manuscripts present the use of a stand-alone method that monitors only one aspect of the system. Additionally, the consideration of competitive NO products is essentially neglected and the NO donor of interest is just assumed to have formed. During the NO releasing process, it is additionally assumed that the NO donor of interest is giving rise to NO without this aspect of the system actually being probed. The material must be fully characterized to understand fully the material during the NO loading and releasing stages and to enable fine control over the NO release kinetics and durations. To overcome these obstacles, fundamental and systematic studies must be performed on model material systems that enable a clear understanding of the NO loading and delivery processes (Figure 1.6).

Achieving selective and efficient NO loading. To work towards the ability to enhance NO reservoirs in polymer systems, the efficiency of the NO loading process must be probed. To accomplish this, the NO products must be characterized for these multi-functional macromolecular polymer systems. The system can then be tuned to achieve the desired NO reservoir, which is dictated by the amount of NO moieties that are formed. Systematic studies must be performed to quantify the NO products in the system based upon tailoring properties, such as the material properties and synthetic conditions employed. By understanding the kinetics of NO donor formation, we can begin to understand which parameters can be tuned to achieve selective and efficient NO loading.

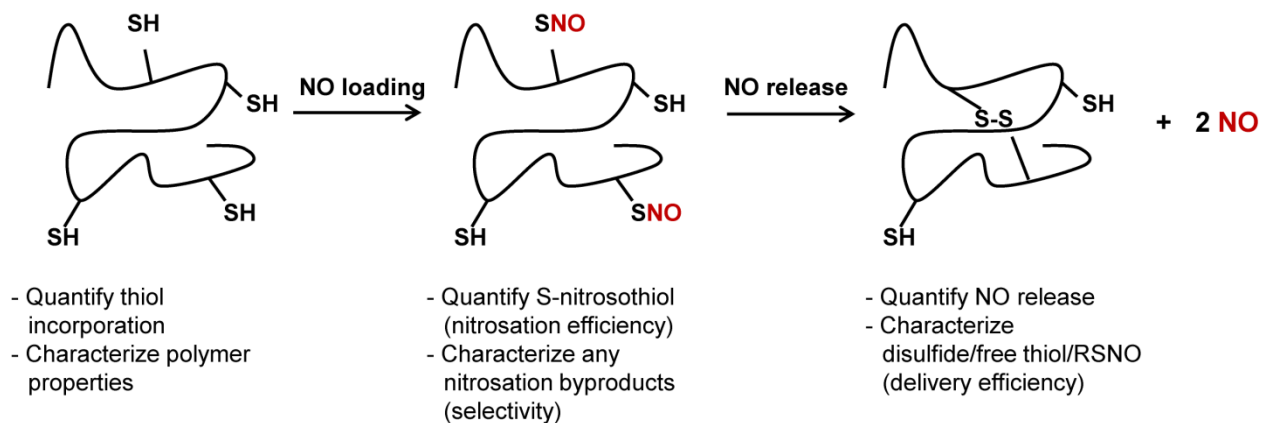


Figure 1.6 The NO loading and release properties must be thoroughly characterized for a polymer system; multiple components in the system must be characterized and quantified.

Herein, systematic studies are presented where the efficiency and nature of *S*-nitrosothiol NO donor formation is investigated in a polymer environment. The nitrosating agent and polymer presence were found to have a significant impact on the kinetics of *S*-nitrosation (Chapter 2). Also, due to the versatile nature of nitrosation, NO byproducts that form competitively with *S*-nitrosothiols have been characterized. By tuning the functional groups within the polymer structure, competitive nitrosation products were eliminated and NO recoveries were enhanced (Chapter 3).

Achieving controllable NO release parameters. Once the NO loading process is characterized and RSNO quantified, molar extinction coefficient values were determined along with nitrosation efficiencies for model polymer systems (Chapters 3 & 4). Further, trends in the NO release kinetics were considered relative to the polymer functionality surrounding the RSNO moiety (Chapter 4). It is subsequently critical to probe the NO donor behavior in conjunction with the direct NO release to ensure that the material processes giving rise to therapeutic release

are fully understood. We can understand the structure-function relationships for these model systems by correlating NO donor behavior and NO release kinetics (Chapter 5). For model polymers containing covalently linked *S*-nitrosothiol moieties, UV-vis spectroscopy was coupled to direct NO detection to fully characterize the NO loading and release stages. Decomposition of the *S*-nitrosothiol moiety was directly correlated to NO release.

S-nitrosothiol blended films were also investigated to determine the spatial distribution of NO release, which is critical to ensure a localized NO effect from the material surface. Methods were coupled to track the leaching of small molecule RSNOs from a material matrix, where initial leaching of surface-bound donor was found, followed by no more subsequent leaching (Chapter 6). Finally, studies are presented that consider the impact of plasma processing on the surface properties and NO releasing capabilities of a model polymer system (Chapter 7).

Summarizing remarks. Overall, this dissertation describes progress towards the development of methods to monitor the formation and decomposition of blended or covalently attached *S*-nitrosothiol donor moieties within both biostable and biodegradable polymer systems. To understand the NO chemistries within material systems, we have investigated a number of model systems and developed the necessary methods for monitoring NO processes within these systems. Taken together, the information is used to develop physical models of how properties within the system as well as synthetic conditions can be tuned to acquire the desired NO properties for a given biological application. The fundamental and systematic studies of NO releasing materials that are presented herein have not been formerly considered by the NO materials community. Only by characterizing these materials completely can this class of biomaterial be better understood.

CHAPTER 1 REFERENCES

1. Ignarro, L. J.; Buga, G. M.; Wood, K. S.; Byrns, R. E.; Chaudhuri, G., Endothelium-Derived Relaxing Factor Produced and Released From Artery and Vein is Nitric Oxide. *Proc. Natl. Acad. Sci. USA* **1987**, *84*, 9265-9269; Palmer, R. M. J.; Ferrige, A. G.; Moncada, S., Nitric Oxide Release Accounts for the Biological Activity of Endothelium-Derived Relaxing Factor. *Nature* **1987**, *327*, 524-526; Rapoport, R. M.; Draznin, M. B.; Murad, F., Endothelium-Dependent Relaxation in Rat Aorta May Be Mediated Through Cyclic GMP-Dependent Protein Phosphorylation. *Nature* **1983**, *306*, 174-176; Furchgott, R. F.; Vanhoutte, P. M., Endothelium-Derived Relaxing and Contracting Factors. *FASEB J.* **1989**, *2*, 2007-2018.
2. Moncada, S.; Higgs, E. A., Endogenous Nitric Oxide: Physiology, Pathology and Clinical Relevance. *Eur. J. Clin. Invest.* **1991**, *21*, 361-374; Marletta, M. A., Nitric Oxide: Biosynthesis and Biological Significance. *Trends Biochem. Sci.* **1989**, *14*, 488-492; Stamler, J. S.; Singel, D. J.; Loscalzo, J., Biochemistry of Nitric Oxide and Its Redox-Activated Forms. *Science* **1992**, *258*, 1898-1902; Wink, D. A.; Grisham, M. B.; Mitchell, J. B.; Ford, P. C., Direct and Indirect Effects of Nitric Oxide in Chemical Reactions Relevant to Biology. *Methods Enzymol.* **1996**, *268*, 12-31; Wink, D. A.; Mitchell, J. B., Chemical biology of nitric oxide: Insights into regulatory, cytotoxic, and cytoprotective mechanisms of nitric oxide. *Free Radical Biol. Med.* **1998**, *25* (4-5), 434-456; Moncada, S.; Palmer, R. M. J.; Higgs, E. A., Nitric Oxide: Physiology, Pathophysiology, and Pharmacology. *Pharmacol. Rev.* **1991**, *43*, 109-142.

3. Knowles, R. G.; Moncada, S., Nitric Oxide Synthases in Mammals. *Biochem. J.* **1994**, *298*, 249-258.
4. Ignarro, L. J., Nitric Oxide: A Unique Endogenous Signaling Molecule in Vascular Biology. *Biosci. Rep.* **1999**, *19*, 51-71.
5. Papapetropoulos, A.; Garcia-Cardena, G.; Madri, J. A.; Sessa, W. C., Nitric Oxide Production Contributes to the Angiogenic Properties of Vascular Endothelial Growth Factor in Human Endothelial Cells. *J. Clin. Invest.* **1997**, *100*, 3131-3139.
6. Azuma, H.; Ishikawa, M.; Sekizaki, S., Endothelium-Dependent Inhibition of Platelet Aggregation. *Br. J. Pharmacol.* **1986**, *88*, 411-415; Radomski, M.; Palmer, R. M. J.; Moncada, S., Comparative Pharmacology of Endothelium-Derived Relaxing Factor, Nitric Oxide and Prostacyclin in Platelets. *Br. J. Pharmacol.* **1987**, *92*, 181-187; Moncada, S.; Radomski, M. W.; Palmer, R. M. J., Endothelium-Derived Relaxing Factor: Identification as Nitric Oxide and Role in the Control of Vascular Tone and Platelet Function. *Biochem. Pharmacol.* **1988**, *37*, 2495-2501; Radomski, M. W.; Moncada, S., The Biological and Pharmacological Role of Nitric Oxide in Platelet Function. *Adv. Exp. Med. Biol.* **1993**, *344*, 251-265; Radomski, M. W.; Palmer, R. M. J.; Moncada, S., The Anti-aggregating Properties of Vascular Endothelium: Interactions Between Prostacyclin and Nitric Oxide. *Br. J. Pharmacol.* **1987**, *92*, 639-646.
7. Radomski, M.; Palmer, R. M. J.; Moncada, S., The Role of Nitric Oxide and cGMP in Platelet Adhesion to Vascular Endothelium. *Biochem. Biophys. Res. Commun.* **1987**, *148*, 1482-1489.
8. Bogdan, C., Nitric Oxide and the Immune Response. *Nat. Immunol* **2001**, *2*, 907-916.

9. Ialenti, A.; Ianaro, A.; Moncada, S.; Di Rosa, M., Modulation of Acute Inflammation by Endogenous Nitric Oxide. *Eur. J. Pharmacol.*
10. Calabrese, V.; Mancuso, C.; Calvani, M.; Rizzarelli, E.; Butterfield, D. A., Nitric Oxide in the Central Nervous System: Neuroprotection Versus Neurotoxicity. *Nat. Rev. Neurosci.* **2007**, *8*, 766-775.
11. Lefebvre, R. A., Nitric Oxide in the Peripheral Nervous System. *Ann. Med.* **1995**, *27*, 379-388; Toda, N.; Okamura, T., The Pharmacology of Nitric Oxide in the Peripheral Nervous System of Blood Vessels. *Pharmacol. Rev.* **2003**, *55*, 271-324.
12. Murad, F., Discovery of Some of the Biological Effects of Nitric Oxide and Its Role in Cell Signaling. *Angew. Chem. Int. Ed.* **1999**, *38*, 1856-1868.
13. Coneski, P. N.; Schoenfisch, M. H., Nitric Oxide Release: Part III. Measurement and Reporting. *Chem. Soc. Rev.* **2012**, *41*, 3753-3758.
14. Janero, D. R., Nitric Oxide (NO)-Related Pharmaceuticals: Contemporary Approaches to Therapeutic NO Modulation. *Free Radical Biol. Med.* **2000**, *28*, 1495-1506; Yamamoto, T.; Bing, R. J., Nitric Oxide Donors. *Proc. Soc. Exp. Biol. Med.* **2000**, *225*; Carpenter, A. W.; Schoenfisch, M. H., Nitric Oxide Release: Part II. Therapeutic Applications. *Chem. Soc. Rev.* **2012**, *41*, 3742-3752.
15. Nichols, S. P.; Storm, W. L.; Koh, A.; Schoenfisch, M. H., Local Delivery of Nitric Oxide: Targeted Delivery of Therapeutic to Bone and Connective Tissues. *Adv. Drug Delivery Rev.* **2012**, *64*, 1177-1188.
16. Marsh, N.; Marsh, A., A Short History of Nitroglycerine and Nitric Oxide in Pharmacology and Physiology. *Clin. Exp. Pharmacol. Physiol.* **2000**, *27*, 313-319.

17. Wang, P. G.; Xian, M.; Tang, X.; Wu, X.; Wen, Z.; Cai, T.; Janczuk, A. J., Nitric Oxide Donors: Chemical Activities and Biological Applications. *Chem. Rev.* **2002**, *102*, 1091-1134.
18. Williams, D. L. H., The Chemistry of S-nitrosothiols. *Acc. Chem. Res.* **1999**, *32*, 869-876.
19. Stamler, J. S.; Toone, E. J., The Decomposition of Thionitrites. *Curr. Opin. Chem. Biol.* **2002**, *6*, 779-785.
20. Hrabie, J. A.; Keefer, L. K., Chemistry of the Nitric Oxide-Releasing Diazeniumdiolate (“Nitrosohydroxylamine”) Functional Group and Its Oxygen-Substituted Derivatives. *Chem. Rev.* **2002**, *102*, 1135-1154.
21. Drago, R. S.; Paulik, F. E., The Reaction of Nitrogen(II) Oxide with Diethylamine. *J. Am. Chem. Soc.* **1960**, *82*, 96-98; Drago, R. S.; Ragsdale, R. O.; Eyman, D. P., Mechanism for Reaction of Diethylamine with Nitric Oxide. *J. Am. Chem. Soc.* **1961**, *83*, 4337-4339.
22. Hrabie, J. A.; Klose, J. R.; Wink, D. A.; Keefer, L. K., New Nitric Oxide-Releasing Zwitterions Derived from Polyamines. *J. Org. Chem.* **1993**, *58*, 1472-1476.
23. Maragos, C. M.; Morley, D.; Wink, D. A.; Dunams, T. M.; Saavedra, J. E.; Hoffman, A.; Bove, A. A.; Isaac, L.; Hrabie, J. A.; Keefer, L. K., Complexes of NO with Nucleophiles as Agents for the Controlled Biological Release of Nitric Oxide - Vasorelaxant Effects. *J. Med. Chem.* **1991**, *34*, 3242-3247.
24. Davies, K. M.; Wink, D. A.; Saavedra, J. E.; Keefer, L. K., Chemistry of the Diazeniumdiolates. 2. Kinetics and Mechanism of Dissociation to Nitric Oxide in Aqueous Solution. *J. Am. Chem. Soc.* **2001**, *123*, 5473-5481.
25. Zhang, H.; Annich, G. M.; Miskulin, J.; Osterholzer, K.; Merz, S. I.; Bartlett, R. H.; Meyerhoff, M. E., Nitric Oxide Releasing Silicone Rubbers with Improved Blood

- Compatibility: Preparation, Characterization, and in vivo Evaluation. *Biomaterials* **2002**, *23*, 1485-1494.
26. Saavedra, J. E.; Southan, G. J.; Davies, K. M.; Lundell, A.; Markou, C.; Hanson, S. R.; Adrie, C.; Hurford, W. E.; Zapol, W. M.; Keefer, L. K., Localizing Antithrombotic and Vasodilatory Activity with a Novel, Ultrafast Nitric Oxide Donor. *J. Med. Chem.* **1996**, *39*, 4361-4365.
 27. Saavedra, J. E.; Booth, M. N.; Hrabie, J. A.; Davies, K. M.; Keefer, L. K., Piperazine as a Linker for Incorporating the Nitric Oxide-Releasing Diazeniumdiolate Group into Other Biomedically Relevant Functional Molecules. *J. Org. Chem.* **1999**, *64*, 5124-5131.
 28. Ramamurthi, A.; Lewis, R. S., Measurement and Modeling of Nitric Oxide Release Rates for Nitric Oxide Donors. *Chem. Res. Toxicol.* **1997**, *10*, 408-413.
 29. Keefer, L. K.; Nims, R. W.; Davies, K. M.; Wink, D. A., NONOates (1-Substituted Diazen- 1-ium- 1,2-diolates) as Nitric Oxide Donors: Convenient Nitric Oxide Dosage Forms. *Methods Enzymol.* **1996**, *268*, 281-293.
 30. Dinh, B.; Dove, K.; Jappar, D.; Hrabie, J. A.; Davies, K. M., Effect of Hydrophobic Structure on the Catalysis of Nitric Oxide Release from Zwitterionic Diazeniumdiolates in Surfactant and Liposome Media. *Nitric Oxide* **2005**, *13*, 204-209.
 31. Saavedra, J. E.; Keefer, L. K., Nitrogen-Based Diazeniumdiolates: Versatile Nitric Oxide-Releasing Compounds in Biomedical Research and Potential Clinical Applications. *J. Chem. Ed.* **2002**, *79*, 1427-1434; Fitzhugh, A. L.; Keefer, L. K., Diazeniumdiolates: Pro- and Antioxidant Applications of the "NONOates". *Free Radical Biol. Med.* **2000**, *28*, 1463-1469; Keefer, L. K., Progress Toward Clinical Application of the Nitric Oxide-Releasing Diazeniumdiolates. *Annu. Rev. Pharmacol. Toxicol.* **2003**, *43*, 585-607; Keefer, L. K.,

- Nitric Oxide (NO)- and Nitroxyl (HNO)-Generating Diazeniumdiolates (NONOates): Emerging Commercial Opportunities. *Curr. Top. Med. Chem.* **2005**, *5*, 625-636; Keefer, L. K., Fifty Years of Diazeniumdiolate Research. From Laboratory Curiosity to Broad-Spectrum Biomedical Advances. *ACS Chem. Biol.* **2011**, *6*, 1147-1155.
32. Williams, D. L. H., Nitrosation Mechanisms. *Adv. Phys. Org. Chem.* **1983**, *19*, 381-428.
33. Byler, D. M.; Gosser, D. K.; Susi, H., Spectroscopic Estimation of the Extent of S-nitrosothiol Formation by Nitrite Action on Sulfhydryl Groups. *J. Agric. Food. Chem.* **1983**, *31*, 523-527; Hart, T. W., Some Observations Concerning the S-nitroso and S-phenylsulphonyl Derivatives of L-cysteine and Glutathione. *Tetrahedron Lett.* **1985**, *26*, 2013-2016.
34. Field, L.; Dilts, R. V.; Ravichandran, R.; Lenhert, P. G.; Carnahan, G. E., An Usually Stable Thionitrite from N-acetyl-D,L-penicillamine; X-Ray Crystal and Molecular Structure of 2-(Acetylamino)-2-carboxy-1,1-dimethylethyl Thionitrite. *J. C. S. Chem. Comm.* **1978**, 249-250; Morakinyo, M. K.; Strongin, R. M.; Simoyi, R. H., Modulation of Homocysteine Toxicity by S-nitrosothiol Formation: A Mechanistic Approach. *J. Phys. Chem. B* **2010**, *114*, 9894-9904; Morakinyo, M. K.; Chipinda, I.; Hettick, J.; Siegel, P. D.; Abramson, J.; Strongin, R.; Martincigh, B. S.; Simoyi, R. H., Detailed Mechanistic Investigation into the S-nitrosation of Cysteamine. *Can. J. Chem.* **2012**, *90*, 724-738; Morris, P. A.; Williams, D. L. H., Kinetics and Mechanism of S-nitrosation of Some Thiol-containing Amino Acids and Other Thiols. *J. Chem. Soc., Perkin Trans. 2* **1988**, 513-516; Collings, P.; Al-Mallah, K.; Stedman, G., Kinetics and Equilibria of the S-nitrosation of Alkylthioureas. *J. Chem. Soc., Perkin Trans. 2* **1975**, 1734-1736; Dix, L. R.; Williams, D. L. H., Kinetics and Mechanism of Thionitrite Formation. Mercapto-

- carboxylic Acids: A New Range of Efficient Nitrous Acid Scavengers. *J. Chem. Soc., Perkin Trans. 2* **1984**, 109-112; Al-Mallah, K.; Collings, P.; Stedman, G., Electrophilic Nitrosation at Sulphur and Nitrogen in Thiourea. *J. Chem. Soc., Dalton Trans.* **1974**, 2469-2472.
35. Roy, B.; Moulinet d'Hardemare, A.; Fontecave, M., New Thionitrites: Synthesis, Stability, and Nitric Oxide Generation. *J. Org. Chem.* **1994**, *59*, 7019-7026.
36. Aldred, S. E.; Williams, D. L. H., Alkyl Nitrites as Nitrosating Agents. Kinetics and Mechanism of the Reactions of Propyl Nitrite in Propan-1-ol. *J. Chem. Soc., Perkin Trans. 2* **1981**, 1021-1024; Crookes, M. J.; Williams, D. L. H., Nitrosation by Alkyl Nitrites. Part 2. Kinetics of Reactions in Aqueous Acid Solution with Isopropyl and t-Butyl Nitrites. *J. Chem. Soc., Perkin Trans. 2* **1988**, 1339-1343; Patel, H. M. S.; Williams, D. L. H., Nitrosation by Alkyl Nitrites. Part 3. Reactions with Cysteine in Water in the pH Range 6-13. *J. Chem. Soc., Perkin Trans. 2* **1989**, 339-341; Crookes, M. J.; Williams, D. L. H., Nitrosation by Alkyl Nitrites. Part 4. S-nitrosation in Acidic Alcohol Solvent. *J. Chem. Soc., Perkin Trans. 2* **1989**, 759-763; Crookes, M. J.; Williams, D. L. H., Nitrosation by Alkyl Nitrites. Part 5. Kinetics and Mechanism of Reactions in Acetonitrile. *J. Chem. Soc., Perkin Trans. 2* **1989**, 1319-1322; Patel, H. M. S.; Williams, D. L. H., Nitrosation by Alkyl Nitrites. Part 6. Thiolate Nitrosation. *J. Chem. Soc., Perkin Trans. 2* **1990**, 37-42.
37. Goldstein, S.; Czapski, G., Mechanism of the Nitrosation of Thiols and Amines by Oxygenated NO Solutions: the Nature of the Nitrosating Intermediates. *J. Am. Chem. Soc.* **1996**, *118*, 3419-3425; Wink, D. A.; Cook, J. A.; Kim, S. Y.; Vodovotz, Y.; Pacelli, R.; Krishna, M. C.; Russo, A.; Mitchell, J. B.; Jourdeuil, D.; Miles, A. M.; Grisham, M. B., Superoxide Modulates the Oxidation and Nitrosation of Thiols by Nitric Oxide-Derived

- Reactive Intermediates. *J. Biol. Chem.* **1997**, *272*, 11147-11151; Schrammel, A.; Gorren, A. C. F.; Schmidt, K.; Pfeiffer, S.; Mayer, B., S-nitrosation of Glutathione by Nitric Oxide, Peroxynitrite, and NO/O₂. *Free Radical Biol. Med.* **2003**, *34*, 1078-1088; Gow, A. J.; Buerk, D. G.; Ischiropoulos, H., A Novel Reaction Mechanism for the Formation of S-nitrosothiol in vivo. *J. Biol. Chem.* **1997**, *272*, 2841-2845; Keszler, A.; Zhang, Y.; Hogg, N., Reaction Between Nitric Oxide, Glutathione, and Oxygen in the Presence and Absence of Protein: How are S-nitrosothiols Formed? *Free Radical Biol. Med.* **2010**, *48*, 55-64; Jour'dheuil, D.; Jour'dheuil, F. L.; Feelisch, M., Oxidation and Nitrosation of Thiols at Low Micromolar Exposure to Nitric Oxide. *J. Biol. Chem.* **2003**, *278*, 15720-15726.
38. Kharitonov, V. G.; Sundquist, A. R.; Sharma, V. S., Kinetics of Nitrosation of Thiols by Nitric Oxide in the Presence of Oxygen. *J. Biol. Chem.* **1995**, *270*, 28158-28164.
39. Keshive, M.; Singh, S.; Wishnok, J. S.; Tannenbaum, S. R.; Deen, W. M., Kinetics of S-nitrosation of Thiols in Nitric Oxide Solutions. *Chem. Res. Toxicol.* **1996**, *9*, 988-993.
40. Holmes, A. J.; Williams, D. L. H., Reaction of Ascorbic Acid with S-nitrosothiols: Clear Evidence for Two Distinct Reaction Pathways. *J. Chem. Soc. Perkin Trans. 2* **2000**, 1639-1644.
41. Smith, J. N.; Dasgupta, T. P., Kinetics and Mechanism of the Decomposition of S-nitrosoglutathione by L-ascorbic Acid and Copper Ions in Aqueous Solution to Produce Nitric Oxide. *Nitric Oxide* **2000**, *4*, 57-66.
42. Singh, R. J.; Hogg, N.; Joseph, J.; Kalyanaraman, B., Mechanism of Nitric Oxide Release from S-nitrosothiols. *J. Biol. Chem.* **1996**, *271*, 18596-18603.
43. Zhelyaskov, V. R.; Gee, K. R.; Godwin, D. W., Control of NO Concentration in Solutions of Nitrosothiol Compounds by Light. *Photochem. Photobiol.* **1998**, *67*, 282-288; Wood, P.

- D.; Mutus, B.; Redmond, R. W., The Mechanism of Photochemical Release of Nitric Oxide from S-nitrosoglutathione. *Photochem. Photobiol.* **1996**, *64*, 518-524.
44. Sexton, D. J.; Muruganandam, A.; McKenney, D. J.; Mutus, B., Visible Light Photochemical Release of Nitric Oxide from S-nitrosoglutathione: Potential Photochemotherapeutic Applications. *Photochem. Photobiol.* **1994**, *59*, 463-467.
45. Munro, A. P.; Williams, D. L. H., Synthesis and Kinetics of Decomposition of Some Novel S-nitrosothiols. *Can. J. Chem.* **1999**, *77*, 550-556.
46. Gu, J.; Lewis, R. S., Effect of pH and Metal Ions on the Decomposition Rate of S-nitrosocysteine. *Ann. Biomed. Eng.* **2007**, *35*, 1554-1560.
47. Williams, D. L. H., S-nitrosothiols and Role of Metal Ions in Decomposition to Nitric Oxide. *Methods Enzymol.* **1996**, *268*, 299-308; Noble, D. R.; Williams, D. L. H., Structure-Reactivity Studies of the Cu²⁺-catalyzed Decomposition of Four S-nitrosothiols Based Around the S-nitrosocysteine/S-nitrosoglutathione Structures. *Nitric Oxide* **2000**, *4*, 392-398; Stubauer, G.; Giuffre, A.; Sarti, P., Mechanism of S-nitrosothiol Formation and Degradation Mediated by Copper Ions. *J. Biol. Chem.* **1999**, *274*, 28128-28133; Askew, S. C.; Barnett, D. J.; McAninly, J.; Williams, D. L. H., Catalysis by Cu²⁺ of Nitric Oxide Release from S-nitrosothiols (RSNO). *J. Chem. Soc., Perkin Trans. 2* **1995**, 741-745; Noble, D. R.; Swift, H. R.; Williams, D. L. H., Nitric Oxide Release from S-nitrosoglutathione (GSNO). *Chem. Commun.* **1999**, 2317-2318.
48. Dicks, A. P.; Swift, H. R.; Williams, D. L. H.; Butler, A. R.; Al-Sa'doni, H. H.; Cox, B. G., Identification of Cu⁺ as the Effective Reagent in Nitric Oxide Formation from S-nitrosothiols (RSNO). *J. Chem. Soc., Perkin Trans. 2* **1996**, 481-487.

49. Gorren, A. C. F.; Schrammel, A.; Schmidt, K.; Mayer, B., Decomposition of S-nitrosoglutathione in the Presence of Copper Ions and Glutathione. *Arch. Biochem. Biophys.* **1996**, *330*, 219-228.
50. de Oliveira, M. G.; Shishido, S. M.; Seabra, A. B.; Morgon, N. H., Thermal Stability of Primary S-nitrosothiols: Roles of Autocatalysis and Structural Effects on the Rate of Nitric Oxide Release. *J. Phys. Chem. A* **2002**, *106*, 8963-8970.
51. Grossi, L.; Montevicchi, P. C., A Kinetic Study of S-nitrosothiol Decomposition. *Chem. Eur. J.* **2002**, *8*, 380-387.
52. Aleryani, S.; Milo, E.; Rose, Y.; Kostka, P., Superoxide-Mediated Decomposition of Biological S-nitrosothiols. *J. Biol. Chem.* **1998**, *273*, 6041-6045.
53. Zhao, Y.; McCarren, P. R.; Houk, K. N.; Choi, B. Y.; Toone, E. J., Nitrosonium-Catalyzed Decomposition of S-nitrosothiols in Solution: A Theoretical and Experimental Study. *J. Am. Chem. Soc.* **2005**, *127*, 10917-10924.
54. Clancy, R. M.; Abramson, S. B., Novel Synthesis of S-nitrosoglutathione and Degradation by Human Neutrophils. *Anal. Biochem.* **1992**, *204*, 365-371.
55. Meyer, D. J.; Kramer, H.; Ozer, N.; Coles, B.; Ketterer, B., Kinetics and Equilibria of S-nitrosothiol-thiol Exchange Between Glutathione, Cysteine, Penicillamines and Serum Albumin. *FEBS Lett.* **1994**, *345*, 177-180.
56. Singh, S. P.; Wishnok, J. S.; Keshive, M.; Deen, W. M.; Tannenbaum, S. R., The Chemistry of the S-nitrosoglutathione/glutathione System. *Proc. Natl. Acad. Sci. USA* **1996**, *93*, 14428-14433.
57. Giustarini, D.; Milzani, A.; Colombo, R.; Dalle-Donne, I.; Rossi, R., Nitric Oxide and S-nitrosothiols in Human Blood. *Clin. Chim. Acta* **2003**, *330*, 85-98; Stamler, J. S., S-

- nitrosothiols in the Blood: Roles, Amounts, and Methods of Analysis. *Circ. Res.* **2004**, *94*, 414-417; Stamler, J. S.; Jaraki, O.; Osborne, J.; Simon, D. I.; Keaney, J.; Vita, J.; Singel, D.; Valeri, C. R.; Loscalzo, J., Nitric Oxide Circulates in Mammalian Plasma Primarily as an S-nitroso Adduct of Serum Albumin. *Proc. Natl. Acad. Sci. USA* **1992**, *89*, 7674-7677; Arnelle, D. R.; Stamler, J. S., NO⁺, NO, and NO⁻ Donation by S-nitrosothiols: Implications for Regulation of Physiological Functions by S-nitrosylation and Acceleration of Disulfide Formation. *Arch. Biochem. Biophys.* **1995**, *318*, 279-285.
58. Ignarro, L. J.; Lipton, H.; Edwards, J. C.; Baricos, W. H.; Hyman, A. L.; Kadowitz, P. J.; Gruetter, C. A., Mechanism of Vascular Smooth Muscle Relaxation by Organic Nitrates, Nitrite, Nitroprusside and Nitric Oxide: Evidence for the Involvement of S-nitrosothiols as Active Intermediates. *J. Pharmacol. Exp. Ther.* **1981**, *218*, 739-749; Mathews, W. R.; Kerr, S. W., Biological Activity of S-nitrosothiols: The Role of Nitric Oxide. *J. Pharmacol. Exp. Ther.* **1993**, *267*, 1529-1537; Stamler, J. S.; Simon, D. I.; Osborne, J. A.; Mullins, M. E.; Jaraki, O.; Michel, T.; Singel, D. J.; Loscalzo, J., S-nitrosylation of Proteins with Nitric Oxide: Synthesis and Characterization of Biologically Active Compounds. *Proc. Natl. Acad. Sci. USA* **1992**, *89*, 444-448.
59. Al-Sa'doni, H. H.; Khan, I. Y.; Poston, L.; Fisher, I.; Ferro, A., A Novel Family of S-nitrosothiols: Chemical Synthesis and Biological Actions. *Nitric Oxide* **2000**, *4*, 550-560.
60. Smith, D. J.; Chakravarthy, D.; Pulfer, S.; Simmons, M. L.; Hrabie, J. A.; Citro, M. L.; Saavedra, J. E.; Davies, K. M.; Hutsell, T. C.; Mooradian, D. L.; Hanson, S. R.; Keefer, L. K., Nitric Oxide-Releasing Polymer Containing the [N(O)NO]- Group. *J. Med. Chem.* **1996**, *39*, 1148-1156.

61. Frost, M. C.; Batchelor, M. M.; Lee, Y.; Zhang, H.; Kang, Y.; Oh, B.; Wilson, G. S.; Gifford, R.; Rudich, S. M.; Meyerhoff, M. E., Preparation and Characterization of Implantable Sensors with Nitric Oxide Release Coatings. *Microchem. J.* **2003**, *74*, 277-288; Reynolds, M. M.; Frost, M. C.; Meyerhoff, M. E., Nitric Oxide-Releasing Hydrophobic Polymers: Preparation, Characterization, and Potential Biomedical Applications. *Free Radical Biol. Med.* **2004**, *37*, 926-936; Frost, M. C.; Reynolds, M. M.; Meyerhoff, M. E., Polymers Incorporating Nitric Oxide Releasing/Generating Substances for Improved Biocompatibility of Blood-Contacting Medical Devices. *Biomaterials* **2005**, *26*, 1685-1693; Hetrick, E. M.; Schoenfisch, M. H., Reducing Implant-Related Infections: Active Release Strategies. *Chem. Soc. Rev.* **2006**, *35*, 780-789; Varu, V. N.; Tsihlis, N. D.; Kibbe, M. R., Nitric Oxide-Releasing Prosthetic Materials. *Vasc. Endovascular Surg.* **2009**, *43*, 121-131; Sortino, S., Light-Controlled Nitric Oxide Delivering Molecular Assemblies. *Chem. Soc. Rev.* **2010**, *39*, 2903-2913; Seabra, A. B.; Duran, N., Nitric Oxide-Releasing Vehicles for Biomedical Applications. *J. Mater. Chem.* **2010**, *20*, 1624-1637; de Mel, A.; Murad, F.; Seifalian, A. M., Nitric Oxide: A Guardian for Vascular Grafts? *Chem. Rev.* **2011**, *111*, 5742-5767; Riccio, D. A.; Schoenfisch, M. H., Nitric Oxide Release: Part I. Macromolecular Scaffolds. *Chem. Soc. Rev.* **2012**, *41*, 3731-3741; Naghavi, N.; de Mel, A.; Alavijeh, O. S.; Cousins, B. G.; Seifalian, A. M., Nitric Oxide Donors for Cardiovascular Implant Applications. *Small* **2012**, *9*, 22-35; Jen, M. C.; Serrano, M. C.; van Lith, R.; Ameer, G. A., Polymer-Based Nitric Oxide Therapies: Recent Insights for Biomedical Applications. *Adv. Funct. Mater.* **2012**, *22*, 239-260.

62. Espadas-Torre, C.; Oklejas, V.; Mowery, K.; Meyerhoff, M. E., Thromboresistant Chemical Sensors Using Combined Nitric Oxide Release/Ion Sensing Polymeric Films. *J. Am. Chem. Soc.* **1997**, *119*, 2321-2322.
63. Mowery, K. A.; Schoenfisch, M. H.; Saavedra, J. E.; Keefer, L. K.; Meyerhoff, M. E., Preparation and Characterization of Hydrophobic Polymeric Films that are Thromboresistant via Nitric Oxide Release. *Biomaterials* **2000**, *21*, 9-21.
64. Zhou, Z.; Meyerhoff, M. E., Preparation and Characterization of Polymeric Coatings with Combined Nitric Oxide Release and Immobilized Active Heparin. *Biomaterials* **2005**, *26*, 6506-6517.
65. Coneski, P. N.; Nash, J. A.; Schoenfisch, M. H., Nitric Oxide-Releasing Electrospun Polymer Microfibers. *ACS Appl. Mater. Interfaces* **2011**, *3* (2), 426-432.
66. Batchelor, M. M.; Reoma, S. L.; Fleser, P. S.; Nuthakki, V. K.; Callahan, R. E.; Shanley, C. J.; Politis, J. K.; Elmore, J.; Merz, S. I.; Meyerhoff, M. E., More Lipophilic Dialkyldiamine-Based Diazoniumdiolates: Synthesis, Characterization, and Application in Preparing Thromboresistant Nitric Oxide Release Polymeric Coatings. *J. Med. Chem.* **2003**, *46*, 5153-5161.
67. Fleser, P. S.; Nuthakki, V. K.; Malinzak, L. E.; Callahan, R. E.; Seymour, M. L.; Reynolds, M. M.; Merz, S. I.; Meyerhoff, M. E.; Bendick, P. J.; Zelenock, G. B.; Shanley, C. J., Nitric Oxide-Releasing Biopolymers Inhibit Thrombus Formation in a Sheep Model of Arteriovenous Bridge Grafts. *J. Vasc. Surg.* **2004**, *40*, 803-811.
68. Skrzypchak, A. M.; Lafayette, N. G.; Bartlett, R. H.; Zhou, Z. R.; Frost, M. C.; Meyerhoff, M. E.; Reynolds, M. M.; Annich, G. M., Effect of Varying Nitric Oxide Release to Prevent

- Platelet Consumption and Preserve Platelet Function in an in vivo Model of Extracorporeal Circulation. *Perfusion* **2007**, *22*, 193-200.
69. Wu, Y. D.; Zhou, Z. R.; Meyerhoff, M. E., In vitro Platelet Adhesion on Polymeric Surfaces with Varying Fluxes of Continuous Nitric Oxide Release. *J. Biomed. Mater. Res., Part A* **2007**, *81A*, 956-963.
70. Smith, D. J.; Simmons, M. L., Transdermal Delivery of Nitric Oxide from Diazeniumdiolates. *J. Controlled Release* **1998**, *51*, 153-159.
71. Schoenfisch, M. H.; Zhang, H.; Frost, M. C.; Meyerhoff, M. E., Nitric Oxide-Releasing Fluorescence-Based Oxygen Sensing Polymeric Films. *Anal. Chem.* **2002**, *74*, 5937-5941.
72. Wu, B.; Gerlitz, B.; Grinnell, B. W.; Meyerhoff, M. E., Polymeric Coatings that Mimic the Endothelium: Combining Nitric Oxide Release with Surface-Bound Active Thrombomodulin and Heparin. *Biomaterials* **2007**, *28*, 4047-4055.
73. Annich, G. M.; Meinhardt, J. P.; Mowery, K. A.; Ashton, B. A.; Merz, S. I.; Hirschl, R. B.; Meyerhoff, M. E.; Bartlett, R. H., Reduced Platelet Activation and Thrombosis in Extracorporeal Circuits Coated with Nitric Oxide Release Polymers. *Crit. Care Med.* **2000**, *28*, 915-920.
74. Xu, H.; Reynolds, M. M.; Cook, K. E.; Evans, A. S.; Toscano, J. P., 2-Hydroxy-5-nitrobenzyl as a Diazeniumdiolate Protecting Group: Application in NO-Releasing Polymers with Enhanced Biocompatibility. *Org. Lett.* **2008**, *10*, 4593-4596.
75. Bohl, K. S.; West, J. L., Nitric Oxide-Generating Polymers Reduce Platelet Adhesion and Smooth Muscle Cell Proliferation. *Biomaterials* **2000**, *21*, 2273-2278.

76. Robbins, M. E.; Oh, B. K.; Hopper, E. D.; Schoenfish, M. H., Nitric Oxide-Releasing Xerogel Microarrays Prepared with Surface-Tailored Poly(dimethylsiloxane) Templates. *Chem. Mater.* **2005**, *17*, 3288-3296.
77. Hetrick, E. M.; Schoenfish, M. H., Antibacterial Nitric Oxide-Releasing Xerogels: Cell Viability and Parallel Plate Fow Cell Adhesion Studies *Biomaterials* **2007**, *28*, 1948-1956.
78. Deupree, S. M.; Schoenfish, M. H., Morphological Analysis of the Antimicrobial Action of Nitric Oxide on Gram-Negative Pathogens Using Atomic Force Microscopy *Acta Biomater.* **2009**, *5*, 1405-1415.
79. Parzuchowski, P. G.; Frost, M. C.; Meyerhoff, M. E., Synthesis and Characterization of Polymethacrylate-Based Nitric Oxide Donors. *J. Am. Chem. Soc.* **2002**, *124*, 12182-12191.
80. Zhou, Z.; Meyerhoff, M. E., Polymethacrylate-Based Nitric Oxide Donors with Pendant N-diazeniumdiolated Alkyldiamine Moieties: Synthesis, Characterization, and Preparation of Nitric Oxide Releasing Polymeric Coatings. *Biomacromolecules* **2005**, *6*, 780-789.
81. Bohl Masters, K. S.; Leibovich, J.; Belem, P.; West, J. L.; Poole-Warren, L. A., Effects of Nitric Oxide Releasing Poly(vinyl alcohol) Hydrogel Dressings on Dermal Wound Healing in Diabetic Mice. *Wound Repair Regen.* **2002**, *10*, 286-294.
82. Marxer, S. M.; Rothrock, A. R.; Nablo, B. J.; Robbins, M. E.; Schoenfish, M. H., Preparation of Nitric Oxide (NO)-Releasing Sol-Gels for Biomaterial Applications. *Chem. Mater.* **2003**, *15*, 4193-4199.
83. Nablo, B. J.; Rothrock, A. R.; Schoenfish, M. H., Nitric Oxide-Releasing Sol-Gels as Antibacterial Coatings for Orthopedic Implants. *Biomaterials* **2005**, *26*, 917-924.
84. Nablo, B. J.; Schoenfish, M. H., In vitro Cytotoxicity of Nitric Oxide-Releasing Sol-Gel Derived Materials. *Biomaterials* **2005**, *26*, 4405-4415.

85. Robbins, M. E.; Hopper, E. D.; Schoenfish, M. H., Synthesis and Characterization of Nitric Oxide-Releasing Sol-Gel Microarrays. *Langmuir* **2004**, *20*, 10296-10302.
86. Dobmeier, K. P.; Schoenfish, M. H., Antibacterial Properties of Nitric Oxide-Releasing Sol-Gel Microarrays *Biomacromolecules* **2004**, *5*, 2493-2495.
87. Zhang, H.; Annich, G. M.; Miskulin, J.; Stankiewicz, K.; Osterholzer, K.; Merz, S. I.; Barlett, R. H.; Meyerhoff, M. E., Nitric Oxide-Releasing Fumed Silica Particles: Synthesis, Characterization and Biomedical Application. *J. Am. Chem. Soc.* **2003**, *125*, 5015-5024.
88. Shin, J. H.; Metzger, S. K.; Schoenfish, M. H., Synthesis of Nitric Oxide-Releasing Silica Nanoparticles. *J. Am. Chem. Soc.* **2007**, *129*, 4612-4619; Shin, J. H.; Schoenfish, M. H., Inorganic/Organic Hybrid Silica Nanoparticles as a Nitric Oxide Delivery Scaffold. *Chem. Mater.* **2008**, *20*, 239-249.
89. Carpenter, A. W.; Slomberg, D. L.; Rao, K. S.; Schoenfish, M. H., Influence of Scaffold Size on Bactericidal Activity of Nitric Oxide-Releasing Silica Nanoparticles. *ACS Nano* **2011**, *5*, 7235-7244; Slomberg, D. L.; Lu, Y.; Broadnax, A. D.; Hunter, R. A.; Carpenter, A. W.; Schoenfish, M. H., Role of Size and Shape on Biofilm Eradication for Nitric Oxide-Releasing Silica Nanoparticles *ACS Appl. Mater. Interfaces* **2013**, *5*, 9322-9329; Hetrick, E. M.; Shin, J.; Paul, H. S.; Schoenfish, M. H., Anti-Biofilm Efficacy of Nitric Oxide-Releasing Silica Nanoparticles. *Biomaterials* **2009**, *30*, 2782-2789; Hetrick, E. M.; Shin, J.; Stasko, N. A.; Johnson, C. B.; Wespe, D. A.; Holmuhamedov, E.; Schoenfish, M. H., Bactericidal Efficacy of Nitric Oxide-Releasing Silica Nanoparticles *ACS Nano* **2008**, *2*, 235-246.

90. Carpenter, A. W.; Reighard, K. P.; Saavedra, J. E.; Schoenfisch, M. H., O₂-Protected Diazeniumdiolate-Modified Silica Nanoparticles for Extended Nitric Oxide Release From Dental Composites. *Biomater. Sci.* **2013**, *1*, 456-459.
91. Koh, A.; Carpenter, A. W.; Slomberg, D. L.; Schoenfisch, M. H., Nitric Oxide-Releasing Silica Nanoparticle-Doped Polyurethane Electrospun Fibers *ACS Appl. Mater. Interfaces* **2013**, *5*, 7956–7964.
92. Lu, Y.; Slomberg, D. L.; Sun, B.; Schoenfisch, M. H., Shape- and Nitric Oxide Flux-Dependent Bactericidal Activity of Nitric Oxide-Releasing Silica Nanorods *Small* **2013**, *9*, 2189–2198.
93. Lowe, A.; Deng, W.; Smith, D. W.; Balkus, K. J., Acrylonitrile-Based Nitric Oxide Releasing Melt-Spun Fibers for Enhanced Wound Healing. *Macromolecules* **2012**, *45*, 5894-5900.
94. Jun, H.; Taite, L. J.; West, J. L., Nitric Oxide-Producing Polyurethanes. *Biomacromolecules* **2005**, *6*, 838-844.
95. Reynolds, M. M.; Hrabie, J. A.; Oh, B. K.; Politis, J. K.; Citro, M. L.; Keefer, L. K.; Meyerhoff, M. E., Nitric Oxide Releasing Polyurethanes with Covalently Linked Diazeniumdiolated Secondary Amines. *Biomacromolecules* **2006**, *7*, 987-994.
96. Reynolds, M. M.; Saavedra, J. E.; Showalter, B. M.; Valdez, C. A.; Shanklin, A. P.; Oh, B. K.; Keefer, L. K.; Meyerhoff, M. E., Tailored Synthesis of Nitric Oxide-Releasing Polyurethanes Using O₂-protected Diazeniumdiolated Chain Extenders. *J. Mater. Chem.* **2010**, *20*, 3107-3114.
97. Rothrock, A. R.; Donkers, R. L.; Schoenfisch, M. H., Synthesis of Nitric Oxide-Releasing Gold Nanoparticles. *J. Am. Chem. Soc.* **2005**, *127*, 9362-9363.

98. Zhou, Z.; Annich, G. M.; Wu, Y.; Meyerhoff, M. E., Water-Soluble Poly(ethylenimine)-Based Nitric Oxide Donors: Preparation, Characterization and Potential Application in Hemodialysis. *Biomacromolecules* **2006**, *7*, 2565-2574.
99. Stasko, N. A.; Schoenfish, M. H., Dendrimers as a Scaffold for Nitric Oxide Release. *J. Am. Chem. Soc.* **2006**, *128*, 8265-8271; Lu, Y.; Sun, B.; Li, C.; Schoenfish, M. H., Structurally Diverse Nitric Oxide-Releasing Poly(propylene imine) Dendrimers. *Chem. Mater.* **2011**, *23*, 4227-4233.
100. Sun, B.; Slomberg, D. L.; Chudasama, S. L.; Lu, Y.; Schoenfish, M. H., Nitric Oxide-Releasing Dendrimers as Antibacterial Agents. *Biomacromolecules* **2012**, *13*, 3343–3354; Lu, Y.; Slomberg, D. L.; Shah, A.; Schoenfish, M. H., Nitric Oxide-Releasing Amphiphilic Poly(amidoamine) (PAMAM) Dendrimers as Antibacterial Agents *Biomacromolecules* **2013**, *14*, 3589–3598.
101. Kou, Y.; Wan, A., Synthesis of Novel N-diazeniumdiolates Based on Hyperbranched Polyethers. *Bioorg. Med. Chem. Lett.* **2008**, *18*, 2337-2341.
102. Zhao, H.; Serrano, M. C.; Popowich, D. A.; Kibbe, M. R.; Ameer, G. A., Biodegradable Nitric Oxide-Releasing Poly(diols citrate) Elastomers. *J. Biomed. Mater. Res., Part A* **2010**, *93A*, 356-363.
103. Carpenter, A. W.; Worley, B. V.; Slomberg, D. L.; Schoenfish, M. H., Dual Action Antimicrobials: Nitric Oxide Release from Quaternary Ammonium-Functionalized Silica Nanoparticles *Biomacromolecules* **2012**, *13*, 3334–3342.
104. Shishido, S. M.; Seabra, A. B.; Loh, W.; de Oliveira, M. G., Thermal and Photochemical Nitric Oxide Release from S-nitrosothiols Incorporated in Pluronic F127 Gel: Potential Uses for Local and Controlled Nitric Oxide Release. *Biomaterials* **2003**, *24*, 3543-3553.

105. Seabra, A. B.; Fitzpatrick, A.; Paul, J.; de Oliveira, M. G.; Weller, R., Topically Applied S-nitrosothiol-containing Hydrogels as Experimental and Pharmacological Nitric Oxide Donors in Human Skin. *Br. J. Dermatol.* **2004**, *151*, 977-983.
106. Georgii, J. L.; Amadeu, T. P.; Seabra, A. B.; de Oliveira, M. G.; Monte-Alto-Costa, A., Topical S-nitrosoglutathione-releasing Hydrogel Improves Healing of Rat Ischaemic Wounds. *J. Tissue Eng. Regener. Med.* **2011**, *5*, 612-619; Amadeu, T. P.; Seabra, A. B.; de Oliveira, M. G.; Costa, A. M. A., S-nitrosoglutathione-containing Hydrogel Accelerates Rat Cutaneous Wound Repair. *J. Eur. Acad. Dermatol. Venereol.* **2007**, *21*, 629-637.
107. Simoes, M. M. D. G.; de Oliveira, M. G., Poly(vinyl alcohol) Films for Topical Delivery of S-Nitrosoglutathione: Effect of Freezing-Thawing on the Diffusion Properties. *J. Biomed. Mater. Res., Part B* **2010**, *93B* (2), 416-424.
108. Seabra, A. B.; de Oliveira, M. G., Poly(vinyl alcohol) and Poly(vinyl pyrrolidone) Blended Films for Local Nitric Oxide Release. *Biomaterials* **2004**, *25* (25), 3773-3782.
109. Seabra, A. B.; da Rocha, L. L.; Eberlin, M. N.; de Oliveira, M. G., Solid Films of Blended Poly(vinyl alcohol)/Poly(vinyl pyrrolidone) for Topical S-nitrosoglutathione and Nitric Oxide Release. *J. Pharm. Sci.* **2005**, *94*, 994-1003.
110. Seabra, A. B.; de Souza, G. F. P.; da Rocha, L. L.; Eberlin, M. N.; de Oliveira, M. G., S-nitrosoglutathione Incorporated in Poly(ethylene glycol) Matrix: Potential Use for Topical Nitric Oxide Delivery. *Nitric Oxide* **2004**, *11*, 263-272.
111. Shishido, S. M.; de Oliveira, M. G., Polyethylene Glycol Matrix Reduced the Rates of Photochemical and Thermal Release of Nitric Oxide from S-nitroso-N-acetylcysteine. *Photochem. Photobiol.* **2000**, *71*, 273-280.

112. Koehler, J. J.; Zhao, J.; Jedlicka, S. S.; Potterfield, D. M.; Rickus, J. L., Compartmentalized Nanocomposite for Dynamic Nitric Oxide Release. *J. Phys. Chem. B* **2008**, *112*, 15086-15093.
113. Frost, M. C.; Meyerhoff, M. E., Controlled Photoinitiated Release of Nitric Oxide from Polymer Films Containing S-Nitroso-N-acetyl-DL-penicillamine Derivatized Fumed Silica Filler. *J. Am. Chem. Soc.* **2004**, *126*, 1348-1349.
114. Frost, M. C.; Meyerhoff, M. E., Synthesis, Characterization, and Controlled Nitric Oxide Release from S-nitrosothiol-Derivatized Fumed Silica Polymer Filler Particles. *J. Biomed. Mater. Res., Part A* **2005**, *72A*, 409-419.
115. Riccio, D. A.; Nugent, J. L.; Schoenfisch, M. H., Stober Synthesis of Nitric Oxide-Releasing S-nitrosothiol-Modified Silica Particles. *Chem. Mater.* **2011**, *23*, 1727-1735.
116. Privett, B. J.; Broadnax, A. D.; Bauman, S. J.; Riccio, D. A.; Schoenfisch, M. H., Examination of Bacterial Resistance to Exogenous Nitric Oxide. *Nitric Oxide* **2012**, *26*, 169-173.
117. Seabra, A. B.; da Silva, R.; de Oliveira, M. G., Polynitrosated Polyesters: Preparation, Characterization, and Potential Use for Topical Nitric Oxide Release. *Biomacromolecules* **2005**, *6*, 2512-2520.
118. Coneski, P. N.; Rao, K. S.; Schoenfisch, M. H., Degradable Nitric Oxide-Releasing Biomaterials via Post-Polymerization Functionalization of Cross-Linked Polyesters. *Biomacromolecules* **2010**, *11*, 3208-3215.
119. Seabra, A. B.; Martins, D.; Simoes, M. M. S. G.; da Silva, R.; Brocchi, M.; de Oliveira, M. G., Antibacterial Nitric Oxide-Releasing Polyester for the Coating of Blood-Contacting Artificial Materials. *Artif. Organs* **2010**, *34*, E204-E214.

120. Coneski, P. N.; Schoenfisch, M. H., Synthesis of Nitric Oxide-Releasing Polyurethanes with S-nitrosothiol-Containing Hard and Soft Segments. *Polym. Chem.* **2011**, *2*, 906-913.
121. Bohl Masters, K. S.; Lipke, E. A.; Rice, E. E. H.; Liel, M. S.; Myler, H. A.; Zygourakis, C.; Tulis, D. A.; West, J. L., Nitric Oxide-Generating Hydrogels Inhibit Neointima Formation. *J. Biomater. Sci., Polym. Ed.* **2005**, *16*, 659-672.
122. Lipke, E. A.; West, J. L., Localized Delivery of Nitric Oxide from Hydrogels Inhibits Neointima Formation in a Rat Carotid Balloon Injury Model. *Acta Biomater.* **2005**, *1*, 597-606.
123. Stasko, N. A.; Fischer, T. H.; Schoenfisch, M. H., S-nitrosothiol-Modified Dendrimers as Nitric Oxide Delivery Vehicles. *Biomacromolecules* **2008**, *9*, 834-841.
124. Johnson, T. A.; Stasko, N. A.; Matthews, J. L.; Cascio, W. E.; Holmuhamedov, E. L.; Johnson, C. B.; Schoenfisch, M. H., Reduced Ischemia/Reperfusion Injury via Glutathione-Initiated Nitric Oxide-Releasing Dendrimers. *Nitric Oxide* **2010**, *22*, 30-36.
125. Riccio, D. A.; Dobmeier, K. P.; Hetrick, E. M.; Privett, B. J.; Paul, H. S.; Schoenfisch, M. H., Nitric Oxide-Releasing S-nitrosothiol-Modified Xerogels. *Biomaterials* **2009**, *30*, 4494-4502.
126. Riccio, D. A.; Coneski, P. N.; Nichols, S. P.; Broadnax, A. D.; Schoenfisch, M. H., Photoinitiated Nitric Oxide-Releasing Tertiary S-nitrosothiol-Modified Xerogels. *ACS Appl. Mater. Interfaces* **2012**, *4*, 796-804.
127. Seabra, A. B.; da Silva, R.; de Souza, G. F. P.; de Oliveira, M. G., Antithrombogenic Polynitrosated Polyester/Poly(methylmethacrylate) Blend for the Coating of Blood-Contacting Surfaces. *Artif. Organs* **2008**, *32*, 262-267.

128. Li, Y.; Lee, P. I., Controlled Nitric Oxide Delivery Platform Based on S-nitrosothiol Conjugated Interpolymer Complexes for Diabetic Wound Healing. *Mol. Pharmaceutics* **2010**, *7*, 254-266.
129. Vaughn, M. W.; Kuo, L.; Liao, J. C., Estimation of nitric oxide production and reaction rates in tissue by use of a mathematical model. *Am. J. Physiol. Heart Circ. Physiol.* **1998**, *274* (6), H2163-H2176.
130. Hunter, R. A.; Storm, W. L.; Coneski, P. N.; Schoenfisch, M. H., Inaccuracies of Nitric Oxide Measurement Methods in Biological Media *Anal. Chem.* **2013**, *85*, 1957–1963; Harding, J. L.; Reynolds, M. M., Accurate Nitric Oxide Measurements from Donors in Cell Media: Identification of Scavenging Agents *Anal. Chem.* **2013**, *In press*.
131. Davies, I. R.; Zhang, X., Nitric Oxide Selective Electrodes. *Methods Enzymol.* **2008**, *436*, 63-95.
132. Tominaga, T.; Sato, S.; Ohnishi, T.; Ohnishi, S. T., Electron Paramagnetic Resonance (EPR) Detection of Nitric Oxide Produced During Forebrain Ischemia of the Rat *J. Cereb. Blood Flow Metab.* *1994*, *14*, 715-722 **1994**, *14*, 715-722.
133. Nagano, T., Practical Methods for Detection of Nitric Oxide. *Luminescence* **1999**, *14*, 283-290.
134. Bates, J. N., Nitric Oxide Measurement by Chemiluminescence Detection. *Neuroprotocols* **1992**, *1*, 141-149; Beckman, J. S.; Congert, K. A., Direct Measurement of Dilute Nitric Oxide in Solution with an Ozone Chemiluminescent Detector. *Methods* **1995**, *7*, 35-38.
135. Reynolds, M. M.; Zhou, Z. R.; Oh, B. K.; Meyerhoff, M. E., Bis-diazeniumdiolates of Dialkyldiamines: Enhanced Nitric Oxide Loading of Parent Diamines. *Org. Lett.* **2005**, *7*, 2813-2816.

136. Pogrebnaya, V. L.; Usov, A. P.; Baranov, A. V.; Nesterenko, A. I.; Bez'yazychnyi, P. I., Oxidation of Nitric Oxide by Oxygen in the Liquid Phase. *J. Appl. Chem. USSR* **1975**, *48*, 1004-1007.
137. *Methods in Nitric Oxide Research*. Wiley & Sons: New York, 1996.
138. Szacilowski, K.; Stasicka, Z., S-nitrosothiols: Materials, Reactivity and Mechanisms. *Prog. React. Kinet. Mech.* **2001**, *26*, 1-58.
139. Zhang, H. Development of Nitric Oxide-Releasing Polymers With Improved Blood Compatibility. The University of Michigan, 2002.
140. Kostyukovskii, Y. L.; Melamed, D. B., Carcinogenic N-nitrosamines. Formation, Properties, and Analysis. *Russ. Chem. Rev.* **1988**, *57*, 350-366.
141. Coneski, P. N.; Schoenfisch, M. H., Competitive Formation of N-Diazeniumdiolates and N-Nitrosamines via Anaerobic Reactions of Polyamines with Nitric Oxide. *Org. Lett.* **2009**, *11* (23), 5462-5465.
142. Ragsdale, R. O.; Karstetter, B. R.; Drago, R. S., Decomposition of the Adducts of Diethylamine and Isopropylamine with Nitrogen(II) Oxide. *Inorg. Chem.* **1965**, *4*, 420-422.
143. Park, J., Reaction of S-nitrosoglutathione with Sulfhydryl Groups in Protein. *Biochem. Biophys. Res. Commun.* **1988**, *152*, 916-920.
144. Wallace, T. J.; Schriesheim, A.; Bartok, W., The Base-catalyzed Oxidation of Mercaptans. III. Role of the Solvent and Effect of Mercaptan Structure on the Rate Determining Step. *J. Org. Chem.* **1963**, *28*, 1311-1314.
145. Hisano, N.; Iwata, H.; Teramura, Y.; Chen, H.; Ikada, Y., Kinetics Analyses of Disulfide Formation Between Thiol Groups Attached to Linear Poly(acrylamide). *J. Polym. Sci., Part A: Polym. Chem.* **2010**, *49*, 671-679.

146. Jen, M. C.; Serrano, M. C.; van Lith, R.; Ameer, G. A., Polymer-Based Nitric Oxide Therapies: Recent Insights for Biomedical Applications. *Adv. Funct. Mater.* **2012**, *22* (2), 239-260.

CHAPTER 2:
SYSTEMATIC EVALUATION OF *S*-NITROSATION KINETICS IN AQUEOUS POLYMER
SOLUTION

2.1 PREFACE

In Chapter 1 of this dissertation, the importance of enhancing the NO loading capacities associated with NO materials was highlighted. In the NO materials literature, a variety of nitrosating agents (nitrous acid, alkyl nitrites) and subsequent nitrosation conditions (nitrosating agent concentration, material phase, solvent choice) are employed to achieve *S*-nitrosothiol formation within a material matrix. While small molecule studies have been reported to assess the rates of nitrosation for a variety of substrates, no systematic studies have been reported in the literature that compare multiple nitrosating agents for a single substrate. Further, no fundamental studies have been reported that assess the efficiency of the nitrosation process within a material system. This work, published in *ACS Applied Materials & Interfaces* (© American Chemical Society 2012), marks the first systematic study that has been performed to assess the efficiency of the *S*-nitrosation of a thiol within a model polymer system. Within these studies, two different nitrosating agents were compared and the corresponding rates of *S*-nitrosation were monitored spectroscopically for varying polymer concentrations. Ultimately, the ability to control nitrosation efficiency depending upon the nitrosation conditions was demonstrated. This research was supported by funds from the Boettcher Foundation's Webb-Waring Biomedical Research Program.

Adapted with permission from Joslin, J. M.; Reynolds, M. M., Kinetics of *S*-Nitrosation Processes in Aqueous Polymer Solution for Controlled Nitric Oxide Loading: Toward Tunable

Biomaterials. *ACS Appl. Mater. Interfaces* **2012**, *4*, 1126-1133. Copyright 2012 American Chemical Society.

2.2 INTRODUCTION

Nitric oxide (NO) is an important bioregulatory agent and has been implicated in a variety of physiologically relevant processes.¹ In addition to the enzymatic production of NO in cells, NO is selectively transported and released *in vivo* via *S*-nitrosothiols (RSNOs).² *S*-nitrosothiols constitute a major class of endogenous and exogenous NO donors and are synthesized upon *S*-nitrosation of thiol moieties. As such, RSNOs have attracted widespread attention as vehicles to incorporate long-term NO storage in biomaterials used for blood- and tissue-contacting devices.³ *S*-nitrosothiol moieties decompose through a variety of decomposition mechanisms,⁴ thus resulting in NO release from the material surface. These materials can exert control over biological functions that occur at the material surface, leading to selective cell proliferation accompanied by minimized platelet activation and adhesion,⁵ vasodilation,⁶ and antibacterial effects.⁷ Therefore, the ability to fine-tune NO loading through the use of NO donors is crucial to develop materials with tailorable reservoirs of NO for a variety of biomedical applications including site-specific delivery for tumor apoptosis, biodegradable tissue scaffolds, extracorporeal circuitry and cardiovascular implants.

Previous work demonstrates the incorporation of RSNO moieties within various materials, including polymers,⁶⁻⁹ hydrogels,^{5, 10} xerogels,¹¹ dendrimers¹² and fumed silica filler particles.^{13, 14} Of further importance for application is the ability to process NO releasing materials in usable forms, such as electrospun fibers.¹⁵ Despite achieving NO loading within the materials, no control has been exhibited over this loading process. Further, the kinetics of

nitrosation in polymer systems have not been reported. If control over NO loading is to be achieved toward a requisite NO storage capacity for a specific treatment, fundamental studies investigating the factors affecting RSNO formation kinetics are a necessity. For certain applications, the maximum amount of NO loaded onto the material is desired to ensure the highest therapeutic dosage of NO. In such cases, the most efficient nitrosation would be ideal in order to load all of the thiol sites. For other applications, of greater importance is the ability to exert fine-tuned control over the nitrosation process. If only a fraction of the thiol sites present require NO loading for material applications where a lower dosage of NO is required, the nitrosation process needs to occur more slowly under conditions where the reaction can be halted at the desired endpoint.

To achieve controllable derivatization of thiol sites, we investigate the rate of RSNO formation under different synthetic conditions with emphasis on the kinetics of *S*-nitrosation in the presence of a polymer. In this work, we present the kinetics of *S*-nitrosothiol formation in a polymer solution and not within a pre-cast solid material. From an applications viewpoint, many materials are often solvent-cast or dip-coated onto medical device substrates, thus the formation of the RSNO in a polymer solution environment is practical. Further, due to the nitrosation reactions involving aqueous (nitrous acid) or liquid (*t*-butyl nitrite) nitrosating agents, it is more feasible to load NO within a polymer solution. The resulting RSNO-polymer can then be cast from solution into its desired forms (thin-film coatings, electrospun nanofibers, etc.). Despite the ultimate application involving nitrosation of thiol sites covalently attached to a polymer, we consider the formation of a small molecule donor in a polymer solution. This system offers better control over factors under consideration as the amount of thiol sites in the system is easily altered by the amount of small molecule thiol added to solution. In the covalently bound thiol instance,

the concentration of thiol in the system would be more difficult to regulate. Additionally, the system described herein allows the amount of thiol to remain constant while altering the amount of polymer added. The general trends for efficiency and tunability of NO loading for the small molecule case can then be extended to the thiol pendant to a polymer situation. The reaction variables that allow the most efficient loading of thiol sites, as well as those that permit fine-tuned control over the nitrosation process are described. The reaction conditions under investigation include a comparison of nitrosating agents as well the effect on the rate of *S*-nitrosation due to different concentrations of a water soluble polymer present during the reaction. During the solution-phase nitrosation, the nitrosating agent and polymer concentration can be altered to control the nitrosation kinetics as we have described, even for a case where a thiol is covalently attached to the polymer. The ability to fine-tune NO loading in such systems is crucial toward the development of tailored NO releasing biomaterials.

2.3 EXPERIMENTAL SECTION

2.3.1 Materials. Glutathione (GSH, Acros Organics, 98%, reduced), sodium nitrite (NaNO_2 , Alfa Aesar, 99.999%), and hydrochloric acid (BDH Aristar, 36-38%) were all used as received unless otherwise noted. For all kinetics studies, *t*-butyl nitrite (*t*-BuONO) was obtained from Acros Organics (90% pure) and dextran (MW = ca 40,000) was from TCI America. For the pH studies described, *t*-butyl nitrite (90%) was from Aldrich and dextran (MW = ca 40,000) was from Sigma. All solutions were prepared using Millipore treated ultrapure water. During all solution preparation and reagent addition, the % purity of each reagent was considered.

2.3.2 Methods. Kinetic runs were performed using a Thermo Evolution 300 UV-vis spectrophotometer equipped with a Smart Peltier thermostatted single cell holder with stir and temperature control capabilities. The temperature of the solution contained within the cuvette was monitored using a temperature probe accessory (Pt100 platinum resistance thermometer installed in a TeflonTM cuvette stopper) connected to the Peltier device.

Glutathione solutions were prepared in EnviroWare amber EPA-certified vials to minimize any metal ion contaminants in contact with the thiol solutions. Solutions were prepared freshly and constantly purged with N₂ gas prior to analysis to deoxygenate the solution, preventing thiol oxidation to disulfide in the presence of O₂. Solutions were purged in a 25 °C water bath to minimize temperature equilibration time upon transfer of the solution to the cuvette within the 25 °C Peltier spectrophotometer accessory. The temperature of the reaction cell remained at 25.0 ± 0.4 °C throughout the course of all spectrophotometric experiments.

Nitrosation with HNO₂. To determine the rate order with respect to each reagent (glutathione, acid and nitrite) involved in the nitrosation process, the isolation method was employed. To establish the rate order in each reagent, the reagent of interest was held as the limiting reagent compared to the other two reagents. The concentration of GSH was always held constant throughout all experiments (6.5×10^{-3} M) while the concentration of acid and nitrite was varied.

For thiol-limiting and nitrite-limiting cases, 2 mL of GSH in acid solution were transferred to a quartz cuvette within the UV-vis spectrophotometer. The temperature was monitored by the temperature probe submerged in the solution. At the start of the kinetic run, a 100 µL aliquot of sodium nitrite solution (prepared in Millipore water) was injected into the cuvette which contained a stir bar. The absorbance at 545 nm was monitored for 4 min with the

temperature probe in place. Despite the sodium nitrite solution being at room temperature, the addition of the 100 μL aliquot did not change the temperature of the overall solution, as indicated by replacement of the temperature probe immediately after injection.

To monitor the pH in the acid-limiting runs to assess acid dependence, a vial containing a stir bar and 4 mL of glutathione solution (25 $^{\circ}\text{C}$) was wrapped in aluminum foil to prevent exposure to light. Sodium nitrite solution (200 μL) was injected, and the pH value was collected at a 3 s interval.

Once the reaction order was established for each reactant, the concentration of GSH was held constant as the limiting reagent (6.5×10^{-3} M) with the concentration of acid and nitrite in 4 \times molar excess (25×10^{-3} M). Rate constants were determined under these conditions to compare to the *t*-butyl nitrite experiments to assess nitrosating agent efficiency. The UV-vis experiments were performed as previously described, where a 100 μL aliquot of sodium nitrite stock solution was injected into 2 mL of the acidic GSH solution. The kinetics profiles were tracked by following the 545 nm absorbance feature as a function of reaction time.

Nitrosation with t-butyl nitrite. 2 mL of glutathione solution (6.5×10^{-3} M, prepared in water) were transferred to a quartz cuvette. The start of the kinetic run was marked by injection of a molar excess of *t*-butyl nitrite (6.75 μL to yield 25×10^{-3} M reagent, 90% purity accounted for) into the cuvette via a Hamilton 25 μL airtight syringe. The temperature probe was employed to determine the initial temperature of the thiol solution. To minimize *t*-butyl nitrite evaporation over the course of the nitrosation period, the temperature probe was replaced with a cuvette lid. The absorbance at 545 nm was monitored for 15 min, and the final temperature of the reaction solution was determined by the temperature probe. The initial and final temperature values were

taken to be the temperature range of the reaction. To assess the effect of EDTA-treated *t*-butyl nitrite on glutathione nitrosation, the nitrosating agent was pretreated with 10 w/v% EDTA and allowed to settle. The *t*-butyl nitrite was drawn from the top of the liquid to minimize EDTA presence in the reaction cell. The *t*-butyl nitrite was not filtered for EDTA removal due to the volatility of the reagent.

pH measurements. To determine pH effects on the kinetics of nitrosation, pH values were determined using a Mettler Toledo InLab[®] Routine Pro pH probe (KCl electrolyte, calibrated at 4, 7, and 10). For nitrous acid nitrosation measurements, glutathione and dextran polymer were dissolved in an HCl solution. Upon injection of 150 μL of NaNO_2 solution into 3 mL of GSH/dextran solution, the final concentrations were 6.5×10^{-3} M GSH, 25×10^{-3} M HCl and 25×10^{-3} M NaNO_2 . The pH measurement was recorded prior to the NO_2^- injection and then 4 min after the injection to mimic the final pH of the solution at the end of the kinetics run. For the *t*-butyl nitrite nitrosation measurements, glutathione and dextran were dissolved in water and, upon injection of 10.1 μL (using a 100 μL Hamilton airtight syringe) of the nitrosating agent into 3 mL of solution, the final concentrations were 6.5×10^{-3} M GSH and 25×10^{-3} M *t*-butyl nitrite. The pH measurement was recorded before *t*-butyl nitrite injection, the vial was then capped and the pH value recorded 15 min after injection.

For the determination of the order in H^+ using the isolation method, *in situ* pH measurements were made on an Accumet Excel XL50 dual channel pH/ion/conductivity meter equipped with an Accumet pH probe combination electrode with Ag/AgCl reference. The pH probe was calibrated using buffer solutions of pH values 4.00, 7.00, and 10.00 and pH

measurements were collected at a minimum of 3 s intervals. Rough pH measurements were also determined using pH-indicator strips (EMD, pH range 0-14).

2.3.3 Statistical analysis. All error bars are reported as the standard deviation for each experiment with an $n \geq 3$ for all trials. The % relative error values reported in figure captions were determined by dividing the standard deviation by the average for the y axis values. The Student's t-test was used to assess any significant difference among sets of data at the indicated confidence level (99%+).

2.4 RESULTS & DISCUSSION

2.4.1 Model system. Due to its water solubility, simplicity as a homopolymer and current use in a range of drug delivery applications,¹⁶ dextran was chosen as the model polymer investigated in these studies (structure shown in Figure 2.1).

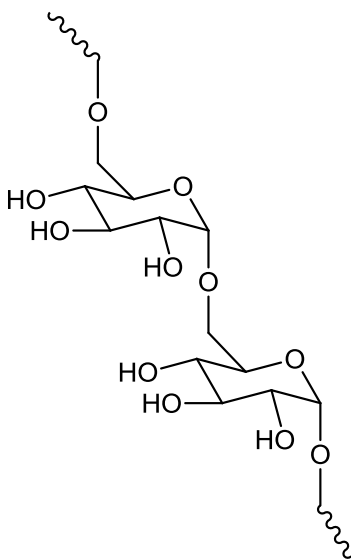


Figure 2.1 Structure of dextran polymer.

Glutathione was used as the thiol substrate for two experimental design reasons: 1) the nitrosated product, *S*-nitrosoglutathione (GSNO), has been well characterized, and 2) GSNO is among the most stable of reported RSNO species.¹⁷ *S*-nitrosoglutathione exhibits two UV-visible absorbance bands ($\lambda_{\text{max}} = 335 \text{ nm}$, $\epsilon_{\text{max}} = 922 \text{ M}^{-1} \text{ cm}^{-1}$; $\lambda_{\text{max}} = 545 \text{ nm}$, $\epsilon_{\text{max}} = 15.9 \text{ M}^{-1} \text{ cm}^{-1}$).¹⁸ The 545 nm peak was monitored to measure the formation of the GSNO product in these studies instead of the 335 nm peak, despite a lower extinction coefficient, due to a lack of interfering species (NO_2^- or HNO_2) at 545 nm.¹⁹ The stability of GSNO is important as the nitrosothiol moiety decomposition will not significantly compete with the rate of its formation. Two commonly reported nitrosating agents were investigated when used in a fixed molar excess relative to glutathione: nitrous acid (HNO_2) and *t*-butyl nitrite. The use of both HNO_2 ¹⁹⁻²³ and *t*-butyl nitrite^{24, 25} for *S*-nitrosation under aqueous conditions has been reported previously, establishing each as a viable nitrosating reagent for these studies. Since the HNO_2 and *t*-butyl nitrite nitrosating agents are aqueous and liquid, respectively, we report RSNO formation in a polymer solution rather than within a cured solid substrate.

2.4.2 Nitrosation under aqueous conditions. The kinetics of GSNO formation using nitrous acid or *t*-butyl nitrite as the nitrosating agent under aqueous conditions serve as a point of comparison for the polymer work presented later. Upon nitrosation of GSH, a nitrosonium cation (NO^+) replaces the proton at the thiol site, as indicated in Figure 2.2.

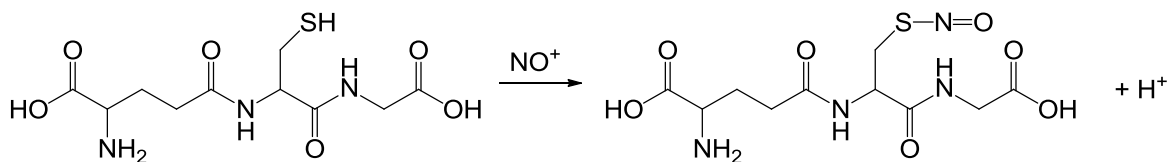


Figure 2.2 Nitrosation of the thiol site on glutathione results in formation of the –SNO moiety.

Previous reports of nitrosation kinetics have commonly used a stop-flow apparatus to accomplish *in situ* formation of HNO₂ prior to addition to the thiol solution.^{19, 20, 22} Here, we employ a simplified method whereby an aliquot of sodium nitrite solution is injected directly into the reaction cell containing a stirring solution of the thiol. Due to the acidic conditions employed (pH < 3, before and after reaction), the HNO₂ species forms rapidly upon nitrite injection into the acidic thiol solution (pK_a = 3.15)²⁶ and is available for reaction at the thiol site. Under these highly acidic conditions, the nitrosonium ion (NO⁺) is the species that reacts with the thiol site.^{19, 27} Because the mechanism of nitrosation remains the same as for the stop-flow apparatus previously described, this method also allows for an appropriate kinetics investigation of HNO₂ nitrosation. For the HNO₂ nitrosation of thiols described herein, a first order dependence on the thiol has been reported.^{19, 20}

Determination of rate law for HNO₂ nitrosation. In general, the rate law for the nitrosation of GSH using any nitrosating agent according to Figure 2.2 should be an equilibrium process, including both the formation of GSNO and the reversible decomposition of GSNO, where k_f and k_r are the forward and reverse rate constants, respectively and δ , ϵ , η and κ correspond to the order in each species.

$$\text{Rate} = k_f [\text{GSH}]^\delta [\text{nitrosating agent}]^\epsilon - k_r [\text{GSNO}]^\eta [\text{H}^+]^\kappa \quad (2.1)$$

However, due to the stability of the GSNO donor, we assume that the second term in the rate law corresponding to reversible GSNO decomposition is negligible due to a very small k_r compared to k_f . Therefore, for the HNO₂ nitrosation described herein, the rate law depends on three reagents: glutathione (GSH), acid (H⁺), and nitrite (NO₂⁻) where k is the rate constant and α , β , and γ represent the rate order for each reagent, respectively (equation 2.2).

$$\text{Rate} = k [\text{GSH}]^\alpha [\text{H}^+]^\beta [\text{NO}_2^-]^\gamma \quad (2.2)$$

Using the isolation method to establish the rate order in each reagent, one reagent served as the limiting reagent and the other two reagents were held in excess ($\sim 4\times$ molar excess). The rate orders with respect to thiol and nitrite were determined by monitoring the formation of the GSNO product whereas the rate order with respect to acid involved direct measurement of the H^+ via a pH probe. The pH values were confirmed to be < 3 for all cases at the beginning and end of each experiment. Under these highly acidic conditions, the nitrosonium ion (NO^+) is the species that reacts with the thiol site.^{19, 27} Differences in the reaction kinetics, therefore, are not due to differences in the mechanism of nitrosation.

For the thiol-limiting and nitrite-limiting cases, the concentration of reagent at time t , $[\text{reagent}]_t$, was calculated from the GSNO concentration at that time, $[\text{GSNO}]_t$, as indicated by equation 2.3. The absorbance was followed at 545 nm ($\epsilon_{\text{max}} = 15.9 \text{ M}^{-1} \text{ cm}^{-1}$), where the Beer-Lambert law holds for the -SNO moiety.¹⁸

$$[\text{reagent}]_t = [\text{reagent}]_0 - [\text{GSNO}]_t \quad (2.3)$$

The initial concentration of reagent, $[\text{reagent}]_0$, was experimentally determined by considering the maximum GSNO concentration, $[\text{GSNO}]_{\text{max}}$, reached. The $[\text{GSNO}]_{\text{max}}$ value is determined from the maximum absorbance point from the absorbance (545 nm) versus time plots, shown in Figure 2.3 (a, b). Once the absorbance values reached a plateau, the maximum value correlates to a maximum $[\text{GSNO}]$, which is correlated to the initial concentration of the limiting reagent. This $[\text{GSNO}]_{\text{max}}$ directly correlates to the limiting reagent initial concentration in a 1:1 molar ratio (equation 2.4).

$$[\text{GSNO}]_{\text{max}} = [\text{reagent}]_0 \quad (2.4)$$

For the acid-limiting case, the acid concentration was directly measured through use of a pH meter as a function of time, where the plot of pH over time is shown in Figure 2.3 (c).

In the case of limiting thiol, the rate law becomes time dependent on only the thiol concentration (equation 2.5), where k_{obs} is the experimentally determined rate constant.

$$-\frac{d[\text{GSH}]}{dt} = k [\text{GSH}]^\alpha [\text{NO}_2^-]_0 [\text{H}^+]_0 = k_{\text{obs}} [\text{GSH}]^\alpha \quad (2.5)$$

Similarly, when generalizing the rate law for the other limiting reagents (NO_2^- , H^+), only the limiting reagent of interest, $[\text{reagent}]_t$, depends on time (equation 2.6), where k_{obs} is unique for each reagent and is dependent upon the initial concentration of the two reagents in excess.

$$-\frac{d[\text{reagent}]}{dt} = k_{\text{obs}} [\text{reagent}]^\alpha \quad (2.6)$$

When the reaction is first order with respect to the reagent ($\alpha = 1$), the integrated rate law results in a linear plot for $\ln([\text{reagent}]_t / [\text{reagent}]_0)$ as a function of time (equation 2.7). The rate constant is then determined from the slope ($k_{\text{obs}} = -\text{slope}$) of the plot and the half-life of the reagent is calculated using equation 2.8.

$$\ln\left(\frac{[\text{reagent}]_t}{[\text{reagent}]_0}\right) = -k_{\text{obs}} t \quad (\text{eq. 2.7})$$

$$t_{1/2} = \frac{\ln(2)}{k_{\text{obs}}} \quad (\text{eq. 2.8})$$

When GSH or nitrite were held as the limiting reagent, the linear relationship between $\ln([\text{reagent}]_t / [\text{reagent}]_0)$ and time, as shown in Figure 2.4 (a, b), demonstrates first order behavior with respect to each reagent. Of note are the differences in the reaction time for near complete nitrosation based on the limiting reagent. For GSH-limiting reaction, nitrosation was complete within 35 s while the nitrite-limiting reaction required 130 s.

For the acid-limiting case, the pH was monitored as a function of time to determine $[\text{H}^+]$. As shown in Figure 2.4 (c), the linear plot for $\ln([\text{H}^+]_t / [\text{H}^+]_0)$ as a function of time indicates first

order kinetics with respect to acid. Only 6 s of each run are shown because the pH exceeds the pK_a of HNO_2 past that point. Thus, the aforementioned nitrosation involving NO^+ is not valid at pH values larger than the pK_a of HNO_2 .

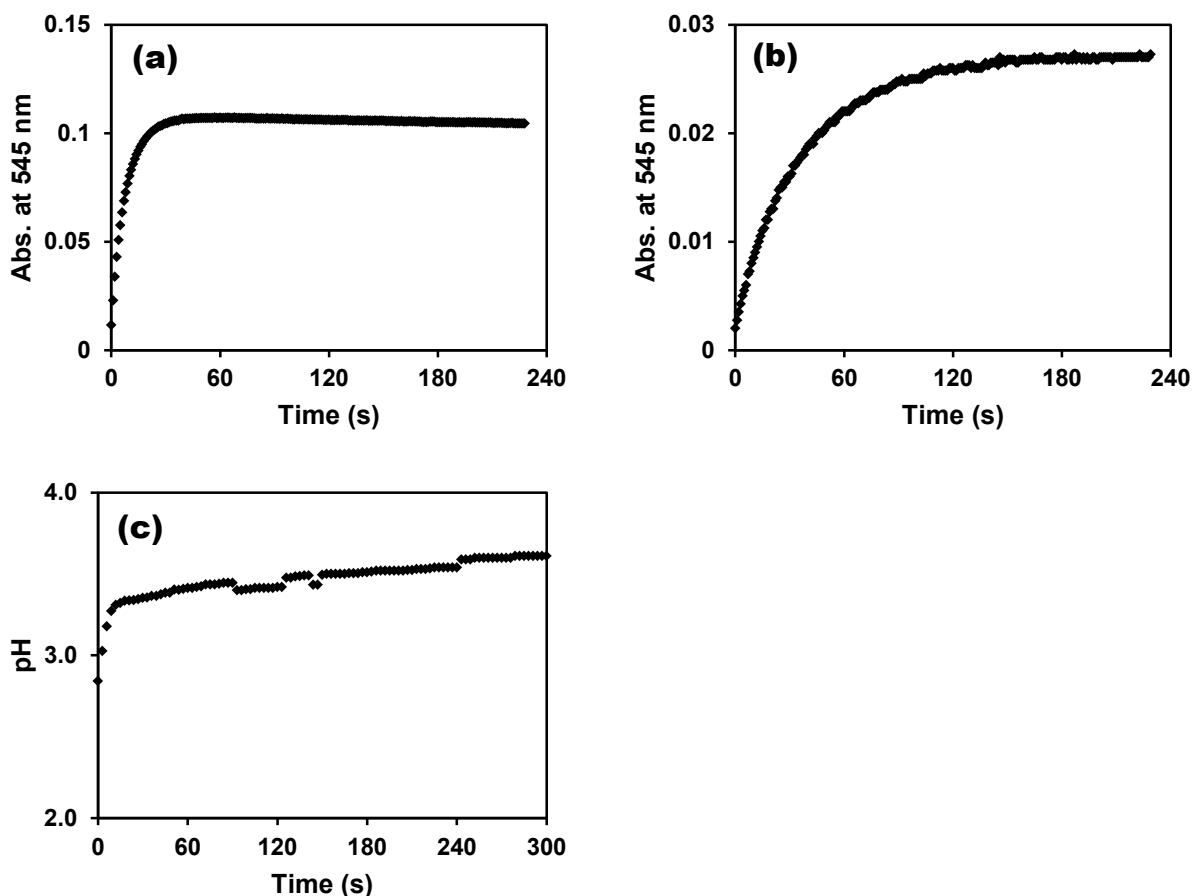


Figure 2.3 Plots of absorbance (545 nm) as a function of time for (a) limiting thiol ($6.76 \pm 0.13 \times 10^{-3}$ M GSH, 0.025 M HCl/ NaNO_2), 2.1% relative error and (b) limiting nitrite (6.5×10^{-3} M GSH/HCl, $1.75 \pm 0.03 \times 10^{-3}$ M NaNO_2), 1.4% relative error. The pH as a function of time for the acid limiting case is shown in (c) (6.5×10^{-3} M GSH/ NaNO_2 , $1.44 \pm 0.15 \times 10^{-3}$ M HCl), 3.1% relative error. For all cases, $n \geq 4$ and $T = 25.0 \pm 0.4$ °C.

Having established first order kinetics with respect to each reagent, we determined the rate constant (k_{obs}) and half-life ($t_{1/2}$) values for each limiting reagent (see Table 2.1 where the limiting reagent is identified). The half-lives are 6.2, 32.2, and 6.1 s for limiting GSH, NO_2^- , and H^+ , respectively. The % nitrosation values listed correspond to the time period indicated. Complete nitrosation was accomplished for the excess acid and nitrite (limiting thiol) case within less than a minute. For the case of limiting nitrite, the process required four times longer to reach complete nitrosation when compared to limiting thiol. The slower reaction time with limiting nitrite indicates that nitrosation will be accomplished more quickly when excess nitrosating agent is present relative to the thiol. Only pH was measured, and not product formation, therefore the % nitrosation was not evaluated for the acid-limiting case. The acid-limiting nitrosation was analyzed directly via pH measurements instead of indirectly, as in the limiting thiol and nitrite cases.

The overall findings indicate first order dependence with respect to each reagent (equation 2.9) which is supported by previous studies.¹⁹



The rate law presented in equation 2.9 was additionally confirmed using the initial rates method. For this method, the absorbance at 335 nm ($\epsilon = 922 \text{ M}^{-1} \text{ cm}^{-1}$)¹⁸ was monitored as a function of time. To ensure that the addition of nitrite ($\lambda_{\text{max}} = 354 \text{ nm}$) was not an interference, the molar extinction coefficient for nitrite was determined to be $22.8 \text{ M}^{-1} \text{ cm}^{-1}$ (see Figure 2.5). Therefore, the concentration of thiol was kept low enough, such that the addition of nitrite would result in absorbance from only the RSNO species and not nitrite interference.

Control experiments were conducted where nitrite was injected into 2 mL of 0.1 M HCl solution. If the final $[\text{NaNO}_2]$ exceeded $2.6 \times 10^{-4} \text{ M}$, the absorbance value at 335 nm exceeded

0.01. Therefore, NaNO_2 concentrations in the cuvette were usually fixed at 2.5×10^{-4} M. It is of interest to note that, for the isolation method described earlier on, the 545 nm absorbance was monitored. To keep the nitrite and *t*-butyl nitrite concentrations among runs the same for comparison purposes, it was not viable to inject such a small amount ($< 1 \mu\text{L}$) of *t*-butyl nitrite into the reaction cell to result in $[\text{t-BuONO}]_{\text{final}} = 2.5 \times 10^{-4}$ M. Therefore, higher concentrations of nitrosating agent were required, and interference at 335 nm would have become a significant issue.

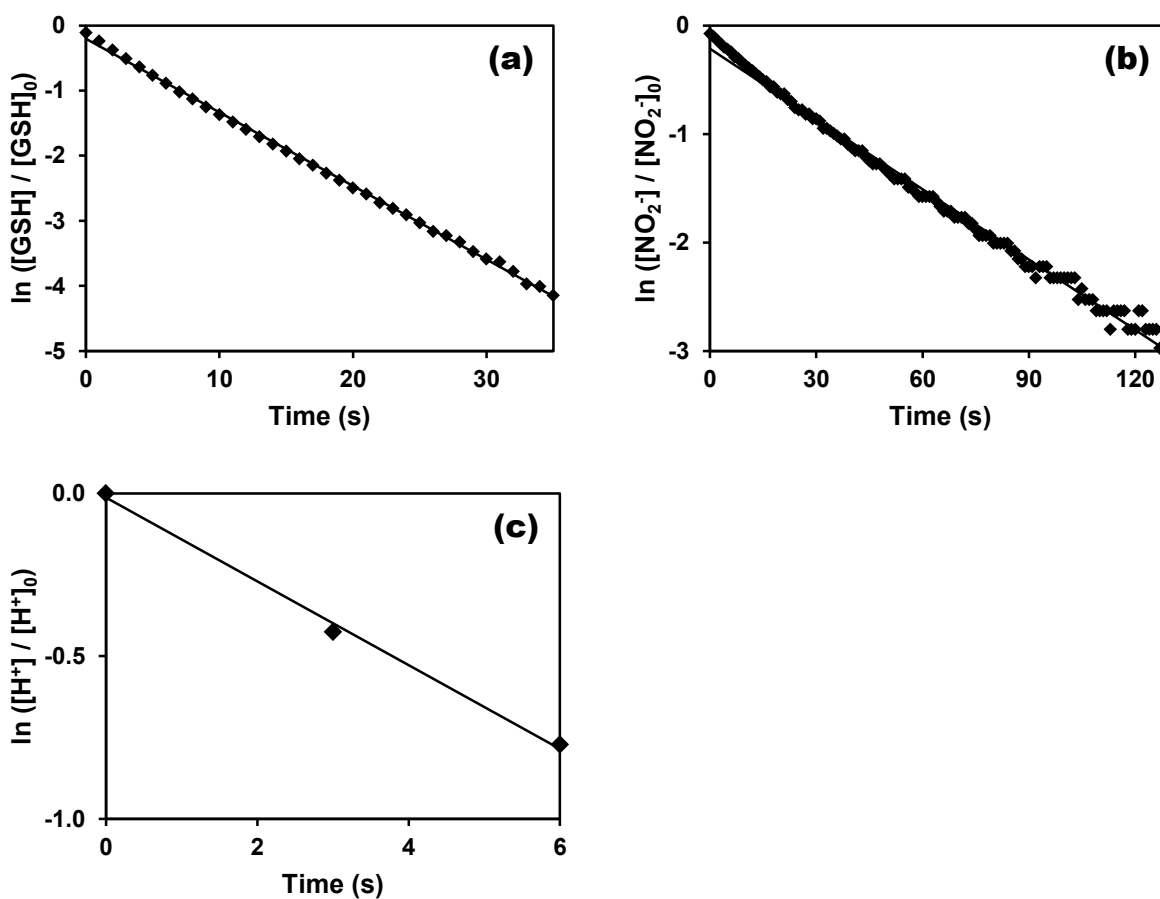


Figure 2.4 First order plots for (a) GSH rate dependence, $R^2 = 0.999$, $n = 10$, 6.1% relative error, (b) NO_2^- rate dependence, $R^2 = 0.994$, 5.2% relative error and (c) H^+ rate dependence, $R^2 = 0.996$, 5.1% relative error. For all cases, $n \geq 4$ and $T = 25.0 \pm 0.4$ °C.

Table 2.1 Summary for nitrous acid nitrosation of glutathione in 0 w/v% dextran solution.^a

[GSH] ($\times 10^{-3}$ M)	[H ⁺] ($\times 10^{-3}$ M)	[NO ₂] ($\times 10^{-3}$ M)	% nitrosation	k_{obs} (s ⁻¹)	$t_{1/2}$ (s)	Time period (s)
$6.76 \pm 0.13^{\text{b}}$	25	25	98.3 ± 0.6	0.113 ± 0.007	6.2 ± 0.4	35
6.5	6.5	$1.75 \pm 0.03^{\text{b}}$	93.7 ± 1.7	0.022 ± 0.001	32.2 ± 2.0	130
6.5	$1.44 \pm 0.15^{\text{b}}$	6.5	-	0.128 ± 0.046	6.1 ± 2.8	6

^a T = 25.0 ± 0.4 °C

^b Experimentally determined reagent concentration

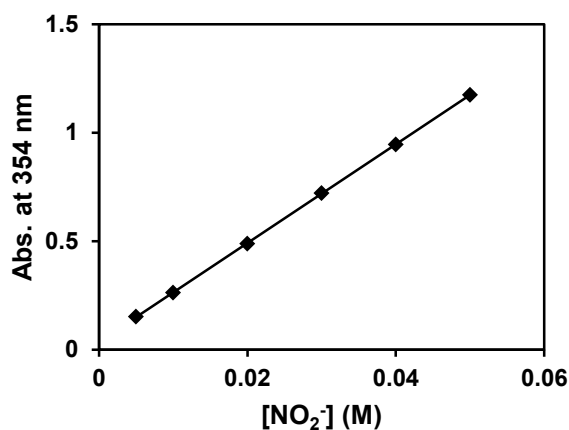


Figure 2.5 Absorbance at 354 nm as a function of nitrite concentration ($R^2 = 1$, relative error < 0.4 %, pathlength of 1 cm). The slope of this calibration curve indicates an ϵ_{max} of $22.8 \text{ M}^{-1} \text{ cm}^{-1}$.

The method of initial rates requires altering a single reagent concentration while keeping the other reagent concentrations constant among 2 runs. Therefore, a total of 9 trials were performed, while altering concentrations of nitrite, acid, or glutathione. The data is summarized in Table 2.2, where equation 2.10 was used to determine the order with respect to each reagent, where R is the initial rate (M s^{-1}) with respect to the concentration, [A], of reagent.

$$\ln\left(\frac{R_1}{R_2}\right) = \alpha \ln\left(\frac{[A]_1}{[A]_2}\right) \quad (2.10)$$

The order was determined to be 0.91 ± 0.04 , 0.94 ± 0.11 , and 1.13 ± 0.13 for glutathione, nitrite, and acid, respectively. Overall, these values round to an order of 1 for each reagent, confirming the following rate law presented in equation 2.9.

Table 2.2 Initial rate values (for the first 5 s) under different reagent concentration conditions.

Trial	[GSH] ($\times 10^{-4}$ M)	[NaNO ₂] ($\times 10^{-4}$ M)	[HCl] (M)	rate _{i, 5s} ($\times 10^{-6}$ M s ⁻¹)
1	1.25	2.50	0.1	4.24 ± 0.11
2	2.50	2.50	0.1	7.76 ± 0.25
3	3.75	2.50	0.1	11.40 ± 0.27
4	2.50	1.25	0.1	4.34 ± 0.09
5	2.50	3.75	0.1	11.90 ± 0.52
6	2.50	2.50	0.05	3.25 ± 0.05
7	2.50	2.50	0.025	1.63 ± 0.05

Glutathione S-nitrosation with HNO₂ for more efficient NO loading.

Since the main goal of this work is to compare the efficiency of *S*-nitrosation kinetics across different nitrosating agents, this section will highlight specifically the limiting thiol with excess nitrous acid. While the previous section establishes the overall rate law for nitrous acid nitrosation of a small molecule thiol, this section will highlight only the experimental conditions that are comparable to *t*-butyl nitrite, which will be presented later, to assess relative nitrosation efficiencies.

We experimentally monitored the formation of *S*-nitrosoglutathione; however, we report the kinetics in terms of the disappearance of the thiol reactant. Theoretically, the disappearance of the thiol could be attributed to either the formation of the *S*-nitrosated product or possible disulfide formation. By measuring the formation of the *S*-nitrosothiol and not the disappearance of the thiol, we consider only the reaction of the thiol to form the product of interest. We report

the kinetics in terms of the disappearance of the reactant to offer insight into how quickly a thiol within a materials system will react under each set of conditions. However, because we have monitored the formation of the *S*-nitrosated product and then calculated the thiol concentration, disulfide formation is not a concern in the data analysis. Further, the final concentration of the *S*-nitrosated product that is formed in all cases suggests that the starting amount of thiol is completely converted to product and that minimal disulfide is formed (the experimentally determined maximum product concentration matches the theoretical amount of thiol added).

As described earlier, the concentration of thiol at time t , $[\text{GSH}]_t$, was calculated from the GSNO concentration at that time, $[\text{GSNO}]_t$, according to equation 2.3, which specifically yields equation 2.11 for GSH as the limiting reagent. Experimentally, the absorbance was followed at 545 nm ($\epsilon_{\text{max}} = 15.9 \text{ M}^{-1} \text{ cm}^{-1}$).¹⁸

$$[\text{GSH}]_t = [\text{GSH}]_0 - [\text{GSNO}]_t \quad (2.11)$$

Briefly, the maximum point on the absorbance curve (Figure 2.3 (a)) corresponded to the initial concentration of thiol, $[\text{GSH}]_0$, according to equation 2.12, where the $[\text{GSNO}]_{\text{max}}$ directly correlates to the $[\text{GSH}]_0$ in a 1:1 molar ratio.

$$[\text{GSNO}]_{\text{max}} = [\text{GSH}]_0 \quad (2.12)$$

Due to the excess of nitrosating agent, HNO_2 , the rate law becomes time dependent on only the thiol concentration (equation 2.13), where k_{obs} is the experimentally determined rate constant.

$$\text{Rate} = k_{\text{obs}} [\text{GSH}]^\alpha \quad (2.13)$$

As described in equation 2.7, when the reaction is first order with respect to the thiol ($\alpha = 1$), a linear plot of $\ln([\text{GSH}]_t / [\text{GSH}]_0)$ as a function of time yields a slope relating to the rate constant ($k_{\text{obs}} = -\text{slope}$). The half-life of the reagent for a first order kinetic process, or the time required

for the thiol concentration to reach one-half its initial value, was calculated using equation 2.8. These values (k_{obs} , $t_{1/2}$) are presented as a point of comparison for the kinetics of nitrosation under different reaction conditions.

The linear relationship between $\ln([\text{GSH}]_t / [\text{GSH}]_0)$ and time shown in Figure 2.4(a) demonstrates first order behavior with respect to glutathione. For this GSH-limiting reaction, $98.3 \pm 0.6\%$ nitrosation was achieved within 35 s. Having confirmed first order kinetics with respect to glutathione, we determined the rate constant, k_{obs} , and half-life of the reagent, $t_{1/2}$, to be $0.113 \pm 0.007 \text{ s}^{-1}$ and $6.2 \pm 0.4 \text{ s}$, respectively (shown in Table 2.1).

Table 2.3 shows the pH values before initiation of the *S*-nitrosation process (1.69 ± 0.03) and 4 min after the reaction (1.73 ± 0.02). The pH values were determined to be statistically of the same population at the 95% confidence level. This indicates no significant change in the pH after the nitrosation process is complete.

Table 2.3 The pH value is given for either set of reaction conditions (nitrous acid and *t*-butyl nitrite) for a variety of dextran concentrations, before and after completion of the *S*-nitrosation process.

Nitrosating agent ^a	w/v% dextran	pH value	
		Before ^b	After ^c
HNO ₂	0	1.69 ± 0.03	1.73 ± 0.02
	2.4	1.68 ± 0.01	1.74 ± 0.01
	4.8	1.69 ± 0.01	1.74 ± 0.01
	9.6	1.68 ± 0.03	1.74 ± 0.01
<i>t</i> -BuONO	0	3.05 ± 0.03	2.71 ± 0.15
	2.5	3.05 ± 0.02	2.73 ± 0.15
	5	3.05 ± 0.02	2.86 ± 0.12
	10	3.09 ± 0.02	2.82 ± 0.18

^a Final concentrations of $6.5 \times 10^{-3} \text{ M}$ GSH and $25 \times 10^{-3} \text{ M}$ nitrosating agent

^b For HNO₂, the pH was measured prior to NaNO₂ injection; for *t*-BuONO, the pH was measured prior to *t*-BuONO injection

^c The pH was measured after 4 min of reaction time for HNO₂ and 15 min for *t*-BuONO

Glutathione S-nitrosation with t-butyl nitrite for more controlled NO loading. Previous reports have established that nitrosation of a thiol via an alkyl nitrite reagent (RONO) is first order in thiol and nitrosating agent with the rate law described in equation 2.14.²⁵

$$\text{Rate} = k [\text{RSH}] [\text{RONO}] \quad (2.14)$$

As such, we explored the limiting thiol case where a fixed [GSH] was reacted with *t*-butyl nitrite upon addition of a fixed volume of nitrosating agent. Like the nitrous acid case, the molar excess of nitrosating agent results in a rate law that is dependent upon thiol concentration only (equation 2.13).

The concentration of glutathione at a given time t , $[\text{GSH}]_t$, was determined from the GSNO concentration at that time, $[\text{GSNO}]_t$, using equation 2.11. The initial thiol concentration, $[\text{GSH}]_0$, was experimentally determined based upon the $[\text{GSNO}]_{\text{max}}$, where 100% nitrosation was assumed based upon the concentration of the limiting reagent, as previously described in the nitrous acid case (equation 2.12). A representative absorbance versus time plot for the process is shown in Figure 2.6.

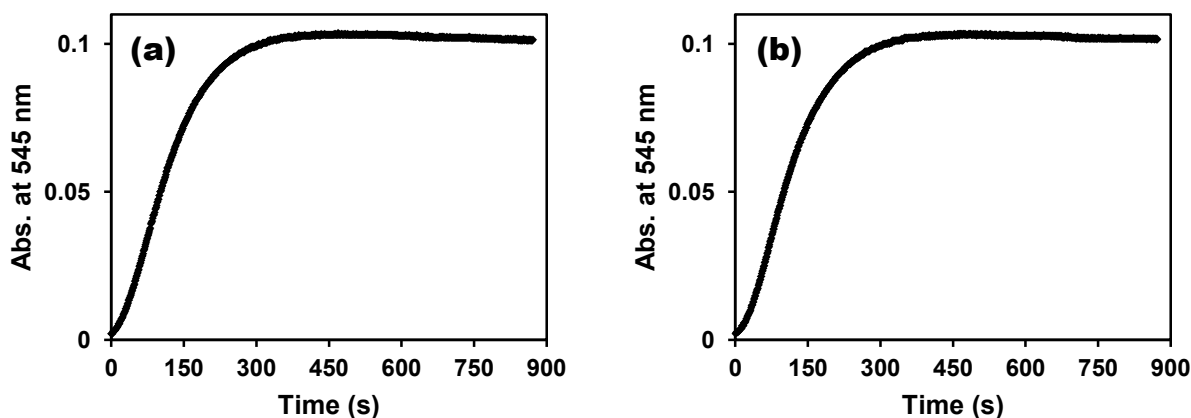


Figure 2.6 Plots of absorbance (545 nm) as a function of time for limiting thiol nitrosation via 0.025 M *t*-butyl nitrite with (a) 10 w/v% EDTA treatment of *t*-butyl nitrite ($6.54 \pm 0.00 \times 10^{-3}$ M

GSH), 1.9% relative error and **(b)** no treatment of *t*-butyl nitrite ($6.50 \pm 0.10 \times 10^{-3}$ M GSH), 3.1% relative error. In both experiments, $n \geq 3$ and $T = 25.0 \pm 0.4$ °C.

Previous synthetic strategies employed treatment of *t*-butyl nitrite with a metal chelator prior to nitrosation.¹⁴ This motivated us to investigate the role of EDTA-treated *t*-butyl nitrite to determine the presence of metal ion impurities in the *t*-butyl nitrite that would result in competitive GSNO decomposition during the synthesis. Figure 2.6 shows the absorbance (545 nm) as a function of time for the *t*-butyl nitrite nitrosation of GSH (a) with and (b) without treatment of the nitrosating agent with 10 w/v% EDTA chelator. Figure 2.7 shows $\ln([GSH]_t / [GSH]_0)$ as a function of time plots (a) with and (b) without the EDTA treatment of *t*-butyl nitrite. The linearity of both plots confirms first order kinetics in thiol for *t*-butyl nitrite nitrosation; Table 2.4 shows the corresponding kinetics data.

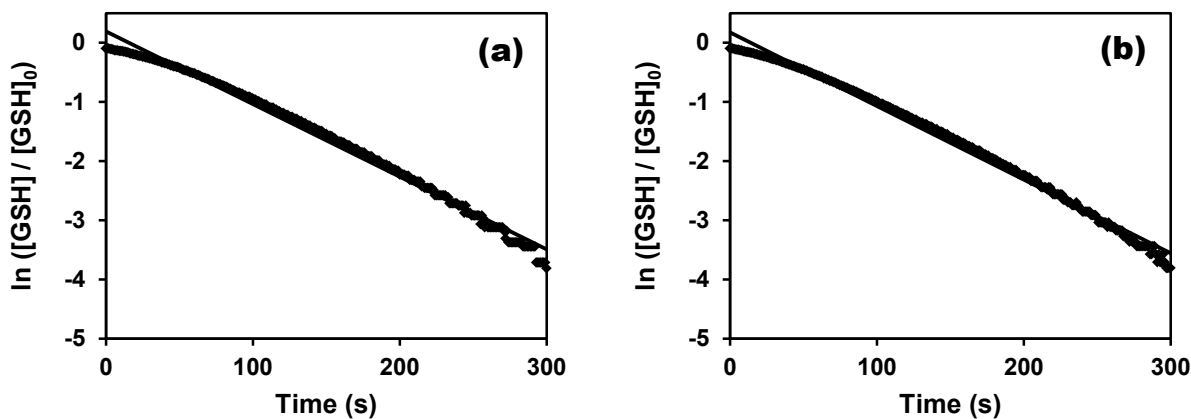


Figure 2.7 Plots of (a) GSH rate dependence with EDTA treatment of *t*-BuONO, $R^2 = 0.990$, 7.6% relative error and (b) GSH rate dependence without treatment, $R^2 = 0.992$, 7.3% relative error. In both experiments, $n \geq 3$ and $T = 25.0 \pm 0.4$ °C.

Table 2.4 Summary for *t*-butyl nitrite nitrosation of glutathione in 0 w/v% dextran solution.^a

[GSH] ($\times 10^{-3}$ M) ^b	[<i>t</i> -BuONO] (M)	10 w/v% EDTA treatment	% nitrosation ^c	k_{obs} ($\times 10^{-2}$ s ⁻¹)	$t_{1/2}$ (s)
6.54 \pm 0.00	0.025	Yes	97.8 \pm 0.6	1.23 \pm 0.10	56.6 \pm 5.0
6.50 \pm 0.10	0.025	No	97.7 \pm 0.5	1.24 \pm 0.08	55.9 \pm 3.9

^a T = 25.0 \pm 0.4 °C^b Experimentally determined reagent concentration^c Extent of nitrosation after a 300 s nitrosation time period

A half-life of 56.6 s and 55.9 s for EDTA treatment and no treatment of *t*-butyl nitrite, respectively, demonstrates no statistically significant difference between the two sets of data at a 99.9% confidence level. This indicates that the EDTA treatment had no significant effect on the nitrosation process, thus no contaminants are present in the *t*-butyl nitrite that would result in competitive GSNO decomposition. For thiol-limiting *t*-butyl nitrite nitrosation, 100% nitrosation was accomplished between 6-10 min. Overall, the chelator treatment of the *t*-butyl nitrite does not impact the kinetics of nitrosation and is thus an unnecessary step in the nitrosation process.

When looking at the shapes of the kinetic curves in Figure 2.7, it can be seen that the initial behavior is observed to deviate slightly from the first order linear behavior, indicating a slower reaction of the nitrosating agent with the thiol initially. This is attributed to the time required for the *t*-butyl nitrite to disperse in solution, either due to limited aqueous solubility of the reagent or insufficient stirring in the reaction cell. The deviation of the kinetic curve from first order behavior could also be due to the reversible decomposition of GSNO in solution, which could be pronounced over the longer time scale associated with GSH nitrosation via *t*-butyl nitrite compared to nitrous acid. However, for a simplistic comparison of nitrous acid and *t*-butyl nitrite agents, reversible formation of GSH from GSNO was neglected for these kinetic analyses. For thiol-limiting *t*-butyl nitrite nitrosation, 100% nitrosation was accomplished within about 5 min. Table 2.3 includes the pH measurements for 0% polymer case, with an initial pH of

3.05 ± 0.03 and a final pH of 2.71 ± 0.15 after 15 min of reaction. This slight drop in pH is not significant as the solution is still acidic enough for the reaction to proceed toward further *S*-nitrosation.

2.4.3 Nitrosation in the presence of dextran polymer solution. With the kinetics of nitrosation of glutathione via nitrous acid or *t*-butyl nitrite established under aqueous conditions, we investigated the effect of polymer concentration on the reaction kinetics. Toward the application of NO loading onto thiol sites pendant to a polymer, the effect of the polymer presence on the *S*-nitrosation process is crucial. The general trends of efficiency and tunability involving the nitrosating agent and the polymer for the small molecule RSNO donor formation can be applied to a polymer containing a pendant thiol.

Glutathione S-nitrosation with HNO₂ in dextran solution for more efficient NO loading. To assess the rate law in the presence of dextran, experiments were run in 2.4 w/v% dextran where each reagent was limited, as described for the HNO₂ nitrosation in 0 w/v% dextran solution. The plots of $\ln([\text{reagent}]_t / [\text{reagent}]_0)$ as a function of time (Figure 2.8 (a-c)) indicate first order kinetics with respect to each reagent. In addition to the rate law remaining the same in the presence or absence of dextran, plots in Figures 2.4 and 2.8 have the same general shape. This implies that the nitrosation process proceeds in the same fashion whether or not polymer is present.

Table 2.5 presents the kinetics data for the HNO₂ nitrosation in 2.4 w/v% dextran solution. A comparison between the thiol half-lives with 0 and 2.4 w/v% dextran experiments (6.2 and 6.8 s, respectively) indicates a statistically significant difference at the 99% confidence

level. Nitrosation in the presence of 2.4 w/v% dextran results in a slight increase in the GSH half-life. However, the cases of limiting nitrite or acid showed no statistically significant difference between the 0 and 2.4 w/v% dextran cases. This can be explained based on an encounter-controlled process where the reaction is dependent upon the nitrosating agent and the thiol site colliding. Because GSH is larger in size relative to H^+ or NO_2^- , the thiol molecule may be diffusion limited in the presence of a polymer while the movement of the proton and nitrite ions is unabated in the polymer solution. Further, the polar amine, amide, thiol, and carboxylic acid functional groups present on GSH may likely interact with the polar alcohol groups in dextran, perhaps limiting availability of the thiol site for reaction.

To assess the effect of polymer concentration on the rate and % nitrosation, polymer concentrations were increased to 4.8 and 9.6 w/v% for the thiol-limiting case only. The rate constant (k_{obs}) and half-life ($t_{1/2}$) values are shown in Table 2.6 for varying concentrations of dextran in the reaction solution. Figure 2.9 (a) shows the linear dependence of the half-life on the increasing polymer concentration. Subsequently, the % nitrosation achieved within 35 s linearly decreases with increasing polymer concentration, as shown in Figure 2.9 (b).

The significant slowing of the reaction kinetics with increasing polymer concentration suggests an encounter-controlled mechanism, as a higher polymer content serves to hinder the collision of the HNO_2 reagent with the thiol. Of further note is the fact that the pH values before and after *S*-nitrosation do not change with increasing polymer concentration. This indicates that the presence of the polymer is not affecting the mechanism of nitrosation, which is expected to be dependent upon the protonation of the HNO_2 species.²⁸ Instead, these pH data confirm that the presence of the polymer can prevent the collision of the nitrosating agent with the thiol site.

As shown in Table 2.6, the experimentally determined $[\text{GSH}]_0$ varies with increasing polymer concentration. To determine whether the source of the rate constant decrease arises from increasing polymer concentration or varying $[\text{GSH}]_0$, the rate constants were normalized by $[\text{GSH}]_0$. A linear decrease of normalized k with increasing polymer concentration was still observed (Figure 2.10), establishing that the decrease in the rate constant is due to the increase in polymer concentration and not a slight variance in the experimental $[\text{GSH}]_0$.

Table 2.5 Summary for nitrous acid nitrosation of glutathione in 2.4 w/v% dextran solution.^a

[GSH] ($\times 10^{-3}$ M)	[H ⁺] ($\times 10^{-3}$ M)	[NO ₂ ⁻] ($\times 10^{-3}$ M)	% nitrosation	k_{obs} (s ⁻¹)	$t_{1/2}$ (s)	Time period (s)
$6.59 \pm 0.09^{\text{b}}$	25	25	97.5 ± 0.5	0.102 ± 0.002	6.8 ± 0.1	35
6.5	6.5	$1.74 \pm 0.03^{\text{b}}$	94.9 ± 1.9	0.023 ± 0.003	32.2 ± 2.0	130
6.5	$1.59 \pm 0.04^{\text{b}}$	6.5	-	0.137 ± 0.012	5.1 ± 0.5	6

^a T = 25.0 ± 0.4 °C

^b Experimentally determined reagent concentration

Table 2.6 Summary for nitrous acid nitrosation of GSH in the indicated w/v% dextran solution.^a

[GSH] ($\times 10^{-3}$ M) ^b	w/v% dextran	% nitrosation ^c	k_{obs} (s ⁻¹)	$t_{1/2}$ (s)	R ² value ^d
6.76 ± 0.13	0	98.3 ± 0.6	0.113 ± 0.007	6.2 ± 0.4	0.999
6.59 ± 0.09	2.4	97.5 ± 0.5	0.102 ± 0.002	6.8 ± 0.1	0.997
6.44 ± 0.10	4.8	96.5 ± 1.3	0.094 ± 0.011	7.5 ± 0.9	0.997
6.39 ± 0.13	9.6	94.4 ± 2.1	0.078 ± 0.010	9.0 ± 1.3	0.993

^a T = 25.0 ± 0.4 °C, $[\text{NO}_2^-]_0 = [\text{H}^+]_0 = 0.025$ M

^b Experimentally determined reagent concentration

^c Extent of nitrosation after a 35 s nitrosation time period

^d R² is indicated for the $\ln([\text{GSH}]_t / [\text{GSH}]_0)$ vs. time

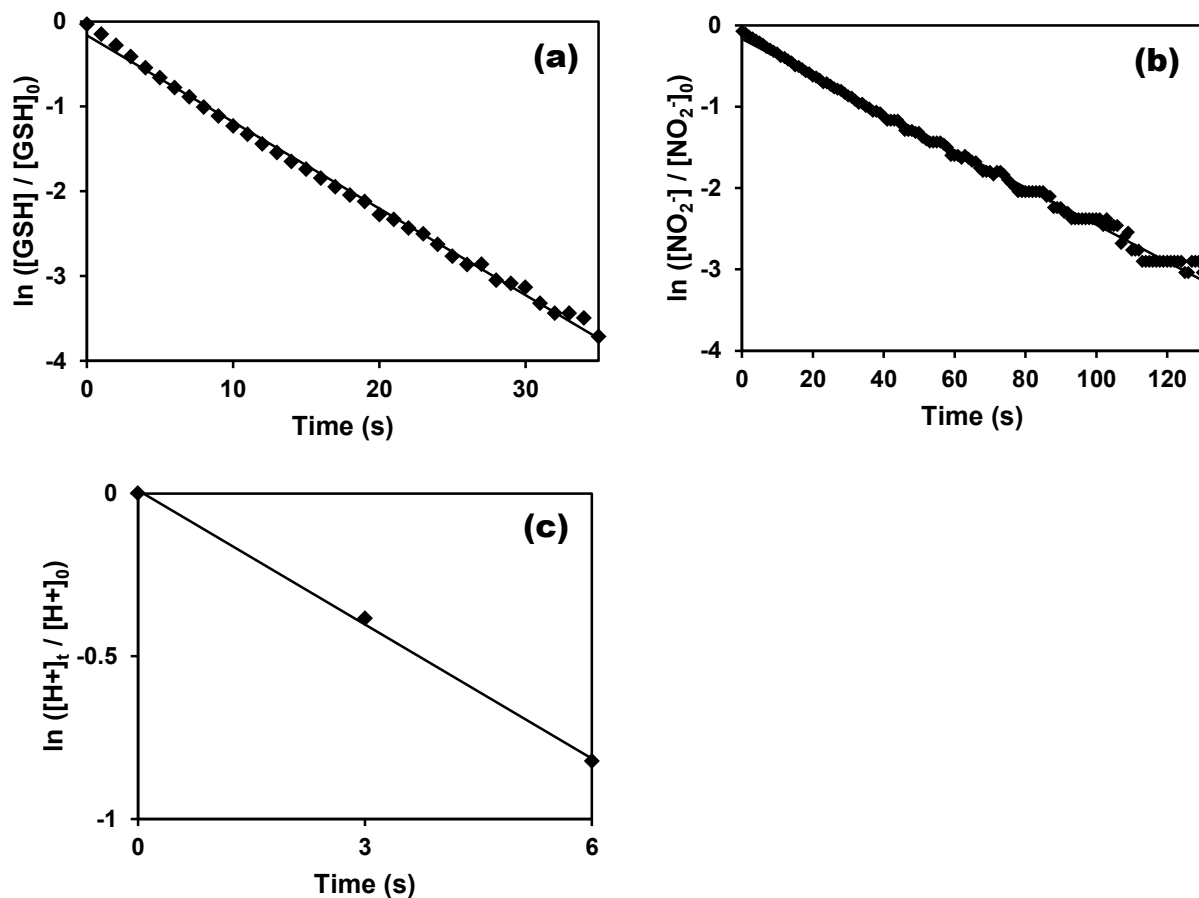


Figure 2.8 Plots for (a) GSH rate dependence, $R^2 = 0.997$, 6.3% relative error, (b) NaNO₂ rate dependence, $R^2 = 0.995$, 7.5% relative error and (c) HCl rate dependence, $R^2 = 0.998$, 9.2% relative error. All experiments conducted in 2.4 w/v% dextran solution with $n = 5$ and $T = 25.0 \pm 0.4$ °C.

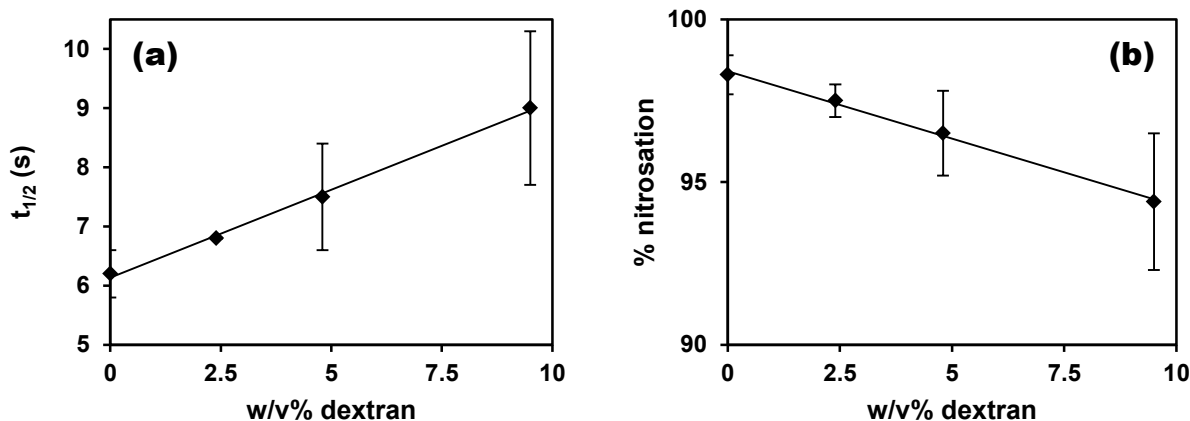


Figure 2.9 Dependence of (a) thiol half-life, $t_{1/2}$, and (b) % nitrosation on the w/v% dextran present in solution during nitrosation with HNO_2 nitrosating agent. Slopes are $0.30 \text{ s} / \% \text{ dextran}$ ($R^2 = 0.997$) and $-0.42 \% \text{ nitrosation} / \% \text{ dextran}$ ($R^2 = 0.996$), respectively.

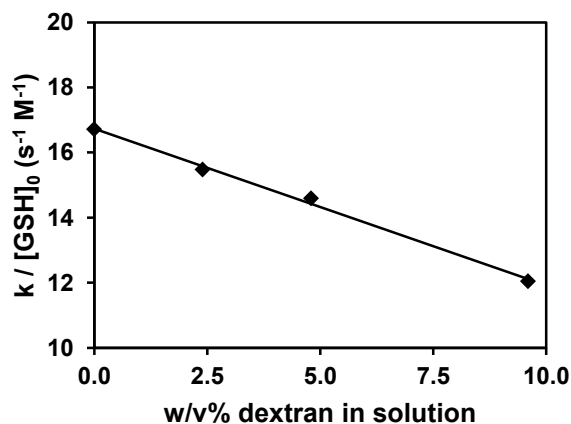


Figure 2.10 Rate constant values normalized by $[\text{GSH}]_0$ for each trial plotted against w/v% dextran in the reaction solution, $R^2 = 0.996$, slope = $-0.48 \text{ s}^{-1} \text{ M}^{-1} \text{ w/v}\%^{-1}$, 8.4% relative error.

Glutathione S-nitrosation with t-butyl nitrite in dextran solution for more controlled NO loading. Nitrosation via *t*-butyl nitrite in the presence of 2.5 w/v% dextran confirmed first order kinetics with respect to the thiol (Figure 2.11).

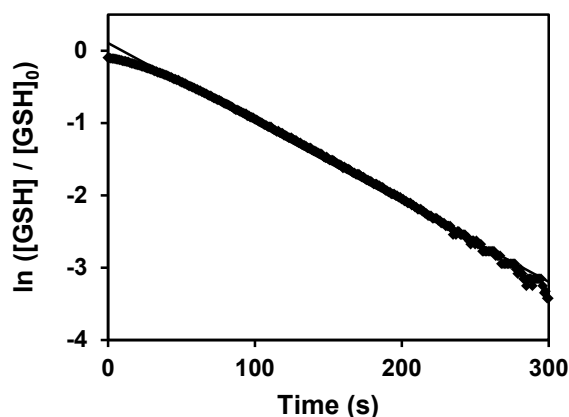


Figure 2.11 First order plot for GSH rate dependence versus time for *t*-BuONO nitrosation in 2.5 w/v% dextran, $n = 3$, $R^2 = 0.995$, 9.1% relative error, $T = 25.0 \pm 0.4$ °C.

Further, regardless of polymer concentration increasing to 5 and 10 w/v%, the $\ln([GSH]_t / [GSH]_0)$ vs. time plots yielded linear trends. The kinetics of *t*-butyl nitrite nitrosation for solutions of increasing dextran concentration are summarized in Table 2.7, while Figure 2.12 shows the dependence of the thiol half-life and % nitrosation over 300 s as a function of w/v% dextran in solution.

Table 2.7 Summary for *t*-butyl nitrite nitrosation of GSH in various w/v% dextran solutions.^a

[GSH] ($\times 10^{-3}$ M) ^b	w/v% dextran	% nitrosation ^c	k_{obs} ($\times 10^{-2}$ s ⁻¹)	$t_{1/2}$ (s)	R^2 value ^d
6.50 ± 0.10	0	97.7 ± 0.5	1.24 ± 0.08	55.9 ± 3.9	0.992
6.39 ± 0.04	2.5	96.7 ± 0.6	1.10 ± 0.05	62.9 ± 2.9	0.995
6.52 ± 0.10	5	87.1 ± 1.9	0.68 ± 0.05	102.8 ± 7.8	0.991
6.27 ± 0.10	10	69.6 ± 7.8	0.38 ± 0.10	189.6 ± 45.2	0.998

^a $T = 25.0 \pm 0.4$ °C, $[t\text{-BuONO}]_0 = 0.025$ M

^b Experimentally determined reagent concentration

^c Extent of nitrosation after a 300 s nitrosation time period

^d R^2 is indicated for the $\ln([GSH]_t / [GSH]_0)$ vs. time

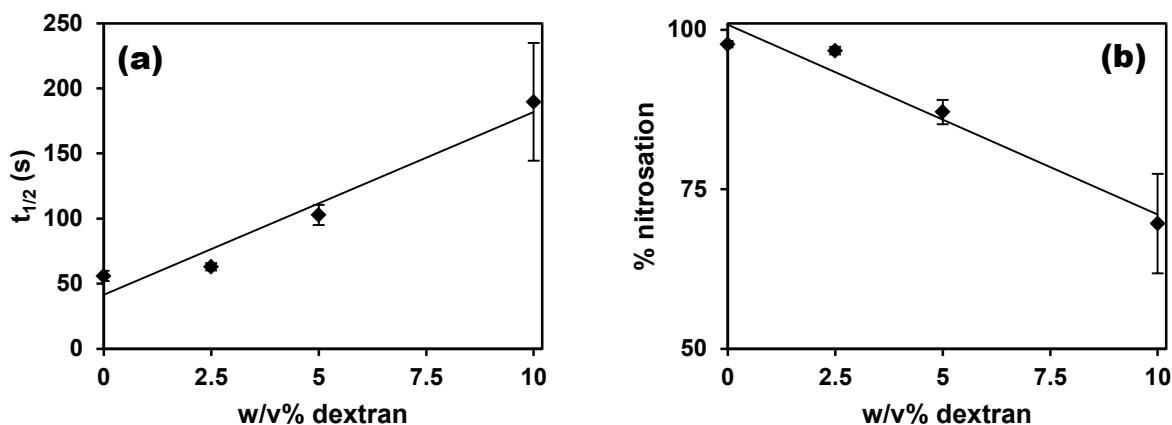


Figure 2.12 Dependence of (a) the half-life, $t_{1/2}$, and (b) % nitrosation on the w/v% dextran present in solution during nitrosation with *t*-butyl nitrite nitrosating agent. Slopes are 14.0 s / % dextran ($R^2 = 0.952$) and -3.0 % nitrosation / % dextran ($R^2 = 0.952$), respectively.

Larger $t_{1/2}$ values for GSH and a lesser extent of nitrosation in dextran solutions with higher % polymer once again provide evidence that the rate of nitrosation depends on polymer concentration. Similar to the case of 0% dextran, the *t*-butyl nitrite reagent results in slower nitrosation kinetics than the nitrous acid reagent in the presence of dextran for each polymer concentration. However, the percent nitrosation is more significantly inhibited over the indicated time frame for *t*-butyl nitrite than for nitrous acid due to increasing polymer concentration as indicated by a larger slope value for *t*-butyl nitrite's % nitrosation vs. time plot (see Figures 2.9 and 2.12). As in the case of HNO_2 , an increase in the dextran concentration did not yield significantly different (95% confidence level) pH values before and after the *S*-nitrosation process. This once again suggests that the polymer does not affect the pH of the reaction solution; however, the polymer presence serves to delay the nitrosating agent from meeting the thiol.

2.4.4 A comparison of HNO₂ and *t*-butyl nitrite reagents.

Efficiency of nitrosation. We investigated the effect of polymer presence on the efficiency of *S*-nitrosation of GSH as a function of the nitrosating agent: nitrous acid and *t*-butyl nitrite. We found that, for the case of limiting thiol with the same molar excess of nitrosating agent, the process was slower for *t*-butyl nitrite. Excess nitrous acid will result in the most efficient nitrosation, as evidenced by nearly 100% nitrosation within 35 s, compared to 300 s for *t*-butyl nitrite. Additionally, the half-life of GSH for the HNO₂ reagent (6.2 ± 0.4 s) is an order of magnitude smaller than the half-life of GSH using *t*-butyl nitrite (55.9 ± 3.9 s). The differences in the efficiency of reaction in either case could be due to effects that limit the diffusion of the nitrosating reagent to the thiol site or pH effects.

It has been previously established that nitrosation occurs through an encounter-controlled process.^{20, 23} When considering the two nitrosating agents in the same molar excess of thiol, the *t*-butyl nitrite agent is bulkier than the nitrous acid. Therefore, it might be expected that the nitrous acid will interact more readily with the thiol site where reaction toward RSNO formation can proceed. When considering the structures of *t*-butyl nitrite and nitrous acid, the differences in reactivity could be due to electronic or steric effects. Previous reports suggest that, for either nitrosating agent, the nitrosation process is dependent upon the protonation of the O bearing the *t*-butyl or proton side group.²⁸ Considering that the inductive effect of the *t*-butyl nitrite would result in a more negatively charged O bound to the *t*-butyl group than the O bound to the proton in nitrous acid, the rate of nitrosation would be expected to occur more quickly for *t*-butyl nitrite due to a more efficient protonation of the O bound to the *t*-butyl group under acidic conditions. However, our data indicate a quicker nitrosation with nitrous acid, suggesting that the *t*-butyl group hinders the protonation of the O bound to it. As a result, the formation of the NO⁺

nitrosating species is limited. Other steric hindrance contributions can be considered that support an encounter-controlled nitrosation process due to a lesser availability of the *t*-butyl nitrite compared to the nitrous acid. In addition to the bulkier *t*-butyl side group preventing interaction of the thiol site and the –ONO moiety of the nitrosating agent for NO⁺ transfer to occur, the results could reflect a slowed diffusion of the *t*-butyl nitrite reagent to the thiol site, *t*-butyl nitrite's limited solubility in water due to the hydrocarbon side group, or *t*-butyl nitrite's relatively high volatility (b.p. 61-63 °C).²⁹ If the nitrosating agent is evaporating from the cell during analysis, the nitrosation rate will slow. To minimize this evaporation, the cuvette was capped during analysis; however, the cuvette was only half full of solution (2 mL solution in a 4 mL volume cuvette), leaving headspace in the cuvette to house *t*-butyl nitrite gas. However, 100% nitrosation accomplished with respect to limiting thiol occurs for the *t*-butyl nitrite runs, indicating that, despite possible volatility issues, the *t*-butyl nitrite is still present in enough excess within the solution to drive the reaction to completion. Any of these factors could slow the encounter-controlled process, thus nitrosation will occur at a slower rate for *t*-butyl nitrite.

The shapes of the kinetic curves for the nitrous acid and *t*-butyl nitrite cases also indicate that the HNO₂ species reaches the thiol site more quickly than *t*-butyl nitrite. The HNO₂ curve shows an initial steep decrease in ln[GSH]_t, followed by a linear decrease, until the function reaches 100% nitrosation (see Figures 2.4 and 2.8). The *t*-butyl nitrite kinetic curve shows an initial slight decrease in thiol concentration but is less steep than the linear portion (see Figures 2.7 and 2.11). Slower diffusion of *t*-butyl nitrite due to its larger size and limited solubility when compared to HNO₂ can account for these differences. The steep initial decrease for HNO₂ indicates a fast encounter between the nitrosating agent and the thiol, resulting in nitrosation. The remainder of the nitrosation period is marked by a slightly slower reaction process (less steep

plot) due to fewer thiol sites available for reaction. Overall, the half-life and % nitrosation data, as well as the shapes of the kinetic curves, indicate that, for an encounter-controlled nitrosation process, the HNO_2 species is able to react more efficiently with the thiol site than the *t*-butyl nitrite.

In addition to steric and diffusion effects that could slow the nitrosation process involving *t*-butyl nitrite, the kinetics results can also be explained due to the differences in pH of each system. Despite the same concentrations of thiol and nitrosating reagent, the HNO_2 system consistently exhibited a pH of 1.7, whereas the *t*-BuONO system exhibited a pH of ~ 3 (see Table 2.3). If the process is dependent upon protonation of the nitrosating agent, the system with the lower pH will result in a more efficient NO^+ production at the thiol site, resulting in more efficient nitrosation for the HNO_2 system.

Despite the nitrosating agent employed, the reactions likely proceed through the same mechanism, which includes reaction of the NO^+ species with the thiol site. The pH values of the final solutions after nitrosation were confirmed to be about 2-3 for both nitrous acid and *t*-butyl nitrite in all limiting reagent cases. At such low pH values, the thiol is likely to be protonated (-SH) and reaction of the NO^+ species will displace the proton from the thiol site. This is of interest as some reports indicate that, at higher pH values, nitrosation via *t*-butyl nitrite involves the thiolate ion (RS^-) as the reactive thiol species.²⁴ However, the thiol will not exist in the deprotonated form at the low pH values indicated in our systems. Therefore, the slower reaction of *t*-butyl nitrite with the thiol site cannot be attributed to the additional step involving deprotonation of the thiol moiety prior to NO^+ transfer. Instead, the less efficient nitrosation by *t*-butyl nitrite is attributed to the factors that will inhibit encounter of the reagent with the thiol site.

In the presence of 9.6 w/v% dextran, the nitrous acid nitrosation reached $94.4 \pm 2.1\%$ nitrosation within 35 s, only a 4% decrease compared to the 0 w/v% dextran case. This indicates that, despite relatively high polymer concentrations, nitrous acid will essentially drive the system toward 100% nitrosation very quickly, within less than a minute. Therefore, these results demonstrate the effectiveness of HNO_2 to maximize nitrosation of thiol groups pendant to a polymer. A greater effect on the half-life and % nitrosation due to increasing polymer concentration was exhibited by the *t*-butyl nitrite, making it less efficient over a fixed time frame in the presence of a polymer. For materials applications that require higher amounts of NO delivery, the most efficient *S*-nitrosation would be desired to maximize the NO reservoir. In such a case, nitrous acid offers the most efficient NO loading despite the presence of a polymer.

Control over nitrosation. A decrease of nearly 30% nitrosation was achieved for the *t*-butyl nitrite reagent when increasing the polymer concentration from 0 to 10 w/v% for a 5 min analysis period, indicating a more significant effect on the kinetics than seen with HNO_2 . This larger impact of the polymer concentration on the reaction rate indicates that the use of *t*-butyl nitrite as the nitrosating agent can exert finer control over NO loading. For instance, if a polymer has a fixed number of thiol sites and only a fraction of those sites need to be nitrosated to result in the desired amount of NO incorporated into the material, the use of nitrous acid will essentially drive all thiol sites toward nitrosation. However, *t*-butyl nitrite would be a more viable reagent as, for a fixed polymer concentration, the extent of reaction can essentially be controlled to reach the desired % nitrosation based upon the required NO reservoir for the material application, especially for applications in which excess NO could cause local toxicity.

Due to *t*-butyl nitrite's low boiling point, once the reaction has spanned the desired time period, vacuum applied to the system can remove the reagent, effectively halting the nitrosation process.

In addition to control over the extent of nitrosation, another benefit of *t*-butyl nitrite involving removal of the nitrosating agent due to the reagent's low boiling point is that residual nitrite in the product due to the nitrosating agent is minimized. This is important as residual nitrite in the material could contribute to the measurement of NO under RSNO reduction conditions due to nitrite reduction in the presence of copper. For example, NO is released from RSNOs upon exposure to copper metal ion and appropriate reducing agents.^{17,30} Residual nitrite in the system is also reduced to NO under similar conditions and will thus contribute to the total NO measured using a direct NO measurement technique. To demonstrate that residual nitrite contributes to directly detected NO under Cu²⁺/GSH reducing conditions, an aqueous solution of sodium nitrite (NaNO₂) was added to a reaction cell, connected to a Sievers 280i Nitric Oxide Analyzer (NOA). Upon injection of a solution of Cu²⁺ and GSH, NO was detected. In the reaction cell, 2 μmol of NO₂⁻ were present, in a limiting concentration to 3 μmol of Cu²⁺ and GSH. In just over 1.5 h, 84% of the theoretical amount of NO₂⁻ was recovered as NO, where 1 mol of NO₂⁻ is converted to 1 mol NO. These findings serve to confirm that residual nitrite present in the system can be directly detected as NO under Cu²⁺/GSH reducing conditions. As RSNO species are decomposed under the same conditions, NO detected from a sample of RSNO containing residual nitrite would include NO detected from the decomposition of the RSNO as well as the reduction of nitrite to NO. As such, a falsely high amount of NO based on the amount of RSNO would be detected due to the nitrite contribution under reducing conditions.

A commonly employed analytical method for the indirect measurement of NO is the Griess assay, a colorimetric assay for nitrite determination. Since NO is readily oxidized to NO₂⁻

in oxygenated aqueous conditions,³¹ many researchers measure the amount of nitrite in the material soaking solution and report the amount of nitrite as the apparent NO release from a system. Using the Griess assay, residual nitrite from the synthesis of RSNO materials will give falsely high apparent NO release measurements for the materials, which could have significant clinical outcomes. Complete nitrite removal is more difficult when using nitrous acid to create RSNOs, as multiple washes would be required to remove the nitrite ion from the product. Therefore, the removal of *t*-butyl nitrite from the nitrosated product is critical depending upon the NO characterization technique that is employed for the *S*-nitrosated system.

Alkyl nitrites have been demonstrated as useful agents under a variety of solvent conditions such as aqueous pH 6-13,²⁴ alcohol solvent,³² and organic solvent,³³ in addition to acidic aqueous conditions,³⁴ making this class of agents more versatile than nitrous acid. The synthesis of NO releasing materials under aqueous conditions would limit the nitrosation of hydrophobic polymers in organic solvent solution. Further, polymers that degrade via hydrolysis cannot be nitrosated under aqueous HNO₂ conditions without compromising the integrity of the polymer, therefore *t*-butyl nitrite nitrosation under organic solvent conditions have been recently employed.⁹ The ability of *t*-butyl nitrite to nitrosate under a variety of solvent conditions is a significant benefit to the synthesis of materials under versatile conditions.

Despite *t*-butyl nitrite's benefits, slightly poorer linearity is exhibited for the % nitrosation as a function of polymer concentration for the *t*-butyl nitrite system, indicating that the % nitrosation may be less predictable than for HNO₂. This could reflect the slight insolubility of *t*-butyl nitrite in water as well as its low boiling point. If the concentration of *t*-butyl nitrite in reaction solution varies more significantly than that of nitrous acid due to these physical properties, a less predictable extent of nitrosation when using *t*-butyl nitrite may result.

Clearly, both reagents offer advantages. Nitrous acid allows fast and complete nitrosation while slower nitrosation with *t*-butyl nitrite leads to better control of the extent of nitrosation and permits removal of excess reagent after the reaction. Figure 2.13 summarizes the efficiency and fine-tuned control associated with *S*-nitrosation for either reagent under 0 and 10 w/v% polymer conditions. The use of HNO₂ results in nearly 100% nitrosation much more quickly than with *t*-butyl nitrite for the 0% polymer cases. For the 0% and 10% dextran comparison, the % nitrosation over time profiles do not change nearly as significantly for the HNO₂ case as compared to the *t*-butyl nitrite case. These trends involving the use of nitrosating agent and polymer concentration to control the NO loading process can be expanded to systems involving thiol groups covalently attached to polymers. This improves the ability to exert control over the NO loading of polymer materials for particular biomedical device applications.

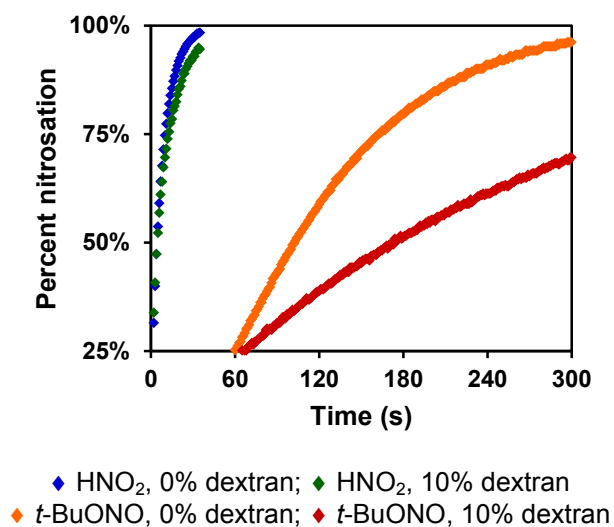


Figure 2.13 The rate of nitrosation is dependent on the nitrosating agent employed as well as the concentration of polymer in solution.

2.5 CONCLUSIONS

We have demonstrated that, in the presence of a polymer solution, the most efficient reaction conditions for glutathione *S*-nitrosation involve the use of nitrous acid with near-complete nitrosation achieved within 35 s. This process is less significantly affected by polymer concentration than for the *t*-butyl nitrite reagent. However, to exert tunable control over the amount of NO loaded in the presence of a polymer, the *t*-butyl nitrite reagent is most viable as the use of this reagent has a larger impact on the nitrosation kinetics with nearly a 30% decrease in the extent of nitrosation with 10 w/v% dextran present. Regardless of the nitrosating agent, first order kinetics were established with respect to thiol. The experiments described herein involve the nitrosation of a small molecule thiol in a polymer solution, yet similar trends can be expected for the use of these nitrosating agents for the nitrosation of thiol sites pendant to polymer backbones. Taken together, reaction conditions can now be exploited for optimal performance of NO loading onto or in the presence of polymer materials for a range of clinical applications, such as the development of materials for wound-healing, anti-thrombogenic or anti-microbial properties, where different doses of NO are required.

CHAPTER 2 REFERENCES

1. Ignarro, L. J.; Buga, G. M.; Wood, K. S.; Byrns, R. E.; Chaudhuri, G., Endothelium-Derived Relaxing Factor Produced and Released From Artery and Vein is Nitric Oxide. *Proc. Natl. Acad. Sci. USA* **1987**, *84*, 9265-9269; Marletta, M. A., Nitric Oxide: Biosynthesis and Biological Significance. *Trends Biochem. Sci.* **1989**, *14*, 488-492; Moncada, S.; Palmer, R. M. J.; Higgs, E. A., Nitric Oxide: Physiology, Pathophysiology, and Pharmacology. *Pharmacol. Rev.* **1991**, *43*, 109-142; Stamler, J. S.; Singel, D. J.; Loscalzo, J., Biochemistry of Nitric Oxide and Its Redox-Activated Forms. *Science* **1992**, *258*, 1898-1902; Wink, D. A.; Grisham, M. B.; Mitchell, J. B.; Ford, P. C., Direct and Indirect Effects of Nitric Oxide in Chemical Reactions Relevant to Biology. *Methods Enzymol.* **1996**, *268*, 12-31; Wink, D. A.; Mitchell, J. B., Chemical Biology of Nitric Oxide: Insights into Regulatory, Cytotoxic, and Cytoprotective Mechanisms of Nitric Oxide. *Free Radical Biol. Med.* **1998**, *25*, 434-456; Ford, P. C., Reactions of NO and Nitrite with Heme Models and Proteins. *Inorg. Chem.* **2010**, *49*, 6226-6239.
2. Ignarro, L. J.; Lippton, H.; Edwards, J. C.; Baricos, W. H.; Hyman, A. L.; Kadowitz, P. J.; Gruetter, C. A., Mechanism of Vascular Smooth Muscle Relaxation by Organic Nitrates, Nitrite, Nitroprusside and Nitric Oxide: Evidence for the Involvement of S-nitrosothiols as Active Intermediates. *J. Pharmacol. Exp. Ther.* **1981**, *218*, 739-749; Stamler, J. S.; Jaraki, O.; Osborne, J.; Simon, D. I.; Keaney, J.; Vita, J.; Singel, D.; Valeri, C. R.; Loscalzo, J., Nitric Oxide Circulates in Mammalian Plasma Primarily as an S-nitroso Adduct of Serum Albumin. *Proc. Natl. Acad. Sci. USA* **1992**, *89*, 7674-7677; Stamler, J. S.; Simon, D. I.; Osborne, J. A.; Mullins, M. E.; Jaraki, O.; Michel, T.; Singel, D. J.; Loscalzo, J., S-

- nitrosylation of Proteins with Nitric Oxide: Synthesis and Characterization of Biologically Active Compounds. *Proc. Natl. Acad. Sci. USA* **1992**, *89*, 444-448; Mathews, W. R.; Kerr, S. W., Biological Activity of S-nitrosothiols: The Role of Nitric Oxide. *J. Pharmacol. Exp. Ther.* **1993**, *267*, 1529-1537; Simon, D. I.; Stamler, J. S.; Jaraki, O.; Keaney, J. F.; Osborne, J. A.; Francis, S. A.; Singel, D. J.; Loscalzo, J., Antiplatelet Properties of Protein S-nitrosothiols Derived from Nitric Oxide and Endothelium-Derived Relaxing Factor. *Arterioscler., Thromb., Vasc. Biol.* **1993**, *13*, 791-799.
3. Frost, M. C.; Reynolds, M. M.; Meyerhoff, M. E., Polymers Incorporating Nitric Oxide Releasing/Generating Substances for Improved Biocompatibility of Blood-Contacting Medical Devices. *Biomaterials* **2005**, *26*, 1685-1693; Varu, V. N.; Tsihlis, N. D.; Kibbe, M. R., Nitric Oxide-Releasing Prosthetic Materials. *Vasc. Endovascular Surg.* **2009**, *43*, 121-131.
 4. Bartberger, M. D.; Mannion, J. D.; Powell, S. C.; Stamler, J. S.; Houk, K. N.; Toone, E. J., S-N Dissociation Energies of S-nitrosothiols: On the Origins of Nitrosothiol Decomposition Rates. *J. Am. Chem. Soc.* **2001**, *123* (36), 8868-8869; Stamler, J. S.; Toone, E. J., The Decomposition of Thionitrites. *Curr. Opin. Chem. Biol.* **2002**, *6*, 779-785; Williams, D. L. H., The Chemistry of S-nitrosothiols. *Acc. Chem. Res.* **1999**, *32*, 869-876.
 5. Bohl, K. S.; West, J. L., Nitric Oxide-Generating Polymers Reduce Platelet Adhesion and Smooth Muscle Cell Proliferation. *Biomaterials* **2000**, *21*, 2273-2278; Lipke, E. A.; West, J. L., Localized Delivery of Nitric Oxide from Hydrogels Inhibits Neointima Formation in a Rat Carotid Balloon Injury Model. *Acta Biomater.* **2005**, *1*, 597-606.

6. Seabra, A. B.; da Silva, R.; de Oliveira, M. G., Polynitrosated Polyesters: Preparation, Characterization, and Potential Use for Topical Nitric Oxide Release. *Biomacromolecules* **2005**, *6*, 2512-2520.
7. Seabra, A. B.; Martins, D.; Simoes, M. M. S. G.; da Silva, R.; Brocchi, M.; de Oliveira, M. G., Antibacterial Nitric Oxide-Releasing Polyester for the Coating of Blood-Contacting Artificial Materials. *Artif. Organs* **2010**, *34*, E204-E214.
8. Li, Y.; Lee, P. I., Controlled Nitric Oxide Delivery Platform Based on S-nitrosothiol Conjugated Interpolymer Complexes for Diabetic Wound Healing. *Mol. Pharmaceutics* **2010**, *7*, 254-266; Coneski, P. N.; Schoenfisch, M. H., Synthesis of Nitric Oxide-Releasing Polyurethanes with S-nitrosothiol-Containing Hard and Soft Segments. *Polym. Chem.* **2011**, *2*, 906-913.
9. Damodaran, V. B.; Reynolds, M. M., Biodegradable S-nitrosothiol Tethered Multiblock Polymer for Nitric Oxide Delivery. *J. Mater. Chem.* **2011**, *21*, 5870-5872.
10. Bohl Masters, K. S.; Lipke, E. A.; Rice, E. E. H.; Liel, M. S.; Myler, H. A.; Zygourakis, C.; Tulis, D. A.; West, J. L., Nitric Oxide-Generating Hydrogels Inhibit Neointima Formation. *J. Biomater. Sci., Polym. Ed.* **2005**, *16*, 659-672.
11. Riccio, D. A.; Dobmeier, K. P.; Hetrick, E. M.; Privett, B. J.; Paul, H. S.; Schoenfisch, M. H., Nitric Oxide-Releasing S-nitrosothiol-Modified Xerogels. *Biomaterials* **2009**, *30*, 4494-4502.
12. Stasko, N. A.; Fischer, T. H.; Schoenfisch, M. H., S-nitrosothiol-Modified Dendrimers as Nitric Oxide Delivery Vehicles. *Biomacromolecules* **2008**, *9*, 834-841.

13. Frost, M. C.; Meyerhoff, M. E., Controlled Photoinitiated Release of Nitric Oxide from Polymer Films Containing S-Nitroso-N-acetyl-DL-penicillamine Derivatized Fumed Silica Filler. *J. Am. Chem. Soc.* **2004**, *126*, 1348-1349.
14. Frost, M. C.; Meyerhoff, M. E., Synthesis, Characterization, and Controlled Nitric Oxide Release from S-nitrosothiol-Derivatized Fumed Silica Polymer Filler Particles. *J. Biomed. Mater. Res., Part A* **2005**, *72A*, 409-419.
15. Coneski, P. N.; Nash, J. A.; Schoenfisch, M. H., Nitric Oxide-Releasing Electrospun Polymer Microfibers. *ACS Appl. Mater. Interfaces* **2011**, *3*, 426-432.
16. Broaders, K. E.; Cohen, J. A.; Beaudette, T. T.; Bachelder, E. M.; Frechet, J. M. J., Acetalated Dextran is a Chemically and Biologically Tunable Material for Particulate Immunotherapy. *Proc. Natl. Acad. Sci. USA* **2009**, *106*, 5497-5502.
17. Askew, S. C.; Barnett, D. J.; McAninly, J.; Williams, D. L. H., Catalysis by Cu²⁺ of Nitric Oxide Release from S-nitrosothiols (RSNO). *J. Chem. Soc., Perkin Trans. 2* **1995**, 741-745.
18. Hart, T. W., Some Observations Concerning the S-nitroso and S-phenylsulphonyl Derivatives of L-cysteine and Glutathione. *Tetrahedron Lett.* **1985**, *26*, 2013-2016.
19. Morakinyo, M. K.; Strongin, R. M.; Simoyi, R. H., Modulation of Homocysteine Toxicity by S-nitrosothiol Formation: A Mechanistic Approach. *J. Phys. Chem. B* **2010**, *114*, 9894-9904.
20. Collings, P.; Al-Mallah, K.; Stedman, G., Kinetics and Equilibria of the S-nitrosation of Alkylthioureas. *J. Chem. Soc., Perkin Trans. 2* **1975**, 1734-1736.

21. Byler, D. M.; Gosser, D. K.; Susi, H., Spectroscopic Estimation of the Extent of S-nitrosothiol Formation by Nitrite Action on Sulfhydryl Groups. *J. Agric. Food. Chem.* **1983**, *31*, 523-527.
22. Dix, L. R.; Williams, D. L. H., Kinetics and Mechanism of Thionitrite Formation. Mercapto-carboxylic Acids: A New Range of Efficient Nitrous Acid Scavengers. *J. Chem. Soc., Perkin Trans. 2* **1984**, 109-112.
23. Morris, P. A.; Williams, D. L. H., Kinetics and Mechanism of S-nitrosation of Some Thiol-containing Amino Acids and Other Thiols. *J. Chem. Soc., Perkin Trans. 2* **1988**, 513-516.
24. Patel, H. M. S.; Williams, D. L. H., Nitrosation by Alkyl Nitrites. Part 3. Reactions with Cysteine in Water in the pH Range 6-13. *J. Chem. Soc., Perkin Trans. 2* **1989**, 339-341.
25. Patel, H. M. S.; Williams, D. L. H., Nitrosation by Alkyl Nitrites. Part 6. Thiolate Nitrosation. *J. Chem. Soc., Perkin Trans. 2* **1990**, 37-42.
26. Harris, D. C., *Quantitative Chemical Analysis*. 7 ed.; W. H. Freeman and Company: 2007.
27. Williams, D. L. H., Nitrosation Mechanisms. *Adv. Phys. Org. Chem.* **1983**, *19*, 381-428.
28. Williams, D. L. H., *Nitrosation Reactions and the Chemistry of Nitric Oxide*. Elsevier: 2004.
29. Sigma-Aldrich, tert-Butyl nitrite Material Safety Data Sheet.
30. Dicks, A. P.; Swift, H. R.; Williams, D. L. H.; Butler, A. R.; Al-Sa'doni, H. H.; Cox, B. G., Identification of Cu⁺ as the Effective Reagent in Nitric Oxide Formation from S-nitrosothiols (RSNO). *J. Chem. Soc., Perkin Trans. 2* **1996**, 481-487.
31. Pogrebnaya, V. L.; Usov, A. P.; Baranov, A. V.; Nesterenko, A. I.; Bez'yazychnyi, P. I., Oxidation of Nitric Oxide by Oxygen in the Liquid Phase. *J. Appl. Chem. USSR* **1975**, *48*, 1004-1007; Wink, D. A.; Darbyshire, J. F.; Nims, R. W.; Saavedra, J. E.; Ford, P. C.,

Reactions of the Bioregulatory Agent Nitric Oxide in Oxygenated Aqueous Media: Determination of the Kinetics for Oxidation and Nitrosation by Intermediates Generated in the NO/O₂ Reaction. *Chem. Res. Toxicol.* **1993**, *6*, 23-27.

32. Crookes, M. J.; Williams, D. L. H., Nitrosation by Alkyl Nitrites. Part 4. S-nitrosation in Acidic Alcohol Solvent. *J. Chem. Soc., Perkin Trans. 2* **1989**, 759-763.
33. Crookes, M. J.; Williams, D. L. H., Nitrosation by Alkyl Nitrites. Part 5. Kinetics and Mechanism of Reactions in Acetonitrile. *J. Chem. Soc., Perkin Trans. 2* **1989**, 1319-1322.
34. Crookes, M. J.; Williams, D. L. H., Nitrosation by Alkyl Nitrites. Part 2. Kinetics of Reactions in Aqueous Acid Solution with Isopropyl and t-Butyl Nitrites. *J. Chem. Soc., Perkin Trans. 2* **1988**, 1339-1343.

CHAPTER 3:
CHARACTERIZATION OF MAJOR NITROSATION PRODUCTS FOR THIOLATED
POLYMERS AND ACHIEVING SELECTIVE *S*-NITROSATION

3.1 PREFACE

In Chapter 1 of this dissertation, the importance of characterizing potential nitrosation byproducts for NO loaded materials was highlighted. Since nitrosation chemistry is quite diverse, there is the potential to form a variety of nitroso products onto multiple functional groups within diverse, macromolecular polymer scaffolds. Generally speaking, it is assumed in the literature that polymers subjected to nitrosation are expected to yield exclusively *S*-nitrosothiol moieties, where the possible formation of other nitroso derivatives is not considered. As such, these studies serve to investigate the potential for different nitroso species to form on dextran derivatives. Two different synthetic routes are described which yield different functional groups in addition to the thiol site of interest, which has a large affect on the nitroso products that form. This work, published in *RSC Advances* (© The Royal Society of Chemistry 2013), serves as the first account of the consideration of a polymer system to undergo nitrosation to yield competitive products. Ultimately, by tuning the functional groups in the polymer, we can achieve selective *S*-nitrosation, which is the ultimate goal for creating NO releasing *S*-nitrosated polymers. Specifically for this work, I would like to thank Dr. Vinod Damodaran for his contribution to the studies presented, where he synthesized all dextran derivatives required for the subsequent analysis described herein. We would like to acknowledge the financial support for this research from Colorado State University and the Department of Defense Congressionally Directed Medical Research Program (DOD-CDMRP). This research was supported by funds from the

Boettcher Foundation's Webb-Waring Biomedical Research Program. V.B.D was supported from the DOD-CDMRP and J.M.J. was supported by the Boettcher Foundation's Webb-Waring Biomedical Research Program.

Adapted from Joslin, J. M.; Damodaran, V. B.; Reynolds, M. M., Selective Nitrosation of Modified Dextran Polymers. *RSC Advances* **2013**, 3, 15035-15043 with permission from The Royal Society of Chemistry. Copyright 2013 The Royal Society of Chemistry.

3.2 INTRODUCTION

The ability to load nitric oxide (NO) onto polymer backbones in the form of an NO moiety is fundamental to the development of NO releasing polymers, which demonstrate promising results as biomaterials.¹ Since NO is a highly reactive radical, NO functional groups enable stable storage until the therapeutic NO action is required from the material. The key feature associated with NO releasing polymers is to exert fine control over the type, distribution and concentration of NO donor in the system for highly tunable materials. One popular NO functional group is the *S*-nitrosothiol (RSNO) moiety, which is formed by nitrosation of a thiol site. *S*-nitrosothiols can be triggered to liberate NO through a variety of pathways, including heat-, light-, and metal ion-mediated,² making this class of NO donor versatile depending upon the material application. The incorporation of RSNOs directly onto polymer supports via nitrosation of thiol sites has been previously noted.^{3, 4} The primary method of investigation for these materials has been based upon the quantification of NO generated by the nitrosated material. However, due to the complexity of the macromolecular polymers, there is the potential for the formation of alternate NO donor groups, other than the intended RSNOs. Characterization of the NO moieties formed during the nitrosation process is critical to elucidate the contribution

of various functional groups on the resultant NO groups that form on the material and determining which groups subsequently give rise to NO release.

Complete characterization of the NO loaded material must be two-fold: first, the NO moiety should be characterized to determine the nature and efficiency of the nitrosation process and, secondarily, the NO release from the material should be measured in correspondence with the decomposition of the NO moiety. Depending upon the complexity of the polymer functionality and due to the versatility of nitrosation chemistry,⁵ a variety of NO moieties can form during the nitrosation process (addition of NO^+). In particular, this work will emphasize the competitive formation of *S*-nitrosothiol and *N*-nitrosamine (RNNO) moieties on a mixed functional group model polymer, dextran. As shown in Figure 3.1, RSNO and RNNO moieties can form upon nitrosation of thiol and amine sites, respectively, that are present in the dextran system. It is important to characterize which NO moieties form and which give rise to NO, as well as consider which byproducts are undesirable. Specifically, *N*-nitrosamines have been demonstrated as toxic and carcinogenic compounds.⁶ We therefore aim to prevent RNNO formation on polymer backbones, especially the biodegradable dextran polymers described herein, where small molecule RNNO degradation products would be made available in biological systems. To our knowledge, no reports concerning the formation of RNNO moieties during nitrosation of a thiol-containing material have been reported, which is a critical concern toward applying the materials as clinically relevant devices.

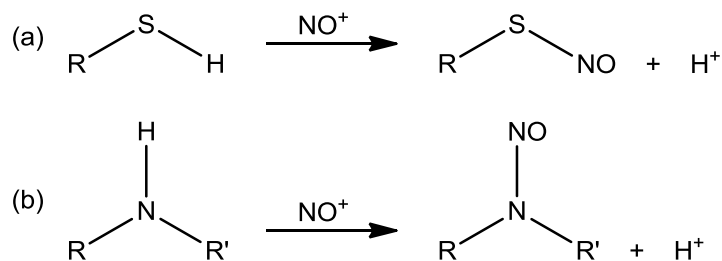


Figure 3.1 Nitrosation of (a) 1° thiol or (b) 2° amine sites is accomplished when either functional group is exposed to a nitrosating agent (a source of NO⁺).

The competitive formation of RNNOs has been considered for other small molecule and polymer systems containing amine sites for other classes of NO donors (*i.e.* *N*-diazoniumdiolates).⁷⁻⁹ If RNNO formation has been considered for other NO donor systems that do not directly involve nitrosation, there is certainly a larger cause for concern regarding side reactions during the nitrosation of materials containing thiols among other functional groups. More specifically, *N*-nitrosamine formation has been noted as a competitive process for small molecules undergoing NO exposure toward *N*-diazoniumdiolate moiety formation.⁷ This concern was further realized for polymers doped with *N*-diazoniumdiolate donors, where donor was found to leach from the material and *N*-nitrosamines were subsequently detected in the soaking solution.¹⁰ Even though nitrosation conditions aren't employed for *N*-diazoniumdiolate systems, any oxidized NO in the system could result in nitrosation due to the formation of NO⁺. As such, RNNO formation has been considered for other NO donor systems that do not directly involve nitrosation. For thiol-containing systems that rely on nitrosation processes for NO loading, there is certainly a larger cause for concern regarding side reactions during the nitrosation of materials containing thiols among other functional groups. Methods are therefore required to differentiate between the formation of these different NO donors in materials systems.

Small molecule RSNO and RNNO moieties have been spectroscopically characterized, both with reported λ_{max} values of 330-350 nm.¹¹ Polymer systems containing RSNO or RNNO functionalities have been demonstrated to maintain similar absorbance features as their respective small molecule analogues.^{4, 8} Overall, because these moieties absorb in the same wavelength region, it is difficult to characterize the formation of one over the other after initial nitrosation using UV-visible spectroscopy. Minimal donor characterization reported in the literature for NO loaded materials in addition to the overlapping UV-visible absorbance features associated with RSNO and RNNO functionalities have led to a further lack of consideration of nitrosation byproducts on these NO loaded polymers.

As an alternative spectroscopic method, small molecule RSNO and RNNO moieties have been characterized by IR spectroscopy.¹² The N=O stretch of the nitroso group is evident for both moieties. However, the frequency differences between the N-S stretch of the RSNO (700-600 cm^{-1}) and the N-N stretch of the RNNO (1000-900 cm^{-1}) have been reported in distinguishably different regions. As such, the characteristic IR absorbance properties could differentiate between each moiety to determine which form during nitrosation.

In addition to spectroscopic characterization, the RSNO and RNNO moieties can be distinguished from one another due to the different stabilities of each functional group arising from the different bond dissociation energies associated with the homolytic cleavage of the X-NO bond. In general, theoretical methods have indicated that the N-NO bond is stronger than the S-NO bond, making the RNNO more stable than the RSNO moiety.¹³ Both moieties must undergo homolytic cleavage of the X-NO bond to yield the NO radical. Theoretical methods have investigated the bond dissociation energies (BDE) of different X-NO species, where the N(H)-NO BDE was on average 30-40 kcal mol^{-1} and the S-NO BDE was 15-20 kcal mol^{-1} .¹³

Despite this theoretical study involving nitrosated 1° amines, the BDE would be even higher for nitrosated 2° amines due to the strengthening of the N-NO bond via the inductive effect. In general, the N-NO bond is stronger than the S-NO bond, indicating the *N*-nitrosamines are more stable moieties than *S*-nitrosothiols. *N*-nitrosamines also require harsher conditions to initiate decomposition toward NO formation (*i.e.* trifluoroacetic acid and hydrogen peroxide mixture)¹⁴ when compared to *S*-nitrosothiols (*i.e.* heat or light).¹⁵ These differences in stability can be exploited to differentiate between the formation of either moiety in a materials system. The stability of some NO moieties relative to others has consequences on the final application of the material. If the ultimate goal is to result in the maximum amount of NO release possible from the material, the formation of NO moieties that cannot contribute to NO release will not accomplish this, particularly if the formation of these stable moieties competes with the formation of NO donor sites. It would instead be more beneficial to tune the chemistry of the system to maximize formation of the NO products (*i.e.* *S*-nitrosothiols) that will decompose under physiological conditions.

Toward the development of highly tunable NO materials (*i.e.* control over the types of NO moieties formed as well as their concentrations), we report a system in which various NO functional groups were incorporated onto the backbone of a dextran polymer. Dextran is a non-toxic polysaccharide polymer that degrades naturally via enzymatic activity and has been implicated as a therapeutic material.¹⁶ Dextran in combination with NO release appears promising for biomaterials development due to the biodegradability and structural properties of dextran coupled to the therapeutic action of NO.^{17, 18} As such, functionalized dextran derivatives serve as a good model system for understanding the nitrosation processes that can give rise to different NO functionalities to exert control over the NO loading process in a material system.

Two different polymer synthesis routes are presented that give rise to different sites available for nitrosation. Depending upon the presence of different functional groups (thiol, amine and amide), the NO moiety formation (RSNO, RNNO) was impacted. Overall, we demonstrate that, depending upon the functionality of the polymer system, selective *S*-nitrosation can be achieved. In addition to spectroscopically monitoring the major nitrosation products, we track the behavior of the functional groups after NO release and are able to discern which groups give rise to NO.

This work demonstrates that spectrophotometric methods can be used to identify the formation of unwanted nitrosation byproducts in mixed NO moiety systems. Synthetic conditions can then be tuned to allow for selective formation of *S*-nitrosothiol donor moieties onto a model dextran backbone, which nearly completely release their NO payload. Overall, the nitrosation processes described herein serve as a fundamental basis toward the investigation of *S*-nitrosothiol formation on polymers with mixed functional groups and the resulting NO release behavior.

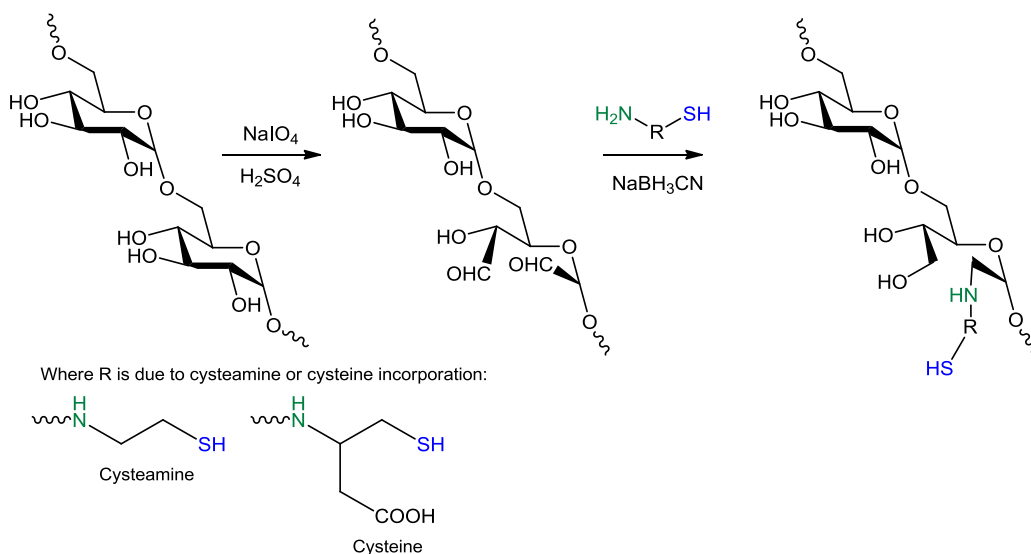
3.3 EXPERIMENTAL SECTION

3.3.1 Materials. Dextran (from *Leuconostoc* spp. MW ~40,000) was obtained from Sigma (St. Louis, MO), L-cysteine (98+ %) from Alfa Aesar, cysteamine hydrochloride (>97%) from Fluka Analytical, and *t*-butyl nitrite (90%) from Aldrich. Unless otherwise stated, all phosphate buffered saline (PBS) was prepared from tablet (OmniPur, EMD) and pH balanced to 7.4 using acid or base, if necessary. All solutions were prepared using Millipore filtered ultrapure water unless otherwise stated.

3.3.2 Polymer synthesis. Dextran was modified to contain pendant cysteine or cysteamine groups using two different synthetic approaches. Syntheses and their respective characterization

were repeated in at least triplicate to ensure reproducibility of the procedures. All experiments were performed in triplicate with the average and standard deviation reported.

Scheme 1: Reductive amination. The first synthetic approach used to modify dextran with a thiol pendant involved the use of reductive amination to attach a cysteamine (**1a**) or cysteine (**1b**) group onto the polymer backbone, as shown in Scheme 3.1.¹⁹



Scheme 3.1 Dextran modification via reductive amination results in the linkage of cysteamine (**1a**) or cysteine (**1b**) to the polymer backbone via a 2° amine linkage.

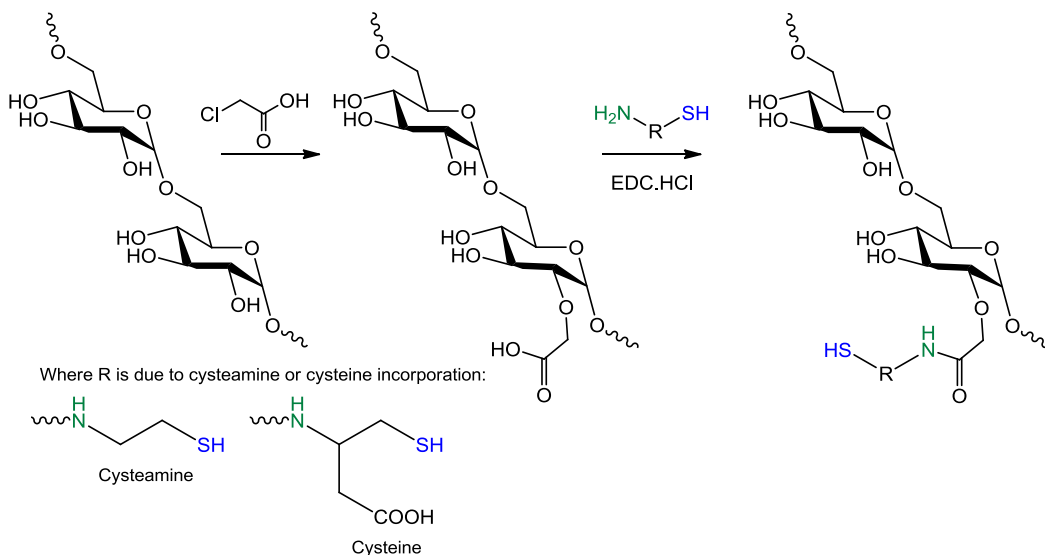
To accomplish this, dextran (1 g) was prepared in water (30 mL), followed by treatment with sodium periodate (0.8 g, 3.73 mmol, Sigma Aldrich) and concentrated sulfuric acid (0.3 g, 3 mmol, 0.8 eq. of periodate, BDH). The mixture was shielded from light under stirring for 1.5 h to allow for periodate oxidation of the dextran. The reaction was terminated via treatment with ethylene glycol (0.18 g, 2.84 mmol, 0.76 eq., 95%, Acros) for a half an hour followed by neutralization with sodium acetate (0.2 M, Mallinckrodt) solution. Dextran aldehyde derivative was isolated by dialysis using a Spectra/Por® dialysis membrane with a molecular weight cut-off

of 8000 Da using Millipore water with multiple changes. The dialyzed dextran aldehyde solution was cooled to 0 °C in an ice bath and subsequently treated with cysteamine hydrochloride or cysteine (1.05 eq. relative to periodate quantity). The pH was adjusted to 8.5 via sodium hydroxide (1 M, Fisher Scientific) addition and stirred at 0 °C for 1 h. To accomplish the reductive amination, sodium cyanoborohydride (0.25 g, 1 eq., Acros) was added to the solution and stirred at 0 °C for 2 h, after which time the product was neutralized by adding acetic acid (10%, BDH). Following an overnight dialysis, the product was treated with dithiothreitol (0.05 g, Fluka) for one hour at room temperature to reduce any disulfide bonds that may have formed during the reaction period. The final thiolated product was further extensively dialyzed and finally isolated after freeze drying.

¹H NMR and ATR-IR were employed to characterize the reductive amination products. ¹H NMR δ/ppm (400 MHz, D₂O) Dextran-cysteamine (**1a**): 2.87 (m, -CH₂-CH₂-SH), 3.35 – 3.85 (m, dextran **H** C₂ – C₆) and 4.83 (m, dextran **H** C₁). Dextran-cysteine (**1b**): 2.74 – 3.25 (m, -CH₂-SH), 3.35 – 3.85 (m, -NH-CH- overlapped with dextran **H** C₂ – C₆) and 4.83 (m, dextran **H** C₁). IR ν_{max}/cm⁻¹Dextran-cysteamine (**1a**): 3600-3000 (-OH), 2890 (-CH), 1247 (-C-N-), and 984 (-CH₂ of α-1,6-linkage). Dextran-cysteine (**1b**): 3600-3000 (-OH), 2890 (-CH), 1577 (-COOH), 1256 (-C-N-), and 1003 (-CH₂ of α-1,6-linkage).

Scheme 2: Carboxymethyl intermediate. The second synthetic approach to achieve thiol-modification of dextran involved the formation of a carboxymethyl intermediate that was further functionalized with cysteamine (**2a**) or cysteine (**2b**), as shown in Scheme 3.2. The dextran derivatives were synthesized and characterized by ¹H NMR and ATR-IR as reported in a previous publication from our group.¹⁷ In brief, dextran hydroxyl groups were first modified with

a carboxymethyl tether by treating with monochloroacetic acid (MCA) under alkaline conditions followed by acidification with acetic acid. Carboxyl groups of the modified dextran derivatives were then covalently modified with aminothiols derivatives through stable amide linkages using carbodiimide chemistry.



Scheme 3.2 Dextran modification via a carboxymethyl intermediate results in the linkage of cysteamine (**2a**) or cysteine (**2b**) to the polymer backbone via an amide linkage.

3.3.3 Ellman's assay for thiol quantification. The Ellman's assay was performed to quantify the amount of thiol that was incorporated onto the dextran backbone for all derivatives. All standard, sample and Ellman's reagent solutions were prepared in a phosphate buffer (100 mM), which was prepared by adding NaH_2PO_4 (100 mM, sodium phosphate, monobasic, anhydrous, molecular biology grade, BDH) to Na_2HPO_4 (100 mM, sodium phosphate, dibasic, anhydrous, ACS grade, Mallinckrodt Chemicals) until pH 8 was reached. Thiol standards were prepared from a stock solution of cysteine (0.012 M) via serial dilution. A solution of DTNB (10 mM, 5,5'-dithiobis(2-nitrobenzoic acid), Sigma), the Ellman's reagent, was prepared. Each modified dextran sample was dissolved in buffer at 5 mg mL^{-1} concentration. Aliquots (100 μL) of each

standard/sample solution were added to DTNB solution (100 μ L) and brought to a final volume of 4 mL. The solutions were agitated for 1 h at room temperature, and the resulting solutions were pipetted into a 96-well plate in 200 μ L aliquots. The absorbance values of the DTNB-treated samples were read at 414 nm on a Synergy 2 microtiter plate reader (BioTek, Winooski, VT, USA).

3.3.4 Nitric oxide loading. Nitrosation of each dextran derivative was achieved by adding anhydrous methanol (4 mL, ACS grade, Macron Chemicals, stored over 4 Å molecular sieves) to the respective dextran derivative (50 mg) in an amber, EPA-certified vial (EnviroWare, Fisher Scientific) with a septum-containing lid. The *t*-butyl nitrite reagent was pretreated with 10 w/v% EDTA ((ethylenedinitrilo)tetraacetic acid, disodium salt, dihydrate, ACS grade, EMD) and subsequently injected (0.4 mL) into the dextran suspension. The sample remained under stirring overnight, protected from light. After nitrosation, the sample was pumped under vacuum for 2 h to remove the methanol and excess *t*-butyl nitrite.

To serve as an *N*-nitrosamine control for characterization comparison, *N*-nitrosoproline was prepared. Proline (50 mg, 99%, Alfa Aesar) was suspended in anhydrous methanol (4 mL), followed by injection of EDTA-treated *t*-butyl nitrite (0.4 mL). The solution was stirred overnight, and the nitrosated product was isolated by vacuum as described above.

3.3.5 Nitric oxide donor, byproduct and NO characterization. All nitrosated products were analyzed before and after NO analysis by solution phase UV-visible spectroscopy on a Nicolet Evolution 300 spectrophotometer (Thermo Electron Corporation, Madison, WI, USA). The polymer solutions were prepared at 0.75 mg mL⁻¹ concentration, where the samples were

sonicated for the time required to solubilize the polymer. The derivatives prepared via reductive amination (**1a**, **1b**) were analyzed before and after nitrosation using a Nicolet 6700 FT-IR fitted with an ATR sample stage for solid-phase IR measurements.

NO release was directly detected via chemiluminescence using Sievers 280i Nitric Oxide Analyzers (NOA, GE Analytical, Boulder, CO, USA). All samples were dissolved in PBS (0.75 mg mL⁻¹) and agitated for the amount of time required for the sample to completely dissolve, followed by injection into the NOA cell. NOA measurements were performed at a 5 s time interval over the duration of time necessary for the measurements to reach baseline. The derivatives prepared via reductive amination (**1a**, **1b**) required about 10 h to reach baseline. The cysteamine derivative prepared via carboxymethyl intermediate (**2a**) required about 10 h to reach baseline, while the cysteine derivative (**2b**) required about 20 h. It is important to note that all NOA experiments were performed under solution phase (PBS, pH 7.4) at room temperature, exposed to ambient light. The mode of RSNO decomposition employed in these experiments, therefore, is due to heat and light initiated NO release.

The Griess assay was performed to assess nitrite in the polymer solution recovered after NO analysis. Sodium nitrite (99.999%, Alfa Aesar) standards were prepared in the concentration range 0-32 μ M via serial dilution from a stock 10 mM solution. Aliquots (212 μ L) of recovered polymer PBS solutions (0.75 mg mL⁻¹) and nitrite standards were pipetted into a 96-well plate and further treated with sulfanilic acid solution (21 μ L of 12.5 mM, prepared from 99%, Aldrich) and hydrochloric acid solution (21 μ L of 6 M, prepared from 36.5-38.0%, BDH Aristar) after refrigeration. Further treatment with NEDA solution (22 μ L of 12.5 mM, N-(1-naphthyl)ethylenediamine dihydrochloride, Acros) resulted in pink-colored solutions (λ_{max} of

540 nm). After 15 minutes of agitation, the absorbance values at 540 nm were measured using a BioTek Synergy 2 microtiter plate reader.

3.4 RESULTS & DISCUSSION

3.4.1 Dextran derivatives prepared by reductive amination. Thiol incorporation using **Scheme 1** resulted in 0.459 ± 0.004 and 0.296 ± 0.007 mmol thiol g⁻¹ for the cysteamine (**1a**) and cysteine (**1b**) derivatives, respectively, (Table 3.1) with the thiol pendant group attached through an amine linkage.

Table 3.1 The thiol content associated with each thiolated dextran derivative as determined by the Ellman's assay and the amount of NO recovered from the corresponding nitrosated materials. All measurements are reported as an average and standard deviation of $n \geq 3$ trials.

Pendant group	Sample ID	Thiol content [mmol g ⁻¹]	NO recovery [mmol g ⁻¹] [a]	% NO recovery (vs. thiol content)
cysteamine	1a [b]	0.459 ± 0.004	0.037 ± 0.003	8%
	2a [c]	0.485 ± 0.007	0.161 ± 0.007	33%
cysteine	1b [b]	0.296 ± 0.007	0.057 ± 0.009	19%
	2b [c]	0.299 ± 0.005	0.158 ± 0.007	53%

[a] NO recovery conditions at room temperature, exposed to ambient light under pH 7.4 phosphate buffered saline at 0.75 mg mL⁻¹ concentration

[b] Thiol attachment accomplished through Scheme 1: reductive amination

[c] Thiol attachment accomplished through Scheme 2: carboxymethyl intermediate

Nitrosation of each derivative was accomplished by adding *t*-butyl nitrite, a well-established nitrosating agent that serves to transfer a nitrosonium ion (NO⁺) to a nucleophilic site. Figure 3.2 indicates the spectra for both derivatives after nitrosation where an absorbance feature at 325-

350 nm indicates the presence of nitroso products. Each nitrosated dextran derivative underwent NO analysis of the dextran solutions (0.75 mg mL^{-1} in PBS) while exposed to ambient light for the time required for the NO measurements to reach baseline. Table 3.1 outlines the NO recoveries over the duration of the NO analysis period, where 0.037 ± 0.003 and 0.057 ± 0.009 mmol NO g^{-1} were recovered for derivatives **1a** and **1b**, respectively. The persistence of an absorbance feature between 325-350 nm for the both derivatives after complete NO recovery (Figure 3.2) indicates a stable byproduct that has formed either during nitrosation or the NO release period.

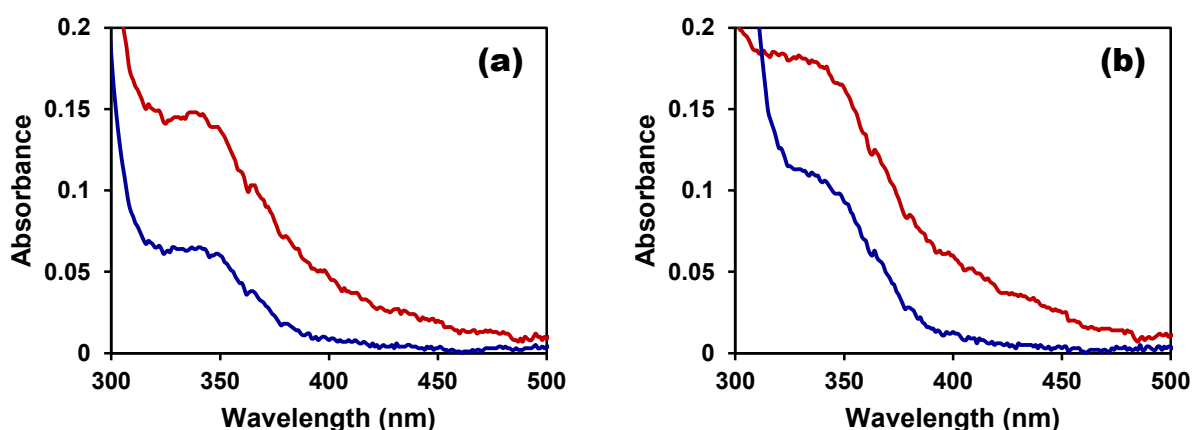


Figure 3.2 (a) UV-vis spectra for the nitrosated cysteamine dextran derivative (**1a**) prepared via reductive amination before (red) and after (blue) NO analysis. (b) UV-vis spectra of nitrosated dextran-cysteine (**1b**) prepared via reductive amination in PBS (0.75 mg mL^{-1}) before and after NO analysis. All spectra represent an average of $n = 3$ trials with a standard deviation $< 10\%$.

The IR spectra shown in Figure 3.3 for the cysteamine derivative (**1a**) indicate the appearance of a frequency band at $\sim 1365 \text{ cm}^{-1}$ which is indicative of the N=O stretch of the nitroso moiety. Further, the appearance of S-N and N-N stretching bands at $\sim 750 \text{ cm}^{-1}$ and ~ 830

cm⁻¹, respectively, indicates the formation of both *S*-nitrosothiol and *N*-nitrosamine moieties after the nitrosation period. The same absorbance features are present in the IR spectrum of the cysteine derivative (**1b**) after nitrosation, shown in Figure 3.4. These absorbance features that occur in the spectra of the nitrosated derivatives are of low intensity; however, to establish that these features were discernible from baseline, an average of 3 baseline spectra was subtracted from the average of 3 nitrosated spectra. The absorbance features were still distinguishable in the baseline-corrected spectrum for each nitrosated derivative, indicating that these features are not contributions from the spectral background but rather absorbance features corresponding to nitroso moieties. The initial UV-vis spectrum of either derivative after nitrosation does not allow for the distinction between the RSNO and RNNO moieties; however, the IR bands present after nitrosation indicate that mixed nitroso products are forming. Overall, spectroscopic evidence qualitatively suggests that both the 2° amine linkages and the 1° thiol sites present in the system experience nitrosation when the dextran system is exposed to *t*-butyl nitrite nitrosation conditions (see Figure 3.5). For all spectroscopic analysis of the dextran derivatives prepared via reductive amination, similar absorbance features are exhibited for either the cysteamine or cysteine derivative.

Controls were run to account for any absorbance contribution due to interferences or remaining RSNO in the system to ensure that the persistence of the 325-350 nm absorbance feature is due predominantly to stable RNNOs in the system. There are various factors other than RNNO formation that could contribute to an absorbance feature in the 350 nm region: a) residual *t*-butyl nitrite nitrosating agent, b) nitrite formed in the system due to prematurely released NO reacting under oxygenated conditions, c) any *O*- or *C*- nitrosation occurring on the dextran backbone, or d) any shift in the polymer solution baseline during the NO analysis period.

Overall, it was found that nitrite was present in the system at low enough concentrations to not interfere in the UV-vis spectrum. Additionally, non-thiolated dextran was subjected to nitrosation conditions and the resulting spectrum indicated no absorbance features due to detectable residual *t*-butyl nitrite or *O*/*C*- nitrosation. The absorbance spectra before and after NO analysis did not experience any shift in the baseline that would contribute to the appearance of an absorbance feature. Additionally, exposure of the polymer to UV light did not result in decomposition of the absorbance feature, which would be expected for any remaining RSNO.

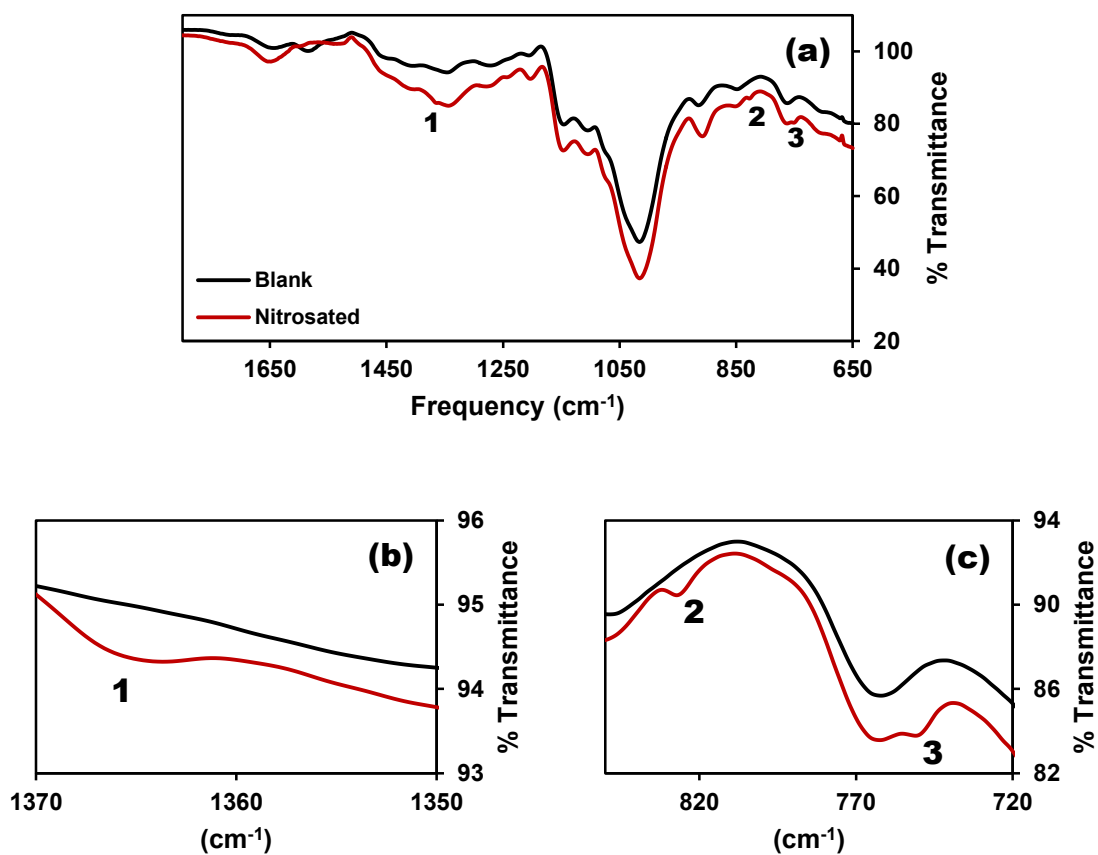


Figure 3.3 (a) Full ATR-IR spectra of dextran-cysteamine (**1a**) prepared via reductive amination before and after nitrosation. Highlighted IR regions for dextran-cysteamine derivative (**1a**) prepared via reductive amination before and after nitrosation where (b) the 1370-1350 cm^{-1}

region indicates an absorbance feature **(1)** corresponding to a N=O stretch and (c) the 850-720 cm^{-1} region indicates absorbance features **(2)** corresponding to a N-N stretch and **(3)** corresponding to a S-N stretch. Each spectrum represents the average of $n=3$ trials with a standard deviation $\leq 2\%$.

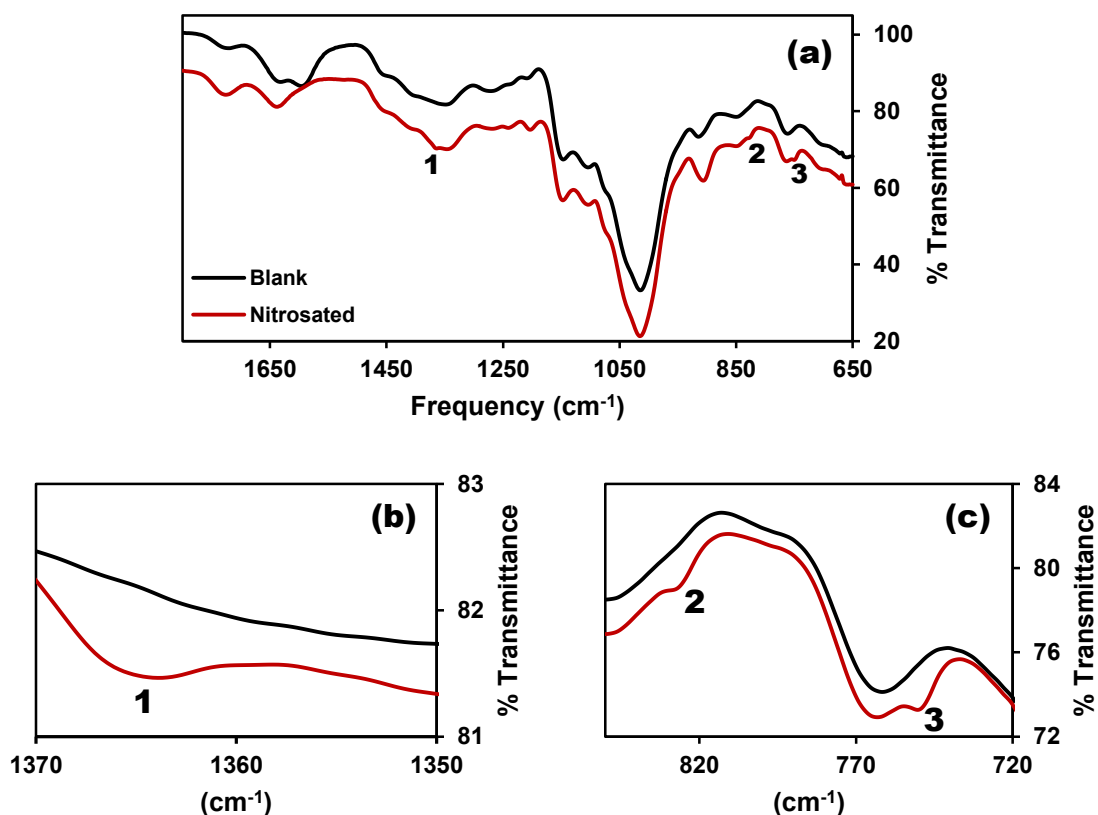


Figure 3.4 (a) Full ATR-IR spectra of dextran-cysteine **(1b)** prepared via reductive amination before and after nitrosation. Highlighted IR regions for dextran-cysteine **(1b)** prepared via reductive amination before and after nitrosation where (b) the 1370-1350 cm^{-1} region indicates an absorbance feature **(1)** corresponding to a N=O stretch and (c) the 850-720 cm^{-1} region indicates absorbance features **(2)** corresponding to a N-N stretch and **(3)** corresponding to a S-N stretch.

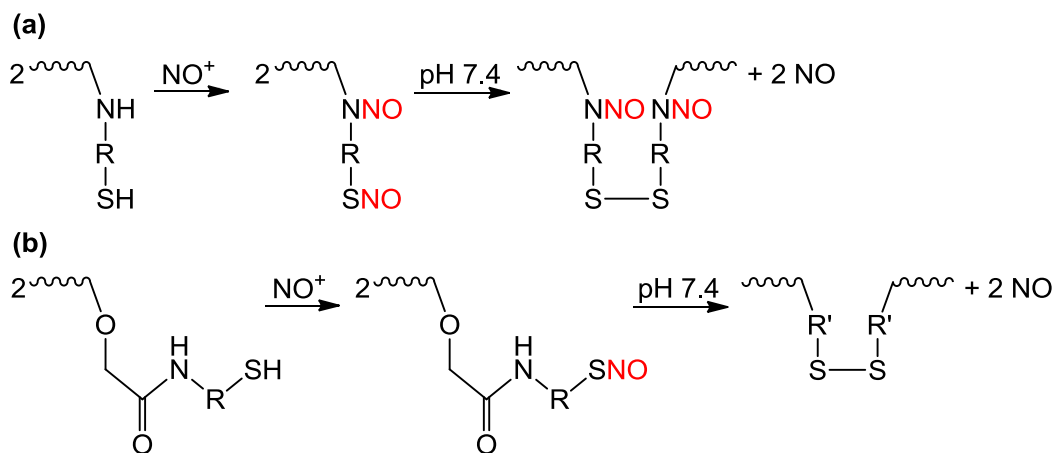


Figure 3.5 (a) For the dextran derivatives (**1a**, **1b**) containing both 2° amine and 1° thiol sites, the introduction of *t*-butyl nitrite results in competitive nitrosation to form *N*-nitrosamine and *S*-nitrosothiol moieties, respectively. (b) Dextran derivatives (**2a**, **2b**) containing amide and 1° thiol sites will selectively yield *S*-nitrosothiol moieties, which decompose completely to give rise to NO.

Nitrite interference. During the preparation of the nitrosated dextran solution in PBS, the cysteine (**1a**) and cysteamine (**1b**) derivatives were sonicated for 15-20 minutes to allow the dextran to solubilize. Any NO released during solution preparation occurred under oxygenated conditions, which could have resulted in the formation of nitrite. Nitrite has an absorbance maximum at 354 nm which could serve as an interfering feature at high enough nitrite concentrations. The molar extinction coefficient for nitrite (ϵ_{\max}) was determined to be $22.8 \text{ M}^{-1} \text{ cm}^{-1}$ from the slope of the Beer's law plot shown in Chapter 2 (Figure 2.5).

The Griess assay was performed on the resulting polymer solutions after NO analysis to determine if the concentration of nitrite was high enough to allow for interference around 350 nm. The nitrite concentrations were determined to be on the order of 5-10 μM , which would result in <0.0005 absorbance contribution, which is below the sensitivity of the spectrometer

measurements. Therefore, the amount of nitrite formed during solution preparation is not significant enough to contribute to any absorbance at 350 nm.

Nitrosated dextran control. To account for any detectable residual *t*-butyl nitrite reagent in the system as well as any potential *C*- or *O*- nitrosation of the dextran backbone, a non-thiolated dextran blank was subjected to the same nitrosation procedure as all the other thiolated dextran derivatives. The dextran product was isolated from methanol/*t*-butyl nitrite under vacuum and analyzed via solution-phase UV-visible spectroscopy (0.75 mg mL⁻¹ in PBS). The dextran product recovered after exposure to *t*-butyl nitrite exhibited no features in the 300-500 nm range, shown in Figure 3.6 (a), and did not release any detectable NO. Different *O*-nitroso groups, such as those due to nitrosation of alcohols and carbohydrates, have been demonstrated to result in an absorbance in the region of 300-400 nm.²⁰ The lack of an absorbance feature demonstrates that no detectable nitrosation occurs due to reaction of *t*-butyl nitrite with the dextran backbone, which in turn does not contribute to the recovered NO. Additionally, the lack of any absorbance features after dextran exposure to *t*-butyl nitrite indicates that no detectable residual nitrosating agent is trapped in the isolated dextran product. The presence of detectable levels of *t*-butyl nitrite would result in a multiplet absorbance feature, as shown in Figure 3.6 (b).

Baseline shift for thiolated dextran derivatives after NO analysis. It is possible that the polymer behavior in soaking solution during the duration of the analysis could lead to a shift in the UV-vis baseline. To account for this, the non-nitrosated thiolated dextran derivatives (**1a**, **1b**) were analyzed in solution (0.75 mg mL⁻¹ in PBS) via UV-vis and NOA on the same timescales as reported for the nitrosated derivatives, where no significant shift was seen in the baselines

(Figure 3.7). Since dextran degradation is not expected under the analysis conditions employed, we would not expect a shift in the baseline.

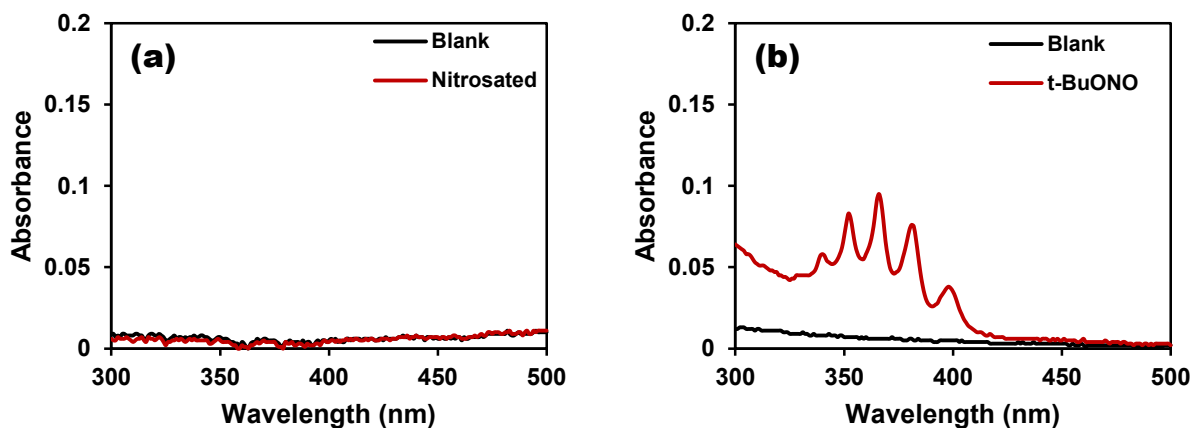


Figure 3.6 (a) 0.75 mg mL^{-1} isolated dextran in PBS with (red) and without (black) exposure to *t*-butyl nitrite nitrosating conditions and (b) 0.75 mg mL^{-1} dextran in PBS with (red) and without (black) the addition of 3 v/v% *t*-butyl nitrite.

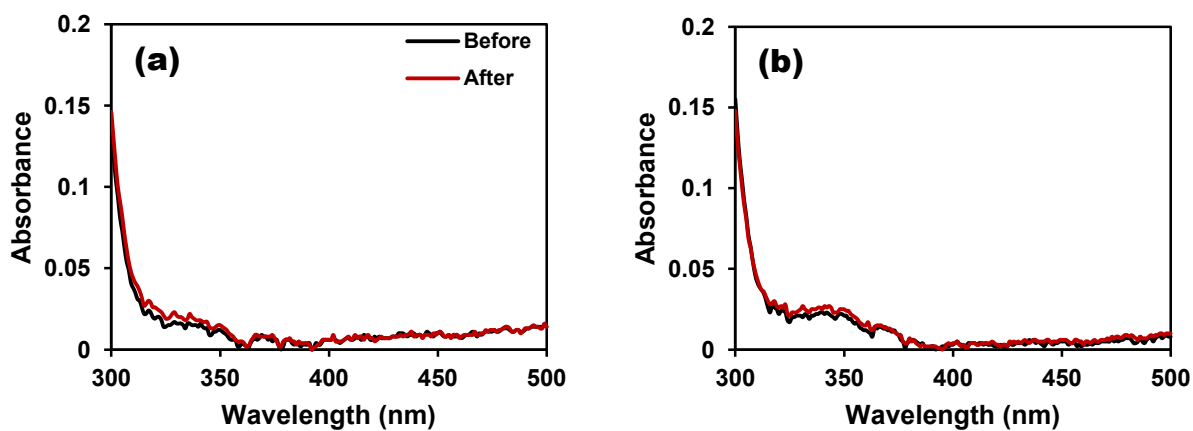


Figure 3.7 Representative UV-vis spectra for the (a) cysteamine and (b) cysteine dextran derivatives prepared via reductive amination before (black) and after (red) NO analysis of each derivative in solution (0.75 mg mL^{-1} in PBS).

Check for remaining RSNO in the system. The recovered dextran solution for the cysteamine (**1a**) derivative was exposed to intense UV light (Blak-Ray B-100AP High Intensity UV lamp; 100 Watt, 365 nm) for 30 min to ensure that the remaining absorbance feature of the nitrosated dextran derivatives prepared via reductive amination was not due to remaining RSNOs in the system. Figure 3.8 demonstrates no significant decrease in the ~350 nm feature, indicating that the feature is not due to residual RSNO. If RSNO moieties were present in the system, near complete decomposition of the RSNOs and corresponding UV-vis feature would be expected since RSNOs are known to decompose via a light-initiated pathway.² Figure 3.9 shows the decrease in absorbance (335 nm) for a representative small molecule RSNO, *S*-nitrosoglutathione, in PBS which experiences 100% decomposition after 30 min UV exposure.

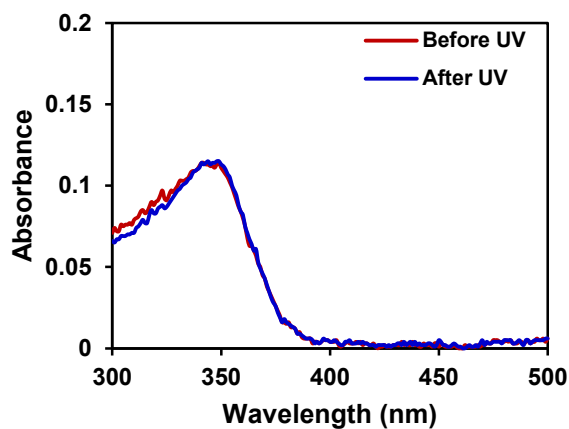


Figure 3.8 Representative absorbance spectra for dextran cysteamine (**1a**) derivative after NO analysis before and after exposure to intense UV light.

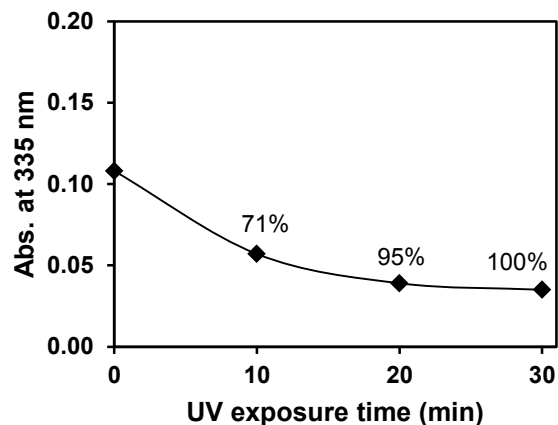


Figure 3.9 Upon exposure of a 0.1 mM *S*-nitrosoglutathione solution to intense UV light, the RSNO experiences 71% decomposition at 10 min, 95% decomposition at 20 min and 100% decomposition at 30 min exposure.

N-nitrosamine control. To consider the formation of the *N*-nitrosamine moiety during nitrosation of dextran derivatives (**1a**, **1b**) prepared via reductive amination with *t*-butyl nitrite, a model amine-containing substrate, proline, was nitrosated. *N*-nitrosoproline serves as a good model *N*-nitroso compound because, compared to other carcinogenic *N*-nitrosamines, it has demonstrated no carcinogenic activity.²¹ Its use in the laboratory is therefore safe as toxic products are not unnecessarily formed. The resulting *N*-nitrosoproline was prepared at 5 mg mL⁻¹ in a 0.75 mg mL⁻¹ dextran solution, which yielded the spectrum shown in Figure 3.10. The absorbance feature at 345 nm due to the *N*-nitroso group matches the absorbance location of the nitrosated dextran derivatives **1a** and **1b** after NO analysis. Of further note is that the *N*-nitrosoproline solution did not release any detectable NO for up to 5 h, after which time there was no significant change in the absorbance spectrum. This indicates that *N*-nitrosamine formation is feasible under *t*-butyl nitrite nitrosation conditions in methanol, resulting in RNNO formation. Further, this suggests

that the RNNO moiety is stable under the conditions reported herein, so the RNNO is not a significant source of NO under these conditions. Due to this stability factor, any remaining RNNO species on the polymer backbone could be available after biodegradation of the material. Due to the toxic and carcinogenic nature of *N*-nitrosamines in general, this is undesirable.

Overall, the only contribution to the remaining 325-350 nm absorbance feature was due to the presence of stable RNNOs in the system. Therefore, the persistent absorbance feature at ~350 nm exhibited by the nitrosated derivatives **1a** and **1b** after NO analysis is not due to nitrite formation, a shift in polymer baseline, remaining RSNO or any features that could occur due to nitrosation of the polymer backbone or residual nitrosating agent.

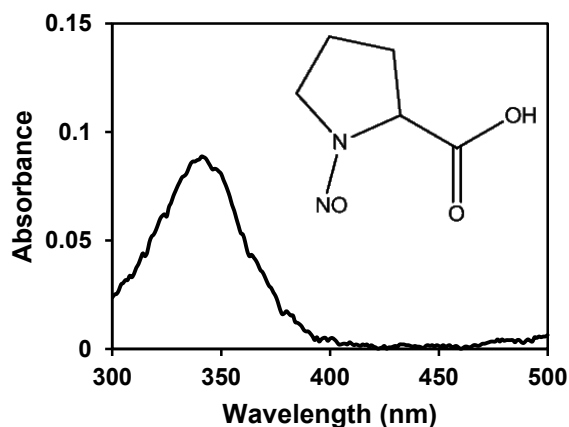


Figure 3.10 Representative absorbance spectrum for *N*-nitrosoproline (structure shown) in 0.75 mg mL⁻¹ dextran solution.

For these dextran derivatives with mixed functional groups, competitive nitrosation is occurring on the amine and thiol sites. Competitive RNNO and RSNO formation has been reported for small molecules under acidic nitrite conditions where, depending upon the reaction

conditions (*i.e.* pH), RNNO formation was enhanced.²² We find that RNNO formation must also be a consideration for polymers exposed to *t*-butyl nitrite conditions. Previous literature suggests that for small molecule mixed systems, during the nitrosation process, RSNO formation could dominate followed by transnitrosation to result in RNNO formation.²³ However, the appearance of both the S-N and N-N stretching modes in the IR after nitrosation suggests that the RNNO forms during the nitrosation period.

3.4.2 Dextran derivatives prepared by carboxymethyl intermediate. As mentioned previously, *N*-nitrosamines are carcinogenic and toxic thus formation on these dextran systems is a critical drawback for use in biomedical applications. To eliminate RNNO formation on the modified dextran backbone, a different synthetic approach was taken. By using chemistries involving a carboxymethyl intermediate (Scheme 3.2), the cysteamine (**2a**) and cysteine (**2b**) residues were attached to the dextran by an amide linkage instead of an amine linkage. The incorporation of the thiol group using this synthetic approach resulted in 0.485 ± 0.007 and 0.299 ± 0.005 mmol thiol g⁻¹ for the cysteamine (**2a**) and cysteine (**2b**) derivatives, respectively. Solutions of each nitrosated derivative (0.75 mg mL^{-1} in PBS) underwent NO analysis at room temperature with the samples exposed to ambient light. The cysteamine (**2a**) and cysteine (**2b**) derivatives released 0.161 ± 0.007 and 0.158 ± 0.007 mmol NO g⁻¹, respectively (Table 3.1).

Figure 3.11 shows the representative UV-vis absorbance spectra for the cysteamine (**2a**) and cysteine (**2b**) derivatives before and after NO analysis. The initial absorbance feature occurred near 335 nm, indicating nitroso product formation. For either derivative, the initial 335 nm peak decayed nearly completely during NO analysis (89% decomposition for **2a**, 91% for **2b**) leaving no significant absorbance feature. The lack of an absorbance feature after NO release

indicates that no RNNOs were present in the system and that the initial absorbance feature after nitrosation is due predominantly to RSNOs formed during nitrosation.

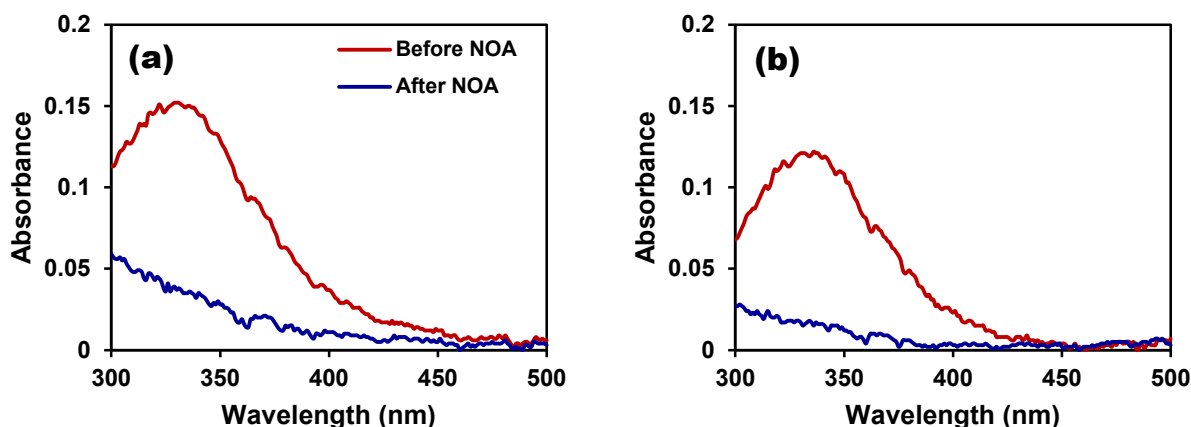


Figure 3.11 UV-vis spectra for the nitrosated (a) cysteamine (**2a**) and (b) cysteine (**2b**) dextran derivatives prepared via carboxymethyl intermediate approach before (red) and after (blue) NO analysis. All spectra represent $n \geq 3$ with a standard deviation $\leq 9\%$ for 0.75 mg mL^{-1} polymer concentration in PBS.

RNNO formation was effectively eliminated by tuning the polymer functionality and the RSNO moieties formed during nitrosation nearly completely decomposed to result in NO release. The electron-withdrawing nature of the carbonyl group of the amide functional group serves to make the amine less nucleophilic when compared to the 2° amine case, making it less susceptible to electrophilic attack by the nitrosating species during nitrosation. Additionally, the steric crowding due to the carbonyl group could block significant interaction of the NO^+ with the nitrogen of the amide. Thus, nitrosation of the amide nitrogen is eliminated, resulting in predominant and selective *S*-nitrosation for the derivatives prepared via carboxymethyl intermediate approach.

Molar extinction coefficient values were determined by correlating the absorbance value at 335 nm to the concentration of RSNO moiety. Solutions of each nitrosated dextran derivative were prepared via serial dilution (0.05, 0.25, 0.50, 0.75 and 1.0 mg polymer mL⁻¹ standard concentrations). The amount of NO recovered during the NOA analysis period was normalized by the mass of polymer present in the 0.75 mg mL⁻¹ solution. This value was further corrected to account for the fact that the RSNO moiety experienced around 90% decomposition (based upon UV-vis analysis) to yield a value that allowed for the conversion of the mg mL⁻¹ polymer concentrations to mol RSNO L⁻¹ (assuming a 1 NO: 1 RSNO molar ratio). Figure 3.12 shows the Beer's law plots associated with the cysteamine (**2a**) and cysteine (**2b**) dextran derivatives. The slope of each plot corresponds to the molar extinction coefficient (M⁻¹ cm⁻¹) of each nitrosated material, where the ϵ_{max} values corresponding to 335 nm were determined to be $1115 \pm 42 \text{ M}^{-1} \text{ cm}^{-1}$ for the cysteamine derivative (**2a**) and $869 \pm 12 \text{ M}^{-1} \text{ cm}^{-1}$ for the cysteine derivative (**2b**). Both molar extinction coefficient values are within the reported order of magnitude ($\sim 10^3 \text{ M}^{-1} \text{ cm}^{-1}$) as those reported for small molecule *S*-nitrosothiols in aqueous solution,² indicating once again that RSNOs are the predominant nitrosation product.

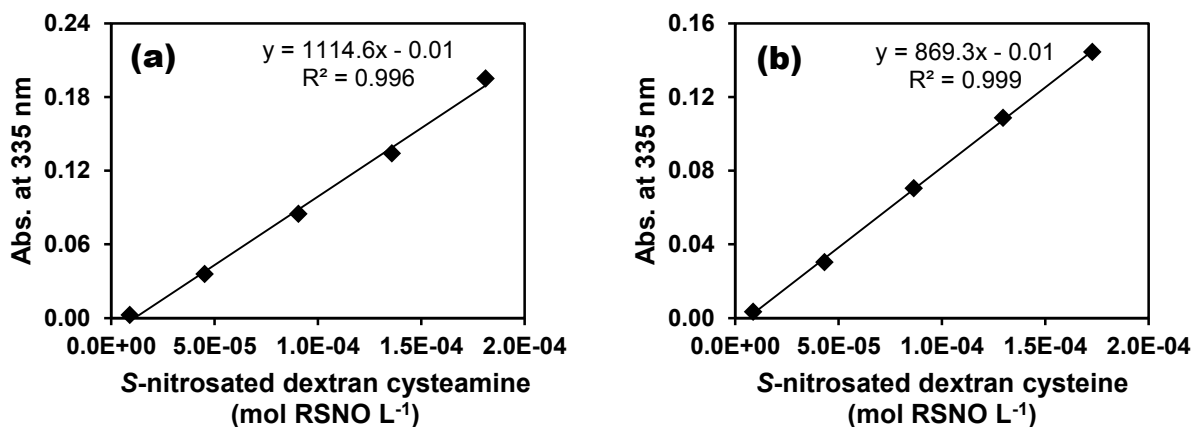


Figure 3.12 Beer's law plots associated (a) cysteamine and (b) cysteine derivatives prepared via carboxymethyl intermediate approach in PBS where the slope of each plot indicates molar extinction coefficients of $1115 \text{ M}^{-1} \text{ cm}^{-1}$ and $869 \text{ M}^{-1} \text{ cm}^{-1}$, respectively, associated with the 335 nm absorbance. Error bars are smaller than the size of the data point (% error < 6% for all data points).

3.4.3 Impact of NO moiety formation on NO loading and release. The absorbance values at 335 nm associated with the nitrosated dextran derivatives containing an amide linkage (baseline corrected with a 0.75 mg mL^{-1} solution of the corresponding non-nitrosated derivative) were 0.143 ± 0.002 for the cysteamine derivative (**2a**) and 0.116 ± 0.004 for the cysteine derivative (**2b**). By converting the absorbance values using the corresponding molar extinction coefficients, the initial RSNO concentrations were found to be $0.171 \pm 0.007 \text{ mmol g}^{-1}$ for **2a** and $0.177 \pm 0.007 \text{ mmol g}^{-1}$ for **2b**, which corresponds to 35 ± 2 and 59 ± 3 % nitrosation based upon the initial thiol content for the cysteamine and cysteine derivatives, respectively.

It is interesting that, despite significantly different thiol content for the carboxymethyl intermediate polymers ($0.459 \pm 0.004 \text{ mmol g}^{-1}$ for **2a**, $0.296 \pm 0.007 \text{ mmol g}^{-1}$ for **2b**), similar RSNO concentrations resulted after nitrosation. In fact, the RSNO concentrations after

nitrosation ($0.171 \pm 0.007 \text{ mmol g}^{-1}$ for **2a**, $0.177 \pm 0.007 \text{ mmol g}^{-1}$ for **2b**) are statistically of the same population at the 90% confidence level (CL). Despite different amounts of thiol residues present in each system, this would suggest a fundamental limit to the nitrosation under these conditions. Additionally, each derivative with the same RSNO concentration decomposed to the same extent (90%), resulting in total NO payloads that are statistically of the same population (90% CL). Despite the same total NO recoveries, the cysteamine (**2a**) and cysteine (**2b**) derivatives yielded different release kinetic profiles (Figure 3.13). Each profile exhibits a relatively flat, steady state NO release, followed by decay to baseline. However, the cysteamine derivative (**2a**) releases a steady state value of $\sim 0.8 \text{ nmol NO}$, which is roughly twice the steady state NO of the cysteine derivative (**2b**), which releases $\sim 0.4 \text{ nmol NO}$ at steady state. Additionally, the cysteamine derivative (**2a**) has completed its NO release within $\sim 10 \text{ h}$, while the cysteine derivative (**2b**) requires $\sim 20 \text{ h}$ to release the same NO payload. Overall, we find that the functionality associated with the thiol pendant group (cysteamine, cysteine) results in different NO release kinetics. The ability to tune the NO release kinetics based upon differences in the polymer functionality is a critical requirement for polymer systems intended for different therapeutic applications. Since the UV-vis absorbance features of the RNNO and RSNO moieties for the reductive amination dextran derivatives (**1a**, **1b**) overlap, we cannot quantify the extent of nitrosation associated with these derivatives. However, the total NO recoveries quantified from the NO profiles shown in Figure 3.14 are impacted depending upon the functionality of the nitrosated polymer. The ratio of released NO relative to the amount of available thiol sites (see Table 3.1) is much lower for the amine containing materials ($\sim 10\text{-}20\%$) compared to the amide containing materials ($\sim 30\text{-}50\%$).

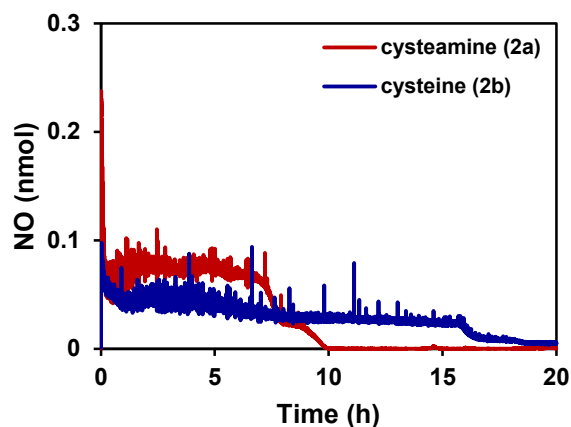


Figure 3.13 Representative NO release profiles for the cysteamine (**2a**) and cysteine (**2b**) dextran derivatives prepared via carboxymethyl intermediate approach (0.75 mg mL^{-1} in PBS, room temperature). The cysteamine derivative (**2a**) exhibits a steady state NO release of ~ 0.8 nmol, while the cysteine derivative (**2b**) exhibits ~ 0.4 nmol NO.

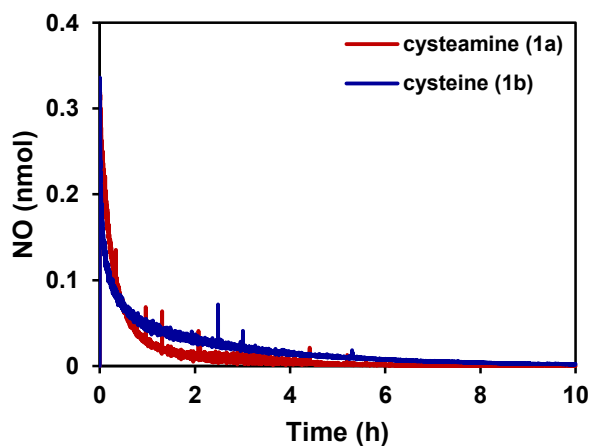


Figure 3.14 NO release profiles associated with solutions (0.75 mg mL^{-1} in PBS, room temperature) of the cysteamine (**1a**) and cysteine (**1b**) dextran derivatives prepared via reductive amination.

The polymers containing the amine linkage resulted in lower overall NO recovery when compared to those with the amide linkage. Since the amine-containing polymers can experience nitrosation of both the thiol and the amine sites, and because the RNNO moieties are relatively stable, only the RSNO is giving rise to the detected NO. In general, the formation of stable RNNO moieties during the nitrosation process will not contribute to the NO release, thus lowering the NO yield associated with the amine containing derivatives. By making available for nitrosation only the thiol sites using the carboxymethyl intermediate approach, this alternate amine sink for the NO is eliminated and most of the NO loaded as RSNO is recovered as indicated by near-complete disappearance of the 335 nm RSNO absorbance band. It can also be considered that the formation of disulfide in the presence of oxygen due to thiol oxidation²⁴ could be resulting in lower thiol availability, which would also impact the amount of RSNO formed. However, because similar thiol contents are exhibited for a given thiol pendant regardless of the synthetic scheme employed (Table 3.1) the rate of disulfide formation will be similar, not impacting the thiol availability significantly between synthetic approaches. Therefore, the increase in NO recovery when switching from the reductive amination to the carboxymethyl intermediate approach can be attributed to the elimination of competitive RNNO formation. The elimination of harmful RNNO species on the polymer backbones is additionally helpful toward the implementation of these materials for bioapplications.

3.5 CONCLUSIONS

Herein, we have reported the synthesis and characterization of nitrosated biodegradable dextran derivatives containing cysteine and cysteamine pendant groups. Depending upon the synthetic approach employed to prepare the derivative, amine or amide functional groups were

available in addition to the thiol sites. After spectroscopic analysis of the nitrosated amine-containing derivatives, it was found that *N*-nitrosamine functional groups formed competitively with *S*-nitrosothiols. The *S*-nitrosothiol moiety gave rise to NO release, while the *N*-nitrosamine remained stable. *N*-nitrosamines are undesirable side products due to their toxic and carcinogenic nature. As such, tuning the polymer chemistry such that the material contained amide instead of amine linkages resulted in primarily *S*-nitrosothiol formation. *S*-nitrosothiol groups completely decomposed, giving rise to higher amounts of released NO when compared to the nitrosated amine-containing derivatives. Overall, we present that the functional groups surrounding the thiol site on a polymer can be tuned to impact directly the NO moieties that are formed during nitrosation and the corresponding NO release properties. Special care must be taken when nitrosating polymer systems that contain multiple functional groups. Toward the ultimate goal of creating NO releasing polymers with increased NO capacities, it is critical to identify and quantify how the NO is stored on the polymer and which of the NO moieties in the system are capable of releasing NO for bioactivity.

CHAPTER 3 REFERENCES

1. Frost, M. C.; Reynolds, M. M.; Meyerhoff, M. E., Polymers Incorporating Nitric Oxide Releasing/Generating Substances for Improved Biocompatibility of Blood-Contacting Medical Devices. *Biomaterials* **2005**, *26*, 1685-1693; Varu, V. N.; Tsihlis, N. D.; Kibbe, M. R., Nitric Oxide-Releasing Prosthetic Materials. *Vasc. Endovascular Surg.* **2009**, *43*, 121-131; Seabra, A. B.; Duran, N., Nitric Oxide-Releasing Vehicles for Biomedical Applications. *J. Mater. Chem.* **2010**, *20*, 1624-1637; Riccio, D. A.; Schoenfisch, M. H., Nitric Oxide Release: Part I. Macromolecular Scaffolds. *Chem. Soc. Rev.* **2012**, *41*, 3731-3741; Carpenter, A. W.; Schoenfisch, M. H., Nitric Oxide Release: Part II. Therapeutic Applications. *Chem. Soc. Rev.* **2012**, *41*, 3742-3752.
2. Williams, D. L. H., The Chemistry of S-nitrosothiols. *Acc. Chem. Res.* **1999**, *32*, 869-876.
3. Bohl, K. S.; West, J. L., Nitric Oxide-Generating Polymers Reduce Platelet Adhesion and Smooth Muscle Cell Proliferation. *Biomaterials* **2000**, *21*, 2273-2278; Frost, M. C.; Meyerhoff, M. E., Synthesis, Characterization, and Controlled Nitric Oxide Release from S-nitrosothiol-Derivatized Fumed Silica Polymer Filler Particles. *J. Biomed. Mater. Res., Part A* **2005**, *72A*, 409-419; Riccio, D. A.; Dobmeier, K. P.; Hetrick, E. M.; Privett, B. J.; Paul, H. S.; Schoenfisch, M. H., Nitric Oxide-Releasing S-nitrosothiol-Modified Xerogels. *Biomaterials* **2009**, *30*, 4494-4502; Li, Y.; Lee, P. I., Controlled Nitric Oxide Delivery Platform Based on S-nitrosothiol Conjugated Interpolymer Complexes for Diabetic Wound Healing. *Mol. Pharmaceutics* **2010**, *7*, 254-266; Seabra, A. B.; Martins, D.; Simoes, M. M. S. G.; da Silva, R.; Brocchi, M.; de Oliveira, M. G., Antibacterial Nitric Oxide-Releasing Polyester for the Coating of Blood-Contacting Artificial Materials. *Artif. Organs* **2010**, *34*,

- E204-E214; Coneski, P. N.; Rao, K. S.; Schoenfisch, M. H., Degradable Nitric Oxide-Releasing Biomaterials via Post-Polymerization Functionalization of Cross-Linked Polyesters. *Biomacromolecules* **2010**, *11*, 3208-3215; Coneski, P. N.; Schoenfisch, M. H., Synthesis of Nitric Oxide-Releasing Polyurethanes with S-nitrosothiol-Containing Hard and Soft Segments. *Polym. Chem.* **2011**, *2*, 906-913; Damodaran, V. B.; Joslin, J. M.; Wold, K. A.; Lantvit, S. M.; Reynolds, M. M., S-nitrosated Biodegradable Polymers for Biomedical Applications: Synthesis, Characterization and Impact of Thiol Structure on the Physicochemical Properties. *J. Mater. Chem.* **2012**, *22*, 5990-6001; Riccio, D. A.; Coneski, P. N.; Nichols, S. P.; Broadnax, A. D.; Schoenfisch, M. H., Photoinitiated Nitric Oxide-Releasing Tertiary S-nitrosothiol-Modified Xerogels. *ACS Appl. Mater. Interfaces* **2012**, *4*, 796-804.
4. Seabra, A. B.; da Silva, R.; de Oliveira, M. G., Polynitrosated Polyesters: Preparation, Characterization, and Potential Use for Topical Nitric Oxide Release. *Biomacromolecules* **2005**, *6*, 2512-2520.
 5. Williams, D. L. H., *Nitrosation Reactions and the Chemistry of Nitric Oxide*. Elsevier: 2004.
 6. Shank, R. C., Toxicology of N-Nitroso Compounds. *Toxicol. Appl. Pharmacol.* **1975**, *31*, 361-368.
 7. Coneski, P. N.; Schoenfisch, M. H., Competitive Formation of N-Diazeniumdiolates and N-Nitrosamines via Anaerobic Reactions of Polyamines with Nitric Oxide. *Org. Lett.* **2009**, *11* (23), 5462-5465.

8. Zhou, Z.; Meyerhoff, M. E., Polymethacrylate-Based Nitric Oxide Donors with Pendant N-diazeniumdiolated Alkyldiamine Moieties: Synthesis, Characterization, and Preparation of Nitric Oxide Releasing Polymeric Coatings. *Biomacromolecules* **2005**, *6*, 780-789.
9. Zhang, H. Development of Nitric Oxide-Releasing Polymers With Improved Blood Compatibility. The University of Michigan, 2002.
10. Mowery, K. A.; Schoenfisch, M. H.; Saavedra, J. E.; Keefer, L. K.; Meyerhoff, M. E., Preparation and Characterization of Hydrophobic Polymeric Films that are Thromboresistant via Nitric Oxide Release. *Biomaterials* **2000**, *21*, 9-21.
11. Wang, P. G.; Xian, M.; Tang, X.; Wu, X.; Wen, Z.; Cai, T.; Janczuk, A. J., Nitric Oxide Donors: Chemical Activities and Biological Applications. *Chem. Rev.* **2002**, *102*, 1091-1134.
12. Szacilowski, K.; Stasicka, Z., S-nitrosothiols: Materials, Reactivity and Mechanisms. *Prog. React. Kinet. Mech.* **2001**, *26*, 1-58; Williams, R. L.; Pace, R. J.; Jeacocke, G. J., Applications of Solvent Effects 1. The Spectra of Secondary Nitrosamines. *Spectrochim. Acta* **1964**, *20*, 225-236.
13. Fu, Y.; Mou, Y.; Lin, B. L.; Liu, L.; Guo, Q. X., Structures of the X-Y-NO Molecules and Homolytic Dissociation Energies of the Y-NO Bonds (Y = C, N, O, S). *J. Phys. Chem. A* **2002**, *106*, 12386-12392.
14. Kostyukovskii, Y. L.; Melamed, D. B., Carcinogenic N-nitrosamines. Formation, Properties, and Analysis. *Russ. Chem. Rev.* **1988**, *57*, 350-366.
15. Jen, M. C.; Serrano, M. C.; van Lith, R.; Ameer, G. A., Polymer-Based Nitric Oxide Therapies: Recent Insights for Biomedical Applications. *Adv. Funct. Mater.* **2012**, *22*, 239-260.

16. Naessens, M.; Cerdobbel, A.; Soetaert, W.; Vandamme, E. J., Leuconostoc Dextranase and Dextran: Production, Properties and Applications. *J. Chem. Technol. Biotechnol.* **2005**, *80* (8), 845-860.
17. Damodaran, V. B.; Place, L. W.; Wold, K. A.; Kipper, M. J.; Reynolds, M. M., Enzymatically Degradable Nitric Oxide Releasing Dextran Derivatives for Biomedical Applications. *J. Mater. Chem.* **2012**, *22*, 23038-23048.
18. Reynolds, M. M.; Witzeling, S. D.; Damodaran, V. B.; Medeiros, T. N.; Edwards, M. A.; Lookian, P. P.; Brown, M. A., Applications for Nitric Oxide in Halting Proliferation of Tumor Cells. *Biophys. Biochem. Res. Comm.* **2013**, *431*, 647-651; Reynolds, M. M.; Witzeling, S. D.; Damodaran, V. B.; Jarigese, D. M.; Edwards, M. A.; Knodle, R. D.; Lookian, P. P.; Brown, M. A., Application of a Nitric Oxide-Releasing Pro-drug for Halting Growth of Human Breast and Canine Mammary Carcinoma Cells. *J. Vet. Sci. Med.* **2012**, *1* (1), ISSN 2323-4645.
19. Damodaran, V. B.; Joslin, J. M.; Reynolds, M. M., Nitric Oxide Releasing Dextran Derivatives. *PMSE Prepr.* **2011**, *105*, 814-815.
20. Aldred, S. E.; Williams, D. L. H.; Garley, M., Kinetics and Mechanism of the Nitrosation of Alcohols, Carbohydrates, and a Thiol. *J. Chem. Soc., Perkin Trans. 2* **1982**, (7), 777-782.
21. Nagasawa, H. T.; Fraser, P. S.; Yuzon, D. L., A New Method for Nitrosation of Proline and Related sec-Amino Acids to N-nitrosamino Acids with Possible Oncogenic Activity. *J. Med. Chem.* **1973**, *16*, 583-585; Nixon, J. E.; Wales, J. H.; Scanlan, R. A.; Bills, D. D.; Sinnhuber, R. O., Null Carcinogenic Effect of Large Doses of Nitrosoproline and Nitrosohydroxyproline in Wistar Rats. *Food Cosmet. Toxicol.* **1976**, *14* (2), 133-135.

22. Davies, R.; Massey, R. C.; McWeeny, D. J., A Study of the Rates of the Competitive Nitrosations of Pyrrolidine, p-Cresol and L-cysteine Hydrochloride. *J. Sci. Food Agric.* **1978**, *29*, 62-70.
23. Dennis, M. J.; Davies, R.; McWeeny, D. J., The Transnitrosation of Secondary Amines S-nitrosocysteine in Relation to N-nitrosamine Formation in Cured Meats. *J. Sci. Food Agric.* **1979**, *30*, 639-645; Shenoy, N. R.; Choughuley, A. S. U., Inhibitory Effect of Diet Related Sulfhydryl Compounds on the Formation of Carcinogenic Nitrosamines. *Cancer Lett.* **1992**, *65* (3), 227-232; Keshive, M.; Singh, S.; Wishnok, J. S.; Tannenbaum, S. R.; Deen, W. M., Kinetics of S-nitrosation of Thiols in Nitric Oxide Solutions. *Chem. Res. Toxicol.* **1996**, *9*, 988-993.
24. Hisano, N.; Iwata, H.; Teramura, Y.; Chen, H.; Ikada, Y., Kinetics Analyses of Disulfide Formation Between Thiol Groups Attached to Linear Poly(acrylamide). *J. Polym. Sci., Part A: Polym. Chem.* **2010**, *49*, 671-679.

CHAPTER 4:
COMPLETE CHARACTERIZATION OF NITRIC OXIDE LOADING AND RELEASE
PROPERTIES FOR S-NITROSATED BIODEGRADABLE POLYMER DERIVATIVES

4.1 PREFACE

This chapter includes the analysis of both the nitrosation efficiency and NO release parameters for a model *S*-nitrosated polymer system. The polymer that was characterized was based upon poly(lactic-*co*-glycolic acid), where a multi-block polymer was composed of lactic acid and glycolic acid monomers with hydroxymethyl propionic acid (HMPA) chain extenders. The resulting PLGH material was derivatized to contain pendant thiol groups, which were subsequently nitrosated. Methods were developed to quantify the RSNO content in the system via molar extinction coefficient value determination for each *S*-nitrosated derivative. This quantification enabled the determination of nitrosation efficiency. A subsequent NO release analysis considered the effect of the thiol functional group on the kinetics of NO release for each derivative, where significantly different NO release profiles and % NO recoveries were determined depending upon the derivative employed. Overall, this work, published in *Journal of Materials Chemistry* (© The Royal Society of Chemistry 2012), serves as the first report of NO releasing biodegradable materials that are characterized to consider RSNO quantification combined with consideration of variable NO release parameters. Overall, the pendant thiol group was found to greatly impact the extent of *S*-nitrosation as well as the subsequent NO release properties.

Specifically for this work, I would like to recognize Dr. Vinod Damodaran as the primary author of the original manuscript due to his contribution to the synthesis and characterization of

the thiolated PLGH derivatives, as well as subsequent nitrosation, NO analysis and biodegradation studies. Kate Wold was responsible for fabricating the polymers into electrospun nanofibers, while Sarah Lantvit performed surface analysis to assess surface wettability. My major contributions to this work included the quantification of the RSNO moiety to determine the impact of each derivative on the % *S*-nitrosation and % NO recovery values. This chapter will highlight predominantly the characterization of the NO loading and releasing stages; the specific details regarding the biodegradation profiles, surface analysis, toxicity and processing will not be presented in whole since that work was not performed by this author. In section 4.5.1 of the Results & Discussion, the characterization of the thiolated polymer as performed by Dr. Damodaran is included to complete the picture of the PLGH derivatives before and after nitrosation. We would like to acknowledge the financial support for this research from Colorado State University and the Department of Defense Congressionally Directed Medical Research Program (DOD-CDMRP). This research was further supported by funds from the Boettcher Foundation's Webb-Waring Biomedical Research Program. V.B.D and K.A.W were supported from the DOD-CDMRP and J.M.J. and S.M.L were supported by the Boettcher Foundation's Webb-Waring Biomedical Research Program.

Adapted from Damodaran, V. B.; Joslin, J. M.; Wold, K. A.; Lantvit, S. M.; Reynolds, M. M., *S*-nitrosated Biodegradable Polymers for Biomedical Applications: Synthesis, Characterization and Impact of Thiol Structure on the Physicochemical Properties. *J. Mater. Chem.* **2012**, *22*, 5990-6001 with permission from The Royal Society of Chemistry. Copyright 2012 The Royal Society of Chemistry.

4.2 INTRODUCTION

The need for synthetic materials to aid in the repair and regeneration of tissues in prominent biomedical applications has resulted in a shift from the development of biostable to biodegradable materials over the last 20 years.¹ In fact, many biodegradable polymers are currently being investigated for tissue engineering scaffolds, cardiovascular stents, and orthopaedic and intestinal anastomosis devices.² However, many of these first generation materials cause localized cell death and work against cell regeneration processes. Furthermore, these materials still initiate the foreign body response and cause platelet activation. This lack of integration with cells and tissues and the instigation of various bioresponses results in severe complications both initially and long-term. Taken together, the biological processes invoked by a synthetic material can ultimately lead to functional failure of implanted devices and significant health hazards to patients. In this regard, biointeractive materials are required that control initial blood activation and infection events followed by complete degradation after cell regeneration occurs.³

Nitric oxide is a naturally occurring signalling agent responsible for maintaining the functional performance of cells that line the blood vessels. Some of NO's vascular functions include modulating hemostasis, regulating vascular tone and promoting revascularization.⁴ Moreover, NO is involved in other physiological processes such as monocyte inactivation, anti-inflammatory responses,⁵ and wound-healing.⁶ Overall, compelling evidence suggests that biodegradable materials that release NO at tunable levels may provide the ideal approach for creating a class of biointeractive materials. As shown schematically in Figure 4.1, it is of utmost importance to develop a biodegradable polymer that promotes certain processes and inhibits others to modulate a range of events.

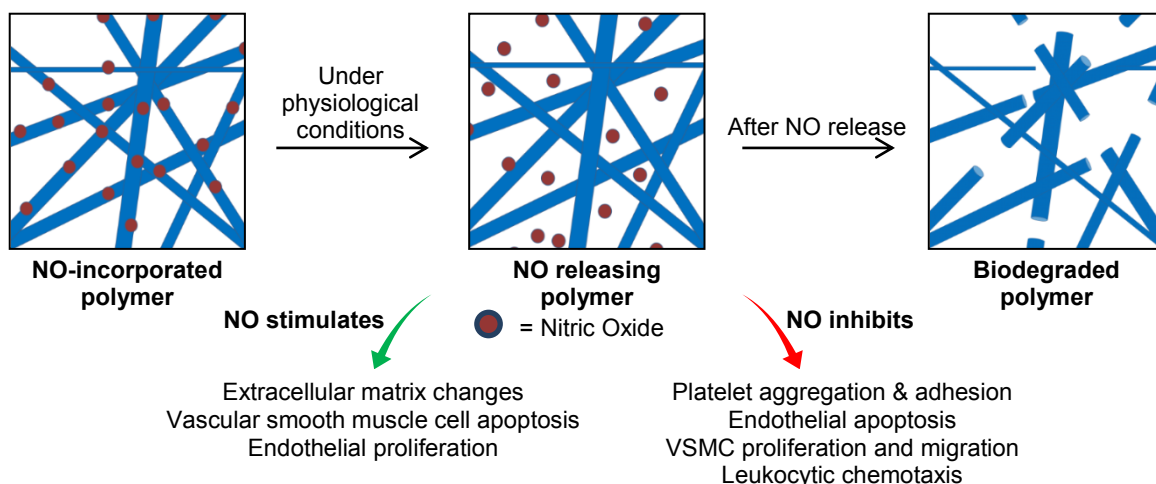


Figure 4.1 Concept schematic of the multifunctional behaviour of a biointeractive material, where the material both up-regulates the important biological processes needed to promote wound-healing and suppresses the processes that cause adverse bioresponses.

Due to its short half-life and high reactivity, NO has to be stably stored within a material in the form of various donors such as nitrites, *S*-nitrosothiols and *N*-diazoniumdiolates.^{7, 8} In these studies, we employed the *S*-nitrosothiol (RSNO) moiety for the storage and delivery of NO since RSNOs are endogenous, non-toxic NO donors *in vivo* and their decomposition is triggered through several mechanisms such as heat, light and metal ions.^{8, 9} The variety of RSNO decomposition mechanisms marks an advantage for applications since the materials reported herein can be tailored to deliver NO over a wide range of conditions, including phototherapeutic treatments.

Extensive research exists on the development of hydrophobic NO releasing materials that are biostable, including materials prepared from blends or covalent attachment of NO donor moieties to polymer backbones.^{10, 11} However, little work has been published regarding biodegradable, NO releasing materials. Coneski *et al.* recently synthesized degradable *S*-

nitrosated polyesters by post-synthetically incorporating cysteamine and penicillamine, followed by nitrosation via nitrous acid.¹² These materials delivered a range of 0.04-2.28 μmol NO and the degradation rates of the non-nitrosated polymers ranged from 0-100% degradation within 10 weeks. However, acidic conditions associated with the nitrosation process resulted in premature hydrolysis of the polymer. Discussion of the different release rates of NO from the materials largely included the monomer composition and degree of cross-linking due to the curing temperature employed. Further, the amount of NO loaded into the polymer initially was assumed to be the amount of NO recovered, and no characterization of the *S*-nitrosation process was included. The latter assumption is common in the field of NO releasing polymers and a thorough characterization of the extent of NO loading separate from the NO release data has not been previously reported. Zhao *et al.* have reported the synthesis of biodegradable elastomers containing secondary amines that were reacted to form *N*-diazoniumdiolate NO donor moieties.¹¹ The materials exhibited 20% weight loss after 6 weeks in buffer, indicating biodegradation, and preliminary studies indicated cell compatibility. However, NO release was indirectly assessed using the Griess assay for nitrite determination and the formation of the NO donor moiety was not characterized. Our research group recently reported on a synthetic method in which a poly(lactic-*co*-glycolic-*co*-hydroxymethyl propionic acid) (PLGH) polymer was modified to contain a pendant thiol.¹³ Upon nitrosation with *t*-butyl nitrite under non-aqueous conditions, we were able to load NO onto the modified polymer backbone while avoiding hydrolysis of the polymer linkages to maintain the polymer integrity.

Herein, we describe the incorporation of a variety of thiols as pendant groups on a modified PLGH polymer, which undergo nitrosation in non-aqueous conditions. The main impact of this work involves the ability to tune the extent of NO loading and recovery based

upon the thiol pendant to the polymer backbone and its functional environment. The thiol structure and extent of incorporation is related to the properties of the resulting material. Moreover, multiple and independent analytical methodologies were adapted and developed to quantify the extent of NO loading as well as NO recovery that corresponds to RSNO decomposition. By considering the loading and recovery processes separately, we can quantify the % NO recovery based upon the amount that was loaded onto the material initially as opposed to only directly quantifying the NO recovery. The ability to exert control over the thiol structure, extent of incorporation and the subsequent nitrosation is crucial to the resulting range of NO release kinetics that are yielded. The functional utility of these materials is demonstrated since these non-toxic polymers release NO under physiological conditions and can be prepared as electrospun nanofibers, commonly used in tissue and bone regeneration applications.¹⁴ Overall, the synthesis of a class of *S*-nitrosated biodegradable polymers is described that allows for control over the incorporation of the thiol moiety, resulting in materials that can be tailored for NO storage and kinetically controlled NO delivery.

4.3 EXPERIMENTAL SECTION

4.3.1 Materials. *N*-hydroxysuccinimide (NHS) and *t*-butyl nitrite were purchased from Acros Organics (Morris Plains, NJ, USA), disodium ethylenediamine tetraacetate dihydrate (EDTA disodium salt), *N,N*-dimethylformamide (DMF) and phosphate buffered saline (PBS) were from EMD Chemicals (Gibbstown, NJ, USA) and tetrahydrofuran (THF) was from Mallinckrodt Chemicals (Phillipsburg, NJ, USA). All other chemicals were procured from Sigma-Aldrich (St. Louis, MO, USA). Dry dichloromethane (DCM) was prepared by refluxing over calcium hydride

for 1 h; constant boiling fractions were collected and stored over 4 Å molecular sieves under N₂. Anhydrous DMF was stored after purchase over 4 Å molecular sieves under N₂.

4.3.2 Preparation of *S*-nitrosated PLGH copolymers. The method previously reported for the preparation of the (a) cysteamine-modified PLGH polymer¹³ was extended for the incorporation of (b) cysteine, (c) homocysteine, (d) glutathione, and (e) penicillamine. The polymer synthesis was performed by Dr. Vinod Damodaran, and the full details can be found in the original *J. Mater. Chem.* manuscript.¹⁵ Briefly, a carboxyl functionalized multiblock polymer was initially prepared via ring opening polymerization of lactide (LA), glycolide (GL), and hydroxymethyl propionic acid (HMPA) monomers. Post-synthetic modification allowed for the incorporation of pendant thiol groups. Subsequent *S*-nitrosation with *t*-butyl nitrite resulted in the formation of the RSNO moiety.

Nitrosation of the thiol sites within each polymer was accomplished by dissolving 50 mg of polymer in 2 mL of 2 methanol: 1 dichloromethane in an amber colored EPA vial (Fisher Scientific). In a separate vial, 1 mL of 2 methanol: 1 dichloromethane was added to 8.4 mg of *t*-butyl nitrite, where the *t*-butyl nitrite solution was then added to the polymer solution. The polymer solution was stirred and protected from light for a fixed period of time (4 h for the cysteamine (**1a**) and homocysteine (**1c**) derivatives, 8 h for the cysteamine (**1b**) derivative), after which time the polymer was isolated under vacuum by removal of excess *t*-butyl nitrite and solvent. The general structures of the thiolated and nitrosated polymers are shown in Figure 4.2.

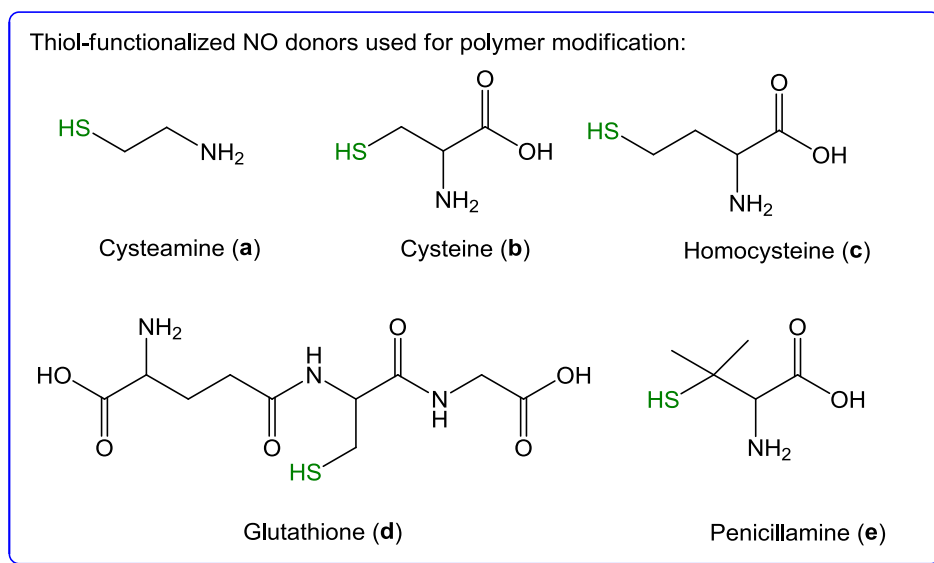
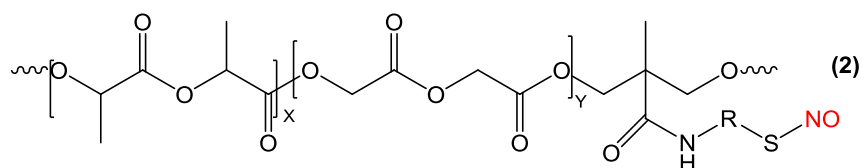
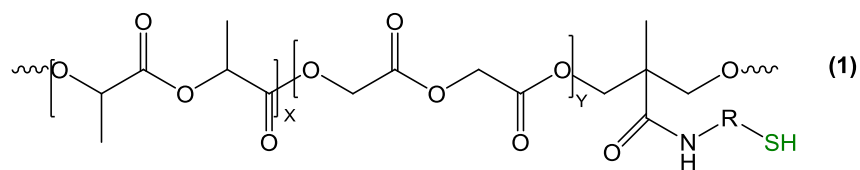


Figure 4.2 To assess the impact of the thiol pendant on the properties of the resulting polymers, different structurally unique thiols were incorporated onto the PLGH copolymer (1), followed by *S*-nitrosation to yield NO releasing biodegradable polymers (2).

4.3.3 Characterization of PLGH derivatives.

Thiol incorporation. To assess the formation of PLGH and the subsequent incorporation of each thiol (1), ^1H NMR spectra of the polymer samples were recorded in CDCl_3 using a Varian Inova 400 MHz FT-NMR (Varian NMR Systems, Palo Alto, CA, USA). To further evaluate the functionalization of PLGH and the thiolated derivatives, FTIR-ATR spectra were recorded for

solid polymer samples in the range of 600-4000 cm^{-1} using a Nicolet 6700 (Thermo Electron Corporation Madison, WI, USA).

Nitrosation of pendant thiols. To characterize formation of the final *S*-nitrosated products (**2**), UV-vis spectroscopy was employed. UV absorbance studies were performed using a Nicolet Evolution 300 spectrophotometer (Thermo Electron Corporation). All samples were dissolved in anhydrous 2 methanol: 1 dichloromethane solvent and protected from light for solution-phase UV measurements ($n \geq 3$). The UV absorbance was assessed before and after NO release studies were performed to assess the % donor decomposition.

Molecular weight. The number average molecular weight (M_n) and polydispersity index (PDI) values of each sample were measured via gel permeation chromatography (GPC) using a Waters University 1500 GPC (Waters, Milford, MA, USA). A chloroform eluent was employed at a flow rate of 1.0 mL min^{-1} and values were calculated relative to PMMA standards after chromatogram processing via Waters Empower software (version 2002).

Thermal properties: Decomposition (T_d) and glass transition (T_g) temperatures. The thermal properties of PLGH and each thiol derivative were determined by thermal gravimetric analysis (TGA) and differential scanning calorimetry (DSC). TGA analysis (TGA 2950, TA Instruments, New Castle, DE, USA) was performed by heating each polymer sample up to 500 $^{\circ}\text{C}$ at a heating rate of 10 $^{\circ}\text{C min}^{-1}$, thereby yielding heat decomposition temperatures (T_d). DSC experiments employed sealed hermetic aluminum pans (DSC model 2920, TA Instruments) in which samples were heated up to 200 $^{\circ}\text{C}$ (10 $^{\circ}\text{C min}^{-1}$) followed by a 2 min isothermal period and subsequent

cooling to 25 °C (10 °C min⁻¹) during the first cycle. The second cycle involved an initial isotherm (-10 °C for 2 min) followed by a heating period to 150 °C (10 °C min⁻¹) to determine the glass transition temperature (T_g).

Morphology. Small angle X-ray scattering (SAXS, Rigaku S-Max 3000 High Brilliance three pinhole system) was used to evaluate the morphology of each PLGH-thiol derivative. Components of the system included a MicroMax-007HFM rotating anode (CuKR), Confocal Max-Flux Optic, Gabriel multiwire area detector, and a Linkam thermal stage. Samples were sandwiched between Kapton[®] discs and placed into the SAXS instrument for a 7200 s exposure time. The data was assessed for the presence of lamellar peaks to determine the degree of crystallinity.

4.3.4 Characterization of PLGH derivatives for bioapplications. Additional studies were performed to describe the feasibility of the materials for biomedical applications. Polymer degradation studies were performed by Dr. Vinod Damodaran, surface wettability was determined by Sarah Lantvit and the polymers were processed into electrospun nanofibers by Kate Wold. The full details regarding these analyses are outside the scope of this dissertation and are presented in full in the original *J. Mater. Chem.* manuscript.¹⁵ Briefly, polymer degradation studies were performed in 1 week increments for up to 6 weeks total of soaking in PBS (pH 7.4) 37 °C. Cytotoxicity studies were performed on the thiolated PLGH derivatives according to International Organization for Standardization (ISO-10993-5: *Biological Evaluation of Medical Devices, Part 5: Tests for In Vitro Cytotoxicity*) at NAMSA (Northwood, OH, USA). In addition

to biodegradation and cytotoxicity studies, the PLGH derivatives were electrospun into nanofiber networks and characterized via scanning electron microscopy.

4.3.5 Nitric oxide analysis. NO release profiles associated with the nitrosated PLGH derivatives were collected via chemiluminescent NO detection using NO analyzers (NOA, Sievers 280i, GE Analytical, Boulder, CO, USA). Each NOA was calibrated before each analysis using nitrogen as the zero gas and a 45 ppm NO gas. NO release from each *S*-nitrosated polymer sample was analyzed in deoxygenated 10 mM PBS (pH 7.4) at 37 °C, shielded from direct exposure to light. Measurements were recorded in triplicate at a data interval of 5 sec at a flow rate of 200 mL min⁻¹ with a cell pressure of 9.7 Torr and an oxygen pressure of 6 psi.

4.4 RESULTS & DISCUSSION

4.4.1 Influence of thiol incorporation on polymer properties. A relatively straightforward synthetic strategy was adopted to prepare a series of thiolated PLGH polymers that allowed for a thorough investigation of the effect of thiolation on the chemical and physical attributes of the NO releasing polymers. The structures of the different thiolated polymers are shown in Figure 4.2. Key to this post-polymerization modification is the use of non-aqueous reaction conditions to prevent any possible polymer degradation during the nitrosation step. A number of thiol-functionalized amino acids such as cysteine, homocysteine, glutathione and penicillamine as well as the simplest stable aminothiols, cysteamine, were chosen as suitable thiol candidates because of their unique structural differences. For all thiol modifications, the composition of the PLGH backbone was held constant at 85% lactide, 10% glycolide and 5% HMPA by weight. To assess the post-synthetic modification of the PLGH backbone and the subsequent incorporation of each

thiol, ^1H NMR, FTIR-ATR, GPC and elemental analysis of the thiolated derivatives were performed.

Extent of thiol incorporation. As described in the original manuscript, the polymer structure and subsequent thiol incorporation was confirmed using FT-IR and ^1H NMR methods. Complete ^1H NMR and IR spectra were collected by Dr. Vinod Damodaran and are presented in the original *J. Mater. Chem.* manuscript.¹⁵ Preservation of the polymer backbone was indicated by the strong absorbance feature at 1752 cm^{-1} arising from the ester carbonyl group, while absorbance bands at 1180 , 1126 and 1083 cm^{-1} correspond to C-O-C stretching from the ester linkages for both the PLGH and PLGH-thiol derivatives (**1**). Incorporation of the thiol derivative onto the polymer backbone through an amide linkage was confirmed from the absorbance band at 1649 cm^{-1} due to amide carbonyl groups.

Quantification of the extent of thiol incorporation was performed by integrating the NMR intensities of the thiol protons and those of the PLGH backbone. The ratio of the average NMR proton intensities between the corresponding thiol protons with that from the HMPA segment of the polymer backbone gives the extent of thiol modification to the polymers. Overall, cysteamine demonstrated the largest extent of thiol incorporation based upon the available -COOH groups (>90%), followed by cysteine (63%) and homocysteine (29%). Glutathione and penicillamine were not successfully added to the polymer under the reaction conditions employed. The extent of thiol incorporation is summarized in Table 4.1.

Table 4.1 Polymer characterization summary of PLGH and thiol derivatives

PLGH derivative	Thiol modification ^(a)		MW profile ^(b)		Thermal properties	
	mmol SH g ⁻¹	% based on COOH ^(e)	M_n g mol ⁻¹	PDI	T_d ^(c) °C	T_g ^(d) °C
PLGH	-	-	4400 ± 700*	1.39 ± 0.06*	219 ± 1*	40.5 ± 0.5*
Cysteamine (1a)	0.57 ± 0.03	92	5500 ± 700*	1.49 ± 0.04*	272 ± 3	25.0 ± 0.4*
Cysteine (1b)	0.39 ± 0.02	63	5600 ± 830	1.50 ± 0.06	263 ± 5	34.4 ± 0.9
Homocysteine (1c)	0.18 ± 0.05	29	6540 ± 175	1.42 ± 0.03	258 ± 2	28.6 ± 0.7

Values Determined by ^(a)integration of ¹H NMR proton peak, ^(b)GPC, ^(c)TGA and ^(d)DSC

^(e)All % conversion values are based upon 0.62 ± 0.05 mmol COOH g⁻¹ polymer associated with the PLGH

*V. B. Damodaran and M. M. Reynolds, *J. Mater. Chem.* 2011, **21**, 5870.

Impact of thiol on polymer properties. The full manuscript also describes the characterization of the molecular weight (MW) profiles and thermal properties associated with PLGH and its thiolated derivatives, which are shown in Table 4.1. Overall, the MW profiles of the polymers studied via GPC analysis indicated no significant differences in the number average MW (M_n) or polydispersity index (PDI) as a function of thiol incorporation. This is expected given that the same PLGH composition was used for each post-synthetic thiol derivatization. These data also suggest that slight-to-no cross-linking occurred as a result of disulfide bond formation under the conditions of the derivatization reaction. All polymers exhibited similar PDI values and fair MW distribution.

The thermal properties of the thiolated PLGH polymers were measured via TGA and DSC analysis and are also summarized in Table 4.1. From TGA, all modified polymers presented a one-step decomposition profile for the parent as well as thiolated polymers. The heat decomposition temperature (T_d) of each thiolated polymer was comparatively higher than that of the unmodified polymer, indicating a stabilization of the polymer matrix by cross-linking via disulfide bridging. Unlike the minimal disulfide formation indicated by MW analysis, disulfide formation will increase significantly with the increasing temperatures associated with TGA

analysis. Cross-linking stabilization is further supported due to the T_d of PLGH-cysteamine (**1a**), which is higher compared to the other derivatives due to a greater extent of thiol groups capable of disulfide formation. The glass transition temperatures (T_g) were determined using DSC following a heat-cool-heat cycle and the midpoint of the transition from the second cycle was taken as the T_g of the sample. The T_g values suggest an amorphous structure for all polymers at room temperature. The observed T_g values associated with the thiol-modified polymers are lower than that of the unmodified polymer, indicating an increase in randomness in the polymer lattice from the introduction of thiol functionalities on the HMPA segment of the polymer.

Morphological structure is important in the eventual use of polymers in medical applications. As such, we were also interested in the effect of thiolation on the crystallinity of the modified PLGH materials. Using SAXS, we found that the thiol derivatives presented a diffusion of the scattering curves in all cases without reaching any scattering maximum. Consequently, the absence of any characteristic lamellar peaks in these profiles confirms a lack of cluster structures in the polymer lattice, suggesting a disordered microstructural array.¹³ Thus, the incorporation of the thiol groups did not significantly impact the morphological structure of the polymer.

4.4.2 NO storage and delivery as a function of thiol structure.

Characterizing S-nitrosation. To efficiently load S-nitrosothiol moieties onto the thiolated polymers, a non-aqueous nitrosation methodology was adopted that allowed for removal of the nitrosating agent, thereby eliminating the possibility of non-thiol bound NO release from the final material. The S-nitrosated polymers were characterized by the distinctive RSNO UV absorbance band at 335-338 nm. Figure 4.3 demonstrates the appearance of the absorbance

feature after nitrosation for each PLGH derivative compared to the non-nitrosated thiolated polymer.

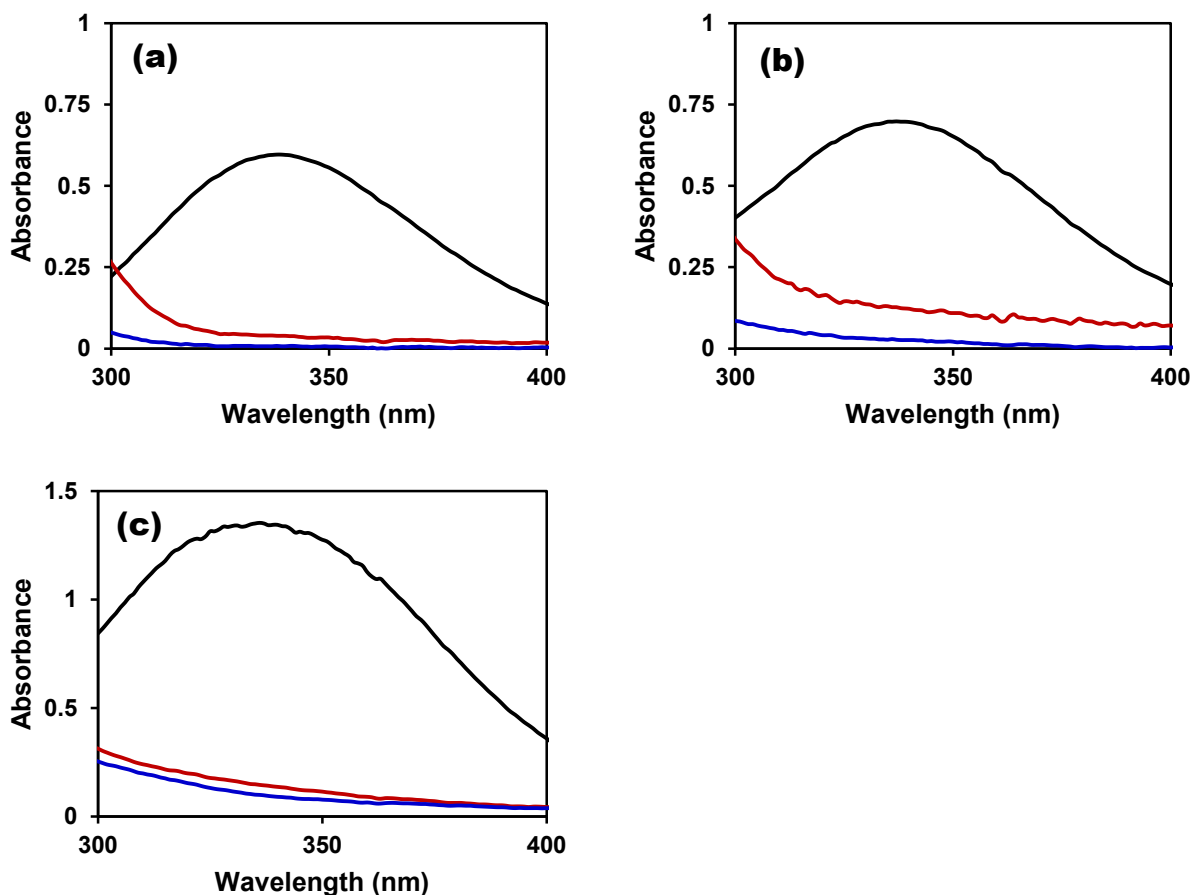


Figure 4.3 Representative absorbance spectra for (a) cysteamine (1.5 mg mL⁻¹), (b) cysteine (4 mg mL⁻¹) and (c) homocysteine (20 mg mL⁻¹) dissolved in 2 methanol: 1 dichloromethane for freshly *S*-nitrosated samples (black), samples after NOA analysis (red) and non-nitrosated control samples (blue).

Optimal nitrosation time determination. To determine the nitrosation time required for optimal NO loading, the formation of the *S*-nitrosated product was monitored via the respective λ_{\max}

(338, 335, and 336 nm for the cysteamine (**2a**), cysteine (**2b**), and homocysteine (**2c**) derivative, respectively). The extent of nitrosation over time for each thiolated PLGH derivative was influenced by the thiol pendant of choice. Figure 4.4 summarizes the kinetics of RSH conversion to RSNO, determined by monitoring the λ_{max} of each *S*-nitrosated polymer as a function of nitrosation time. The highest extent of *S*-nitrosation occurred at 4 h for PLGH-cysteamine (**1a**) and PLGH-homocysteine (**1c**). Extending the nitrosation time past 4 h, however, resulted in a lesser extent of *S*-nitrosation, likely due to product instability in the solvent system under the given reaction conditions. Thus, preparation of *S*-nitrosated PLGH-cysteamine (**2a**) and PLGH-homocysteine (**2c**) involved a 4 h reaction time with *t*-butyl nitrite. However, Figure 4.4 demonstrates a slower rate of NO loading for PLGH-cysteine (**1b**), requiring 8 h with a comparatively lower yield under similar reaction conditions.

Determination of molar extinction coefficient values and thermal NO recovery. To determine a molar extinction coefficient value (ϵ_{max}) associated with the λ_{max} of each *S*-nitrosated PLGH derivative, an absorbance analysis was performed. The ϵ_{max} is required to correlate the absorbance value at the λ_{max} to a concentration of RSNO moiety. Because the ϵ_{max} is dependent on the environment around the *S*-nitrosothiol moiety, the ϵ_{max} specific to each polymer was determined.

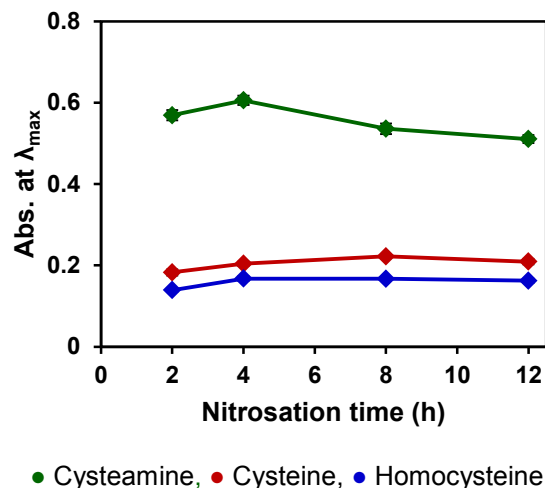


Figure 4.4 *S*-nitrosation reaction kinetics associated with the absorbance value at the λ_{\max} (338 nm for PLGH-cysteamine, **2a**; 335 nm for PLGH-cysteine, **2b**; and 336 nm for PLGH-homocysteine, **2c**) as a function of nitrosation time.

A series of freshly *S*-nitrosated polymer solutions were prepared in a concentration range of 0-1.75, 0-4.0, and 0-10.0 mg polymer mL⁻¹ (2 methanol: 1 dichloromethane solvent) for cysteamine (**2a**), cysteine (**2b**), and homocysteine (**2c**) derivatives, respectively. The calibration curves shown in Figure 4.5 indicate the absorbance values at the λ_{\max} as a function of polymer concentration for each derivative. The absorbance values for the non-nitrosated samples were taken to be the 0 mg mL⁻¹ point on each calibration curve.

To determine the ϵ_{\max} value from the slope of the Beer's Law plot ($A=\epsilon bc$ where b is a pathlength of 1 cm and c is the concentration of RSNO in mol L⁻¹), the polymer concentration values (mg mL⁻¹) were converted to mol RSNO L⁻¹, where the conversion factor of mol NO g⁻¹ was determined via thermal analysis. Thermal analysis was performed to determine the extent of NO recovery from each nitrosated derivative, where samples were directly heated under dry conditions in a step-wise manner (37-100 °C) until baseline reading was reached on the NOAs.

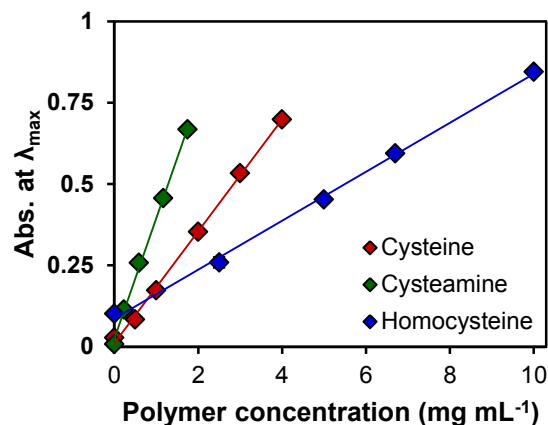


Figure 4.5 Absorbance at 338 nm, 335 nm and 336 nm as a function of polymer concentration where the linear regression analysis yielded a slope of 0.372, 0.172, and 0.075 mL mg⁻¹ for the cysteamine (**2a**), cysteine (**2b**), and homocysteine (**2c**) PLGH derivatives, respectively. All calibration curves yielded an $R^2 \geq 0.998$ with relative % error values of $\leq 2\%$ associated with each absorbance value.

It was necessary to determine the % RSNO decomposition that corresponded to the amount of NO recovered from each material, since it cannot be assumed that the recovered NO corresponds to 100% of the NO reservoir within the material since some residual absorbance is present after NO recovery. To determine the % RSNO decomposition, freshly *S*-nitrosated polymer solutions were prepared for UV absorbance analysis at a concentration of 1.5, 4, and 20 mg mL⁻¹ for cysteamine (**2a**), cysteine (**2b**) and homocysteine (**2c**), respectively. After the NOA thermal decomposition analysis, each material was recovered and dissolved to the same concentration as the freshly *S*-nitrosated sample. The absorbance values at the λ_{max} before and after RSNO decomposition determined the % RSNO decomposition relative to a blank non-nitrosated sample (*i.e.* the blank sample represented 100% decomposition while the freshly *S*-nitrosated sample represented 0% decomposition; the % decomposition of the RSNO after NOA

analysis was determined accordingly). The % decomposition of each nitrosated derivative can be visualized according to the spectra shown in Figure 4.3.

Table 4.2 indicates the amount of NO recovered via thermal NO analysis, where the % decomposition associated with the absorbance feature after NO release, as well as the ϵ_{\max} corresponds to the indicated λ_{\max} for each derivative. The ϵ_{\max} value for each derivative was determined from the slope of the Beer's Law plot shown in Figure 4.6, where the error bars associated with the ϵ_{\max} values were determined by performing a linear regression analysis to find the error in the slope.

Table 4.2 The NO recovery associated with the thermal degradation of the RSNO moiety, the % decomposition of the absorbance feature and the corresponding ϵ_{\max} value for the λ_{\max} corresponding to each nitrosated PLGH derivative.

<i>S</i> -nitrosated polymer derivative	NO recovered ($\times 10^{-4}$ mol g ⁻¹) ^a	λ_{\max} (nm)	% RSNO decomposition	ϵ_{\max} (M ⁻¹ cm ⁻¹)
Cysteamine (2a)	4.61 ± 0.36	338	94.9 ± 2.5	766.0 ± 19.7
Cysteine (2b)	1.68 ± 0.19	335	86.2 ± 0.2	882.9 ± 18.2
Homocysteine (2c)	1.11 ± 0.08	336	95.9 ± 0.6	652.1 ± 16.7

^aNO recovery corresponds to the thermal RSNO degradation studies performed under dry conditions.

The ϵ_{\max} value was determined for each nitrosated PLGH derivative instead of using the literature reported ϵ_{\max} values corresponding to the small molecule *S*-nitrosothiol since the electronic environment for the S-NO moiety is different for the polymer versus the small molecule case. Table 4.3 highlights the differences in the λ_{\max} and ϵ_{\max} values for each polymer derivative compared to the small molecule analogue. In order to appropriately quantify the starting *S*-nitrosothiol concentration for each nitrosated PLGH derivative, the appropriate ϵ_{\max} was required.

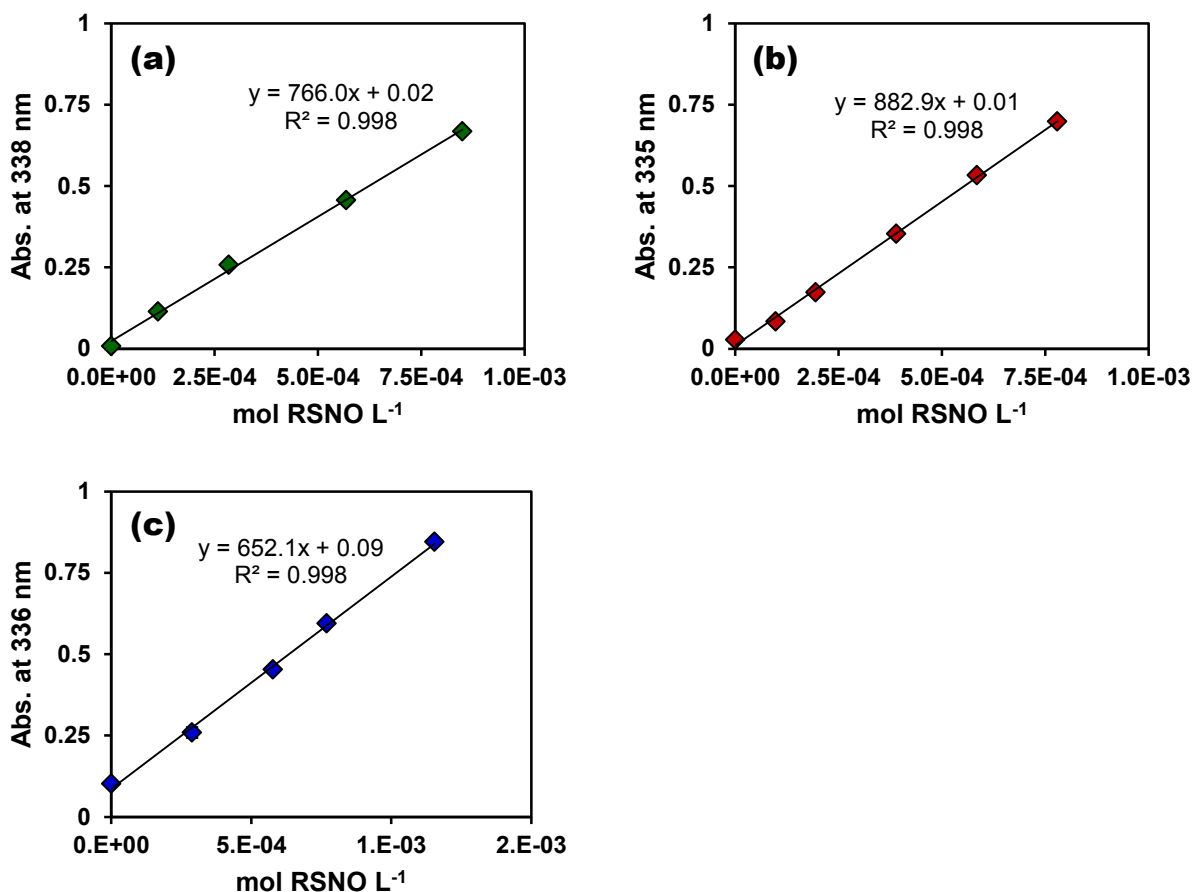


Figure 4.6 The Beer's Law plots are shown for (a) the cysteamine derivative, **2a**; (b) the cysteine derivative, **2b**; and (c) the homocysteine derivative, **2c**. At each point, the error bars are smaller than the size of the data point.

Table 4.3 Molar extinction coefficients for nitrosated cysteamine, cysteine and homocysteine small molecules compared to the nitrosated PLGH derivatives.

<i>S</i> -nitroso small molecule	λ_{\max} (nm)	ϵ_{\max} ($M^{-1}cm^{-1}$)	<i>S</i> -nitrosated polymer derivative	λ_{\max} (nm)	ϵ_{\max} ($M^{-1}cm^{-1}$)
Cysteamine ^a	333	793	Cysteamine (2a)	338	766.0 ± 19.7
Cysteine ^b	334	900	Cysteine (2b)	335	882.9 ± 18.2
Homocysteine ^c	333	740	Homocysteine (2c)	336	652.1 ± 16.7

^aB. Roy, A. du Moulinet d'Hardemare and M. Fontecave, *J. Org. Chem.* 1994, **59**, 7019.

^b(i) T. M. Greco, R. Hodara, I. Parastatidis, H. F. G. Heijnen, M. K. Dennehy, D. C. Liebler, and H. Ischiropoulos, *Proc. Natl. Acad. Sci. USA*, 2006, **103**, 7420; (ii) M. John Dennis, R. Davies, and D. J. McWeeny, *J. Sci. Food Agric.* 1979, **30**, 639.

^cM. P. Gordge, J. S. Hothersall and A. A. Noronha-Dutra, *Brit. J. Pharmacol.* 1998, **124**, 141.

Quantifying S-nitrosothiol content for PLGH derivatives. Once the ϵ_{\max} value was determined for each nitrosated PLGH derivative, the initial RSNO content was determined based upon the initial absorbance value for each derivative. Table 4.4 summarizes the mmol of SNO formed per g polymer, indicating nearly complete RSH conversion to RSNO for PLGH-homocysteine (**2c**) and PLGH-cysteamine (**2a**) within 4 h. PLGH-cysteine (**2b**), however, experiences less than 50% nitrosation of thiol sites within an 8 h period. When considering the structure of each polymer, it can be seen that PLGH-homocysteine (**1c**) experiences the thiol site furthest away from either the polymer backbone or a carboxyl group, thus minimizing steric hindrance and allowing thiol contact with the nitrosating agent to occur. PLGH-cysteine (**1b**) does not experience steric hindrance from a carboxyl group on the pendant thiol; however, the thiol group is closer to the polymer chain than in the case of the homocysteine derivative (**1c**), resulting in a slightly lesser extent of conversion when compared to PLGH-homocysteine (**1c**). The cysteine derivative (**1b**) experiences the smallest extent of thiol conversion to RSNO in the longest period of time due to steric hindrance of the neighboring carboxyl group and the polymer backbone.

Table 4.4 Summary of NO loading efficiency for each nitrosated PLGH derivative.

<i>S</i> -nitrosated polymer derivative	mmol RSNO g ⁻¹	% NO loaded ^a
Cysteamine (2a)	0.53 ± 0.01	93 ± 3
Cysteine (2b)	0.17 ± 0.01	43 ± 1
Homocysteine (2c)	0.17 ± 0.01	96 ± 3

^aThe NO loading efficiency was determined by considering the amount of RSNO that formed during nitrosation relative to the amount of thiol available in the polymer.

Nitric oxide recovery under aqueous conditions. To determine the release of NO from each nitrosated PLGH derivative under simulated physiological conditions, polymer films (mass ~4-6

mg, thickness ~10 mm) were prepared on pre-cleaned glass slides by spin-coating the corresponding polymer solution in anhydrous dichloromethane, protected from light.

NO release profiles over 48 h, as well as the initial 5 h window, are shown in Figure 4.7. For comparison, the NO flux associated with the natural endothelium (EC, 0.5×10^{-10} mol cm⁻² min⁻¹) is included.¹⁶ It can be seen that the homocysteine derivative (**2c**) releases a quick burst of NO within the first hour, followed by a nearly steady release of NO below that of the EC. The flux of homocysteine (**2c**) remains significantly lower than that of cysteine (**2b**) or cysteamine (**2a**) past the first hour of analysis, indicating a greater stability of the *S*-nitrosated homocysteine moiety. The behavior of the cysteine (**2b**) and cysteamine (**2a**) derivatives is significantly different as both polymers release an increasing NO flux for the first hour, followed by a gradual decay over the remaining 48 h. For both polymer derivatives, at nearly 25 h, the NO flux reaches below the EC. The characteristic and controlled NO release profiles associated with the cysteine (**2b**) and cysteamine (**2a**) derivatives may be an added advantage in designing particular biomedical devices.

A summary of NO release from each polymer derivative under physiological conditions is given in Table 4.5. It is interesting to note that a higher extent of thiol conversion to *S*-nitrosothiol was observed with the cysteamine (**2a**) and homocysteine (**2c**) derivatives (nearly 100%, see Table 4.4), and a greater % NO recovery was achieved with the cysteine (**2b**) modified polymer under physiological conditions. Near-complete release of the available NO was achieved with the *S*-nitrosated PLGH-cysteine (**2b**) polymer within 48 h under physiological conditions. However, only half of the available NO was released by the cysteamine (**2a**) and less than 25% was released by the homocysteine (**2c**) analogues under the same conditions. These relative differences in the extent of NO release can be attributed to variation in the stability of the

S-nitrosated species and also due to the influence of neighboring groups. Considering that the trend of % NO recovery follows cysteine > cysteamine > homocysteine, the trend involving stability of the *S*-nitrosated polymer must follow the opposite trend (which is also supported by the NO release profiles).

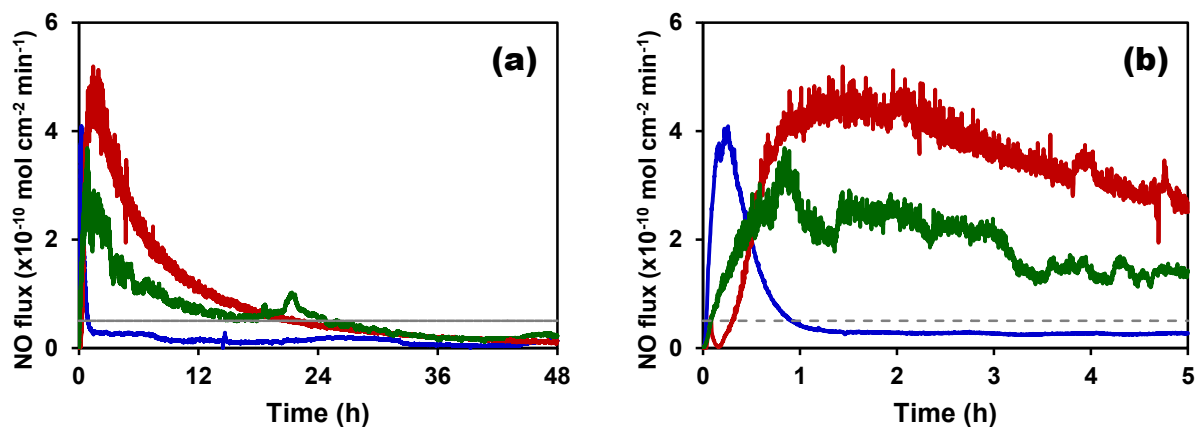


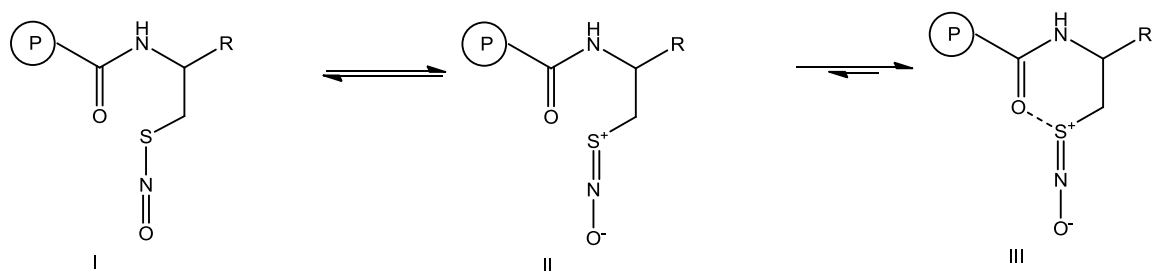
Figure 4.7 Representative NO release profiles for each nitrosated PLGH derivative (homocysteine (**2c**) in blue, cysteine (**2b**) in red and cysteamine (**2a**) in green). (a) Polymer thin films were exposed to phosphate buffered saline soaking conditions at a physiological pH of 7.4 and temperature of 37 °C for (a) 48 h. (b) To highlight the initial NO release profiles, the first 5 h of analysis is shown. For comparison, the lower-limit NO flux released by the natural endothelium is indicated by the dashed line.

Table 4.5 Summary of NO release from various polymers under physiological conditions.

<i>S</i> -nitrosated polymer derivative	mmol RSNO g ⁻¹	% NO recovery ^a
Cysteamine (2a)	0.241 ± 0.004	46 ± 1
Cysteine (2b)	0.155 ± 0.009	93 ± 5
Homocysteine (2c)	0.033 ± 0.007	20 ± 4

^aThe NO recoveries were determined by considering the amount of NO that was recovered over 48 h relative to the amount of RSNO available in the polymer.

The relative stabilities of the different *S*-nitrosated PLGH derivatives can be explained through electronic and steric effects. The thiol residues could be stabilized by a 6-membered ring intermediate, wherein a resonance form results in a double bond between the S and N of the SNO moiety, which will strengthen the S-N bond and minimize the SNO decomposition via homolytic cleavage.¹⁷ PLGH-cysteamine (**2a**) and PLGH-cysteine (**2b**) involve a ring intermediate wherein the S atom containing the NO moiety interacts with the carbonyl of the amide linkage that holds the thiol to the polymer backbone (Figure 4.8). Resonance of the SNO moiety results in a positive charge on the S that strongly interacts with the slightly negative carbonyl group, thus stabilizing the intermediate state. However, in the case of cysteine (**2b**), there is a nearby electron withdrawing carboxyl group on the thiol pendant that can decrease the electron density on the carbonyl group, thus decreasing the charge interaction of the S and the carbonyl O. Also, the pi bond of the S=N that is formed can be delocalized over the electron withdrawing carboxyl group, minimizing the strength of the S-N bond. This results in an increased instability of the intermediate, making homolytic cleavage of the S-NO bond more likely to occur as the cysteine derivative (**2b**) was seen to be the least stable. The homocysteine derivative (**2c**) forms a different ring intermediate, involving interaction of the carboxyl group O from the thiol pendant with the S housing the NO moiety (Figure 4.9). The strong electron withdrawing nature of the double bonded carboxyl O results in a strong partial negative charge that interacts with the S, therefore increasing the stability of the intermediate and leading the smallest amount of S-NO cleavage compared to the other derivatives.



where R = H for cysteamine and COOH for cysteine

Figure 4.8 Stabilization of the *S*-nitrosated cysteamine (**2a**) and cysteine (**2b**) derivatives may be attributed to a 6-membered ring intermediate.

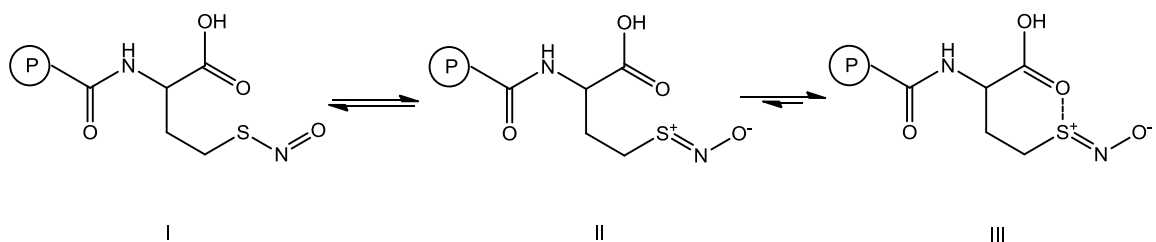


Figure 4.9 Stabilization of the *S*-nitrosated homocysteine derivative (**2c**) may be due to a 6-membered ring intermediate.

4.4.3 Feasibility for biomaterial applications.

In the original manuscript, a thorough description was included of the surface wettability, biodegradation profiles, and cytotoxicity assessment, as well as the preliminary development of nanofibers to serve as biomedical scaffolds.¹⁵ For the purposes of this dissertation, these studies will be described only briefly since they were not performed by this author. Overall, these studies demonstrated the potential for the use of these nitrosated PLGH materials to be processed into non-toxic, NO releasing scaffolds with predictable biodegradation behavior.

The surface properties of the PLGH thin films were characterized by a water contact angle between 75-80°; however, no other surface analyses were performed. Simulated biodegradation studies in PBS predicted complete degradation of the material over nearly 40 weeks for PLGH-cysteamine (**1a**), 30 weeks for PLGH-cysteine (**1b**) and 20 weeks for PLGH and PLGH-homocysteine (**1c**) polymer derivatives. According to the ISO 10993-5 cytotoxicity elution method, all thiolated PLGH derivatives received a reactivity grade score of 0, corresponding to no cytotoxicity, cell lysis or reduction of cell growth associated with the polymer material. Preliminary processing studies demonstrated that the nitrosated materials can be effectively electrospun into nanofibers and still maintain the majority of their NO releasing capabilities.

4.5 CONCLUSIONS

A series of new thiolated PLGH polymers were synthesized and extensively characterized that allowed for tunable NO loading and recovery efficiencies based upon the thiol that was incorporated. Employing advanced methods, we were able to quantify the NO donor moiety incorporation to enable % NO loading calculations. Additionally, the NO release parameters could be determined in terms of % NO recovery. This approach provides new insights for designing suitable materials with predictable and tailorable kinetics of NO release for medical applications. The nature of the thiol tether was found to greatly influence the overall properties of the polymer, including NO storage as well as the resulting NO release properties. These *S*-nitrosated PLGH derivatives represent progress towards the development of processable biodegradable NO releasing polymeric nanofibers for biomedical applications.

CHAPTER 4 REFERENCES

1. Ulery, B. D.; Nair, L. S.; Laurencin, C. T., Biomedical Applications of Biodegradable Polymers. *J. Polym. Sci., Part B: Polym. Phys.* **2011**, *49*, 832-864; Kroeze, R. J.; Helder, M. N.; Govaert, L. E.; Smit, T. H., Biodegradable Polymers in Bone Tissue Engineering. *Materials* **2009**, *2*, 833-856; Navarro, M.; Michiardi, A.; Castaño, O.; Planell, J. A., Biomaterials in Orthopaedics. *J. R. Soc., Interface* **2008**, *5*, 1137-1158.
2. Coulembier, O.; Degée, P.; Hedrick, J. L.; Dubois, P., From Controlled Ring-Opening Polymerization to Biodegradable Aliphatic Polyester: Especially Poly([beta]-malic acid) Derivatives. *Prog. Polym. Sci.* **2006**, *31*, 723-747; Kumbar, S. G.; Nukavarapu, S. P.; James, R.; Nair, L. S.; Laurencin, C. T., Electrospun Poly(lactic acid-co-glycolic acid) Scaffolds for Skin Tissue Engineering. *Biomaterials* **2008**, *29*, 4100-4107; Nair, L. S.; Bhattacharyya, S.; Bender, J. D.; Greish, Y. E.; Brown, P. W.; Allcock, H. R.; Laurencin, C. T., Fabrication and Optimization of Methylphenoxy Substituted Polyphosphazene Nanofibers for Biomedical Applications. *Biomacromolecules* **2004**, *5*, 2212-2220; Nukavarapu, S. P.; Kumbar, S. G.; Brown, J. L.; Krogman, N. R.; Weikel, A. L.; Hindenlang, M. D.; Nair, L. S.; Allcock, H. R.; Laurencin, C. T., Polyphosphazene/Nano-Hydroxyapatite Composite Microsphere Scaffolds for Bone Tissue Engineering. *Biomacromolecules* **2008**, *9*, 1818-1825; Su, Q.; Zhao, A.; Peng, H.; Zhou, S., Preparation and Characterization of Biodegradable Electrospun Polyanhydride Nano/Microfibers. *J. Nanosci. Nanotechnol.* **2010**, *10*, 6369-6375; Betz, M. W.; Modi, P. C.; Caccamese, J. F.; Coletti, D. P.; Sauk, J. J.; Fisher, J. P., Cyclic Acetal Hydrogel System for Bone Marrow Stromal Cell Encapsulation and Osteodifferentiation. *J. Biomed. Mater. Res., Part A* **2008**,

- 86A, 662-670; Welle, A.; Kröger, M.; Döring, M.; Niederer, K.; Pindel, E.; Chronakis, I. S., Electrospun Aliphatic Polycarbonates as Tailored Tissue Scaffold Materials. *Biomaterials* **2007**, *28*, 2211-2219; Macario, D. K.; Entersz, I.; Bolikal, D.; Kohn, J.; Nackman, G. B., Iodine Inhibits Antiadhesive Effect of PEG: Implications for Tissue Engineering. *J. Biomed. Mater. Res., Part B* **2008**, *86B*, 237-244; Asai, T.; Lee, M.-H.; Arrecubieta, C.; von Bayern, M. P.; Cespedes, C. A.; Baron, H. M.; Cadeiras, M.; Sakaguchi, T.; Marboe, C. C.; Naka, Y.; Deng, M. C.; Lowy, F. D., Cellular Coating of the Left Ventricular Assist Device Textured Polyurethane Membrane Reduces Adhesion of Staphylococcus Aureus. *J. Thorac. Cardiovasc. Surg.* **2007**, *133*, 1147-1153; Uttayarat, P.; Perets, A.; Li, M.; Pimton, P.; Stachelek, S. J.; Alferiev, I.; Composto, R. J.; Levy, R. J.; Lelkes, P. I., Micropatterning of Three-Dimensional Electrospun Polyurethane Vascular Grafts. *Acta Biomater.* **2010**, *6*, 4229-4237.
3. Smith, B. S.; Yoriya, S.; Grissom, L.; Grimes, C. A.; Popat, K. C., Hemocompatibility of Titania Nanotube Arrays. *J. Biomed. Mater. Res., Part A* **2010**, *95A*, 350-360; Stevens, M. M., Biomaterials for Bone Tissue Engineering. *Mater. Today* **2008**, *11*, 18-25.
 4. Furchgott, R. F., Endothelium-Derived Relaxing Factor: Discovery, Early Studies, and Identification as Nitric Oxide. *Angew. Chem., Int. Ed.* **1999**, *38*, 1870-1880; Ignarro, L. J.; Buga, G. M.; Wood, K. S.; Byrns, R. E.; Chaudhuri, G., Endothelium-Derived Relaxing Factor Produced and Released From Artery and Vein is Nitric Oxide. *Proc. Natl. Acad. Sci. USA* **1987**, *84*, 9265-9269; Luque Contreras, D.; Vargas Robles, H.; Romo, E.; Rios, A.; Escalante, B., The Role of Nitric Oxide in the Post-Ischemic Revascularization Process. *Pharmacol. Ther.* **2006**, *112*, 553-563; Gallo, O.; Fini-Storchi, I.; Vergari, W. A.; Masini,

- E.; Morbidelli, L.; Ziche, M.; Franchi, A., Role of Nitric Oxide in Angiogenesis and Tumor Progression in Head and Neck Cancer. *J. Natl. Cancer Inst.* **1998**, *90*, 587-596.
5. Hill, B. G.; Dranka, B. P.; Bailey, S. M.; Lancaster, J. R.; Darley-USmar, V. M., What Part of NO Don't You Understand? Some Answers to the Cardinal Questions in Nitric Oxide Biology. *J. Biol. Chem.* **2010**, *285*, 388-398; Massion, P. B.; Feron, O.; Dessy, C.; Balligand, J.-L., Nitric Oxide and Cardiac Function: Ten Years After, and Continuing. *Circ. Res.* **2003**, *93*, 388-398; Radomski, M. W., Nitric Oxide: Biological Mediator, Modulator and Effector. *Ann. Med.* **1995**, *27*, 321-329.
 6. Isenberg, J. S.; Ridnour, L. A.; Espey, M. G.; Wink, D. A.; Roberts, D. A., Nitric Oxide in Wound-Healing. *Microsurgery* **2005**, *25*, 442-451; Rizk, M.; Witte, M. B.; Barbul, A., Nitric Oxide and Wound Healing. *World J. Surg.* **2004**, *28*, 301-306.
 7. Wang, P. G.; Xian, M.; Tang, X.; Wu, X.; Wen, Z.; Cai, T.; Janczuk, A. J., Nitric Oxide Donors: Chemical Activities and Biological Applications. *Chem. Rev.* **2002**, *102*, 1091-1134.
 8. Al-Sa'doni, H. H.; Khan, I. Y.; Poston, L.; Fisher, I.; Ferro, A., A Novel Family of S-nitrosothiols: Chemical Synthesis and Biological Actions. *Nitric Oxide* **2000**, *4*, 550-560.
 9. Szacilowski, K.; Stasicka, Z., S-nitrosothiols: Materials, Reactivity and Mechanisms. *Prog. React. Kinet. Mech.* **2001**, *26*, 1-58; Williams, D. L. H., The Chemistry of S-nitrosothiols. *Acc. Chem. Res.* **1999**, *32*, 869-876.
 10. Mowery, K. A.; Schoenfish, M. H.; Saavedra, J. E.; Keefer, L. K.; Meyerhoff, M. E., Preparation and Characterization of Hydrophobic Polymeric Films that are Thromboresistant via Nitric Oxide Release. *Biomaterials* **2000**, *21*, 9-21; Coneski, P. N.; Schoenfish, M. H., Synthesis of Nitric Oxide-Releasing Polyurethanes with S-nitrosothiol-

- Containing Hard and Soft Segments. *Polym. Chem.* **2011**, *2*, 906-913; Parzuchowski, P. G.; Frost, M. C.; Meyerhoff, M. E., Synthesis and Characterization of Polymethacrylate-Based Nitric Oxide Donors. *J. Am. Chem. Soc.* **2002**, *124*, 12182-12191; Smith, D. J.; Chakravarthy, D.; Pulfer, S.; Simmons, M. L.; Hrabie, J. A.; Citro, M. L.; Saavedra, J. E.; Davies, K. M.; Hutsell, T. C.; Mooradian, D. L.; Hanson, S. R.; Keefer, L. K., Nitric Oxide-Releasing Polymer Containing the [N(O)NO]- Group. *J. Med. Chem.* **1996**, *39*, 1148-1156; Seabra, A. B.; Martins, D.; Simoes, M. M. S. G.; da Silva, R.; Brocchi, M.; de Oliveira, M. G., Antibacterial Nitric Oxide-Releasing Polyester for the Coating of Blood-Contacting Artificial Materials. *Artif. Organs* **2010**, *34*, E204-E214; Jun, H.; Taite, L. J.; West, J. L., Nitric Oxide-Producing Polyurethanes. *Biomacromolecules* **2005**, *6*, 838-844; Reynolds, M. M.; Saavedra, J. E.; Showalter, B. M.; Valdez, C. A.; Shanklin, A. P.; Oh, B. K.; Keefer, L. K.; Meyerhoff, M. E., Tailored Synthesis of Nitric Oxide-Releasing Polyurethanes Using O₂-protected Diazeniumdiolated Chain Extenders. *J. Mater. Chem.* **2010**, *20*, 3107-3114; Seabra, A. B.; Duran, N., Nitric Oxide-Releasing Vehicles for Biomedical Applications. *J. Mater. Chem.* **2010**, *20*, 1624-1637.
11. Zhao, H.; Serrano, M. C.; Popowich, D. A.; Kibbe, M. R.; Ameer, G. A., Biodegradable Nitric Oxide-Releasing Poly(diols citrate) Elastomers. *J. Biomed. Mater. Res., Part A* **2010**, *93A*, 356-363.
 12. Coneski, P. N.; Rao, K. S.; Schoenfisch, M. H., Degradable Nitric Oxide-Releasing Biomaterials via Post-Polymerization Functionalization of Cross-Linked Polyesters. *Biomacromolecules* **2010**, *11*, 3208-3215.
 13. Damodaran, V. B.; Reynolds, M. M., Biodegradable S-nitrosothiol Tethered Multiblock Polymer for Nitric Oxide Delivery. *J. Mater. Chem.* **2011**, *21*, 5870-5872.

14. Li, W. J.; Laurencin, C. T.; Caterson, E. J.; Tuan, R. S.; Ko, F. K., Electrospun Nanofibrous Structure: A Novel Scaffold for Tissue Engineering. *J. Biomed. Mater. Res.* **2002**, *60*, 613-621; Prabhakaran, M. P.; Venugopal, J.; Ramakrishna, S., Electrospun Nanostructured Scaffolds for Bone Tissue Engineering. *Acta Biomater.* **2009**, *5*, 2884-2893; Prabhakaran, M. P.; Ghasemi-Mobarakeh, L.; Ramakrishna, S., Electrospun Composite Nanofibers for Tissue Regeneration. *J. Nanosci. Nanotechnol.* **2011**, *11*, 3039-3057; Orlova, Y.; Magome, N.; Liu, L.; Chen, Y.; Agladze, K., Electrospun Nanofibers as a Tool for Architecture Control in Engineered Cardiac Tissue. *Biomaterials* **2011**, *32*, 5615-5624.
15. Damodaran, V. B.; Joslin, J. M.; Wold, K. A.; Lantvit, S. M.; Reynolds, M. M., S-nitrosated Biodegradable Polymers for Biomedical Applications: Synthesis, Characterization and Impact of Thiol Structure on the Physicochemical Properties. *J. Mater. Chem.* **2012**, *22*, 5990-6001.
16. Vaughn, M. W.; Kuo, L.; Liao, J. C., Estimation of Nitric Oxide Production and Reaction Rates in Tissue by use of a Mathematical Model. *Am. J. Physiol. Heart Circ. Physiol.* **1998**, *274*, H2163-H2176.
17. Roy, B.; Moulinet d'Hardemare, A.; Fontecave, M., New Thionitrites: Synthesis, Stability, and Nitric Oxide Generation. *J. Org. Chem.* **1994**, *59*, 7019-7026.

CHAPTER 5:
CORRELATING *S*-NITROSOTHIOL DECOMPOSITION WITH NITRIC OXIDE RELEASE
FOR POLYMER FILMS

5.1 PREFACE

Toward the application of *S*-nitrosated polymers as biomaterials, it is essential that the physical processes occurring within the film during the NO releasing period are completely understood. To guarantee that the source of NO from the system is due to the decomposition of the NO donor within a model polymer, thin films of *S*-nitrosated PLGH-cysteine were analyzed by (a) UV-vis spectroscopy to track donor behavior and (b) chemiluminescent detection of the NO release. Overall, the % NO recovery and % RSNO decomposition values matched within error at each time point under various conditions, demonstrating that the RSNO is the predominant source of NO release in the system. These methods are intended to be applied across all NO releasing materials to ensure that each system is yielding NO from the intended source, rather than potential byproducts or residual species present in the system. I would like to acknowledge Dr. Vinod Damodaran for his help with the synthesis of the PLGH-cysteine derivative used for these studies. Additionally, he helped perform NOA measurements for the PBS soak, 48 h analysis described. I would like to also acknowledge Bella Neufeld for her involvement in the experiments performed in sections 5.4.1, 5.4.2 and 5.4.3.

5.2 INTRODUCTION

As discussed in great detail throughout this dissertation, there are many materials currently reported that have the capability to release NO at therapeutically relevant levels.¹ These

materials all operate on the basis of incorporating an NO donor into a material, where NO is released upon the initiation of donor decomposition. However, there can be several possible sources of NO in the system. During the NO loading process to form *N*-diazoniumdiolate or *S*-nitrosothiol donors, there is the potential for byproduct formation due to exposure of the polymer to NO or nitrosating agents, respectively. If any oxygen or moisture is present in the system, a wide array of NO_x species can form. As addressed in Chapter 3, the functional groups present within the polymer must also be taken into account when considering potential byproduct formation.

In addition to byproduct formation during the NO loading stage, it is also possible that residual NO or nitrosating agent (*i.e.* inorganic or alkyl nitrite) could remain trapped within the system and undergo further reaction during material exposure to oxygen or during prolonged material storage. Additionally, the exposure of *S*-nitrosated polymers to reducing conditions (*i.e.* copper ion) to initiate donor decomposition could also have an effect on any residual NO_x species present in the system. For instance, in Chapter 2, experiments were presented in which a solution of nitrite was exposed to a mixture of Cu²⁺/thiol, where nearly 90% of the nitrite present in solution was recovered as NO within just over an hour. This demonstrates that residual nitrite in the system will be reduced under the copper conditions employed to initiate RSNO decomposition. Therefore, if any residual nitrite is present in the polymer, NO release values will be falsely high relative to the amount of RSNO that is decomposed.

Due to the versatility of nitrosation chemistry and the wide array of nitrosating agents available, it is necessary to consider potential products that could contribute to NO release from the material. However, the current approach in the literature is to characterize the material predominantly by NO detection methods, which indicates nothing about the donor behavior.

Polymers exposed to copper consistently demonstrate significantly enhanced NO recovery compared to heat or light initiated decomposition, thus many research groups will expose their *S*-nitrosated polymer to copper in order to “completely” reduce the RSNO to yield a total NO recovery, which is attributed back to initial RSNO content.² Additionally, depending upon the species in the system, toxicity and leaching concerns must be addressed. One study that attempted to completely decompose *S*-nitrosothiols via copper was not 100% effective, likely due to Cu²⁺ coordination to thiol sites in the system.³ Therefore, attempts to quantify initial RSNO due to the introduction of copper to the system may not completely decompose the available RSNO.

Overall, it is crucial that the donor within the material be probed on the same time scale as the NO release to ensure that the NO is coming from the donor of interest. If the kinetics of donor decomposition and NO release do not match up, this indicates that other physical processes are occurring within the film to give rise to NO. Before these materials can be considered for use in biomedical applications, the source of NO must be identified to eliminate the possibility of side reactions occurring. In these studies, a model polymer, *S*-nitrosated PLGH-cysteine, was investigated (presented in Chapter 4). *S*-nitrosated PLGH-cysteine films were prepared for subsequent donor decomposition studies and NO release measurements.

5.3 EXPERIMENTAL SECTION

5.3.1 Materials. The PLGH-cysteine derivative was prepared according to the synthetic scheme presented in Chapter 4.⁴ Methanol (MeOH) and dichloromethane (DCM) were both purchased (ACS grade) from Fisher Scientific, while *t*-butyl nitrite (90%) was purchased from Aldrich.

Phosphate buffered saline (PBS) was prepared from OmniPur tablet with Millipore ultrapure water and pH adjusted to 7.4.

5.3.2. Methods.

Polymer nitrosation. Nitrosation of the PLGH-cysteine was accomplished by dissolving 50 mg polymer in 2 mL of 2 MeOH: 1 DCM solvent in an amber colored, EPA-certified vial (Fisher Scientific). In a separate vial, 8.4 mg of *t*-butyl nitrite was added to 1 mL of 2 MeOH: 1 DCM; the *t*-butyl nitrite solution was then added to the polymer solution. The vial was protected from light and the polymer solution underwent stirring for 4 h, after which time the nitrosated polymer was isolated under vacuum (2 h).

Polymer film preparation. The nitrosated polymer was prepared in solution at 50 mg mL⁻¹ in 2 MeOH: 1 DCM. 75 μ L aliquots were dispensed on round glass slides (12 mm diameter, VWR micro cover glass) or 100 μ L aliquots were dispensed on custom-cut glass slides (9 \times 25 \times 1 mm); polymer films were dried overnight.

Nitric oxide detection and RSNO characterization. To correlate donor decomposition with NO release, the RSNO donor was characterized via solution-phase UV-vis spectroscopy while the NO release was determined using Sievers 280i nitric oxide analyzers (NOAs, GE, Boulder, CO).

For the dry/thermal conditions, each UV-vis sample was placed into a 1 dram glass vial, fitted with a septum, purged with N₂ for 15 min and then placed into a water bath (37 °C). Initial dry/thermal studies were also investigated without the N₂ purge step, where the films were exposed to ambient O₂ during the analysis period. Films were removed at 3 h increments over

the course of a 9 or 12 h total analysis period and dissolved in 1 mL of 2 MeOH: 1 DCM solvent for UV-vis analysis. Spectral scans (200-600 nm) were collected at a 1 nm interval in a 1 cm-pathlength quartz cuvette fitted with a lid to prevent solvent evaporation. The corresponding NO samples were placed each into an NOA cell for direct NO detection over the full 12 h analysis period.

For the PBS/thermal experiments, each sample was placed into a 1 dram glass vial, fitted with a septum and purged with N₂ for 15 min. A stock solution of PBS was deoxygenated via N₂ purge in a 37 °C water bath for at least 30 min. At t=0, 4 mL of the deoxygenated PBS was injected into the deoxygenated vial using a 5 mL airtight Hamilton syringe. In 12 h increments over a 48 h analysis period, samples were removed from the soaking buffer in triplicate, pat dry with a Kimwipe and placed in a desiccator (shielded from light) for 30 min to remove excess water. The films were then dissolved in 1 mL of 2 MeOH: 1 DCM for UV-vis analysis. The corresponding NO samples were placed each into an NOA cell for direct detection during PBS soak over the 48 h analysis period.

Donor decomposition studies were also performed for *S*-nitrosated PLGH-cysteine films exposed to UV light (Blak-Ray B-100AP High Intensity UV lamp; 100 Watt, 365 nm). Since the total analysis required a maximum 30 min analysis period, films were placed into an NOA cell and exposed to UV light for 10, 20 or 30 min under dry conditions for NO data collection. The film was then removed from the NOA cell for subsequent UV-vis analysis.

5.4 RESULTS & DISCUSSION

5.4.1 Analysis under thermal, oxygenated conditions. Nitrosated PLGH-cysteine films were analyzed under thermal (37 °C), dry conditions. For the films analyzed in 3 h increments via

UV-vis, the polymer films were exposed to ambient oxygen during the analysis period. However, the films that were analyzed on the NOAs were under deoxygenated conditions since the NOA setup relies upon a continual N₂ purge to carry the NO to the instrument for detection. Figure 5.1 shows the initial UV-vis spectrum of the *S*-nitrosated polymer, where the absorbance at each wavelength has been normalized by the polymer concentration. The initially nitrosated polymer exhibits a λ_{max} of 335 nm, which confirms nitrosation. The UV-vis spectra clearly reflect that the films analyzed under deoxygenated conditions do not exhibit significant decomposition of the 335 nm absorbance feature after 9 h of NO release. However, the films analyzed under ambient oxygen conditions (37 °C, 9 h) exhibited near-complete decomposition of the absorbance feature, a significant increase in RSNO decomposition compared to the deoxygenated conditions. Therefore, these experimental conditions where NOA data is collected under deoxygenated conditions, while the UV-vis timed decomposition studies are performed under oxygenated conditions, are not sufficient for comparability. Previous reports have demonstrated that RSNOs undergo accelerated decomposition under aerobic conditions compared to anaerobic conditions due to the presence of N₂O₃.⁵

5.4.2 Analysis under thermal, deoxygenated conditions. Due to accelerated decomposition of the RSNO under oxygenated conditions compared to the deoxygenated conditions associated with the NOA setup, the experimental setup was modified. Instead of analyzing the UV-vis decomposition under ambient oxygen conditions, each film was sealed into a vial with a septum and purged with N₂. Films were removed in 3 h increments for UV-vis analysis over a 12 h analysis period.

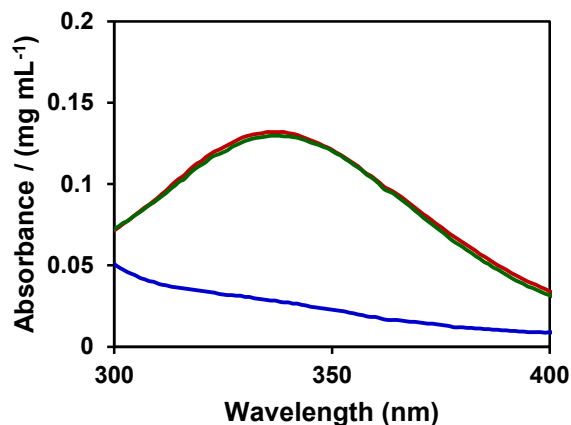


Figure 5.1 Representative UV-vis spectra of absorbance normalized by polymer concentration (mg mL^{-1}) versus wavelength are shown for *S*-nitrosated PLGH-cysteine films dissolved in 2 MeOH: 1 DCM for (red) the initial sample before analysis, (green) after 9 h under deoxygenated conditions and (blue) after 9 h under oxygenated conditions.

All absorbance values were baseline corrected by subtracting out the absorbance contribution due to the non-nitrosated polymer from the raw absorbance value. Since the mass of each film slightly varied and each film was dissolved in 1 mL of solvent, the polymer concentration (mg mL^{-1}) differed slightly among trials ($2.5\text{-}3.5 \text{ mg mL}^{-1}$). Therefore, to consider any concentration dependence of the absorbance contribution due to non-nitrosated PLGH-cysteine, a calibration curve was prepared (Figure 5.2) where the absorbance at 335 nm was measured as a function of blank PLGH-cysteine concentration ($2\text{-}5 \text{ mg mL}^{-1}$). Since dependence of the absorbance at 335 nm on polymer concentration was exhibited, the appropriate baseline value to subtract from the raw absorbance value was determined from the best fit line of the blank calibration curve, where each baseline value was specific to the polymer concentration for that trial.

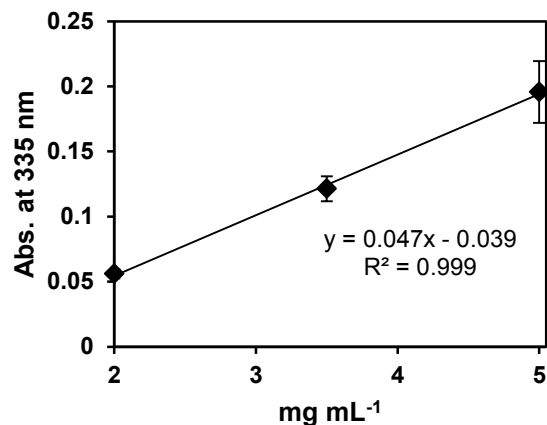


Figure 5.2 The calibration plot for non-nitrosated PLGH-cysteine blank is shown as the dependence of the 335 nm absorbance on polymer concentration.

Once the baseline corrected absorbance values were determined for each sample, the RSNO content (mmol g^{-1}) could be determined from the molar extinction coefficient value previously determined (Chapter 4) for the *S*-nitrosated PLGH-cysteine derivative ($882.9 \pm 18.2 \text{ M}^{-1} \text{ cm}^{-1}$).⁴ Table 5.1 shows the RSNO content as a function of analysis time in 3 h increments for the samples analyzed under deoxygenated conditions, where no significant decrease in the RSNO content is seen over 12 h. The final RSNO content after a 12 h analysis period for films within deoxygenated vials ($0.114 \pm 0.010 \text{ mmol g}^{-1}$) matches within error to the final RSNO content for the samples recovered from the NOAs after 12 h ($0.125 \pm 0.011 \text{ mmol g}^{-1}$). These data demonstrate that the experimental conditions are satisfactory to analyze the donor decomposition and the NO release. However, the 12 h window under dry, thermal conditions is not long enough to probe significant enough donor decomposition within the sensitivity of the UV-vis measurements.

Table 5.1 The RSNO content is shown for *S*-nitrosated PLGH-cysteine films as a function of analysis time. Each value corresponds to the average of $n \geq 6$ samples.

time (h) ^a	RSNO content (mmol g ⁻¹)
0	0.117 ± 0.010
3	0.111 ± 0.019
6	0.118 ± 0.024
9	0.115 ± 0.016
12	0.114 ± 0.010
NOA ^b	0.125 ± 0.011

^a The values shown for the 3 h analysis increments correspond to the deoxygenated UV-vis samples

^b The value shown corresponds to the 12 h analysis performed on the NOAs

5.4.3 Analysis under deoxygenated buffer soak conditions. To monitor significant changes in the donor decomposition, studies were performed to analyze the RSNO content and NO release as a function of time for films exposed to buffer soak at 37 °C over a 48 h window. Films for UV-vis analysis were placed into individual vials and purged with N₂; at t=0, 4 mL of deoxygenated PBS (37 °C) were injected into each vial, and the films were placed into a water bath for the duration of the analysis interval. Films were analyzed every 12 h, while the films analyzed via NOA underwent a 48 h period.

Figure 5.3 shows the plot of RSNO content and NO release as a function of the 48 h soaking period, while Table 5.2 shows the values at each time point. It can be seen in Figure 5.3 that the mmol g⁻¹ over time traces are inverse of one another for NO release and RSNO content. Additionally, the slope corresponding to the 12-48 h data as determined by a linear regression analysis was found to be $1.39 \pm 0.29 \times 10^{-4}$ mmol g⁻¹ h⁻¹ for the NO release and $-2.16 \pm 0.60 \times 10^{-4}$ mmol g⁻¹ h⁻¹ for RSNO content. At the 95% CL, there is no statistically significant difference between these slopes, indicating that NO release indeed correlates inversely to RSNO decomposition.

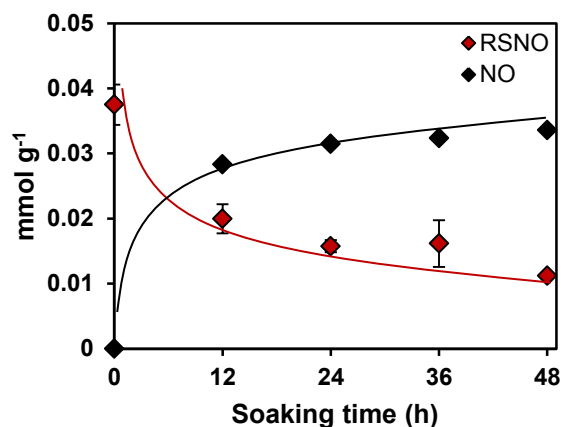


Figure 5.3 The RSNO decomposition (red) and NO release (black) as a function of soaking time for nitrosated PLGH-cysteine films exposed to 37 °C buffer soak over 48 h.

Table 5.2 The RSNO content and NO release is shown as a function of PBS soak time at 37 °C for *S*-nitrosated PLGH-cysteine films. Each value corresponds to the average of $n = 3$ samples.

time (h)	$\mu\text{mol RSNO g}^{-1}$	$\mu\text{mol NO g}^{-1}$
0	37.5 ± 3.1	0.0 ± 0.0
12	20.0 ± 2.2	28.3 ± 0.1
24	15.8 ± 0.9	31.5 ± 0.3
36	16.2 ± 3.6	32.4 ± 0.4
48	11.2 ± 0.4	33.6 ± 0.5

5.4.4 Analysis under deoxygenated exposure to UV light. Additional conditions were considered to analyze RSNO decomposition and NO release under UV light exposure conditions. UV light triggers efficient RSNO decomposition,⁶ thus enabling analysis within a reasonable time duration. *S*-nitrosated PLGH-cysteine films were individually loaded into an NOA cell and exposed to a high intensity UV lamp (365 nm) for 10, 20 or 30 min. After this analysis period, films were collected for UV-vis analysis. The 335 nm absorbance value was baseline corrected according to the blank PLGH-cysteine calibration (Figure 5.2) and the baseline-corrected values

were converted to mmol RSNO g^{-1} using the $882.9 \pm 18.2 \text{ M}^{-1} \text{ cm}^{-1}$ molar extinction coefficient value. Figure 5.4 shows the NO release and RSNO content as a function of UV exposure time, while Table 5.3 shows the values at each time point. The slopes corresponding to NO release and RSNO content were determined to be $1.14 \pm 0.11 \times 10^{-3} \text{ mmol g}^{-1} \text{ h}^{-1}$ and $-1.11 \pm 0.12 \times 10^{-3} \text{ mmol g}^{-1} \text{ h}^{-1}$, respectively, from a linear regression analysis. At the 95% CL, there is no statistically significant difference between these slopes, indicating that the RSNO decomposition initiated by UV light is directly giving rise to the NO that is detected. This correlation can be further seen because the total RSNO that decomposed over the 30 min period was $0.034 \pm 0.025 \text{ mmol g}^{-1}$, while the total NO release was $0.033 \pm 0.006 \text{ mmol g}^{-1}$.

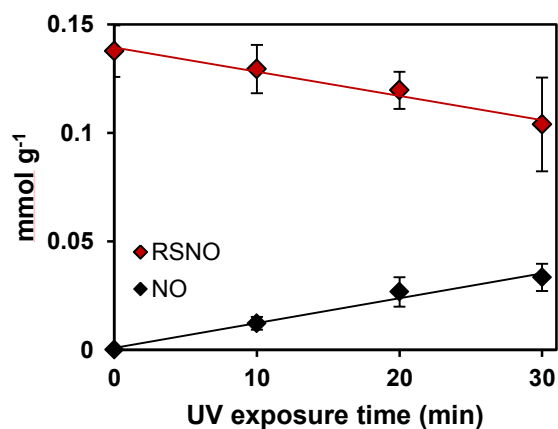


Figure 5.4 The RSNO decomposition (red) and NO release (black) as a function of UV exposure time for nitrosated PLGH-cysteine films.

Table 5.3 The RSNO content and NO release is shown as a function of UV exposure time for *S*-nitrosated PLGH-cysteine films. Each value corresponds to the average of $n \geq 6$ samples.

time (h)	mmol RSNO g ⁻¹	mmol NO g ⁻¹
0	0.138 ± 0.012	0.000 ± 0.000
10	0.129 ± 0.011	0.012 ± 0.003
20	0.120 ± 0.009	0.027 ± 0.007
30	0.104 ± 0.022	0.033 ± 0.006

5.5 CONCLUSIONS

Overall, the presence of oxygen in the reaction vessel was found to have a great impact on the RSNO decomposition. Thus, deoxygenated conditions were employed to correlate NO release with RSNO decomposition. RSNO decomposition correlated to NO release for *S*-nitrosated PLGH-cysteine films exposed to buffer at 37 °C as well as films exposed to UV light under dry, ambient temperature conditions. The ability to correlate NO release with RSNO decomposition is important for confirming that decomposition of the RSNO in the polymer is responsible for the NO release. These methods are intended to be applied to all NO releasing materials, not just the model PLGH system described here. The ability to confirm that NO reservoirs within materials are predominantly due to the donor of interest will enable understanding of the NO material behavior in an application. If the RSNO is confirmed as the predominant source of NO, this will also eliminate the possibility of alternate sources of NO due to byproducts or residual species.

CHAPTER 5 REFERENCES

1. Frost, M. C.; Reynolds, M. M.; Meyerhoff, M. E., Polymers Incorporating Nitric Oxide Releasing/Generating Substances for Improved Biocompatibility of Blood-Contacting Medical Devices. *Biomaterials* **2005**, *26*, 1685-1693; Riccio, D. A.; Schoenfisch, M. H., Nitric Oxide Release: Part I. Macromolecular Scaffolds. *Chem. Soc. Rev.* **2012**, *41*, 3731-3741; Seabra, A. B.; Duran, N., Nitric Oxide-Releasing Vehicles for Biomedical Applications. *J. Mater. Chem.* **2010**, *20*, 1624-1637; Varu, V. N.; Tsihlis, N. D.; Kibbe, M. R., Nitric Oxide-Releasing Prosthetic Materials. *Vasc. Endovascular Surg.* **2009**, *43*, 121-131; Naghavi, N.; de Mel, A.; Alavijeh, O. S.; Cousins, B. G.; Seifalian, A. M., Nitric Oxide Donors for Cardiovascular Implant Applications. *Small* **2012**, *9*, 22-35; Jen, M. C.; Serrano, M. C.; van Lith, R.; Ameer, G. A., Polymer-Based Nitric Oxide Therapies: Recent Insights for Biomedical Applications. *Adv. Funct. Mater.* **2012**, *22*, 239-260.
2. Frost, M. C.; Meyerhoff, M. E., Synthesis, Characterization, and Controlled Nitric Oxide Release from S-nitrosothiol-Derivatized Fumed Silica Polymer Filler Particles. *J. Biomed. Mater. Res., Part A* **2005**, *72A*, 409-419; Johnson, T. A.; Stasko, N. A.; Matthews, J. L.; Cascio, W. E.; Holmuhamedov, E. L.; Johnson, C. B.; Schoenfisch, M. H., Reduced Ischemia/Reperfusion Injury via Glutathione-Initiated Nitric Oxide-Releasing Dendrimers. *Nitric Oxide* **2010**, *22*, 30-36; Riccio, D. A.; Dobmeier, K. P.; Hetrick, E. M.; Privett, B. J.; Paul, H. S.; Schoenfisch, M. H., Nitric Oxide-Releasing S-nitrosothiol-Modified Xerogels. *Biomaterials* **2009**, *30*, 4494-4502; Riccio, D. A.; Nugent, J. L.; Schoenfisch, M. H., Stober Synthesis of Nitric Oxide-Releasing S-nitrosothiol-Modified Silica Particles. *Chem. Mater.* **2011**, *23*, 1727-1735; Stasko, N. A.; Fischer, T. H.; Schoenfisch, M. H., S-nitrosothiol-

- Modified Dendrimers as Nitric Oxide Delivery Vehicles. *Biomacromolecules* **2008**, *9*, 834-841.
3. Li, Y.; Lee, P. I., Controlled Nitric Oxide Delivery Platform Based on S-nitrosothiol Conjugated Interpolymer Complexes for Diabetic Wound Healing. *Mol. Pharmaceutics* **2010**, *7*, 254-266.
 4. Damodaran, V. B.; Joslin, J. M.; Wold, K. A.; Lantvit, S. M.; Reynolds, M. M., S-nitrosated Biodegradable Polymers for Biomedical Applications: Synthesis, Characterization and Impact of Thiol Structure on the Physicochemical Properties. *J. Mater. Chem.* **2012**, *22*, 5990-6001.
 5. Grossi, L.; Montecchi, P. C., A Kinetic Study of S-nitrosothiol Decomposition. *Chem. Eur. J.* **2002**, *8*, 380-387.
 6. Singh, R. J.; Hogg, N.; Joseph, J.; Kalyanaraman, B., Mechanism of Nitric Oxide Release from S-nitrosothiols. *J. Biol. Chem.* **1996**, *271*, 18596-18603; Zhelyaskov, V. R.; Gee, K. R.; Godwin, D. W., Control of NO Concentration in Solutions of Nitrosothiol Compounds by Light. *Photochem. Photobiol.* **1998**, *67*, 282-288; Wood, P. D.; Mutus, B.; Redmond, R. W., The Mechanism of Photochemical Release of Nitric Oxide from S-nitrosoglutathione. *Photochem. Photobiol.* **1996**, *64*, 518-524; Sexton, D. J.; Muruganandam, A.; McKenney, D. J.; Mutus, B., Visible Light Photochemical Release of Nitric Oxide from S-nitrosoglutathione: Potential Photochemotherapeutic Applications. *Photochem. Photobiol.* **1994**, *59*, 463-467.

CHAPTER 6:
STUDIES IN DONOR LEACHING AND LOCALIZED NITRIC OXIDE RELEASE FOR
DONOR-BLENDED POLYMER FILMS

6.1 PREFACE

In Chapter 1 of this dissertation, NO donor-blended polymer films were presented as a useful approach toward creating NO releasing materials. Fine control over the NO reservoir is dictated by the amount of donor that is added to the system, and the NO release kinetics can be easily tuned by the choice of donor and polymer. However, issues with significant donor leaching have limited the use of these materials due to issues with potential donor toxicity as well as downstream effects that result in non-localized NO release. The NO materials community is largely moving toward the use of polymers with covalently attached NO donors; unfortunately, these systems have significant limitations in terms of the extent of functionalization that can be achieved. Therefore, donor-blended films still represent a useful approach toward enhancing and controlling NO reservoirs if formulations can be developed that eliminate leaching.

This work, published in *ACS Applied Materials & Interfaces* (© American Chemical Society 2013), serves to describe *S*-nitrosothiol donor-blended polymer films where the donor that is leached is predominantly due to the loss of surface donor. Subsequently, over the course of a fixed soaking period, the NO release from the material is primarily due to donor decomposition in the polymer film. This work presents the first detailed account of a donor-blended polymer system where bulk leaching is overcome, thus resulting in the desired localized NO release at the material-buffer interface. For this work, I would like to thank Sarah Lantvit for her contribution to the surface analyses that are presented, specifically the water contact angle

goniometry, optical profilometry and SEM-EDS analyses. Major additions to this dissertation that were not included in the original manuscript include the complete characterization of the *S*-nitrosoglutathione donor (UV-vis, IR, ^1H NMR, bond dissociation energy and residual nitrite studies). This research was supported by funds from the Boettcher Foundation's Webb-Waring Biomedical Research Program. We would like to further acknowledge Colorado State University (Fort Collins, CO) and the National Science Foundation for their support. J.M.J. was supported by the Boettcher Foundation and S.M.L. was supported by the National Science Foundation (NSF) under the grant DGE-0841259. Additionally, we acknowledge Alec Lutzke for his help collecting the ^1H NMR spectra of the nitrosated glutathione.

Adapted with permission from Joslin, J. M.; Lantvit, S. M.; Reynolds, M. M., Nitric Oxide Releasing Tygon Materials: Studies in Donor Leaching and Localized Nitric Oxide Release at a Polymer-Buffer Interface. *ACS Appl. Mater. Interfaces* **2013**, *5*, 9285-9294. Copyright 2013 American Chemical Society.

6.2 INTRODUCTION

Extracorporeal circuits (ECCs) are critical to a number of medical procedures that involve blood transport, including blood oxygenation, transfusion, and hemodialysis. Tygon is a proprietary blend of plasticized poly(vinyl chloride) commonly used in ECC applications. There are many drawbacks associated with the use of polymers in ECCs due to a combination of mechanical failures and adverse physiological responses. The most serious complications typically involve blood clot formation in the ECC device, patient infection, and bleeding out due to the use of systemic anti-coagulants. When the material is exposed to blood, platelet activation and adhesion are immediately initiated, leading to blood clot formation during the blood transfer

process within the Tygon tubing. Additionally, serious infection can result at the implant site, which could lead to sepsis. Clotting of the device results in serious complications, including gross thromboembolic aggregation and even death; therefore, systemic anti-coagulants, such as heparin, are usually administered to the patient to prevent clotting. However, the habitual use of systemic anti-coagulants can result in a number of dangerous effects downstream from the site of the ECC device, including platelet consumption and bleeding out at alternate sites of injury. A 2012 report from the Extracorporeal Life Support Organization revealed some alarming statistics regarding the use of ECC devices.¹ Of the patients (16 yrs+) who received ECC treatment, 7.4% were reported to experience mechanical failure due to clotting in the device, and those who experienced clotting had a 33% chance of surviving to discharge or transfer. This leads to an overall expected mortality rate of 5% due to clotting incidents. The report also revealed a 12% mortality rate for hemorrhaging at the site of cannulation and a 12% mortality rate due to infection. Of the hundreds-to-thousands of patients who receive ECC related treatments annually, this is a staggering failure rate. To overcome the issues associated with blood-clotting and infection in ECCs as well as to prevent the use of systemic anti-coagulants that increase the risk of hemorrhaging, different approaches must be taken to develop a more biocompatible ECC material.

One major approach to ECC development is to design materials that are capable of releasing therapeutics at the site of blood contact that would serve to control the initial bioresponse to the material. Nitric oxide (NO) is a promising therapeutic agent for these applications and has previously been shown to retain ECC functionality.^{2, 3} Nitric oxide is released from endothelial cells that line blood vessels to serve as an anti-platelet agent to control coagulation,⁴ and recent research indicates that NO also has an effect on the adsorption of blood-

clotting proteins to a material surface.⁵ In addition to NO's role as a natural anti-coagulant, it also serves other critical physiological functions, such as preventing inflammation⁶ and infection,⁷ which is critical to the performance of ECCs. Overall, creating Tygon coatings capable of releasing NO in a controllable fashion is a promising approach for ECC development. In general, NO releasing materials have gained much interest in a variety of bioapplications, including cardiovascular materials (stents, grafts) and biosensors.^{8,9}

Nitric oxide donors allow for the storage of NO within a material until initiation of release. There are several classes of NO donors which can be pre-formed and isolated as stable small molecules with further incorporation into a material matrix. The most popular donor-incorporated polymer systems have utilized *N*-diazoniumdiolates^{3, 10-14} or *S*-nitrosothiols (RSNOs)¹⁵⁻¹⁸ to facilitate NO storage and release. The major advantage to a donor-incorporated system is that the concentration and type of donor can be tuned to obtain the NO reservoir and release kinetics desired for a given application. Additionally, depending upon the donor type, different stimuli can be employed to initiate donor decomposition (*i.e.* *S*-nitrosothiol decomposition is triggered by heat, light or metal-ion presence¹⁹). The major drawback to these systems is the prevalence of significant donor leaching from the material into the soaking solution.^{11, 15, 17, 18} For instance, *N*-diazoniumdiolate donors have been found to leach from hydrophobic polymer films and attempts at top coating methods and covalent attachment of the donor have been employed to overcome this.¹¹ Additional attempts have been made to create more lipophilic donors that will not leach as significantly into the aqueous soaking phase,^{13, 20, 21} however, donor leaching still remains a problem without time intensive methods to apply multiple top coats.⁵ If the donor leaches significantly into the soaking fluid, this will result in non-localized NO release as the therapeutic NO action will occur downstream from the implant

site. In order to help control thrombus proliferation and prevent infection, NO release needs to be localized at the material-biology interface. Additionally, some NO donors, namely *N*-diazoniumdiolates, have potentially toxic decomposition products (*i.e.* *N*-nitrosamines) that are not intended for release into the bloodstream.^{11, 20} Essentially, in order to perform appropriately, the NO donor must stay fixed in the material matrix, releasing the intended flux of NO for ECC applications. The target NO release is that of the natural endothelium ($0.5-4 \times 10^{-10}$ mol NO cm⁻² min⁻¹).²² To overcome issues with donor leaching, the field has largely steered towards polymers that contain donor groups that are covalently attached to the backbone, resulting in the desired localized NO release.^{8, 10, 23} However, these materials require significant polymer modification, and the NO loading efficiencies are variable depending upon the polymer functionality,²⁴ making it difficult to tailor the exact reservoir of NO contained within the polymer. Due to ease of material preparation and stringent control over the NO reservoirs, donor-incorporated systems remain a viable approach toward the development of NO releasing materials.

Despite prior demonstration of significant donor leaching for different polymer systems, it is important to note that no studies have been performed to investigate how tuning the material properties (*i.e.* polymer type, donor concentration) will overcome leaching while maintaining the requisite NO profiles. There have been studies performed to consider the impact of the polymer type and *S*-nitrosothiol donor concentration on the NO release profiles, but these systems have been found to still result in significant donor leaching from the system.¹⁵ It is additionally important to determine if, despite donor leaching, the majority of the NO released from the system is occurring in the material phase, yielding a truly localized effect, or if the NO is releasing predominantly in the solution phase. The goal of this work, therefore, was to take a model *S*-nitrosothiol-incorporated Tygon system and determine (a) if significant donor leaching

occurs and (b) if leached donor in the solution phase (*i.e.* buffer) contributes significantly to the overall NO release. The second piece is key to understanding whether the NO release occurs in a localized or downstream fashion relative to the material surface.

The model donor in these studies was *S*-nitrosoglutathione (GSNO). The benefit of using GSNO is that any leaching of the donor will not produce harmful byproducts as GSNO and its parent thiol, glutathione, are readily available in the body.²⁵ Additionally, the NO release and donor leaching studies are considered for a 5 h duration, which is relevant to ECC systems,²⁶ more specifically hemodialysis, where a 4-6 h time duration has been considered an acceptable window of time to study biology-material interactions for such applications.^{2, 3, 20, 27} Overall, we establish the fate of the NO donor that is incorporated into a Tygon polymer system and determine the location of NO release relative to the material-buffer interface. In addition to understanding the behavior of the GSNO in the system, we perform surface analyses to determine surface wettability and roughness, which inform the use of this system for blood-contacting bioapplications in general.

6.3 EXPERIMENTAL SECTION

6.3.1 Materials. Glutathione (GSH, 98%, reduced, Acros Organics, Fair Lawn, NJ, USA), sodium nitrite (NaNO₂, ACS grade, EMD Chemicals Inc., Gibbstown, NJ, USA), glutathione disulfide (GSSG, oxidized glutathione, Sigma-Aldrich, St. Louis, MO, USA), hydrochloric acid (HCl, 36-38%, BDH Aristar, Seastar Chemicals Inc., Sidney, BC, Canada), sodium borohydride (NaBH₄, MP Biomedicals, Solon, OH, USA), sodium hydroxide (NaOH, ACS grade, Fisher Scientific, Fair Lawn, NJ, USA), DTNB (Ellman's reagent, 5,5'-dithiobis(2-nitrobenzoic acid), Sigma-Aldrich, St. Louis, MO, USA) and tetrahydrofuran (THF, LC grade, Macron Chemicals,

Phillipsburg, NJ, USA) were all used as received. All solutions of GSH, GSNO and GSSG were prepared using phosphate buffered saline (PBS, prepared from OmniPur tablet with Millipore treated ultrapure water and pH adjusted to 7.4). The model polymer in all studies was Tygon (Formula R-3603, Saint-Gobain Performance Plastics, Akron, OH, USA).

6.3.2 Methods. In brief, GSNO-incorporated Tygon films were prepared in the bottom of polypropylene test tubes. The films were then exposed to simulated physiological conditions (1 mL PBS, pH 7.4, 37 °C) for a 5 h period to simulate hemodialysis conditions. The soaking solution of PBS was analyzed for intact GSNO at different time points during the soaking period to inform any donor leaching from the material phase. Additionally, a modified Ellman's assay was developed to measure total thiol (GSH) in the soaking solution to determine if any solution-phase GSNO decomposed during the soaking period. NO measurements were performed over a 5 h period and NO fluxes were subsequently determined. Surface analyses were also performed on the films pre- and post-soak to understand the interfacial behavior of the film-buffer system.

S-nitrosoglutathione synthesis. The model NO donor for these studies was *S*-nitrosoglutathione (GSNO), which is formed upon nitrosation of the thiol residue of glutathione. The GSNO was synthesized according to a previously published method.²⁸ In brief, 5 mmol of glutathione was added to ice-cold water (8 mL), followed by dissolution upon addition of acid (2 M HCl, 2.5 mL). To initiate nitrosation, sodium nitrite was added (5 mmol) resulting in the formation of nitrous acid, which serves as the nitrosating agent. The solution was kept in an ice bath and stirred for 40 min, followed by addition of acetone (10 mL) to crash out the GSNO product. The final solid product was filtered and washed with water to remove excess nitrite. The product was

rinsed with acetone and dried on filter paper under vacuum for 1.5 h in the dark before transferring the solid to an amber vial (EnviroWare, EPA-certified copper-free, Fisher Scientific, Fair Lawn, NJ, USA) equipped with a septum-containing lid for subsequent drying under vacuum. The isolated GSNO product was stored in the freezer to prevent donor decomposition.

S-nitrosoglutathione characterization. The GSNO donor was characterized by several analytical techniques. For the UV-vis characterization, a Thermo Electron Evolution 300 spectrophotometer was employed with a 1 cm-pathlength quartz cuvette to collect 200-600 nm scans (1 nm resolution). To determine the molar extinction coefficient, GSNO standards were prepared in either Millipore filtered ultrapure water or PBS (pH 7.4) at 1-100 μM concentrations via serial dilution. For the 0 μM standard, blank water or PBS was used. For IR characterization, a Nicolet 6700 FT-IR fitted with an ATR sample stage was employed. An Agilent Inova 300 MHz spectrometer was employed for ^1H NMR analysis of the glutathione before and after nitrosation; 10 mg sample were dissolved in 1 mL D_2O for analysis.

To determine the bond dissociation energy (BDE) of GSNO, an Arrhenius analysis was performed. The kinetics of GSNO decomposition in buffer were monitored at 30, 50, 60 and 70 $^\circ\text{C}$. Full spectral scans were collected (200-600 nm) every 10 min over the course of a 1 h analysis period for 3.5 mL of GSNO solution (1.25 mg mL^{-1} in PBS) present in a 1 cm-pathlength quartz cuvette. An 8 cell accessory was used in the UV-vis spectrometer, which enabled the measurement of 5 samples ($n=5$) for each temperature. The temperature of the cell accessory was set, and the accessory was equipped with a circulating water bath to maintain the temperature and prevent overheating due to the mechanical motion of the device. For each data set, the absorbance value at 336 nm was baseline corrected by the value associated with PBS in the cuvette at that cell position. The baseline-corrected absorbance values were then converted to

[GSNO] (M) using the previously determined ϵ_{\max} value corresponding to the 336 nm feature. All 5 data sets were averaged together at each time point and first order kinetic plots were established by plotting $\ln([\text{GSNO}]_t / [\text{GSNO}]_0)$ as a function of time. The rate constant (k) was taken to be the negative of the slope, and a linear regression analysis was performed to determine the error in the slope. The activation energy was determined from the slope of the Arrhenius plot ($\ln(k)$ versus T^{-1}) and a linear regression analysis was performed to determine the error in the value.

The Griess assay was employed to assess any residual nitrite present in the isolated GSNO product that was due to residual nitrosating agent (nitrous acid). The Griess assay is a solution-phase colorimetric assay where nitrite is reacted with sulfanilic acid (SA) under acidic conditions to create a diazonium salt, which subsequently reacts with *N*-naphthyl ethylenediamine (NEDA) to create an azo chromophore (λ_{\max} of 540 nm). A 1 mM GSNO stock solution was prepared in water and, to minimize GSNO decomposition in solution between absorbance measurements, the solution was prepared freshly before each run in an EPA copper-free vial and stored in an ice bath. A 500 μL aliquot of 1 mM GSNO solution was placed into a quartz cuvette (1 cm pathlength) and was spiked with either 50 μL water (blank) or 50 μL of nitrite standard (10 μM). The solution was then reacted with 50 μL of 6 M HCl, 50 μL of 12.5 mM SA and finally 50 μL of 12.5 mM NEDA, which required a minimum of 60 s before the absorbance spectrum was collected. In addition to the 60 s time delay, increased delay times of 210, 360 and 660 s were also performed to understand the absorbance response as a function of delay time and to take into account any GSNO decomposition occurring under the Griess conditions within the cuvette that could contribute to the nitrite measurement. The absorbance as a function of delay time ($n=3$ for each time point) best fit line enabled extrapolation of the data to

$t=0$, which would be the absorbance contribution due to any residual nitrite in the system. A linear regression analysis was performed to determine the error in the slope and y-intercept values for the absorbance at 540 nm as a function of delay time.

Tygon film preparation. Tygon was dissolved in THF to yield a 0.1 g mL^{-1} polymer solution. The bulk of the analysis was performed on GSNO-incorporated films that were prepared by adding GSNO to the Tygon solution at 20 w/w% of the total Tygon in solution. An aliquot of polymer solution (200 μL) was added to the bottom of a polypropylene test tube (7.3 cm length, 10.5 mm inner diameter, 11.5 mm outer diameter). The polymer films were cured by drying overnight under a cover. For additional GSNO concentration studies, 1, 5, 10, and 30 w/w% GSNO films were prepared in the same fashion by varying the amount of GSNO added to the polymer solution.

Nitric oxide analysis. NO measurements were performed using Sievers 280i Nitric Oxide Analyzers (NOAs, GE Analytical Instruments, Boulder, CO, USA). Baseline measurements were collected on the empty NOA cell for 2 min, prior to addition of 1 mL of PBS (37 °C) per test tube containing the GSNO-incorporated Tygon film. The test tube was inserted into the NOA cell, with the N_2 bubbler adjusted near the top of the soaking solution to prevent disruption of the polymer film. The airtight, deoxygenated cell was then lowered into a 37 °C water bath and NO measurements were collected in 5 s intervals for a 5 h soaking duration, after which the PBS soaking solutions were collected for subsequent analysis. During the soaking of the GSNO-incorporated film, the system was exposed to ambient light. Therefore, the NO release from the system is due to heat- and light-initiated decomposition of the GSNO donor. Additionally, the

Millipore filtered water used in our lab has been analyzed by OES-MS for elemental analysis of any copper content and contains roughly $0.3 \mu\text{g L}^{-1}$. Even at these small concentrations, it is likely that there is some copper-mediated decomposition of the GSNO occurring due to copper in solution. The GSNO-incorporated Tygon films were recovered for surface analysis.

Time-dependent film soaks. In addition to the 5 h total soaking period, it was critical to understand the behavior of the system at different points during the analysis period. As such, additional films were prepared for analysis in a $37 \text{ }^\circ\text{C}$ water bath. At different time intervals (5 min, 1 h, 3 h, 5 h), the PBS soaking solution was collected from the system for GSNO and total GSH analysis. The films were also recovered for surface analysis.

S-nitrosoglutathione assay. To monitor the presence of GSNO in soaking solution due to donor leaching from the Tygon material, a GSNO assay was developed. The PBS soaking solutions from either the NOA or timed-soak experiments were analyzed immediately after collection. Characterization of the GSNO product in PBS was performed by measuring the absorbance at 336 nm, the λ_{max} associated with the SNO moiety of GSNO. A calibration curve was prepared using a set of GSNO standards (5-100 μM) prepared in PBS. Using the corresponding Beer's law plot, the concentration of intact GSNO could be determined in the soaking solution. All measurements involving GSNO quantification were performed by dispensing 300 μL per well in a 96-well UV transparent plate (Thermo Electron Corporation) followed by absorbance readings performed on a Biotek Synergy 2 plate reader (Winooski, VT, USA).

Total thiol assay. To analyze the total thiol content in the PBS soaking solution after film soak and GSNO quantification, the samples were subjected to an Ellman's assay, a colorimetric assay for free thiol detection.²⁹ The assay was modified to contain a sodium borohydride reduction step that served to decompose any GSNO in solution, as well as cleave any GSSG disulfide³⁰ that is a byproduct of GSNO decomposition. Samples (50 μL) in PBS were aliquoted into a 96-well plate setup (Corning® assay plate, polystyrene) and exposed to sodium borohydride (0.2 M NaBH_4 in 0.002 M NaOH , 50 μL) at pH 8-9 to facilitate the GSNO decomposition and GSSG reduction. After a 2 h treatment period, the excess borohydride was quenched with acid (0.2 M HCl , 50 μL) for 10 min (pH 3-4). Addition of NaOH (0.025 M, 50 μL) adjusted the pH to 8, where 50 μL of DTNB (10 mM) was added to produce a yellow-colored chromophore. The absorbance at 414 nm corresponding to the chromophore is directly proportional to the amount of free thiol in solution, as indicated by the standard curve. GSH and GSNO standards were prepared from 5-100 μM and GSSG standards were prepared at half the concentration, 2.5-50 μM (1 mol GSSG: 2 mol GSH after reduction), to determine reduction efficiency.

Surface analysis. Surface analysis of the GSNO-incorporated Tygon films pre- and post-soak was performed using water contact angle goniometry, optical profilometry and SEM-EDS. Sample preparation for all methods involved removing the curved film from the polypropylene test tube and trimming the edges to lay the film flat on double-sided tape.

To assess the wettability of the films, water contact angle was obtained by placing a 2 μL ultrapure water droplet on the surface of the film with subsequent imaging using a Krüss Drop Shape Analysis System DSA 10 (Hamburg, Germany). The angle was obtained from the image of the droplet using the circle fitting parameter on Drop Shape Analysis 1.50 software.

Using optical profilometry, the average surface roughness of the film (Ra) was established to determine the effect of incorporating the GSNO into the Tygon system as well as subsequent film soaking. Three 2×2 stitch scans at 0.424×0.318 mm were performed on each film (control Tygon and pre- or post-soaked GSNO-incorporated films) using a Zometrics ZeScope Optical Profilometer (Tucson AZ, USA) at 20× magnification. The Ra values were assessed and averaged over all replicate samples to obtain an average Ra roughness value.

SEM-EDS surface analysis was further performed to determine the S content on the surface of the GSNO-incorporated Tygon films pre- and post-soak. The film surfaces were imaged with a JEOL JSM-6500F scanning electron microscope (SEM, Peabody, MA, USA) coupled to a Thermo Electron energy dispersive spectrometer (EDS). Scans were collected at 100, 1000, and 5000× magnification with a 15.0 kV accelerating voltage. EDS scans allowed for atomic weight percent of S to be determined across the sample surface.

6.3.3 Statistical analysis. All error bars are reported as the standard deviation for each experiment with an $n \geq 3$ for all trials. The % relative error values reported were determined by dividing the standard deviation by the average. The Q-test was used to determine any outliers in the data sets with a confidence level of 95%. The Student's t-test was used to assess any significant difference among sets of data at the indicated confidence level (95%). To determine comparability within data sets for each method, a pooled t-test was performed to determine whether there was any significant difference between sample populations at the 95% confidence level.

6.4 RESULTS & DISCUSSION

6.4.1 Small molecule *S*-nitrosoglutathione characterization. To fully characterize the small molecule donor *S*-nitrosoglutathione (GSNO), several methods were employed, including UV-vis, IR and ¹H NMR. The BDE was determined and residual nitrite in the final product was determined.

UV-vis characterization of GSNO. UV-vis spectra of different GSNO standards (1, 5, 10, 25, 50, 100 μM) prepared in either water or PBS were collected to confirm the concentration dependence of the characteristic absorbance feature (λ_{max} at 336 nm) due to the $n_{\text{O}} \rightarrow \pi^*$ transition. For a 1 cm pathlength cuvette, the Beer's law plots (shown in Figure 6.1) demonstrated a slope of 808.4 ± 8.0 or $823.9 \pm 10.4 \text{ M}^{-1} \text{ cm}^{-1}$ for GSNO in water or buffer solution, respectively. The reported ϵ_{max} for GSNO is $922 \text{ M}^{-1} \text{ cm}^{-1}$, where the experimentally determined ϵ_{max} for GSNO in water was found to be $808.4 \pm 8.0 \text{ M}^{-1} \text{ cm}^{-1}$, which represents a 12% difference.²⁸ The original report of $922 \text{ M}^{-1} \text{ cm}^{-1}$ does not describe the experimental details regarding the ϵ_{max} value for GSNO in water. Therefore, it is likely that a single GSNO standard was used along with its corresponding absorbance value at 336 nm for this calculation. Additionally, if the concentration of the standard were closer to 1 mM, which is the concentration that would yield an absorbance ≈ 1 , then this value would potentially yield a larger ϵ_{max} value. Since the ϵ_{max} value reported here is for a lower concentration range, it is possible that at higher [GSNO], the ϵ_{max} value will reach closer to the $922 \text{ M}^{-1} \text{ cm}^{-1}$ value that was originally reported due to a more pronounced slope in the absorbance versus [GSNO] plot at higher [GSNO].

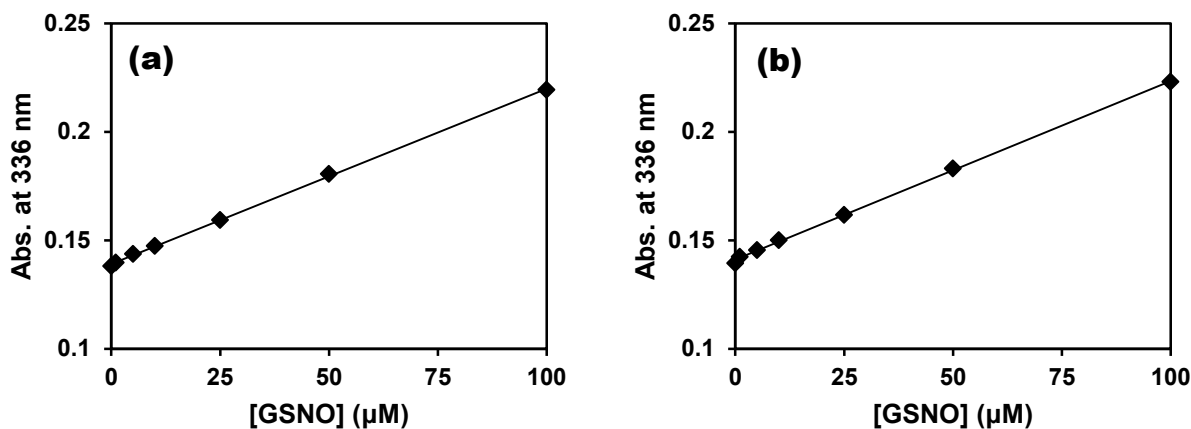


Figure 6.1 The Beer's law plots for GSNO prepared in (a) water and (b) PBS solution yield slope values of $8.08 \pm 0.08 \times 10^{-4}$ and $8.24 \pm 0.10 \times 10^{-4} \mu\text{M}^{-1} \text{cm}^{-1}$ and intercept values of 0.139 and 0.141, respectively. Each data point represents the average of $n=3$ measurements, where the R^2 value for each plot was 0.999.

IR characterization of GSNO. IR spectra were collected for glutathione before and after nitrosation and are shown in Figure 6.2. The fingerprint region (Figure 6.3) demonstrates the appearance of a band at 745 cm^{-1} , corresponding to the S-N stretch, while the feature appearing at 1360 cm^{-1} corresponds to the N=O stretch.³¹ Combined, these features suggest the incorporation of the SNO moiety within the glutathione after nitrosation.

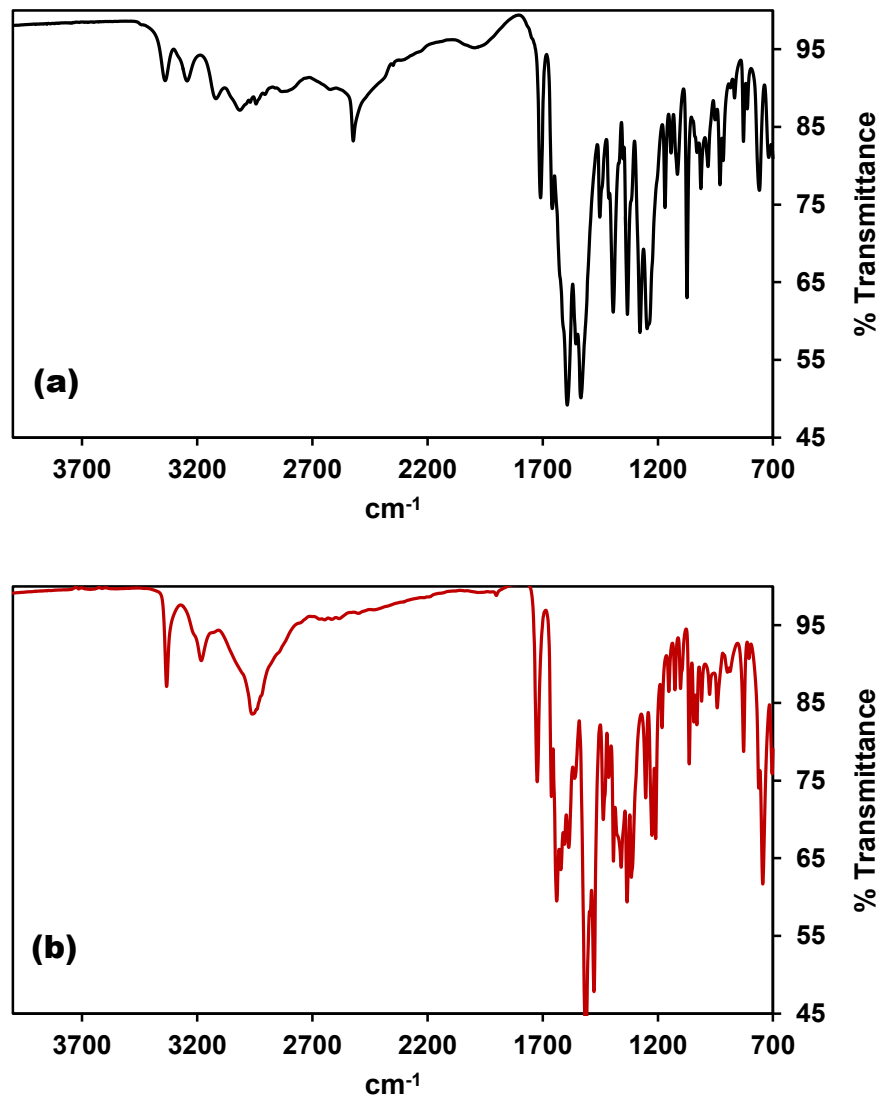


Figure 6.2 The IR spectra are shown for (a) glutathione (black) and (b) nitrosated glutathione (red).

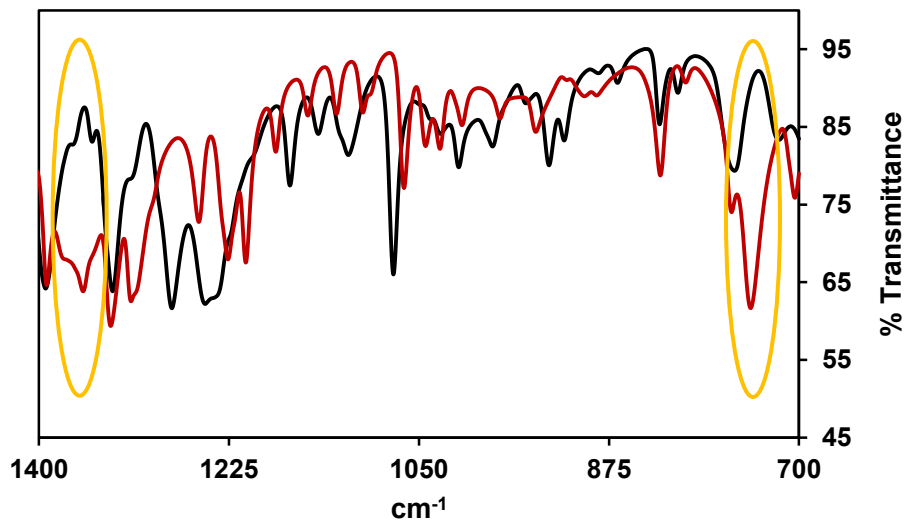


Figure 6.3 The fingerprint region for the IR spectra of glutathione before (black) and after (red) nitrosation suggest the incorporation of SNO moieties.

¹H NMR characterization. ¹H NMR spectra were collected for glutathione before and after nitrosation. Figure 6.4 shows the spectrum corresponding to glutathione in D₂O, where the structure of glutathione shows the protons corresponding to the peak assignments. After nitrosation, the spectrum of nitrosated glutathione was also collected (shown in Figure 6.5). The proton peaks remain in relatively the same location after nitrosation, with the exception of the <D> and <E> protons that are bound to the thiol-containing carbon. Upon the addition of the NO to the thiol site, the presence of this electron-withdrawing moiety causes a significant downfield shift in the peaks for the <D> and <E> protons, which appear closer to 4 ppm after nitrosation compared to the original peaks at ~3 ppm. This ¹H NMR analysis suggests the successful incorporation of the SNO moiety after glutathione nitrosation.

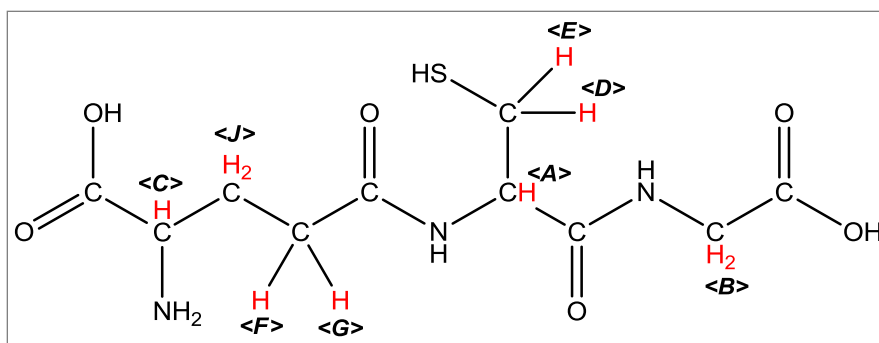
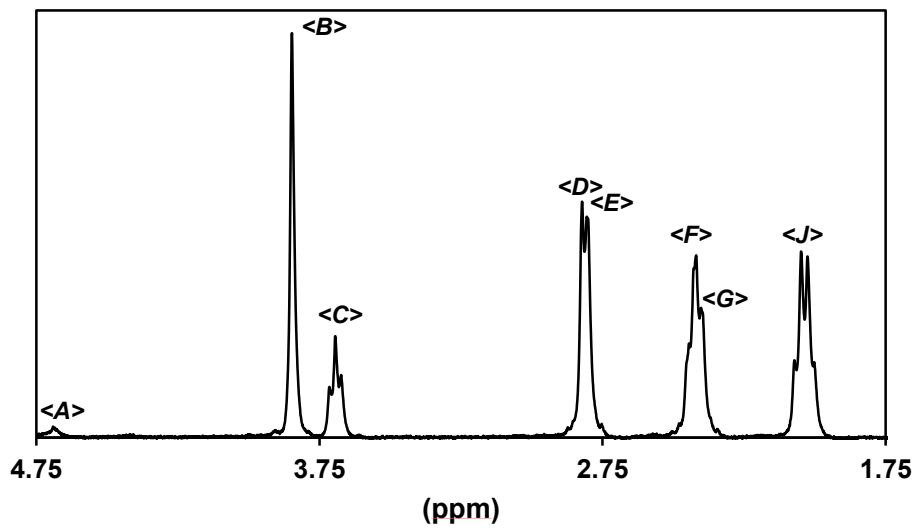


Figure 6.4 The ^1H NMR spectrum of glutathione in D_2O .

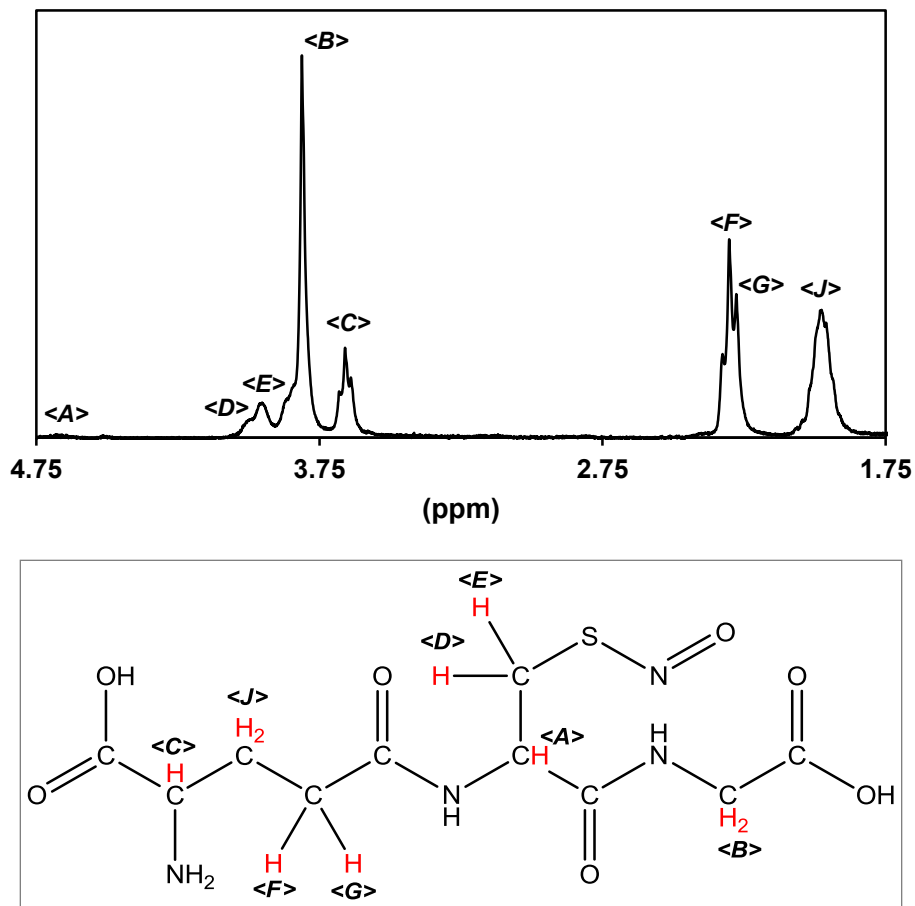


Figure 6.5 The ¹H NMR spectrum of *S*-nitrosoglutathione in D₂O.

Bond dissociation energy determination. The BDE of GSNO was determined via an Arrhenius analysis. The first order kinetics of GSNO decomposition were analyzed at 30, 50, 60 and 70 °C by monitoring the decay of the 336 nm absorbance feature over the course of 1 h. Table 6.1 shows the first order rate constant (k) determined for each temperature, and Figure 6.6 shows the Arrhenius plot of $\ln(k)$ as a function of inverse temperature (K^{-1}). According to equation 6.1, the slope of this plot (5940.4 ± 135.9 K) is related to the activation energy (E_a) which can be taken

as the BDE associated with homolytic S-NO cleavage. The y-intercept (13.8 ± 0.4) of this plot is related to A, the pre-exponential (frequency) factor.

$$\ln(k) = \ln(A) - \frac{E_a}{RT} \quad (6.1)$$

Table 6.1 The rate constant associated with GSNO decomposition in PBS is given for each analysis temperature.

T (°C)	$T^{-1} \times 10^{-3}$ (K ⁻¹)	$k \times 10^{-2}$ (min ⁻¹) ^a	ln(k)
30	3.30	0.30 ± 0.02	-5.80 ± 0.02
50	3.09	1.08 ± 0.05	-4.53 ± 0.02
60	3.00	1.74 ± 0.13	-4.05 ± 0.03
70	2.91	3.03 ± 0.29	-3.50 ± 0.04

^aThe rate constant was determined from the slope of the first order kinetic plot for each temperature

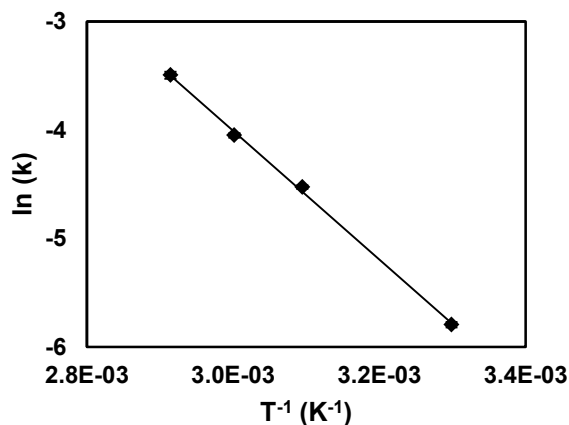


Figure 6.6 The Arrhenius plot of ln(k) versus T^{-1} yielded a slope of 5940.4 ± 135.9 K and y-intercept of 13.8 ± 0.4 (R^2 of 0.999). Each data point represents the average of n=5 kinetic runs.

The final BDE was determined to be 49.4 ± 1.1 kJ mol⁻¹ (11.8 ± 0.3 kcal mol⁻¹), which is on the appropriate order of magnitude for RSNOs where a general BDE value range of 20-30 kcal mol⁻¹

has been reported.³² The BDE values reported for the homolytic cleavage of the S-NO bond have been experimentally and theoretically reported for RSNOs in the gas phase or in organic solvent. Therefore, the determined value of 12 kcal mol⁻¹ reported herein is specific to GSNO in an aqueous buffer environment. The frequency factor, determined from the y-intercept of the Arrhenius plot, was found to be $9.85 \pm 0.29 \times 10^5 \text{ min}^{-1}$.

Residual nitrite quantification. Residual nitrite measurements were performed using the Griess assay to consider any nitrite that might be present in the isolated donor due to the nitrous acid employed for the initial nitrosation. Any residual nitrite in the system could contribute to the NO recovery, depending upon the experimental conditions. To consider any residual nitrite present in the GSNO, the colorimetric response for a GSNO solution with and without the spiked addition of a 10 μM nitrite solution aliquot was considered using the Griess assay for nitrite detection. 500 μL of GSNO solution was spiked with 50 μL of 10 μM nitrite or 50 μL water and further reacted with 50 μL each of HCl (6 M), SA (12.5 mM) and NEDA (12.5 mM) Griess reactants. The minimum time from when the GSNO solution was introduced into the cuvette to the time the absorbance measurement was made required 60 s for all reagents to be added. Therefore, it was critical to consider any decomposition of GSNO in solution which could occur during the time delay associated with addition of the reagents within the cuvette and the absorbance measurement. The delay time was extended from 1 min up to 3.5, 6 and 11 min, where the absorbance response at 540 nm was found to be linearly proportional to the delay time (Figure 6.7). This indicates that the GSNO was decomposing within the cuvette under the conditions of the Griess reaction. However, extrapolation of the curve back to $t=0$ should yield the absorbance contribution due to residual nitrite in solution, independent of any RSNO decomposition

occurring during the analysis period. While extrapolation of the nitrite-spiked curve resulted in an absorbance contribution (0.032 ± 0.002) for the $10 \mu\text{M}$ nitrite spiked solution, the extrapolation of the non-spiked curve essentially resulted in no detectable absorbance contribution. Therefore, it can be determined that the GSNO contained no detectable residual nitrite that was trapped in the donor after it was isolated. However, with increasing delay time, the GSNO will decompose to result in the formation of nitrite, which can be seen due to an increase in the intensity of the Griess chromophore with increasing delay time.

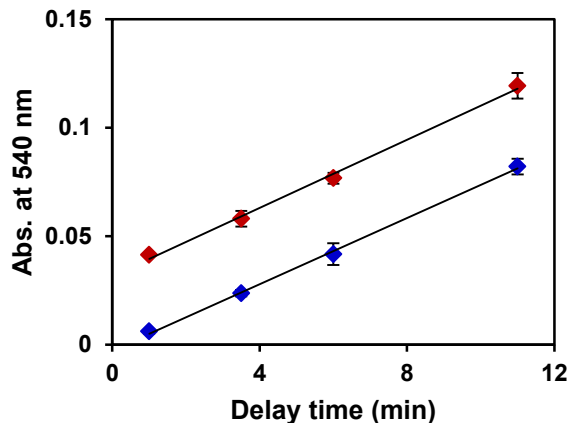


Figure 6.7 Preparation of the Griess-treated 1 mM GSNO solution required a minimum of 60 s between the time of GSNO solution introduction to the cuvette and the absorbance measurement. Extending the delay time resulted in a linear increase in the absorbance response for both the GSNO solution alone (blue) and the GSNO solution spiked with $10 \mu\text{M}$ nitrite (red). For the GSNO solution spiked with $50 \mu\text{L}$ of water before treatment, the slope was found to be $7.62 \pm 0.19 \times 10^{-3} \text{ min}^{-1}$ with a y-intercept of -0.0026 ± 0.0012 (R^2 of 0.999), while the GSNO solution spiked with $50 \mu\text{L}$ of $10 \mu\text{M}$ nitrite before treatment yielded a slope of $7.84 \pm 0.31 \times 10^{-3} \text{ min}^{-1}$ with a y-intercept of 0.032 ± 0.002 (R^2 of 0.997).

Overall, the UV-vis, IR and ^1H NMR analyses confirmed nitrosation of the thiol residue of glutathione to form *S*-nitrosoglutathione. The BDE energy of the S-NO was determined to be $11.8 \pm 0.3 \text{ kcal mol}^{-1}$. No residual nitrite was detected within the GSNO, indicating no significant presence of residual nitrosating agent. Once the GSNO was thoroughly characterized, it was blended into Tygon films for subsequent leaching studies and NO release analysis.

6.4.2 GSNO-blended Tygon films. Upon exposure of a 20 w/w% GSNO-incorporated Tygon film to simulated physiological conditions (1 mL PBS, pH 7.4, 37 °C), the film system exhibited a steady release of NO due to heat and light-initiated GSNO decomposition as well as minor copper content in the buffer solution over a 5 h soaking period (Figure 6.8).

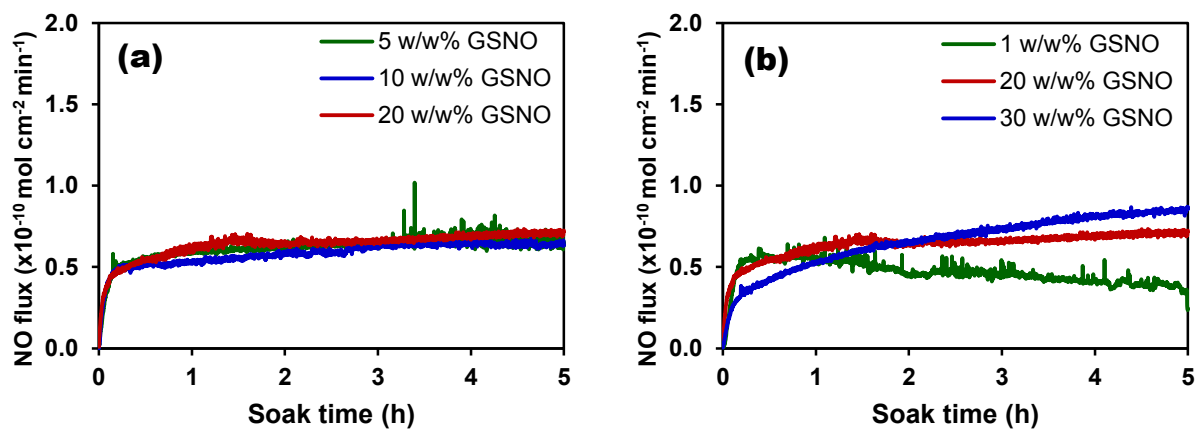


Figure 6.8 The NO release profiles as measured by chemiluminescence for (a) middle-range w/w% films (5, 10) and (b) upper- and lower-range films (1, 30 w/w%) compared to the 20 w/w% GSNO-incorporated Tygon film exposed to 1 mL PBS (pH 7.4) at 37 °C. Each profile represents $n \geq 3$ with an average flux error of 7, 15, 14, 12, and 20% for the 1, 5, 10, 20 and 30 w/w% films, respectively.

Assuming the majority of the NO is being released from the surface of the material, the average NO flux for the 0.25-5 h range was found to be $0.64 \pm 0.05 \times 10^{-10}$ mol NO cm⁻² min⁻¹ for the half-sphere shaped films with an estimated surface area of 1.25 cm². This NO flux marks the lower end of natural endothelial release, which has been reported to range from $0.5-4 \times 10^{-10}$ mol NO cm⁻² min⁻¹.²² Since these films release NO on the order of the natural endothelium, this demonstrates promise to regulate platelets and clotting proteins at the material surface during blood contact. A previous publication demonstrated that a threshold NO flux greater than that of the natural endothelium (13.65×10^{-10} mol NO cm⁻² min⁻¹) was needed in order to completely preserve platelet function and prevent blood clot formation in an ECC model.³ In these same studies, the lowest levels of 2.33×10^{-10} mol NO cm⁻² min⁻¹ demonstrated activated clotting times that were closer to non-NO releasing control surfaces compared to the higher NO flux materials; however, lower flux levels were still found to preserve platelet function while preventing platelet activation and adhesion. Another study considered varying concentrations of *N*-diazeniumdiolate donor in a poly(vinyl chloride) polymer matrix and found, for films exhibiting fluxes ranging from $0.93-7.05 \times 10^{-10}$ mol NO cm⁻² min⁻¹, a significant decrease in platelet adhesion for all samples compared to the control, demonstrating improved performance with increasing NO flux.²¹ Additional investigations of NO releasing scaffolds have demonstrated a reduction in platelet^{33, 34} and bacterial^{33, 35} adhesion while preventing clot formation³⁶ for fluxes below the 13.65×10^{-10} mol NO cm⁻² min⁻¹ threshold, as well as a reduction in platelet adhesion for NO fluxes as low as 0.25×10^{-10} mol NO cm⁻² min⁻¹,³⁷ resulting in improved blood compatibility. A comprehensive review of the NO fluxes reported to have an effect on platelets strongly suggests that the NO flux plus the surface properties contribute to the blood response; thus, a one dosage fits all approach to NO releasing surfaces is not feasible. Overall, the NO flux demonstrated by

the 20 w/w% GSNO-incorporated Tygon films in these studies are on the lower end of the natural endothelial release, but are still promising toward controlling initial bioresponses over the 5 h window necessary for critical care applications since the surface properties were maintained.

Based upon the amount of GSNO incorporated into the material, the theoretical NO reservoir that is available for release over the lifetime of the film is 12 μmol . Over the 5 h analysis period, the films released $0.027 \pm 0.008 \mu\text{mol}$ of NO (Table 6.2), representing only ~0.2% of the total NO reservoir.

Table 6.2 Data summary corresponding to NO release from Tygon films containing various w/w% GSNO. Films were exposed to buffer at 37 °C for a 5 h duration.

w/w% GSNO	NO flux ($\times 10^{-10} \text{ mol cm}^{-2} \text{ min}^{-1}$) ^a	Total NO (nmol) ^b	Theoretical NO _{total} (μmol)	% NO release ^c
1	0.47 ± 0.06	17.3 ± 0.7	0.6	2.91 ± 0.12
5	0.63 ± 0.04	23.1 ± 2.8	3.0	0.78 ± 0.09
10	0.59 ± 0.05	21.8 ± 1.5	5.9	0.37 ± 0.03
20	0.64 ± 0.05	26.9 ± 7.8	11.9	0.23 ± 0.07
30	0.68 ± 0.13	24.7 ± 4.4	17.8	0.14 ± 0.02
20 (with top coat)	0.32 ± 0.10	11.5 ± 1.6	11.9	0.10 ± 0.01

^a NO flux is reported as the average \pm standard deviation for the time duration 0.25-5 h

^b Total NO release is reported as the average \pm standard deviation for the entire time duration (0-5 h)

^c The % NO release is reported relative to a total theoretical NO reservoir based upon w/w% GSNO

Due to the large extent of donor incorporation, these films have the potential to release NO over a prolonged period of time. For example, the 20 w/w% GSNO-incorporated Tygon films released NO over an extended 24 h duration under a PBS soak at 37 °C. The NO flux profile is shown in Figure 6.9, where an average flux of $0.82 \pm 0.08 \times 10^{-10} \text{ mol NO cm}^{-2} \text{ min}^{-1}$ was maintained.

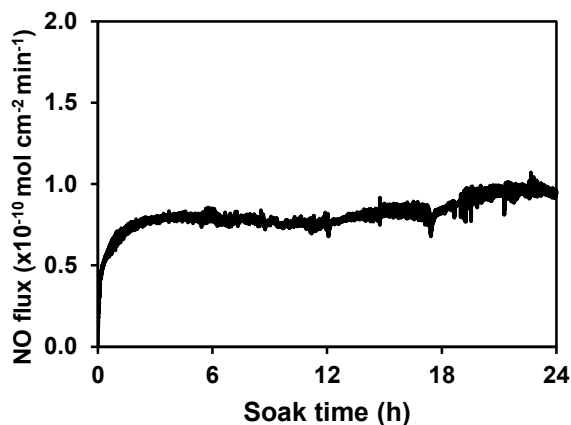


Figure 6.9 The NO release profiles as measured by chemiluminescence demonstrating the average NO flux profile for 20 w/w% GSNO-incorporated Tygon film over a 24 h analysis period (PBS soak, 37 °C) for n=3 samples with an average flux error of 10%.

One of the films was further allowed to soak for 1 week (Figure 6.10), where an average flux of 1.2×10^{-10} mol NO cm⁻² min⁻¹ was exhibited. The average NO flux associated with the 20 w/w% GSNO films slightly increased with increasing soaking time over a week, where a steadier flux was exhibited within the first day of soaking. Of further note, the films that were soaked for 24 h released a total payload of 0.15 ± 0.02 μmol, representing 1.23 ± 0.17 % recovery based upon the 12 μmol GSNO reservoir. The total NO payload was increased by an order of magnitude (1.5 μmol) upon further soak for a 1 week duration. Even after 1 week of soaking, the film only released 12.3% of the available NO, indicating that these materials could be used for applications that required prolonged NO release on the order of weeks-to-months.

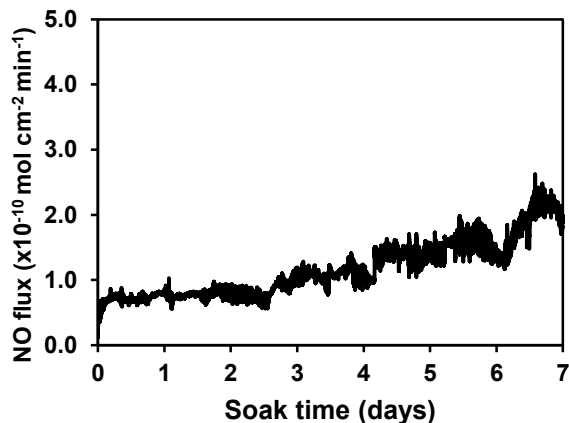


Figure 6.10 The NO release profiles as measured by chemiluminescence demonstrating the average NO flux profile for 20 w/w% GSNO-incorporated Tygon film over a 1 week analysis period (PBS soak, 37 °C) for n=3 samples for the first day and n=1 for the remaining time period.

It is critical toward the application of these materials in an ECC setting to demonstrate that the NO being released from the system is truly localized at the material-buffer interface. Since donor-incorporated systems have been demonstrated to leach significant amounts of donor, it is a serious consideration whether or not any donor leached into the soaking solution will significantly contribute to the detected NO. If solution-phase donor decomposition is primarily responsible for the detected NO, this will result in a non-localized effect of NO at the material-biology interface. Since NO is a free radical with a short half-life, it is critical that the NO be released as close to the material surface as possible where the therapeutic effect is desired. Subsequent GSNO and total thiol assays were performed to determine the extent of donor leaching and the potential for solution-phase donor to contribute to NO release.

6.4.3 GSNO leaching studies. Leaching studies were performed by monitoring the presence of intact GSNO in the soaking solution for 20 w/w% GSNO-incorporated Tygon films exposed to PBS at different time intervals over 5 h. The GSNO concentrations associated with PBS soaking solutions were determined by using the calibration curve presented in Figure 6.11.

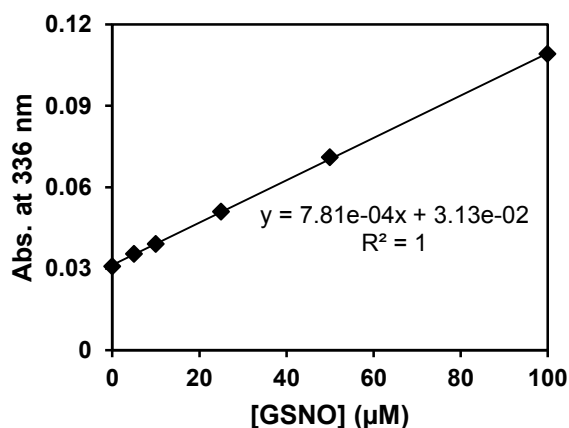


Figure 6.11 The calibration curve associated with the GSNO absorbance assay, where the absorbance value at 336 nm is plotted as a function of [GSNO] (5-100 μM GSNO in PBS, including a PBS blank as the 0 μM point). Each point represents n=3, with an error of $\leq 4\%$ corresponding to each point.

The limit of detection using this assay was 5 μM GSNO in PBS. It is important to note that any GSNO present below this 5 μM detection limit can be significant to the biological application. The GSNO concentration in soaking solution was determined at 5 min, 1 h, 3 h, and 5 h intervals (Figure 6.12).

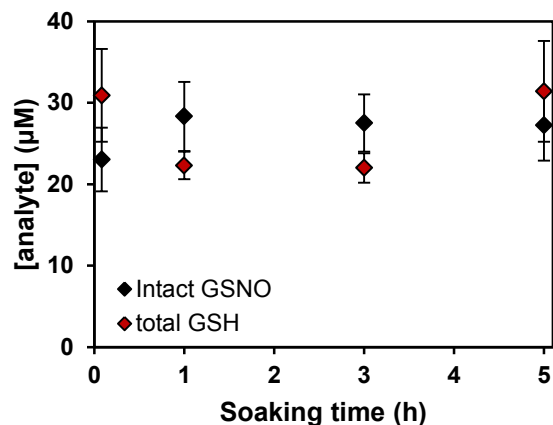


Figure 6.12 Intact GSNO and total GSH concentrations in PBS soaking solution as a function of time for 20 w/w% GSNO-incorporated Tygon film soaks. Donor-incorporated films were exposed to 1 mL PBS (pH 7.4) at 37 °C for a fixed interval of time (5 min, 1 h, 3 h, 5 h). Each point represents the average of 9 films.

A burst of GSNO was released from the film surface between 5 min ($23.1 \pm 3.9 \mu\text{M}$) and 1 h ($28.3 \pm 4.2 \mu\text{M}$) of film soak time (Table 6.3). Soaking the films past this point up to 5 h demonstrated no additional GSNO detected in solution ($27.2 \pm 4.3 \mu\text{M}$ at 5 h; not statistically different from 1 h at 99% CL). No additional GSNO was found intact in the soaking solution past 1 h, indicating that the amount of leached GSNO was removed quickly from the film upon soaking or, if the [GSNO] remained constant, this could indicate continuous leaching if some solution-phase GSNO also decomposed to yield NO. To determine if the GSNO in solution was giving rise to significant amounts of NO, and if so, the total amount of GSNO leached into solution, a total thiol assay was performed.

Table 6.3 Data summary for GSNO leaching and total thiol assays corresponding to 20 w/w% GSNO-incorporated Tygon films exposed to buffer at 37 °C.

Soaking time (h)	20 w/w% GSNO ^a	
	[GSNO] (μM)	[GSH _{total}] (μM)
0.08	23.1 ± 3.9	30.9 ± 5.7
1	28.3 ± 4.2	22.3 ± 1.7
3	27.5 ± 3.5	22.0 ± 1.8
5	27.2 ± 4.3	31.4 ± 6.2

^aData are shown for n=9

6.4.4 Total thiol content in soaking solution. The Ellman's assay for free thiol quantification was modified to include a borohydride reduction step to determine if any of the leached GSNO in solution was giving rise to NO release upon decomposition in PBS. Essentially, any GSNO that leached into the soaking solution and decomposed would yield NO and GSSG according to equation 6.2.



The intact GSNO concentration, [GSNO], is known at the end of the soaking solution from the GSNO assay. Therefore, a method that can quantitatively decompose any remaining GSNO as well as cleave any GSSG that was formed during the soaking period will yield total thiol content, [GSH_{total}]. If [GSH_{total}] = [GSNO], then there no excess thiol due to GSSG was present in the soaking solution at the end of the soaking period and the only source of thiol in the soaking solution was due to the intact GSNO that was detected at the end of the soaking period. In this case, the leached GSNO would not significantly decompose during the soaking period. However, if [GSH_{total}] > [GSNO] at the end of the soaking period, excess thiol would be present due to GSSG from solution-phase GSNO decomposition, indicating that the solution-phase GSNO is contributing to the system's released NO.

To demonstrate that the 2 h borohydride treatment effectively and quantitatively decomposed GSNO and reduced GSSG, GSNO and GSH standards were prepared from 5-100 μM and GSSG standards were prepared at half the concentration (2.5-50 μM) since 1 mol GSSG reduces to 2 mols of GSH. Figure 6.13 demonstrates that the calibration curves for all three analytes overlap, indicating that the borohydride effectively yielded GSH for all samples to result in colorimetric detection of the total thiol content in the soaking solution. When comparing the raw absorbance values from the assay, the GSNO decomposition and GSSG reduction are >95% efficient relative to the GSH standards.

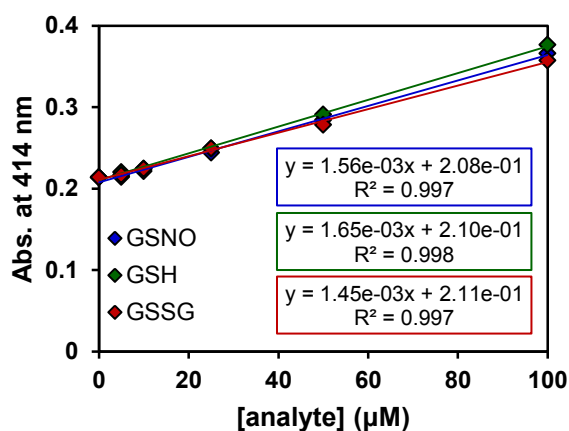


Figure 6.13 Calibration curves associated with GSNO, GSH and GSSG standards that underwent a borohydride reduction step prior to treatment with the Ellman's reagent (DTNB). The absorbance at 414 nm is linearly proportional to the amount of free thiol available in solution for each analyte (5-100 μM thiol). Each point represents an $n=3$ with an error $\leq 3\%$.

To determine the availability for NO release of the 28 μM GSNO that was found intact in the soaking solution from the 20 w/w% GSNO-incorporated Tygon film, the total thiol assay was

performed on the recovered PBS solutions. Figure 6.12 shows that, at each time point, the $[\text{GSH}_{\text{total}}]$ values match up quantitatively with the $[\text{GSNO}]$ values (values do not differ statistically at a 99% CL, Table 6.3). This indicates that the GSNO in the soaking solution did not significantly give rise to any NO release because the total GSH content is due to intact GSNO at the end of the soaking period. If the leached GSNO was a significant source of NO, the total GSH content would be higher than the GSNO due to the presence of GSSG that would form upon decomposition of the solution-phase GSNO.

An additional control experiment was performed where a 28 μM GSNO solution was prepared in PBS and added to a blank polypropylene test tube within an NOA cell under the same conditions as the Tygon film analysis. Minimal NO release was found over a 5 h window compared to the 20 w/w% GSNO-incorporated Tygon film (Figure 6.14).

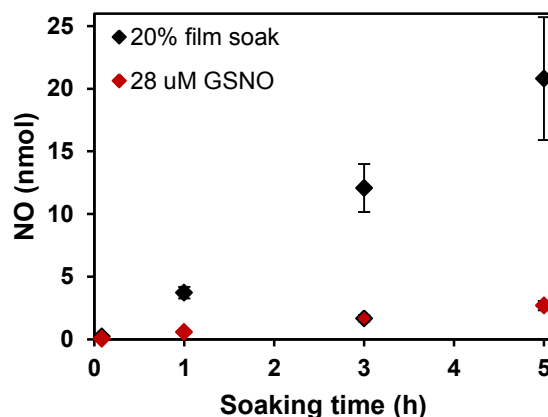


Figure 6.14 The total amount of released NO at various time points (5 min, 1 h, 3 h, 5 h) over a 5 h analysis duration for 20 w/w% GSNO-incorporated Tygon films exposed to 1 mL PBS or 28 μM GSNO in PBS (each at 37 $^{\circ}\text{C}$). Each point represents an $n=3$.

The total NO recovery values of the 28 μM GSNO control that corresponded to the GSNO found in the soaking solution of the films only yielded 2.7 ± 0.4 nmol NO over 5 h. Since the 20 w/w% GSNO-incorporated film system yielded 20.8 ± 4.9 nmol, the 28 μM leachate only contributed 13% of the total NO released from the soaked material. The amount of GSNO that decomposed to yield the NO that was recovered from the 28 μM GSNO solution was not significant enough to result in a detectable change in absorbance after 5 h using the GSNO assay. The amount of GSNO (28 μM) that is detected intact in the soaking solution after the 20 w/w% GSNO-Tygon film soak will give rise to detectable NO. However, the decomposition of the solution-phase GSNO only accounts for $\sim 10\%$ of the total NO that is released from the total GSNO-Tygon/PBS system (not distinguishable within the LOD of the GSNO assay). The GSNO found in solution (0.028 μmol) accounts for only 0.2% of the total GSNO that was blended into the Tygon film (12 μmol GSNO incorporated per film). Because such a small amount of the total GSNO in the system is leaching into the soaking solution, the majority of the GSNO remains in the polymer phase. Subsequently, the majority of the NO that is released from the system is due to the bulk GSNO that is present in the film.

Overall, the GSNO leaching studies and the total thiol assay indicate that a burst of GSNO is released into the soaking solution after only 5 min – 1 h of film soak, followed by no more significant donor leaching for the remainder of the soaking period, with $>80\%$ of the donor leaching within only 5 min. Compared to the theoretical amount of GSNO present in the entire Tygon film (12 μmol), the amount of donor leached into the soaking solution (0.028 μmol) accounts for only $\sim 0.25\%$ of the total GSNO that is available in the system. The amount of NO that is released by the leached, solution-phase GSNO (28 μM) is quite minimal in comparison to the total amount of NO that is released by the GSNO-incorporated Tygon system (13%) and it is

not within the sensitivity of the assays employed to monitor changes in the total thiol content or GSNO concentration in soaking solution.

One approach that has been employed in the field of NO releasing materials is the use of a polymer top coat to prevent the donor at the surface of the film from leaching into the soaking solution.^{2, 11, 14} We recently reported that top coating methods can be an effective way of accomplishing this.⁵ For the Tygon system reported herein, we briefly investigated the effect of a top coat layer to prevent donor leaching for this system. This was accomplished by adding an additional 200 μ L aliquot of blank Tygon polymer solution over top of the cured 20 w/w% GSNO-incorporated Tygon base film. The NO flux profile (Figure 6.15) demonstrated a slowed release over the 5 h duration ($0.32 \pm 0.10 \times 10^{-10}$ mol NO $\text{cm}^{-2} \text{min}^{-1}$) compared to the film that was not top coated ($0.64 \pm 0.05 \times 10^{-10}$ mol NO $\text{cm}^{-2} \text{min}^{-1}$), where the NO flux and total NO recovery was about half that of the non-top coated films (Table 6.2).

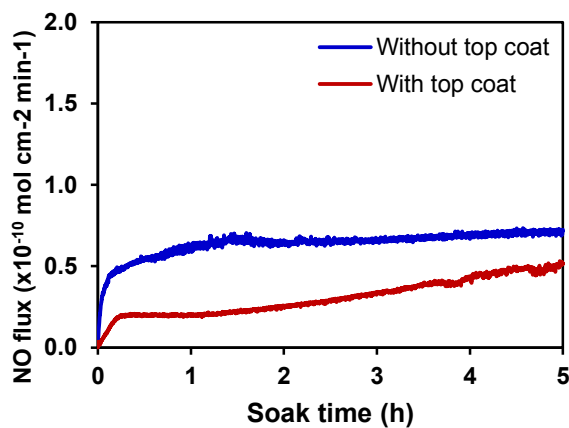


Figure 6.15 The NO release profiles as measured by chemiluminescence for a 20 w/w% GSNO-incorporated Tygon film with or without a top coat, exposed to 1 mL PBS (pH 7.4) at 37 °C. Each profile represents n=3 with an average flux error of 12% for each profile.

Top coat layers have been previously demonstrated to slow the release of NO from donor-incorporated polymer systems.² A GSNO assay performed on the recovered soaking solution from the top coated film quantified $10.8 \pm 1.7 \mu\text{M}$ GSNO (Table 6.4), indicating that some of the donor did leach from the film over the 5 h soaking period. This is a decrease in concentration compared to the non-top coated films ($27.2 \pm 4.3 \mu\text{M}$ after 5 h); however, the addition of the top coat did not completely prevent donor leaching, likely due to mixing of the donor-containing polymer layer and the blank top coat layer. An initial attempt at a top coat, therefore, was not an effective method for entirely preventing donor leaching into the buffer soaking solution. Based on previous work, it is likely that multiple top coats would be required to altogether eliminate donor leaching.⁵

Table 6.4 Data summary for intact GSNO and total thiol (GSH) in the PBS soaking solution recovered from various w/w% GSNO-incorporated Tygon films exposed to buffer at 37 °C for a 5 h duration.

w/w% GSNO	[GSNO] (μM)	[GSH] (μM)
1	2.4 ± 0.1	3.4 ± 0.9
5	5.1 ± 0.4	3.7 ± 0.2
10	9.5 ± 0.7	8.3 ± 0.7
20	27.2 ± 4.3	31.4 ± 6.2
30	31.1 ± 5.4	41.8 ± 6.1
20 (with top coat)	10.8 ± 1.7	13.1 ± 3.8

6.4.5 Monitoring surface sulfur content. Using SEM coupled to Energy Dispersive X-ray Spectroscopy (EDS), the S content on the surface of the 20 w/w% GSNO-incorporated Tygon films was determined before and throughout the soaking period by monitoring the S peak at ~ 2.3

keV. By measuring the surface S as a function of soaking time, this informed the behavior of the GSNO on the surface of the film. The SEM images of the 20 w/w% GSNO-incorporated Tygon films pre- and post-soak are shown in Figure 6.16 (1000 \times magnification) along with the corresponding EDS maps that track the phase containing S.

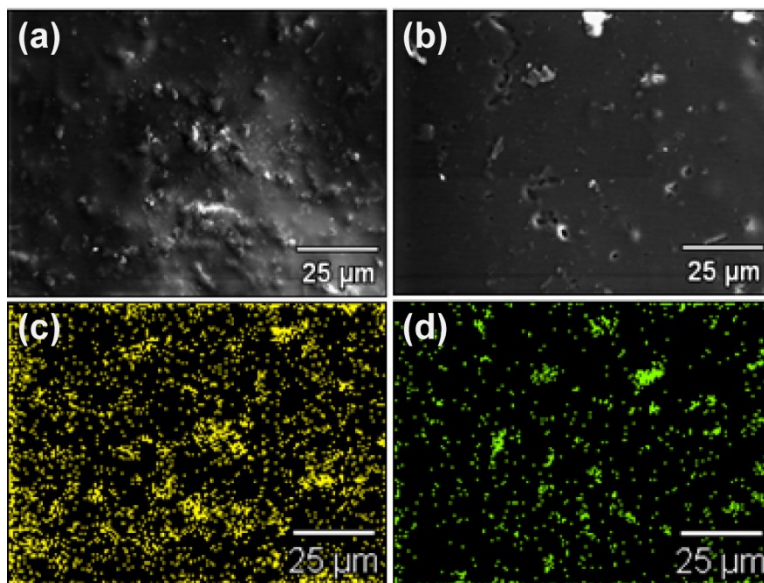


Figure 6.16 Representative SEM images of the 20 w/w% GSNO-incorporated Tygon films at 1000 \times magnification both (a) before and (b) after a 5 h soak (PBS, 37 °C). The corresponding EDS maps are shown for the S-containing phase for the (c) pre- and (d) post-soak samples.

Figure 6.17 shows the EDS map corresponding to the S-containing phase of the surface over time. It can be seen that the % area of the phase containing S decreases over the course of the soaking time. Table 6.5 shows the data corresponding to the % of the total surface area that is composed by the S-containing phase, as well as the atom % of the S-containing phase that is due to S. Based upon these percentages, the % of the total surface area due to S presence was determined.

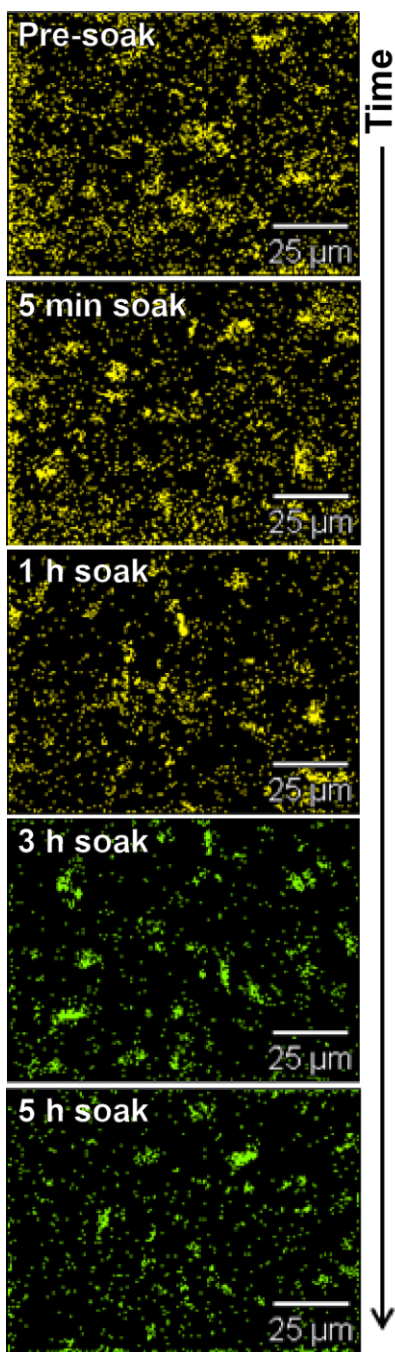


Figure 6.17 The SEM-EDS maps (1000× magnification) corresponding to the S-containing phase of the GSNO-incorporated Tygon films as a function of soaking time.

Table 6.5 Determination of % S on the surface of GSNO-incorporated Tygon films.

Soaking time (h)	Area % of phase ^a	Atom % of S in phase ^b	% of total surface due to S	% of total S removed from surface
0	93.1	0.65 ± 0.02	0.61 ± 0.019	0
0.08	12.8	0.61 ± 0.02	0.08 ± 0.003	87.1 ± 2.9
1	7.7	0.87 ± 0.01	0.07 ± 0.001	89.0 ± 1.0
3	5.3	1.06 ± 0.02	0.06 ± 0.001	90.6 ± 1.7
5	5.4	0.70 ± 0.02	0.04 ± 0.001	93.7 ± 2.7

^a Represents the total surface area that is occupied by the phase that contains S

^b Represents the atom % due to sulfur in the phase that contains S

The SEM-EDS analysis reveals an obvious phase-separation corresponding to the GSNO donor that is present on the surface of the Tygon film. The surface elemental composition of S for the donor-incorporated film pre-soak was $0.61 \pm 0.02\%$, and, as shown in Figure 6.18, 90% of this surface S is removed upon 5 min – 1 h soaking period. This matches, within error, the values associated with the percent of leached GSNO as a function of time (values at each time point are statistically the same at 99% CL). By tracking the surface S in conjunction with the % leached GSNO from the GSNO assay, we see that the GSNO that is found in solution is due to GSNO that is present on the surface of the film, which is removed almost completely within a 5 min exposure of the polymer surface to the soaking buffer. It can be additionally noted that the surface analysis of the blank Tygon film showed no surface S neither pre- nor post-soak, indicating that the S on the surface of the GSNO-incorporated films is due to the presence of donor present on the material surface.

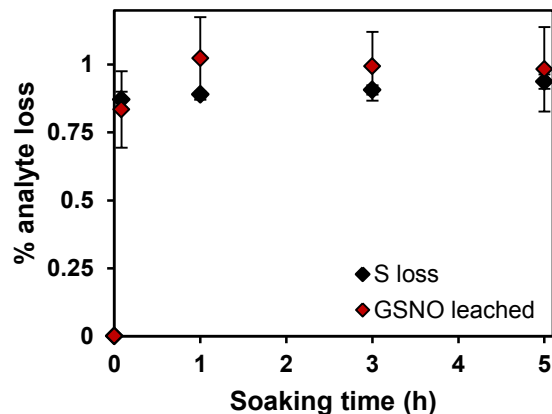


Figure 6.18 For a 20 w/w% GSNO-incorporated Tygon film system, the percent decrease in the amount of elemental surface S or the percent of total leached GSNO into soaking solution is represented. Each point represents an n=9 for the GSNO values, while the elemental S data was taken as the atom % based upon SEM imaging (140 $\mu\text{m} \times 110 \mu\text{m}$ area imaged per sample).

6.4.6 Varying donor concentration in the film. The amount of donor that is incorporated into the Tygon matrix will dictate the amount of NO that is ultimately available for release over the lifetime of the material. As such, it is important to understand how varying the donor concentration will impact the NO release properties as well as the leaching of the GSNO from the system. To investigate this, the amount of donor was varied to include 1, 5, 10, and 30 w/w% GSNO-incorporated films. The average NO fluxes for the films containing 5, 10, and 30 w/w% GSNO were statistically the same as the 20 w/w% GSNO films within error (Table 6.2, Figure 6.8). It was not until the concentration of GSNO was dropped to 1 w/w% that there was a decrease observed in the NO flux ($0.47 \pm 0.06 \times 10^{-10} \text{ mol NO cm}^{-2} \text{ min}^{-1}$). When considering the amount of GSNO that was incorporated into each film, the percent of NO released based upon that available reservoir was < 1% for the 5-30 w/w% films. The kinetics of NO release were the

same for these films because the amount of GSNO that decomposed within the film to yield NO is such a small percentage of the total GSNO reservoir.

Previous studies involving GSNO-blended polymer films have indicated a difference in the NO release profile depending upon the amount of GSNO in the system.¹⁵ However, for the hydrophilic polymer systems considered for those studies, the majority (90%) of the NO reservoir was released within a 24 h time period at physiological temperature, where the kinetics of donor decomposition in the polymer system were found to be significantly slowed compared to solution-phase GSNO decomposition. Overall, this cage effect was found to result in slower donor decomposition kinetics due to the presence of a hydrophilic polymer, which has also been demonstrated for other polymer systems.³⁸ Further studies performed on the hydrophilic polymer system indicated that changes in the pore size and morphology of the polymer resulted in differences in GSNO leaching from the polymer matrix.¹⁸ Considering all of these findings, we can see that the Tygon matrix presented herein is such that the bulk of the GSNO will remain in the polymer film. It can therefore be determined that the morphology of the material is such that the GSNO is severely diffusion limited compared to these other studies that employ higher water uptake polymers, which would result in an even more increased cage effect. This cage effect is clearly reflected in the NO release kinetics for these GSNO-incorporated Tygon films, where the NO release is severely delayed, with only 1% of the NO reservoir being released for the 20 w/w% samples over a 24 h period. Additional slowing of the GSNO in the Tygon matrix could be due to the stabilization of GSNO within acidic microdomains of the polymer film. It is established that the thermal degradation of poly(vinyl chloride) below 600 °C will result in HCl as the major product,³⁹ which could yield acidic microdomains within the Tygon matrix. Since RSNOs have been shown to be stabilized under acidic conditions,⁴⁰ the acidic microdomains

could slow down the GSNO decomposition. This microdomain phenomenon and its influence on NO release rates has been demonstrated previously for *N*-diazoniumdiolate materials.¹³ The microdomain influence on NO release also strongly suggests that the GSNO is likely remaining entrapped in the material phase. Overall, because the donor decomposition is delayed in the Tygon matrix, such a small percentage of the available GSNO actually decomposes, resulting in similar NO release kinetics for the 5-30 w/w% samples.

To consider the effect of donor concentration within the film on the amount of GSNO leachate, a GSNO assay was performed on the soaking solutions for the 1, 5, 10, and 30 w/w% GSNO-incorporated Tygon films. The amount of GSNO found intact in the soaking solution was statistically the same as that of the total GSH concentration (Figure 6.19, Table 6.4), indicating once again that the GSNO that leached into the solution did not contribute to the bulk of the detected NO in the system. There is a dependence on the w/w% of GSNO incorporated into the material matrix and the amount of GSNO donor that was found intact in the PBS solution at the end of the 5 h soaking period. A higher w/w% will result in more surface GSNO which is available to leach into the soaking solution.

An in-depth look at the 10 w/w% GSNO-incorporated samples (Figure 6.20) shows that, in a similar fashion as the 20 w/w% system, the amount of GSNO that leaches from the 10 w/w% donor-incorporated films was nearly completely removed within a 5 min soak period. Additionally, a total thiol assay on the soaking solutions revealed that the $[GSH_{total}]$ values were statistically the same (99% CL) as the $[GSNO]$ values for the 10 w/w% samples (Table 6.6) at different time points across the 5 h soaking duration. This once again demonstrates that the GSNO in solution is not giving rise to the bulk of the NO detected in the system. By cutting the donor concentration in half, we find that the NO release profile is maintained at a flux that

mimics the lower end of the natural endothelium while the amount of surface GSNO that is available to leach from the system is significantly reduced.

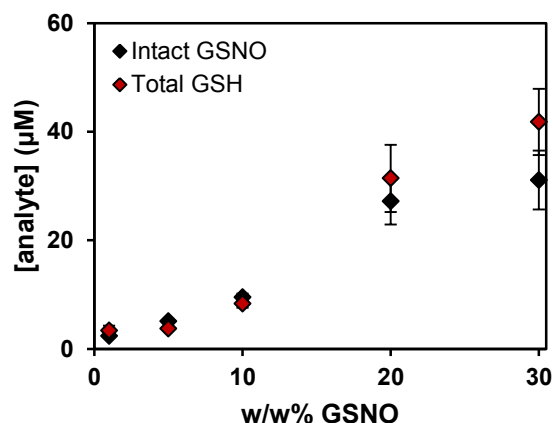


Figure 6.19 GSNO and GSH concentrations in the soaking buffer after a 5 h film soak (pH 7.4, 37 °C) as a function of w/w% GSNO incorporated into the Tygon film ($n \geq 3$).

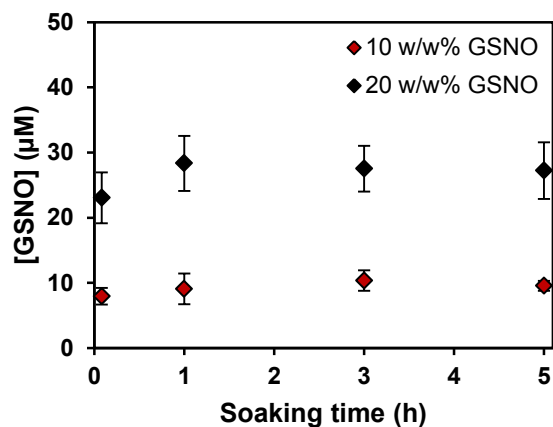


Figure 6.20 GSNO leaching profiles corresponding to the 10 and 20 w/w% GSNO-blended Tygon films upon exposure to 1 mL PBS (pH 7.4) at 37 °C for a 5 h duration. Points for the 20 w/w% samples represent an $n=9$, while the 10 w/w% samples represent an $n=7$.

Table 6.6 Data summary for GSNO leaching and total thiol assays corresponding to GSNO-blended Tygon films exposed to buffer at 37 °C.

Soaking time (h)	20 w/w% GSNO ^a		10 w/w% GSNO ^b	
	[GSNO] (μM)	[GSH _{total}] (μM)	[GSNO] (μM)	[GSH _{total}] (μM)
0.08	23.1 ± 3.9	30.9 ± 5.7	7.9 ± 1.3	6.0 ± 0.3
1	28.3 ± 4.2	22.3 ± 1.7	9.1 ± 2.4	7.4 ± 0.5
3	27.5 ± 3.5	22.0 ± 1.8	10.3 ± 1.6	8.2 ± 0.4
5	27.2 ± 4.3	31.4 ± 6.2	9.5 ± 0.7	8.3 ± 0.7

^aData represents n=9

^bData represents n=7

6.4.7 Surface properties pre- and post-soak. To generally assess the impact of the GSNO-incorporated Tygon film coatings on the biocompatibility of the surface, surface wettability and roughness measurements were made. Each of these surface properties has been found to impact the blood-compatibility of materials in general.⁴¹ The surface wettability was assessed by water contact angle goniometry. The contact angle was established for blank Tygon and 20 w/w% GSNO-incorporated Tygon films pre- and post-soak (Table 6.7). The blank Tygon film exhibited a contact angle of $102.9 \pm 2.9^\circ$ pre-soak and $102.5 \pm 1.8^\circ$ post-soak, compared to $97.1 \pm 2.6^\circ$ for the 20 w/w% GSNO-incorporated Tygon surface pre-soak. The blank Tygon films exhibited the same contact angle before and after 5 h of film soak, indicating no effect on the Tygon surface wettability due to exposure to PBS at 37 °C. Additionally, the contact angle values for the blank Tygon and 20 w/w% GSNO-incorporated Tygon films pre-soak were not statistically different, indicating that the addition of GSNO did not significantly impact the wettability of the Tygon surface. Upon soaking the GSNO-incorporated films, the water contact angle remained the same ($98.4 \pm 1.8^\circ$). Overall, the water contact angle for all samples ranged from 95-103° which indicates generally hydrophobic surfaces. The small difference in the range of the contact angle

values means that the surfaces are of comparable relative hydrophobicity regardless of GSNO incorporation and subsequent exposure to PBS.

Table 6.7 Summary of surface properties corresponding to blank and 20 w/w% GSNO-incorporated Tygon films before and after exposure to buffer at 37 °C.

Sample	Soaking time (h)	Water contact angle (°)	Ra (nm) ^a
Blank Tygon	Pre-soak	102.9 ± 2.9	10.4 ± 1.1
	5	102.5 ± 1.8	12.9 ± 2.0
20 w/w% GSNO Tygon	Pre-soak	97.1 ± 2.6	49.8 ± 8.0
	0.08	97.1 ± 2.0	44.6 ± 15.8
	1	95.6 ± 5.1	37.3 ± 5.9
	3	97.1 ± 3.6	35.0 ± 6.1
	5	98.4 ± 1.8	29.9 ± 5.8

^aAverage surface roughness determined from optical profilometry.

When considering the SEM images of the GSNO-incorporated surfaces pre- and post-soak (Figure 6.16), it is difficult to assess whether or not there were changes in the surface features after soaking. In order to account for the topography of the surfaces, optical profilometry was employed to determine the average surface roughness (Ra). The surface roughness of the blank Tygon film (10.4 ± 1.1 nm) did not vary within statistical error after 5 h of film soak (12.9 ± 2.0 nm) indicating no effect of the soaking process on the roughness of the Tygon surface. Compared to the blank Tygon films, the surface roughness increased after the incorporation of 20 w/w% GSNO (49.8 ± 8.0 nm). After exposure of the GSNO-incorporated Tygon films to soaking solution for different time durations, it appears that there is a trend of decreasing surface roughness with increasing soak time (Table 6.7); however, there is no statistical difference between any of the values at 99% CL. Overall, larger error bars associated with the Ra value due

to variance in the surface upon GSNO incorporation did not result in a clear trend for the surface roughness with increasing film soak time. It is clear from the profilometry analysis that the incorporation of the GSNO into the Tygon matrix definitely increased the surface roughness. However, due to variability in the surface morphology, no statistical difference was seen for the donor-incorporated films upon exposure to PBS. The surface roughness of the Tygon film increased by >20 nm when GSNO was incorporated, thereby potentially impacting the adsorption of biological components compared to the blank Tygon surface. For instance, it has been previously established that a surface roughness change of ~20 nm or greater will fall within the range of surface variability that will impact the interaction of the material with proteins.⁴² This point is mentioned because the incorporation of the GSNO into the Tygon film will likely impact the adsorption of key biological components when compared to the blank Tygon film. Overall, the incorporation of 20 w/w% GSNO into a Tygon film did not affect the surface wettability significantly, but did lead to an increase in surface roughness. The surface roughness values, however, did not change significantly for the GSNO-incorporated films over the course of the soaking period within the range of impacting biological factors, such as proteins.

It was mentioned earlier that the 20 w/w% GSNO formulation underwent analysis for 1 week to assess the ability of the films to release NO for a prolonged period of time. The Tygon film stayed intact for this duration of NO release, and additional surface analysis indicated a water contact angle of $101.5 \pm 0.6^\circ$ and an average surface roughness (Ra) of 21.9 ± 10.6 nm for the films soaked for 1 week. These values are not statistically different at the 99% confidence level from the values corresponding to the 5 h soaked samples, indicating that these surface properties are not changing with a significantly prolonged soaking period.

6.5 CONCLUSIONS

For a model Tygon system, we have demonstrated that the addition of 20 w/w% GSNO into the polymer matrix will result in an NO releasing film. The GSNO on the surface of the film leached into the soaking buffer nearly completely within 5 min of exposure time, after which point the GSNO concentration remained steady (1 h – 5 h). The total amount of leached donor represented <0.25% of the total GSNO reservoir that was contained within the Tygon matrix. Analysis of the S content on the surface of the films further indicated that the surface-bound GSNO was removed from the film almost immediately. Using a total thiol assay, we found that the total thiol content in the soaking solution was due only to intact GSNO at the end of the soaking period, thus demonstrating that the GSNO in the soaking solution did not significantly decompose. The amount of NO recovered due to the solution-phase GSNO decomposition was ~10% of the total NO that was released by the system. Overall, the bulk of the recovered NO was due to GSNO decomposition within the film, resulting in the localized NO delivery that is desired from these systems for bioapplications involving blood-contacting extracorporeal circuitry. The NO flux associated with this Tygon system was $0.64 \pm 0.05 \times 10^{-10}$ mol NO cm⁻² min⁻¹, which mimics the lower end of natural endothelium NO release. The NO release and minimal donor leaching over the 5 h time frame are relevant to ECC applications. Further, the surface properties of the system indicated hydrophobic films with minimal variation in surface roughness upon soaking, making them strong candidates as biomaterials. Upon varying the amount of GSNO in the system from 5-30 w/w%, the NO release properties remained the same, but a smaller amount of GSNO on the surface was available to leach into the soaking solution for the lower w/w% films.

Overall, toward the ability to develop Tygon surfaces with enhanced biocompatibility to overcome blood-clotting and infection-related complications, the incorporation of GSNO appears quite promising. Donor leaching is considered a prevalent problem with donor-incorporated systems, but the only donor that is leached from this system is initially surface-bound GSNO, and it is quickly removed upon soaking (~5 min). To prevent this surface GSNO from being swept into the blood, which could lead to downstream effects, the GSNO-Tygon coated tubing need only be pre-rinsed prior to application. More specifically, the GSNO at the surface of the material will be removed nearly completely within 5 min, and the NO flux will reach a steady state at the lower end of the endothelial release range within roughly 15 min of soaking time. Therefore, treating the material coating with a pre-soak step will effectively eliminate surface bound donor as well as reach a constant NO flux. During the subsequent 5 h time period associated with a typical hemodialysis procedure, these coatings will release NO on the order of the natural endothelium and maintain critical surface properties, such as wettability and roughness, relative to the non-soaked sample. The ability to maintain predominantly localized NO release associated with these coatings is critical to their application as blood-contacting devices.

CHAPTER 6 REFERENCES

1. ECLS Registry Report of the Extracorporeal Life Support Organization (ELSO). ECLS Registry Report of the Extracorporeal Life Support Organization (ELSO), Ann Arbor, Michigan, January, 2012.
2. Major, T. C.; Brant, D. O.; Reynolds, M. M.; Bartlett, R. H.; Meyerhoff, M. E.; Handa, H.; Annich, G. M., The Attenuation of Platelet and Monocyte Activation in a Rabbit Model of Extracorporeal Circulation by a Nitric Oxide Releasing Polymer. *Biomaterials* **2010**, *31*, 2736-2745.
3. Skrzypchak, A. M.; Lafayette, N. G.; Bartlett, R. H.; Zhou, Z. R.; Frost, M. C.; Meyerhoff, M. E.; Reynolds, M. M.; Annich, G. M., Effect of Varying Nitric Oxide Release to Prevent Platelet Consumption and Preserve Platelet Function in an in vivo Model of Extracorporeal Circulation. *Perfusion* **2007**, *22*, 193-200.
4. Radomski, M. W.; Palmer, R. M. J.; Moncada, S., The Anti-aggregating Properties of Vascular Endothelium: Interactions Between Prostacyclin and Nitric Oxide. *Br. J. Pharmac.* **1987**, *92*, 639-646.
5. Lantvit, S. M.; Barrett, B. J.; Reynolds, M. M., Nitric Oxide Releasing Material Adsorbs More Fibrinogen. *J. Biomed. Mater. Res., Part A* **2013**, *101*, 3201-3210.
6. Ialenti, A.; Ianaro, A.; Moncada, S.; Di Rosa, M., Modulation of Acute Inflammation by Endogenous Nitric Oxide. *Eur. J. Pharmacol.* **1992**, *211*, 177-182.
7. Bogdan, C., Nitric Oxide and the Immune Response. *Nat. Immunol* **2001**, *2*, 907-916.
8. Frost, M. C.; Reynolds, M. M.; Meyerhoff, M. E., Polymers Incorporating Nitric Oxide Releasing/Generating Substances for Improved Biocompatibility of Blood-Contacting

- Medical Devices. *Biomaterials* **2005**, *26*, 1685-1693; Riccio, D. A.; Schoenfisch, M. H., Nitric Oxide Release: Part I. Macromolecular Scaffolds. *Chem. Soc. Rev.* **2012**, *41*, 3731-3741.
9. Seabra, A. B.; Duran, N., Nitric Oxide-Releasing Vehicles for Biomedical Applications. *J. Mater. Chem.* **2010**, *20*, 1624-1637; Varu, V. N.; Tsihliis, N. D.; Kibbe, M. R., Nitric Oxide-Releasing Prosthetic Materials. *Vasc. Endovascular Surg.* **2009**, *43*, 121-131; Naghavi, N.; de Mel, A.; Alavijeh, O. S.; Cousins, B. G.; Seifalian, A. M., Nitric Oxide Donors for Cardiovascular Implant Applications. *Small* **2012**, *9*, 22-35.
 10. Smith, D. J.; Chakravarthy, D.; Pulfer, S.; Simmons, M. L.; Hrabie, J. A.; Citro, M. L.; Saavedra, J. E.; Davies, K. M.; Hutsell, T. C.; Mooradian, D. L.; Hanson, S. R.; Keefer, L. K., Nitric Oxide-Releasing Polymer Containing the [N(O)NO]- Group. *J. Med. Chem.* **1996**, *39*, 1148-1156.
 11. Mowery, K. A.; Schoenfisch, M. H.; Saavedra, J. E.; Keefer, L. K.; Meyerhoff, M. E., Preparation and Characterization of Hydrophobic Polymeric Films that are Thromboresistant via Nitric Oxide Release. *Biomaterials* **2000**, *21*, 9-21.
 12. Schoenfisch, M. H.; Zhang, H.; Frost, M. C.; Meyerhoff, M. E., Nitric Oxide-Releasing Fluorescence-Based Oxygen Sensing Polymeric Films. *Anal. Chem.* **2002**, *74*, 5937-5941.
 13. Batchelor, M. M.; Reoma, S. L.; Fleser, P. S.; Nuthakki, V. K.; Callahan, R. E.; Shanley, C. J.; Politis, J. K.; Elmore, J.; Merz, S. I.; Meyerhoff, M. E., More Lipophilic Dialkyldiamine-Based Diazeniumdiolates: Synthesis, Characterization, and Application in Preparing Thromboresistant Nitric Oxide Release Polymeric Coatings. *J. Med. Chem.* **2003**, *46*, 5153-5161.

14. Fleser, P. S.; Nuthakki, V. K.; Malinzak, L. E.; Callahan, R. E.; Seymour, M. L.; Reynolds, M. M.; Merz, S. I.; Meyerhoff, M. E.; Bendick, P. J.; Zelenock, G. B.; Shanley, C. J., Nitric Oxide-Releasing Biopolymers Inhibit Thrombus Formation in a Sheep Model of Arteriovenous Bridge Grafts. *J. Vasc. Surg.* **2004**, *40*, 803-811.
15. Seabra, A. B.; de Oliveira, M. G., Poly(vinyl alcohol) and Poly(vinyl pyrrolidone) Blended Films for Local Nitric Oxide Release. *Biomaterials* **2004**, *25*, 3773-3782.
16. Seabra, A. B.; de Souza, G. F. P.; da Rocha, L. L.; Eberlin, M. N.; de Oliveira, M. G., S-nitrosoglutathione Incorporated in Poly(ethylene glycol) Matrix: Potential Use for Topical Nitric Oxide Delivery. *Nitric Oxide* **2004**, *11*, 263-272.
17. Seabra, A. B.; da Rocha, L. L.; Eberlin, M. N.; de Oliveira, M. G., Solid Films of Blended Poly(vinyl alcohol)/Poly(vinyl pyrrolidone) for Topical S-nitrosoglutathione and Nitric Oxide Release. *J. Pharm. Sci.* **2005**, *94*, 994-1003.
18. Simoes, M. M. D. G.; de Oliveira, M. G., Poly(vinyl alcohol) Films for Topical Delivery of S-nitrosoglutathione: Effect of Freezing-Thawing on the Diffusion Properties. *J. Biomed. Mater. Res., Part B* **2010**, *93B*, 416-424.
19. Williams, D. L. H., The Chemistry of S-nitrosothiols. *Acc. Chem. Res.* **1999**, *32*, 869-876.
20. Annich, G. M.; Meinhardt, J. P.; Mowery, K. A.; Ashton, B. A.; Merz, S. I.; Hirschl, R. B.; Meyerhoff, M. E.; Bartlett, R. H., Reduced Platelet Activation and Thrombosis in Extracorporeal Circuits Coated with Nitric Oxide Release Polymers. *Crit. Care Med.* **2000**, *28*, 915-920.
21. Wu, Y. D.; Zhou, Z. R.; Meyerhoff, M. E., In vitro Platelet Adhesion on Polymeric Surfaces with Varying Fluxes of Continuous Nitric Oxide Release. *J. Biomed. Mater. Res., Part A* **2007**, *81A*, 956-963.

22. Vaughn, M. W.; Kuo, L.; Liao, J. C., Estimation of Nitric Oxide Production and Reaction Rates in Tissue by use of a Mathematical Model. *Am. J. Physiol. Heart Circ. Physiol.* **1998**, *274*, H2163-H2176.
23. Jen, M. C.; Serrano, M. C.; van Lith, R.; Ameer, G. A., Polymer-Based Nitric Oxide Therapies: Recent Insights for Biomedical Applications. *Adv. Funct. Mater.* **2012**, *22*, 239-260.
24. Damodaran, V. B.; Joslin, J. M.; Wold, K. A.; Lantvit, S. M.; Reynolds, M. M., S-nitrosated Biodegradable Polymers for Biomedical Applications: Synthesis, Characterization and Impact of Thiol Structure on the Physicochemical Properties. *J. Mater. Chem.* **2012**, *22*, 5990-6001.
25. Wang, W.; Ballatori, N., Endogenous Glutathione Conjugates: Occurrence and Biological Functions. *Pharmacol. Rev.* **1998**, *50*, 335-356.
26. Malchesky, P. S., Extracorporeal Artificial Organs. In *Biomaterials Science*, 2 ed.; Buddy, D. R.; Hoffman, S. H.; Schoen, F. J.; Lemons, J. E., Eds. Academic Press: San Diego, 1996; pp 514-526.
27. Hennessy, V. L.; Hicks, R. E.; Niewiarowski, S.; Edmunds, L. H.; Colman, R. W., Function of Human Platelets During Extracorporeal Circulation. *Am. J. Physiol. Heart Circ. Physiol.* **1977**, *232*, H622-H628; Zhang, H.; Annich, G. M.; Miskulin, J.; Osterholzer, K.; Merz, S. I.; Bartlett, R. H.; Meyerhoff, M. E., Nitric Oxide Releasing Silicone Rubbers with Improved Blood Compatibility: Preparation, Characterization, and in vivo Evaluation. *Biomaterials* **2002**, *23*, 1485-1494; Major, T. C.; Brant, D. O.; Burney, C. P.; Amoako, K. A.; Annich, G. M.; Meyerhoff, M. E.; Handa, H.; Bartlett, R. H., The Hemocompatibility

- of a Nitric Oxide Generating Polymer that Catalyzes S-nitrosothiol Decomposition in an Extracorporeal Circulation Model. *Biomaterials* **2011**, *32*, 5957-5969.
28. Hart, T. W., Some Observations Concerning the S-nitroso and S-phenylsulphonyl Derivatives of L-cysteine and Glutathione. *Tetrahedron Lett.* **1985**, *26*, 2013-2016.
29. Ellman, G. L., A Colorimetric Method for Determining Low Concentrations of Mercaptans. *Arch. Biochem. Biophys.* **1958**, *74*, 443-450; Ellman, G. L., Tissue Sulfhydryl Groups. *Arch. Biochem. Biophys.* **1959**, *82*, 70-77.
30. Jocelyn, P. C., Chemical Reduction of Disulfides. *Methods Enzymol.* **1987**, *143*, 246-256.
31. Szacilowski, K.; Stasicka, Z., S-nitrosothiols: Materials, Reactivity and Mechanisms. *Prog. React. Kinet. Mech.* **2001**, *26*, 1-58.
32. Lu, J.; Wittbrodt, J. M.; Wang, K.; Wen, Z.; Schlegel, H. B.; Wang, P. G.; Cheng, J., NO Affinities of S-nitrosothiols: A Direct Experimental and Computational Investigation of RS-NO Bond Dissociation Energies. *J. Am. Chem. Soc.* **2001**, *123*, 2903-2904; Grossi, L.; Montecvecchi, P. C., A Kinetic Study of S-nitrosothiol Decomposition. *Chem. Eur. J.* **2002**, *8*, 380-387; Bartberger, M. D.; Mannion, J. D.; Powell, S. C.; Stamler, J. S.; Houk, K. N.; Toone, E. J., S-N Dissociation Energies of S-nitrosothiols: On the Origins of Nitrosothiol Decomposition Rates. *J. Am. Chem. Soc.* **2001**, *123* (36), 8868-8869.
33. Marxer, S. M.; Rothrock, A. R.; Nablo, B. J.; Robbins, M. E.; Schoenfisch, M. H., Preparation of Nitric Oxide (NO)-Releasing Sol-Gels for Biomaterial Applications. *Chem. Mater.* **2003**, *15*, 4193-4199; Riccio, D. A.; Dobmeier, K. P.; Hetrick, E. M.; Privett, B. J.; Paul, H. S.; Schoenfisch, M. H., Nitric Oxide-Releasing S-nitrosothiol-Modified Xerogels. *Biomaterials* **2009**, *30*, 4494-4502.

34. Marxer, S. M.; Robbins, M. E.; Schoenfisch, M. H., Sol-gel Derived Nitric Oxide-Releasing Oxygen Sensors. *Analyst* **2005**, *130*, 206-212.
35. Dobmeier, K. P.; Schoenfisch, M. H., Antibacterial Properties of Nitric Oxide-Releasing Sol-Gel Microarrays *Biomacromolecules* **2004**, *5*, 2493-2495.
36. Zhang, H.; Annich, G. M.; Miskulin, J.; Stankiewicz, K.; Osterholzer, K.; Merz, S. I.; Barlett, R. H.; Meyerhoff, M. E., Nitric Oxide-Releasing Fumed Silica Particles: Synthesis, Characterization and Biomedical Application. *J. Am. Chem. Soc.* **2003**, *125*, 5015-5024.
37. Robbins, M. E.; Hopper, E. D.; Schoenfisch, M. H., Synthesis and Characterization of Nitric Oxide-Releasing Sol-Gel Microarrays. *Langmuir* **2004**, *20*, 10296-10302.
38. Shishido, S. M.; de Oliveira, M. G., Polyethylene Glycol Matrix Reduced the Rates of Photochemical and Thermal Release of Nitric Oxide from S-nitroso-N-acetylcysteine. *Photochem. Photobiol.* **2000**, *71*, 273-280; Shishido, S. M.; Seabra, A. B.; Loh, W.; de Oliveira, M. G., Thermal and Photochemical Nitric Oxide Release from S-nitrosothiols Incorporated in Pluronic F127 Gel: Potential Uses for Local and Controlled Nitric Oxide Release. *Biomaterials* **2003**, *24*, 3543-3553.
39. Stromberg, R. R.; Straus, S.; Achhammer, B. G., Thermal Decomposition of Poly(vinyl chloride). *J. Polym. Sci.* **1959**, *35*, 355-368; Jimenez, A.; Berenguer, V.; Lopez, J.; Sanchez, A., Thermal Degradation Study of Poly(vinyl chloride): Kinetic Analysis of Thermogravimetric Data. *J. Appl. Polym. Sci.* **1993**, *50*, 1565-1573.
40. Roy, B.; Moulinet d'Hardemare, A.; Fontecave, M., New Thionitrites: Synthesis, Stability, and Nitric Oxide Generation. *J. Org. Chem.* **1994**, *59*, 7019-7026.
41. Hallab, N. J.; Bundy, K. J.; Oconnor, K.; Clark, R.; Moses, R. L., Cell Adhesion to Biomaterials: Correlations Between Surface Charge, Surface Roughness, Adsorbed Protein,

- and Cell Morphology. *J. Long-Term Eff. Med. Implants* **1995**, *5*, 209-231; Sethuraman, A.; Han, M.; Kane, R. S.; Belfort, G., Effect of Surface Wettability on the Adhesion of Proteins. *Langmuir* **2004**, *20* (18), 7779-7788; Rechendorff, K.; Hovgaard, M. B.; Foss, M.; Zhdanov, V. P.; Besenbacher, F., Enhancement of Protein Adsorption Induced by Surface Roughness. *Langmuir* **2006**, *22* (26), 10885-10888.
42. Cai, K.; Bossert, J.; Jandt, K. D., Does the Nanometre Scale Topography of Titanium Influence Protein Adsorption and Cell Proliferation? *Colloids Surf., B* **2006**, *49*, 136-144.

CHAPTER 7:
EFFECT OF WATER PLASMA TREATMENT ON NITRIC OXIDE RELEASE AND
SURFACE PROPERTIES OF S-NITROSATED POLYMER FILMS

7.1 PREFACE

In Chapter 1 of this dissertation, approaches were described for the development of functional biomaterials with tunable surface properties and/or therapeutic releasing capabilities. This chapter marks a collaborative study between the Reynolds and Fisher research groups at CSU towards the ability to modify the surface properties of NO releasing materials via plasma treatment. This manuscript is currently in preparation and is authored by A. Pegalajar-Jurado, J. M. Joslin, M. J., Hawker, M. M. Reynolds, and E. R. Fisher. The plasma treatments were performed by Dr. Dori Pegalajar-Jurado and Morgan Hawker, who performed subsequent water contact angle, XPS and SEM-EDS analysis. I performed the thiol and RSNO quantification, NO recovery studies, as well as surface roughness, IR and some SEM-EDS measurements. The data analysis, particularly the XPS interpretation, was a team effort. The authors are grateful for funding received from Colorado State University, the Department of Defense Congressionally Directed Medical Research Program (DOD-CDMRP), and the National Science Foundation (DMR 0847641 and CHE-1152963). We are thankful to Dr. Patrick McCurdy of the CSU Chemistry Central Instrument Facility for XPS, SEM and EDS support and Mr. John Wydallis and the Chuck Henry research group at CSU for profilometry technical support. This research was further supported by funds from the Boettcher Foundation's Webb-Waring Biomedical Research Program.

7.2 INTRODUCTION

Current medical device surfaces are plagued by biofouling issues, predominantly blood clot formation¹ and bacterial infection.² Functional biomaterials are critical to modulate biological responses at the material-biology interface to combat the processes that lead to severe medical complications. The physicochemical properties of a material's surface significantly affect the degree of blood clot formation³ and bacterial infection.⁴ In addition, surface properties control cell attachment and proliferation, critical factors for improving the biocompatibility of a plethora of medical devices.⁵ Surface properties that control the microorganism-surface interactions include surface chemical composition, surface free energy, surface topography, and surface wettability.⁶ It is likewise important to acknowledge that the microorganism surface hydrophobicity, charge and electronegativity also play an important role on the microorganism-surface interactions.⁷ Nonetheless, manipulation of the surface chemistry and wettability of synthetic materials is the most accessible path for controlling microorganism-surface interactions and enhancing biocompatibility. Therefore, the ability to tune material surface properties while retaining the desirable bulk properties can allow for limited bacterial attachment to prevent infection, while simultaneously favoring cell attachment and proliferation to promote material integration and healing processes. Moreover, the incorporation of therapeutic agents in the bulk material for controlled release, such as anti-thrombogenic, reendothelialization and antibiotic drugs, can help to prevent clot formation, promote wound-healing and fight potential infections, respectively.⁸

Surface modification approaches represent a passive approach to control microorganism attachment and adhesion processes, while therapeutic release approaches aim to eradicate bacteria actively and enhance cellular proliferation. Thus, a material that combines these two approaches would represent an advanced functional material that targets different biological

mechanisms, thereby offering precise control over physiological responses at the biomaterial surface. The ability to control multiple pathways associated with biocompatibility is key for developing materials for applications such as tissue engineering, wound dressing fabrication and antimicrobial materials development.

Surface chemical composition and wettability greatly influence the deposition of biological components. For example, Arima and Iwata highlighted the effect of terminal functional groups for self-assembled monolayers (SAMs) on protein adsorption and cell adhesion.⁵ An increase in protein adsorption was observed for surfaces with increasing hydrophilicity for a variety of surface functional groups (i.e. OH, CH₃/COOH). Additionally, endothelial and epithelial cells attached and spread significantly on surfaces with increasing hydrophilicity (i.e. increase in COOH or NH₂ surface groups), which promotes wound healing and device integration. Furthermore, Parreira *et. al.* reported a correlation between the presence of different functional groups on a surface (i.e. CH₃ and OH) and wettability with the increase or reduction of *Helicobacter pylori* (*H. pylori*) adhesion.⁹ Although the 17875/Leb strain showed a distinctive preference for the hydrophilic surface, the remainder of the *H. pylori* strains exhibited the opposite behavior, indicating that bacteria attachment to the material surface is both surface and strain dependent. These observations emphasize the need for materials with tunable surface chemical composition and wettability depending upon the intended application of the material as protein, cell and bacteria behavior changes, depend on the material's surface properties.

Several techniques have been demonstrated to modify the surface properties of different materials, including grafting of polymers, immobilization of biomolecules and plasma treatment.¹⁰ Plasma treatments can be a reproducible approach for modifying surface chemical composition and wettability without changing the bulk properties of the material in a sterile,

solvent-free, and low-temperature environment.¹¹ Plasmas also afford the ability to tune surface chemical composition and wettability by deposition of thin films or via implantation of desirable oxygen and nitrogen-containing functional groups for biological applications.¹² In both approaches, several process variables can be adjusted (e.g. precursor, applied power, treatment time, pressure, substrate position and gas flow rate) to impact the efficacy of the plasma treatment. Previously, we and others have used H₂O vapor plasmas to increase surface wettability of different materials by incorporating OH groups.¹³⁻¹⁵ With hydrophobic polysulfone membranes, not only did H₂O plasma treatment permanently improve wettability, but the change affected the entire membrane cross section and lasted for >2 years. In related work, Lee *et. al.* highlighted an increase in cell adhesion, spreading and growth for H₂O plasma-treated polymers.¹³ Thus, H₂O plasma treatment is a suitable methodology for changing wettability toward enhancing cell-surface compatibility. Unfavorable effects can, however, also be promoted by improved wettability, such as bacterial attachment leading to infection and biofilm formation, and thrombosis. Tuning surface wettability alone is not sufficient for developing targeted biocompatible materials and may need to be combined with additional approaches, including release of a therapeutic agent. Indeed, some approaches have involved the plasma treatment of drug-eluting polymers.¹⁶

One therapeutic agent that has demonstrated excellent antithrombogenic and antimicrobial properties is nitric oxide (NO).¹⁷ As a result of its release from endothelial cells to regulate platelet and clotting activity,¹⁸ as well as its natural role in fighting infection¹⁹ and promoting wound-healing,²⁰ NO is a multi-functional therapeutic agent. Many material platforms have been developed with the capability to release NO and have improved biocompatibility in comparison to control materials.^{3, 21} The use of NO as the agent of choice for a drug-eluting

polymer system is distinctive because NO has the capability to target multiple physiological actions, compared to other agents, such as heparin or antibiotics, which target only a single function. The current objectives in the field involve temporal and spatial control over the NO release, namely achieving appropriate NO fluxes for the intended application and ensuring that the NO release occurs directly at the material-biology interface for a localized effect. Unfortunately, NO releasing materials used for coating medical devices are generally hydrophobic, thereby potentially limiting the attachment and proliferation of cells and increasing the risk of device rejection.²² While NO releasing materials have exhibited desirable properties in terms of preventing blood clot formation and infection, these materials do not specifically address control over cell-surface interactions since the surface properties are not tuned.

An ideal NO releasing material would exhibit (a) bulk mechanical and chemical properties to ensure stability over the device lifetime when exposed to bodily fluids; (b) controllable NO release directed at the microorganism-material interface; and (c) controlled surface hydrophilicity to enhance protein adsorption and cellular adhesion. To date, no attempts to modify the surface properties of an NO releasing polymer while maintaining the bulk properties of the material have been reported. As mentioned previously, the ability to control cellular behavior at the material surface is a critical function which cannot be controlled by NO release alone. Therefore, the combined ability to tune both the NO delivery as well as the surface properties represents a unique approach to creating NO releasing biopolymers that can modulate biological interactions while fighting infection and thrombus formation.

We recently reported on a multiblock polymer system based upon the US Food and Drug Administration (FDA) approved poly(lactic-*co*-glycolic acid) polymer.²³ The polymer backbone was synthesized with covalent attachments of thiol groups, which were subsequently nitrosated

to result in *S*-nitrosated PLGH derivatives with the capability to release NO. The NO reservoir and ultimately the NO release kinetics were controlled based upon the functionality associated with the thiol site. Moreover, we developed advanced methods to enable the characterization and quantification of the *S*-nitrosothiol (RSNO) moieties on the polymer, which serve as the source of NO. When considering the PLGA literature, there are many accounts of plasma treatments to modify the polymer surface properties. Heptylamine and argon plasmas have been employed to impart amine functionality on PLGA scaffolds,²⁴ while argon plasmas have also been employed for PLGA scaffold sterilization.²⁵ Air,²⁶ oxygen^{27, 28} and ammonia²⁸ plasmas have been employed to increase PLGA surface hydrophilicity to improve cell compatibility. Therefore, it is of interest to create a scaffold based on a PLGA backbone that releases NO but also undergoes plasma treatment so that surface properties can be controlled.

Here, we expand the utility of the *S*-nitrosated PLGH system by changing the surface properties of the material by plasma treatment. Using inductively-coupled H₂O plasmas, we assessed the effects of two process parameters, applied rf power (20-50 W) and treatment time (1-5 min), on the surface properties of *S*-nitrosated PLGH polymer thin films. As a result of plasma treatment, the surface chemical composition and functional group distribution changed minimally, but surface wettability underwent a dramatic shift from hydrophobic to complete wetting. Regardless of the treatment parameters, the plasma treatment had no effect on surface roughness, and the majority of the *S*-nitrosothiol content was retained to exhibit identical NO release properties compared to the untreated polymer films. Overall, this work highlights the first demonstration of a plasma-treated NO releasing material, whereby the material retains its therapeutic activity while the surface wettability is tuned based upon the plasma treatment. The ability to controllably achieve a drug-loaded system capable of therapeutic release with tunable

surface properties represents a significant advancement towards developing functional biomaterials.

7.3 EXPERIMENTAL SECTION

7.3.1 Materials. All reagents used for the preparation of the PLGH-cysteine polymer are described elsewhere (see Chapter 4).²³ The *t*-butyl nitrite (90%) was obtained from Aldrich (St. Louis, MO, USA), and the dichloromethane (DCM) and methanol (MeOH) were obtained (ACS grade) from Fisher Scientific (Fair Lawn, NJ, USA). The DCM and MeOH solvents were stored over 4 Å molecular sieves to keep dry. Anhydrous ethanol was obtained from Pharmco Products, Inc. (Brookfield, CT, USA). Potassium carbonate (ACS grade) was purchased from Fisher Scientific (Fair Lawn, NJ, USA).

7.3.2 Preparation of *S*-nitrosated PLGH-cysteine films. The PLGH-cysteine derivative was prepared according to a previously reported synthetic scheme.^{23, 29} The synthetic details regarding the synthesis of the PLGH-cysteine derivative are presented in Chapter 4. Briefly, a carboxyl-functionalized polymer was prepared from L-lactide, glycolide and 2,2-bis(hydroxymethyl propionic acid) (HMPA) via a ring-opening melt polymerization using a stannous octoate catalyst. The carboxyl group of the HMPA polymer segment was further functionalized with cysteine after *N*-hydroxysuccinimide activation. The cysteine group was covalently attached to the PLGH backbone through an amide linkage.

To quantify the amount of thiol present in the form of cysteine pendant to the PLGH backbone, a modified Ellman's assay was performed in 2 MeOH: 1 DCM solvent. The Ellman's assay is a common colorimetric assay that is performed under aqueous conditions to quantify

thiol content.³⁰ Since PLGH is not water soluble, we performed the assay in organic solvent. Due to its solubility in the solvent system, cysteamine was the standard thiol of choice for the calibration of the absorbance response as a function of thiol content. The cysteamine standards were prepared (0-250 μM) in the MeOH/DCM solvent containing 0.5 mg mL^{-1} blank PLGH (non-thiolated) to account for the effect of the blank polymer on the absorbance reading. The PLGH-cysteine samples were prepared at 0.5 mg mL^{-1} in solvent. A 1 mL volume of each standard or sample was treated with 10 mM (1 mL) 5,5'-dithiobis-(2-nitrobenzoic acid), the Ellman's reagent, in the presence of 200 μL of a potassium carbonate-saturated solution that had stirred overnight. Upon reaction with the Ellman's reagent, a yellow chromophore was produced with a λ_{max} of 414 nm. The absorbance of each standard was measured at 414 nm and plotted as a function of the cysteamine standard concentration. All measurements were taken in triplicate to ensure reproducibility.

Nitrosation of the PLGH-cysteine to form the *S*-nitrosated polymer derivative was accomplished by using *t*-butyl nitrite as the nitrosating agent. The PLGH-cysteine (50 mg) was dissolved in 2 MeOH: 1 DCM (2 mL) in an amber, EPA-certified vial (Fisher Scientific, NJ, USA). To facilitate nitrosation, the *t*-butyl nitrite (8.4 mg in 1 mL of 2 MeOH: 1 DCM) was added to the polymer solution. The polymer solution was stirred and protected from light for 4 h, followed by a 2 h vacuum step to remove the solvent and residual *t*-butyl nitrite. The final product was a pink-colored powder which is a visual confirmation of the success of the nitrosation process.

Films of the *S*-nitrosated PLGH-cysteine were prepared by re-dissolving the polymer in 2 MeOH: 1 DCM (50 mg mL^{-1}). Aliquots of the polymer solution (100 μL) were dispensed on round glass slides (VWR micro cover glass, 12 mm diameter, 113 mm^2 area) and dried

overnight, protected from light. The mass of each individual film was determined by subtracting the mass of the glass slide from the mass of the slide containing the polymer film. All *S*-nitrosothiol and NO values were normalized by the mass of the film.

7.3.3 Plasma treatment of polymer films. H₂O plasma treatments on *S*-nitrosated PLGH-cysteine films were performed using a home-built glass tubular reactor, which was inductively coupled via a Ni-plated copper coil. Radio frequency (rf, 13.56 MHz) plasma power was applied through a matching network, and varied between plasma treatments (20, 30 or 50 W). Reactor pressure was monitored using a Baratron capacitance manometer, and was allowed to stabilize at 200 mTorr above base reactor pressure before plasma ignition. A deionized water sample (Millipore, 18 mΩ) was subjected to three freeze-pump-thaw cycles to remove trapped atmospheric gases prior to use and was introduced into the reactor from a 50 mL Pyrex sidearm vacuum flask with a Teflon stopcock. Substrates were placed on a clean glass slide 16 cm downstream from the coil for each treatment, with treatment times of 1, 3, or 5 min. Typically, nine substrates were treated simultaneously for analysis. The plasma treated films were subsequently analyzed for *S*-nitrosothiol content and NO releasing capabilities. Surface and bulk analyses (water contact angle, XPS, SEM-EDS, FTIR, , and optical profilometry) were also performed to assess the wettability, composition and morphology of the polymer films before and after treatment.

7.3.4 *S*-nitrosothiol characterization. Solution phase UV-vis measurements were performed to quantify the *S*-nitrosothiol content for the polymer films before and after plasma treatments. The polymer-coated glass slide was added to an amber, EPA-certified vial and the polymer dissolved

in 2 MeOH: 1 DCM (1 mL). The polymer solution was added to a quartz cuvette (1 cm pathlength) for subsequent UV-vis analysis on an Evolution 300 spectrophotometer (Thermo Electron). To consider the contribution of the blank polymer absorbance, non-nitrosated PLGH-cysteine controls were prepared (2, 3.5, 5 mg mL⁻¹). From this calibration curve (Figure 5.2), the blank response is subtracted from the nitrosated polymer scan based upon the polymer concentration, as described in Chapter 5.

7.3.5 NO release analysis. The NO releasing capabilities of the polymer films before and after plasma treatments were assessed using nitric oxide analyzers (NOAs, Sievers 280i, GE, Boulder, CO, USA). The NOAs are highly selective and sensitive for the direct chemiluminescent detection of NO.³¹ The polymer coated glass substrate was placed into an NOA cell and NO measurements were collected in 5 s intervals over the course of 12 h under dry conditions where the NOA cell was lowered into a 37 °C water bath.

7.3.6 Water contact angle analysis. Static water contact angle (WCA) measurements were collected on both untreated and plasma-treated substrates using a Krüss DSA 30S contact angle goniometer to assess wetting properties. A 6 µL drop of water (Millipore, 18 mΩ) was placed on the substrate. High-speed video recording was performed on each sample (64 frames per second for 10 s). All contact angle measurements were performed in triplicate to gauge reproducibility.

7.3.7 Surface composition analysis: XPS and SEM-EDS. X-ray photoelectron spectroscopy (XPS) analyses were performed on a PHI 5800 XPS system and provided information on surface composition and binding environments. Both the argon ion and electron neutralizers were used to

minimize sample charging. Survey spectra were collected from 10 to 1100 eV for 5 min, and high-resolution C1s, O1s, N1s and S1s spectra were collected over a 15 min period.

A JEOL JSM-6500F scanning electron microscope (SEM) equipped with an energy dispersive spectrometer (EDS) was used to investigate the morphology and elemental mapping of both treated and untreated substrates. An accelerating voltage of 5.0 kV and a working distance of 10.0 mm were used for the analyses of untreated and treated substrates. Three to five images were taken at 50× magnification. EDS spectra were collected for 5 minutes. Samples were grounded using carbon tape.

7.3.8 Surface morphology analysis: SEM and optical profilometry. Surface morphology of the polymer films was assessed both visually and quantitatively by performing SEM and optical profilometry analysis. For SEM analysis, samples were grounded to a sample stage using carbon tape. A JEOL JSM-6500F SEM was used to collect surface images at 100, 250, and 500× magnification. Three to five images were taken of each sample with an accelerating voltage of 1 kV and a working distance of ~10.0 mm.

To assess the surface roughness of the films before and after plasma treatment, a Zometrics ZeScope Optical Profilometer was used. A single scan was collected for a 250 × 350 μm area using a 20× magnification objective with a scan length of 150 μm in the z-axis and a signal threshold of 1.0%. 2 scans were collected on each of 3 samples, for a total of n=6 for each treatment. Both Ra and Rq values were determined from an average of the 6 scans using the ZeMaps Measurement and Analysis software, where the Ra represents the arithmetic mean roughness across a sample scan, while the Rq value represents the root mean square.

7.3.9 Bulk composition analysis: IR. IR analysis was performed on the untreated and treated PLGH-cysteine films to assess functional group incorporation (primarily –OH) on the surface of the plasma-treated film. IR measurements were performed on a Nicolet 6700 FT-IR instrument equipped with an ATR sample stage with a ZnSe window. Scans were performed as an average of 64 scans with resolution of 1 (data spacing of 0.121 cm^{-1}). The ATR sample stage was cleaned with absolute, anhydrous ethanol (product of Pharmco Products, Inc. (Brookfield, CT, USA) between samples. Sample scans were performed in triplicate ($n=3$) for each polymer sample. For these experiments, films were plasma treated and removed from the glass substrate to yield a polymer powder, wherein the surface was blended into the bulk of the polymer during removal.

7.4 RESULTS & DISCUSSION

7.4.1 Effect of plasma treatment on RSNO content and NO release. The main objective of these studies was to assess the effect of plasma treatment on the NO releasing capabilities of a model polymer system, *S*-nitrosated PLGH-cysteine (Figure 7.1).

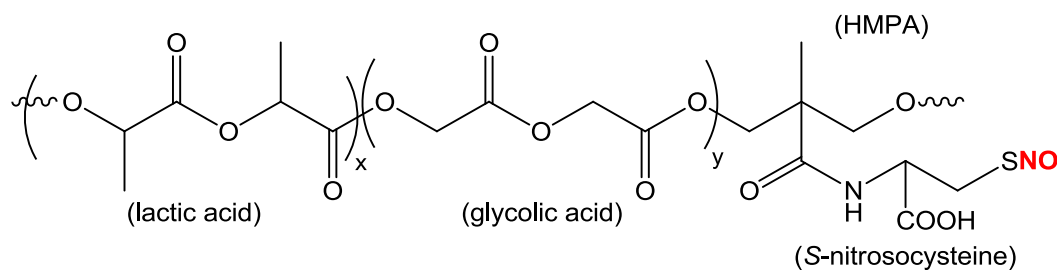


Figure 7.1 The structure of *S*-nitrosated PLGH-cysteine.

The *S*-nitrosothiol functionality was quantified using UV-vis spectroscopy, and direct chemiluminescent detection was used to quantify the real-time NO release under dry, thermal conditions.

Effect of water plasma treatment on S-nitrosothiol content. Figure 7.2 shows a representative UV-vis spectrum corresponding to the *S*-nitrosated PLGH-cysteine polymer dissolved in 2 MeOH: 1 DCM, where the characteristic absorbance feature at 335 nm corresponds to the SNO moiety of the *S*-nitrosated polymer.

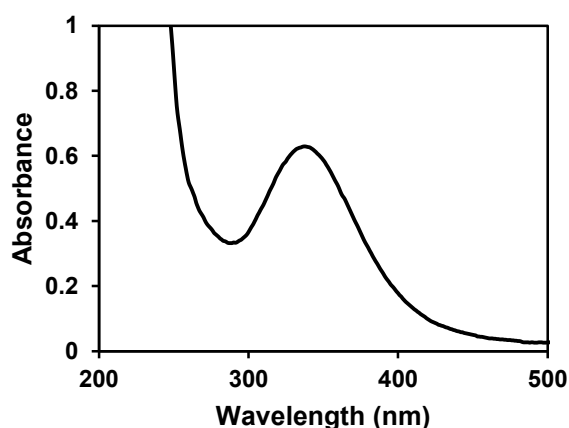


Figure 7.2 A representative UV-vis spectrum for the *S*-nitrosated PLGH-cysteine (3.5 mg mL^{-1} in 2 MeOH: 1 DCM).

We previously determined a molar extinction coefficient value (ϵ_{max}) of $882.9 \pm 18.2 \text{ M}^{-1} \text{ cm}^{-1}$ corresponding to the λ_{max} of 335 nm (described in Chapter 4),²³ which allowed us to characterize an initial RSNO content of $0.155 \pm 0.004 \text{ mmol g}^{-1}$ after polymer nitrosation (Table 7.1). The modified Ellman's assay quantified $0.458 \pm 0.009 \text{ mmol thiol g}^{-1}$ (according to the calibration curve presented in Figure 7.3) which represents a nitrosation efficiency of nearly

35%. These values correlate with previously reported values and confirm a satisfactory nitrosation of the polymer.²³

The RSNO content was subsequently quantified for *S*-nitrosated polymer samples exposed to different H₂O plasma treatments. All samples were placed 16 cm downstream from the coil region of the plasma. For a fixed applied power of 20 W, the treatment time was varied to include 1, 3 and 5 min. Additionally, for a fixed treatment time of 5 min, the power was varied to include 20, 30 and 50 W.

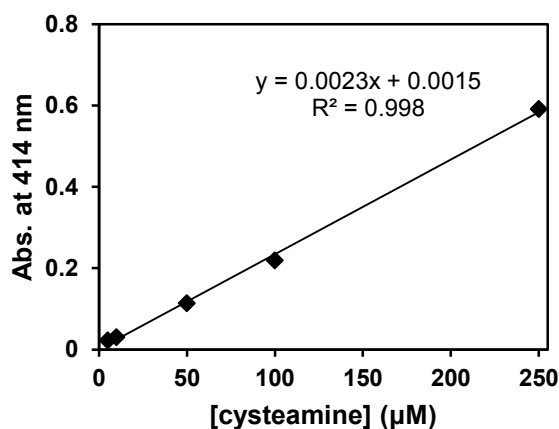


Figure 7.3 Calibration curve for the cysteamine standards treated with the Ellman's reagent in 2 MeOH: 1 DCM solvent containing 0.5 mg mL⁻¹ blank PLGH. The absorbance response at 414 nm is plotted as a function of the cysteamine concentration. The absorbance of each standard was collected in triplicate, with an error < 1% for all measurements.

As shown in Table 7.1, all plasma treatments resulted in a slight decrease in the RSNO content compared to the non-treated samples. The student's t-test reveals that for a fixed 20 W applied power, regardless of the plasma treatment time (1, 3 or 5 min), the RSNO content values for the

post-treatment films were the same as one another within experimental error at the 90% CL. For variable treatment time conditions at a fixed 20 W, the polymer retained $89 \pm 2\%$ of the initial RSNO content. Additionally, for a fixed treatment time of 5 min and an increased applied power of 30 W, the RSNO content was within the error of the 20 W, 5 min treated films. It was not until the applied power was increased to 50 W for a fixed 5 min treatment that a more significant decrease in the RSNO content was exhibited. For all H₂O plasma treatments performed, except for the 50 W applied power, the *S*-nitrosated polymer retained ~90% of the initial RSNO content. An applied power of 50 W for a 5 min treatment resulted in 80% retainment of the RSNO. Overall, the use of H₂O water treatments for ≤ 30 W applied powers and 1-5 min treatment times resulted in only a 10% loss of the total RSNO content.

Table 7.1 RSNO content and NO recovery for plasma-treated *S*-nitrosated PLGH-cysteine films (n=3 for each plasma treatment).

Plasma treatment ^a		RSNO content (mmol g ⁻¹) ^b	NO recovery (mmol g ⁻¹) ^c
Applied Power (W)	Treatment Time (min)		
-	-	0.155 ± 0.004	0.012 ± 0.001
20	1	0.141 ± 0.007	0.013 ± 0.001
20	3	0.136 ± 0.005	0.011 ± 0.001
20	5	0.138 ± 0.004	0.012 ± 0.001
30	5	0.132 ± 0.005	0.011 ± 0.001
50	5	0.126 ± 0.003	0.011 ± 0.002

^aThe *S*-nitrosated PLGH-cysteine films were treated with varying applied power and treatment times

^bThe RSNO content was determined from solution phase UV-vis measurements of the *S*-nitrosated PLGH-cysteine films dissolved in 2 MeOH: 1 DCM using a molar extinction coefficient of $882.9 \text{ M}^{-1} \text{ cm}^{-1}$.

^cThe NO recovery is reported for dry films under 37 °C for a 12 h analysis duration.

Traditionally, the use of *S*-nitrosothiol donors have been viewed as limited due to the minimal stability of the donor as RSNOs decompose under heat and light initiated conditions.³²

We previously demonstrated, however, that these *S*-nitrosated PLGH polymers retained their NO releasing capabilities after being processed into electrospun nanofibers.³³ The current results further demonstrate the ability of the RSNO functionality to survive processing under plasma conditions, as the RSNO content is decreased by only 10% under the vacuum, UV light, temperature and reactivity conditions associated with our H₂O plasma treatments. The stability of the NO functionality under processing and treatment conditions expands the commercial potential of these materials to be processed into materials for clinical use.

Effect of water plasma treatment on NO release kinetics. The NO releasing parameters for a polymer system are largely controlled by the type and concentration of donor, where we have demonstrated a loss of only 10% RSNO content for the lower applied power plasma treatments. The NO release kinetics can, however, be affected by the chemical environment surrounding the RSNO group.²³ Therefore, it was critical to monitor not only the RSNO content, but the real-time NO release profile associated with the *S*-nitrosated PLGH-cysteine films. Figure 7.4 highlights the NO release profile for the *S*-nitrosated PLGH-cysteine pre-treatment, where a characteristic profile of an initial “burst” of NO is followed by a rather steady-state NO release. Over the 12 h analysis window, 0.012 ± 0.001 mmol NO g⁻¹ was released, corresponding to about 8% of the total NO reservoir relative to the initial RSNO content.

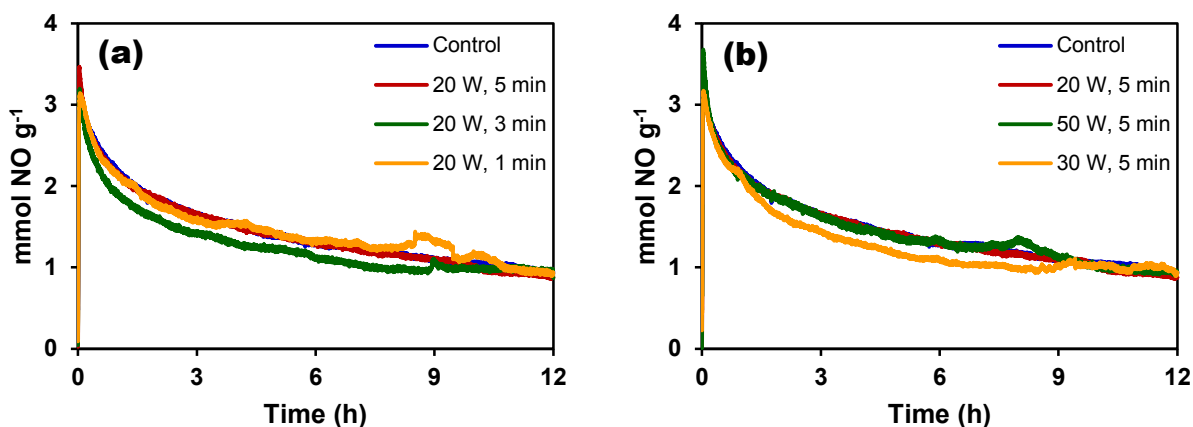


Figure 7.4 NO release profiles for untreated and plasma-treated *S*-nitrosated PLGH cysteine polymer films plasma treated for (a) 1, 3, or 5 min at a constant applied power of 20 W and (b) for 5 min at applied powers of 20, 30, and 50 W. All analyses were performed for an $n = 3$ and the average NO release profile is shown. The error for all profiles is $< \pm 10\%$.

No significant difference was found in the NO release profile or total NO release over 12 h for all of the plasma-treated films compared to the untreated control (Table 7.1). Overall, these data demonstrate that, regardless of plasma power (20-50 W) and treatment time (1-5 min), the polymers still maintained their full NO releasing capabilities in terms of the NO release kinetics.

7.4.2 Effect of plasma treatment on surface wettability. The goal of this work was to tune the surface properties of *S*-nitrosated PLGH-cysteine while maintaining the bulk properties to achieve biostable films with enhanced cell-surface affinity to promote material integration. Water contact angle measurements were performed to assess the effect of H₂O plasma treatments on the surface wettability of the *S*-nitrosated polymer films. The untreated samples exhibited a relatively high water contact angle of $116.6 \pm 3.4^\circ$, indicating these polymers have very

hydrophobic surfaces. After plasma treatment, the surfaces became hydrophilic, with the water droplet spreading in <100 ms. We report water droplet spreading times associated with each plasma-treated surface in Table 7.2.

Table 7.2 Water droplet spreading times (ms) associated with the different plasma treated samples (n=3 for each plasma treatment).

Plasma treatment		Spreading time (ms)
Applied Power (W)	Treatment Time (min)	
20	1	87 ± 16
20	3	65 ± 13
20	5	43 ± 07
30	5	49 ± 13
50	5	70 ± 08

Figure 7.5(a) highlights that, for a fixed applied power of 20 W, increasing the treatment time from 1 to 5 min resulted in faster water spreading. Water droplet spreading time for the 5 min treatment was just 43 ± 7 ms, compared to 87 ± 16 ms for the 1 min treatment. Although we consider both of these surfaces to be hydrophilic, the spreading time values do suggest that the longer treatment time results in a more hydrophilic surface. The increase in hydrophilicity upon plasma treatment can be attributed to multiple factors. Namely, H₂O plasma treatment implants hydroxyl and carbonyl groups which can serve to increase surface hydrophilicity.¹³ Additionally, plasma treatments can initiate shallow reorientation of the polymer microdomains,³⁴ wherein the more hydrophilic regions are brought to the surface of the film.

For a fixed treatment time of 5 min, changing the applied plasma power (20, 30 or 50 W) reveals a slight increase in water spreading time with increasing power as shown in Figure

7.5(b). There is no significant change in the water spreading time between the 20 W and 30 W treatments. However, when the applied power is increased to 50 W, the water spreading time increases significantly in comparison to the 20 and 30 W treatment. This effect at the highest power could result from a competition between implantation of OH functional groups and a mild etching of the polymer surface, which has been previously demonstrated.³⁵ Additionally, since the 50 W treatment results in the loss of an additional 10% of RSNO content compared to all other treatments, the formation of extra disulfide at the surface of the 50 W treated samples could result in a slight decrease in the surface hydrophilicity.

7.4.3 Effect of plasma treatment on surface composition. Both SEM-EDS and XPS analyses were performed to determine the effects of plasma treatments on polymer composition. The C, O, and S elemental percentages derived from SEM-EDS analysis as well as the corresponding elemental ratios for each of the plasma treatment conditions are summarized in Table 7.3. Notably, these data suggest the oxygen content of the materials does not change appreciably with plasma parameters. As SEM-EDS is not a surface sensitive technique with a sampling depth of $\sim 2 \mu\text{m}$,³⁶ we are sampling more of the bulk material than the surface and these elemental composition ratios are essentially identical. This confirms that the bulk of the material is not experiencing significant alteration as a result of plasma treatment, a primary goal of these experiments.

XPS provides information about the surface chemical composition as its sampling depth is only 5-10 nm.³⁷ XPS atomic composition ratios derived from survey and C_{1s} , O_{1s} , N_{1s} and S_{2p} high resolution spectra of treated and untreated *S*-nitrosated PLGH-cysteine films are summarized in Table 7.4.

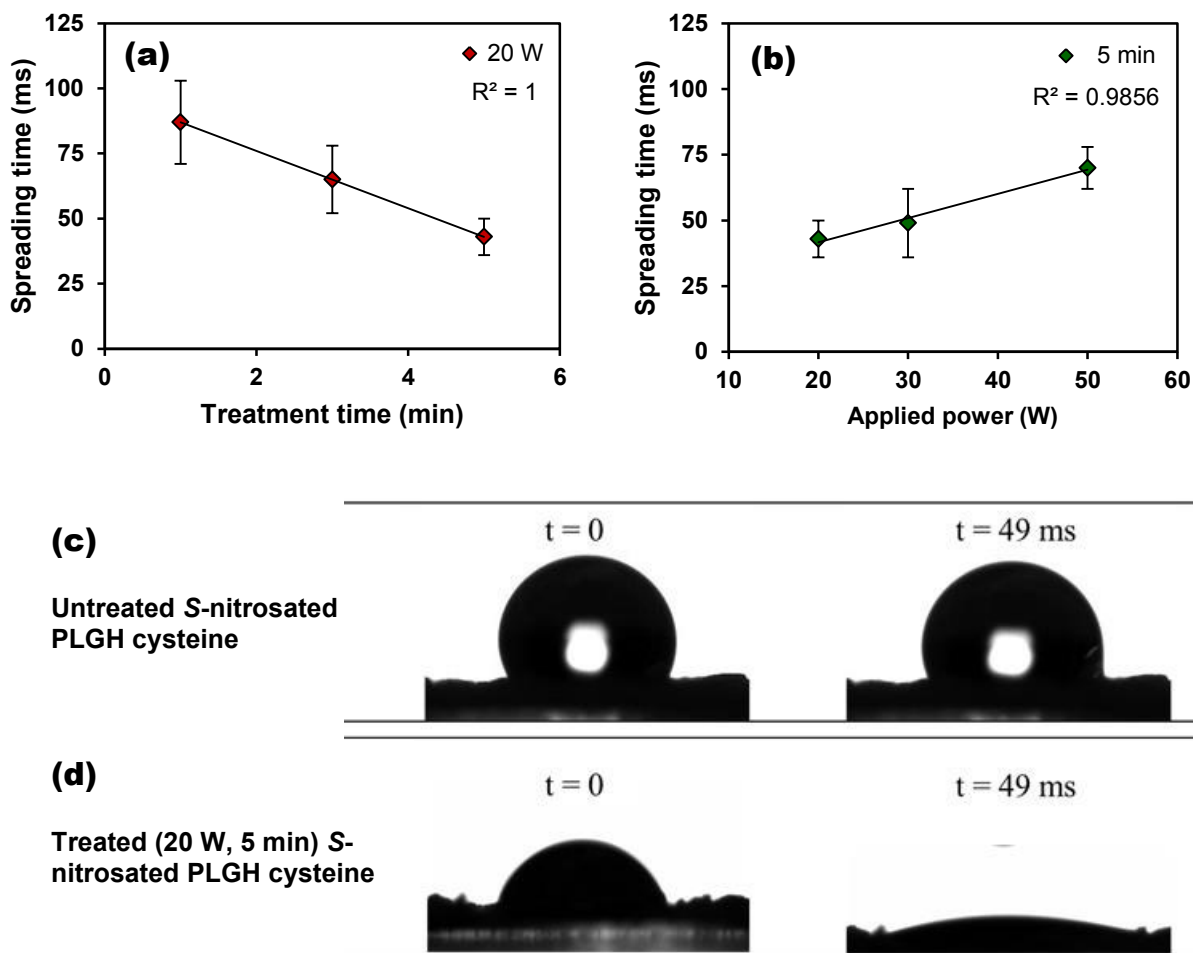


Figure 7.5 (a) Effect of treatment time on water droplet spreading time for *S*-nitrosated PLGH-cysteine films for a fixed power of 20 W; (b) Effect of applied power on water spreading time for *S*-nitrosated PLGH-cysteine films for a fixed 5 min treatment time. Representative images of water droplets on untreated (c) *S*-nitrosated PLGH-cysteine films and (d) plasma treated *S*-nitrosated PLGH-cysteine films. All analyses were performed using 6 μ L droplets and $n = 3$; the average \pm standard deviation are reported.

Table 7.3 SEM-EDS elemental composition and ratios for untreated and plasma treated *S*-nitrosated PLGH-cysteine films (n=3 for each plasma treatment).

Plasma treatment		%C	%O	%S	O/C	S/C
Applied Power (W)	Treatment Time (min)					
-	-	60.5 ± 0.6	39.1 ± 0.4	0.4 ± 0.1	64.8 ± 1.4	0.65 ± 0.14
20	1	62.7 ± 0.4	37.2 ± 0.3	0.1 ± 0.1	59.3 ± 1.1	0.19 ± 0.05
20	3	61.7 ± 0.5	37.9 ± 0.4	0.4 ± 0.1	61.4 ± 1.3	0.60 ± 0.12
20	5	64.8 ± 0.7	35.1 ± 0.5	0.2 ± 0.1	54.8 ± 1.8	0.24 ± 0.11
30	5	60.3 ± 0.5	39.5 ± 0.4	0.2 ± 0.1	65.9 ± 1.3	0.40 ± 0.08
50	5	60.5 ± 0.7	39.1 ± 0.5	0.4 ± 0.1	64.7 ± 1.7	0.68 ± 0.18

Table 7.4 XPS atomic composition ratios of untreated and plasma treated *S*-nitrosated PLGH-cysteine films (n=6 for each plasma treatment).

Plasma treatment		C/O	O/N	C/N
Applied Power (W)	Treatment Time (min)			
-	-	1.67 ± 0.08	18.4 ± 2.5	30.6 ± 3.8
20	1	1.60 ± 0.05	16.4 ± 1.8	26.3 ± 2.7
20	3	1.48 ± 0.05	14.7 ± 1.5	21.7 ± 2.0
20	5	1.43 ± 0.05	12.0 ± 1.1	17.1 ± 2.0
30	5	1.51 ± 0.03	11.6 ± 1.3	17.6 ± 1.8
50	5	1.58 ± 0.03	13.6 ± 1.1	21.5 ± 1.5
20	5 (10 days aged)	1.54 ± 0.02	17.8 ± 1.4	27.5 ± 2.3

Figure 7.6(a) highlights that the C/N ratio decreases with increasing treatment time at a 20 W applied power, indicating an increase in the surface nitrogen. No leaks were detected in the system during treatment, thus it is unlikely that the additional nitrogen arose during the plasma treatment. Thus, there are two possible sources of this surface nitrogen: (a) the plasma treatment creates reactive radical sites at the surface of the polymer, which then react with atmospheric nitrogen following plasma treatment, or (b) the polymer reorganizes as a result of plasma

treatment. Although the former has been observed previously,^{38,39} the small changes observed in surface composition ratios upon sample aging (see Section 7.5.4) suggests the latter explanation may be contributing to the observed nitrogen incorporation, as discussed below. The shallow reorganization of polymer chains when exposed to H₂O plasma treatments has been previously reported in the literature.³⁴ Since the *S*-nitrosated PLGH-cysteine is composed of a hydrophobic backbone with hydrophilic *S*-nitrosocysteine pendant groups, it is likely that the hydrophilic microdomains are reorienting toward the surface when the material is exposed to the H₂O vapor plasma environment.

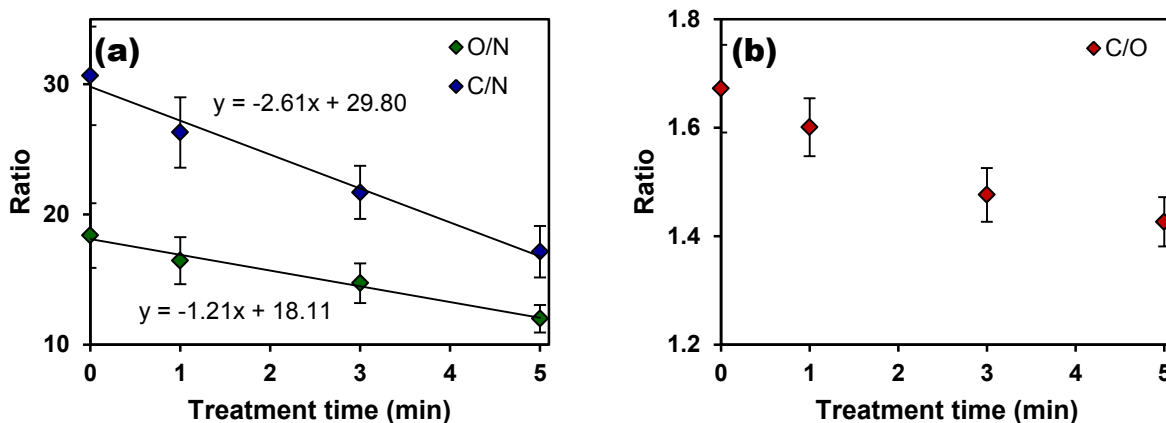


Figure 7.6 Elemental ratios plotted as a function of treatment time for (a) O/C, O/N and (b) C/O from XPS. These values represent the average \pm standard deviation for $n = 6$.

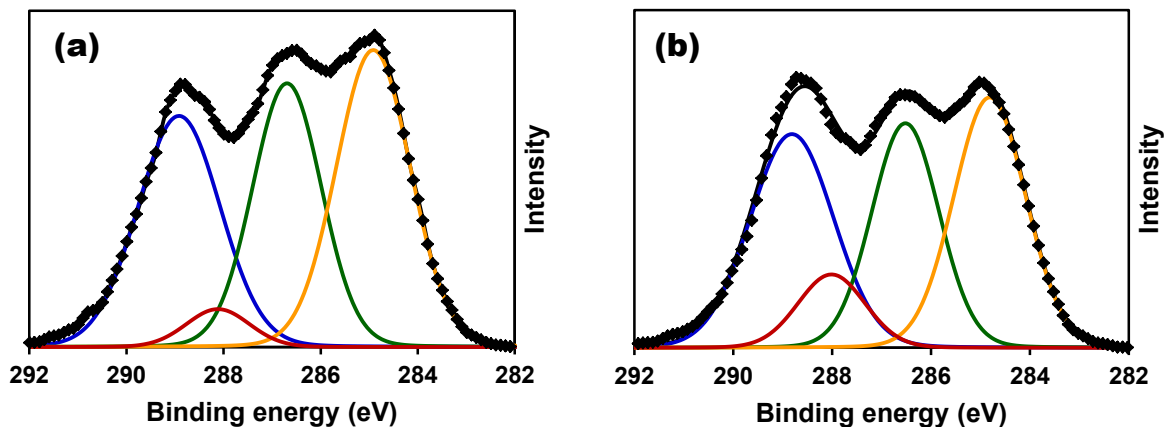
For a fixed 5 min treatment time, an increase in the applied power from 20 to 30 W does not result in a statistically significant difference in the C/N ratio. However, an additional increase in the applied power to 50 W results in a slight increase in the C/N ratio compared to the 20 and 30 W treatments (Table 7.4). Compared to the untreated films ($C/N = 30.6 \pm 3.8$), the C/N ratio for the 50 W treatment (21.5 ± 1.5) is not as low as those measured for the 20 W (17.1 ± 2.0) and

30 W (17.6 ± 1.8) treatments. This could indicate exposure of bulk material due to surface etching at higher applied power conditions, which has been demonstrated to occur for H₂O plasma treatments.⁴⁰

Although our XPS data support the possibility that reorientation of hydrophilic microdomains to the film surface may be occurring, implantation of hydrophilic functional groups that would improve the surface wettability is also an important surface modification to consider. Several reports demonstrate the use of H₂O plasma treatments to implant moieties with a variety of chemical environments (i.e. C=O, C-O, O-C=O) onto polymer surfaces.^{14, 15, 35, 40} To consider the implantation of O-containing moieties on the *S*-nitrosated PLGH-cysteine film surface, we can track the C/O ratio as a function of plasma treatment conditions as seen in Figure 7.6(b). A general trend of decreasing C/O with increasing treatment time is observed for a fixed 20 W applied power, suggesting that there is a relative increase in surface oxygen species with an increasing plasma exposure. We also see a slight decrease in the C/O ratio for the 30 and 50 W power conditions compared to the untreated sample (see Table 7.4). As seen for the C/N ratio, this decrease in the C/O ratio is not as pronounced for increasing applied powers, presumably due to competitive etching under harsher conditions. The O/N and C/N ratios can also be compared as a function of treatment time. In Figure 7.6(a), the slope of the regression line for the C/N plot is steeper than that for O/N. Since there is a greater impact on the N relative to C than for the N relative to O with increasing treatment times, this further suggests O incorporation is occurring along with rearrangement to enhance the N signal.

Despite the elemental ratios suggesting oxygen incorporation, these data do not provide information regarding changes in the oxygen binding environments after plasma treatment. High resolution C_{1s} XPS spectra were deconstructed for untreated samples in addition to 1 and 5 min

treated samples at 20 W applied power to understand changes in surface chemical functionality as a function of plasma treatment time. This process involved fitting each C_{1s} spectrum with four unique binding environments, shown in Figure 7.7, corresponding to C-C/C-H, C=O and O-C-C=O of the polymer backbone and HN-C=O corresponding to the amide linkage of the *S*-nitrosocysteine residue. For the untreated polymer sample, the C=O binding environment comprises multiple functionalities, namely the carboxylic acid moiety on the cysteine residues, as well as the multiple ester linkages in the lactic acid and glycolic acid portions of the polymer backbone, which results in a broadened peak relative to all other binding environments. The binding environments corresponding to the polymer backbone exhibit comparable intensities relative to each other, whereas the HN-C=O of the cysteine residue yields a smaller intensity. These proportions are consistent with the polymer structure (Figure 7.1). In order to focus on changes in chemical functionality as a function of plasma treatment time, the ratios between the C-C/C-H binding environment (285.0 eV) and each of the other O-containing binding environments were calculated from high-resolution C_{1s} spectra (Table 7.5). The C-C/C-H to HN-C=O ratio is 10.12 ± 2.03 for the untreated samples, which decreases to 7.10 ± 0.71 for a 1 min treatment time and 4.55 ± 0.83 for a 5 min treatment time. This increase in the relative intensity of the HN-C=O binding environment further supports the earlier stated hypothesis that the hydrophilic *S*-nitrosocysteine residues are rearranging toward the surface during plasma treatment. Another marked change in the binding environment ratio is the decrease in the C-C/C-H to C=O ratio with increasing treatment time (Figure 7.8). This implies that the C=O binding environment contribution is increased with treatment time, which would suggest the incorporation of carbonyl-containing functionalities during the plasma treatment.



Key: \blacklozenge raw data, — total fit, — C=O fit, — O-C-C=O fit, — C-C/C-H fit, — HN-C=O fit

Figure 7.7 Representative high-resolution C_{1s} XPS spectra and fits for (a) untreated, (b) 20W 5 min treated *S*-nitrosated PLGH-cysteine films.

Table 7.5 The binding environment ratios for the untreated and 20 W treated films with different treatment times as determined from the deconvoluted C_{1s} spectra.

Treatment time (min)	Binding environment relative ratios		
	C-C/C-H to C=O	C-C/C-H to O-C-C=O	C-C/C-H to HN-C=O
0	1.13 ± 0.08	1.14 ± 0.06	10.12 ± 2.03
1	1.06 ± 0.12	1.12 ± 0.12	7.10 ± 0.71
5	0.90 ± 0.06	1.15 ± 0.08	4.55 ± 0.83

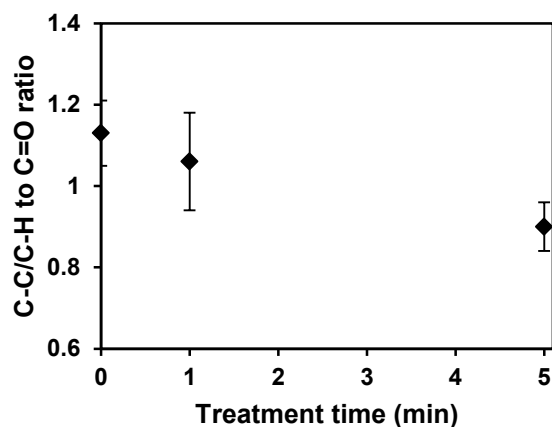


Figure 7.8 C-C/C-H to C=O binding environment ratio as a function of treatment time for a fixed applied power of 20 W (n=6).

Previous studies of H₂O plasma treatment of polysulfone and polyetherimide demonstrated the implantation of O-containing groups at high applied powers (20-200 W) due to the presence of OH and H radicals in the plasma.⁴⁰ Using optical emission spectroscopy (OES), a direct correlation was established between the intensity line attributed to OH• and the concentration of oxygen present in the material surface, as measured by XPS. This relationship further translated to increased wettability for the samples with increased surface oxygen. The deconstructed C_{1s} XPS spectrum for the untreated sample indicated two binding environments corresponding to C-C/C-H and C-O. After H₂O plasma treated, there was an increase in the C-O contribution, followed by the appearance of C=O and O-C=O binding environments. These data suggested that polymer treatment via H₂O plasma treatments resulted in the formation of alcohol, aldehyde/ketone and carboxylic acid/ester functionalities at the material surface, which increased the surface wettability of the samples. Translating these findings to our *S*-nitrosated PLGH-cysteine system, we can infer a direct correlation likely exists between the increase in the surface oxygen content and surface wettability.

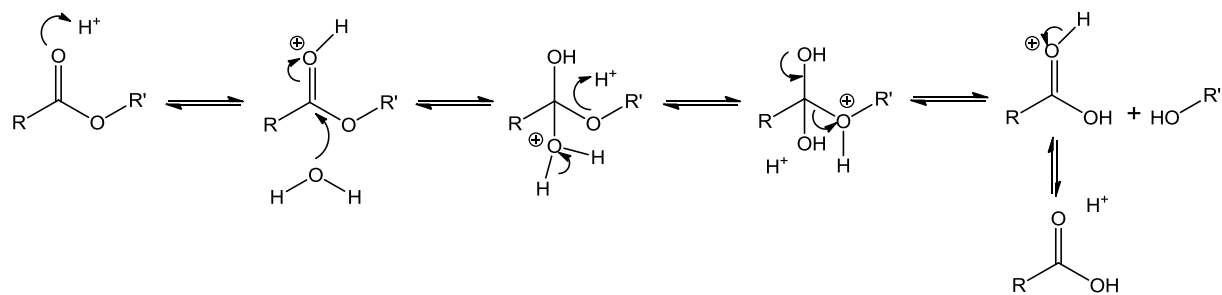
The notable increase in the C=O environment relative to the C-C/C-H binding environment after a 20 W, 5 min treatment observed here can be understood by considering the possible oxidation sites on the polymer. Previous work has demonstrated smaller changes in the C-O binding environment for H₂O plasma-treated polysulfone materials, with a more significant impact on the CO_x groups, such as the aldehyde/ketone and carboxylic acid/ester functional groups.¹⁴ These data suggested the possibility of oxidation of alcohol groups formed during the treatment, or the oxidation of other sites within the polymer backbone, such as methyl groups and quaternary carbon sites, to yield aldehydes and ketones, respectively. Further oxidation of aldehydes could result in carboxylic acid groups. Other studies demonstrated surface functionalization using H₂O plasma treatments for polymers with rigid, aromatic backbones versus linear, hydrocarbon backbones.³⁵ In all cases, similar binding environments and relative elemental compositions similar to those seen here were obtained, with plasma treatment resulting in an increase in C-O and CO_x environments corresponding to hydroxyl- and carbonyl-containing moieties, respectively. Formation of highly oxidized species is supported by the data presented here, where we found a notable increase in the C=O environment relative to C-C/C-H, with no distinguishable difference in the C-C/C-H to -O-C-C=O ratio for an untreated sample compared to a 20 W, 5 min treated sample. This suggests that the oxidation sites associated with the *S*-nitrosated PLGH-cysteine are likely the methyl groups of the lactic acid portion, the secondary carbon sites of the glycolic acid and HMPA portions, and the quaternary carbon site in the HMPA portion to form ketone and aldehyde functional groups (see Figure 7.1).

Another study demonstrated that, at lower applied powers (i.e. 25 W), the OES spectrum as a function of plasma treatment time showed that the O• signal dropped by ~80% when the sample was introduced, which is more significant than the drop in OH•, indicating that the key

player at lower applied powers is $O\cdot$.³⁵ Additionally, it was found that there were notable differences in the resulting functionalities after plasma treatment depending upon the specific material being treated. Differences in the %O incorporation and the corresponding extent of oxidation were attributed to the initial polymer structure and the number of oxidizable sites, in addition to the ability for certain polymers to undergo hydrolysis in aqueous environments. The possibility of polymer chain scission at ester sites is also acknowledged. As *S*-nitrosated PLGH-cysteine polymer is composed of several ester linkages, it could easily undergo acid or base catalyzed hydrolysis to form carboxylic acid groups (Figure 7.9) and result in chain scission.⁴¹

Overall, the XPS data suggest combined pathways that could lead to the observed increase in hydrophilicity of the *S*-nitrosated PLGH-cysteine films surface after plasma treatment. An increase in the N content relative to both O and C content, combined with a decrease in the C-C/C-H to HN-C=O ratio with increasing treatment time, suggests polymer rearrangement to reorient the amide linked, hydrophilic *S*-nitrosocysteine pendant groups to the surface. Additionally, an increase in the surface oxygen, specifically the C=O binding environment relative to C-C/C-H, suggests the implantation of OH groups at the alkyl sites along the polymer backbone, which subsequently oxidize to carbonyl sites, including ketone/aldehyde and carboxylic groups. Chain scission via ester hydrolysis is also a possibility due to the large number of ester sites on the backbone.

(a)



(b)

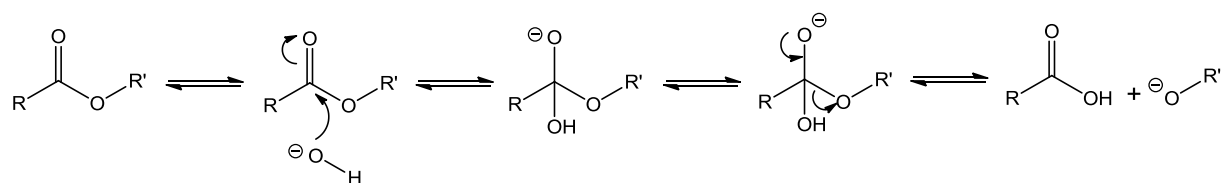


Figure 7.9 (a) Acid catalyzed ester hydrolysis occurs due to reaction with H⁺ and H₂O species and yields carboxylic acid and alcohol products. (b) Base catalyzed ester hydrolysis occurs due to reaction with OH⁻ and yields carboxylic acid and alkoxide products.

7.4.4 Effect of prolonged treatment time on surface composition. Since we found greater changes occurring in the film chemistry with prolonged plasma exposure, an increased treatment time of 60 min was further performed. Films of PLGH-cysteine were prepared and treated for 5 or 60 min at 20 W. Since the plasma treatment does not impact the majority of the RSNO species and the RSNO does not contribute to any of the binding environments for XPS analysis, it was not necessary for the thiol to be nitrosated to probe functionality differences pre- and post-treatment. Therefore, non-nitrosated PLGH-cysteine films were prepared for treatment. Figure 7.10 shows the C/O ratio for both the *S*-nitrosated and non-nitrosated PLGH-cysteine films as a function of treatment time, which appear comparable within the ≤ 5 min treatment times. This indicates that the non-nitrosated samples are sufficient to consider surface functionalization at

longer treatment times. Figure 7.10 also shows that the C/O ratio decreases with increasing treatment time out to 60 min for non-nitrosated PLGH-cysteine films, suggesting that increasing treatment times will enhance any O-containing functional groups that are being incorporated at the material surface.

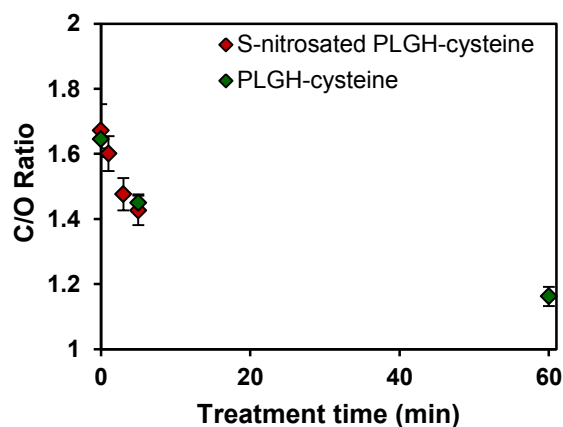


Figure 7.10 (a) High-resolution C_{1s} XPS spectrum with deconstructed fits for individual components for PLGH-cysteine films (60 min treatment time, 20 W applied power). (b) The C/O ratio is presented as a function of treatment time (20 W applied power) for films of *S*-nitrosated and non-nitrosated PLGH-cysteine.

Polymer samples were treated and analyzed using ATR-IR to evaluate the hypothesis that implantation of OH and C=O groups occurs with longer plasma treatment times. We again utilized non-nitrosated PLGH-cysteine films for these analyses to simplify the analysis. The plasma-treated samples were removed from the glass substrate, resulting in a polymer powder where the surface was blended into the bulk. The 20 W, 5 min treatment yielded no significant changes in the IR spectrum compared to the non-treated, indicating that the extent of functionalization was not significant enough to detect against the bulk of the polymer. Therefore,

the plasma treatment time was extended to 60 min to enhance the signal of any functional groups formed during the plasma treatment.

Figure 7.11 highlights changes in the IR spectrum at 3300-3200 and 800 cm^{-1} , corresponding to the O-H stretching and out-of-plane bending modes, respectively, for alcohol and carboxylic acid groups. The PLGH-cysteine spectrum also exhibits a strong feature at 1750 cm^{-1} corresponding to the overlap of the ester (higher frequency) and carboxylic acid (lower frequency) carbonyl groups on the polymer. Since this feature is present in all spectra, we cannot deduce changes in the C=O content after plasma treatment. Nonetheless, the IR analysis suggests that H_2O plasma treatment indeed results in the incorporation of OH into the PLGH polymer structure, likely due to the formation of carboxylic acid groups, similar to what has been observed previously with other polymers.^{13,35}

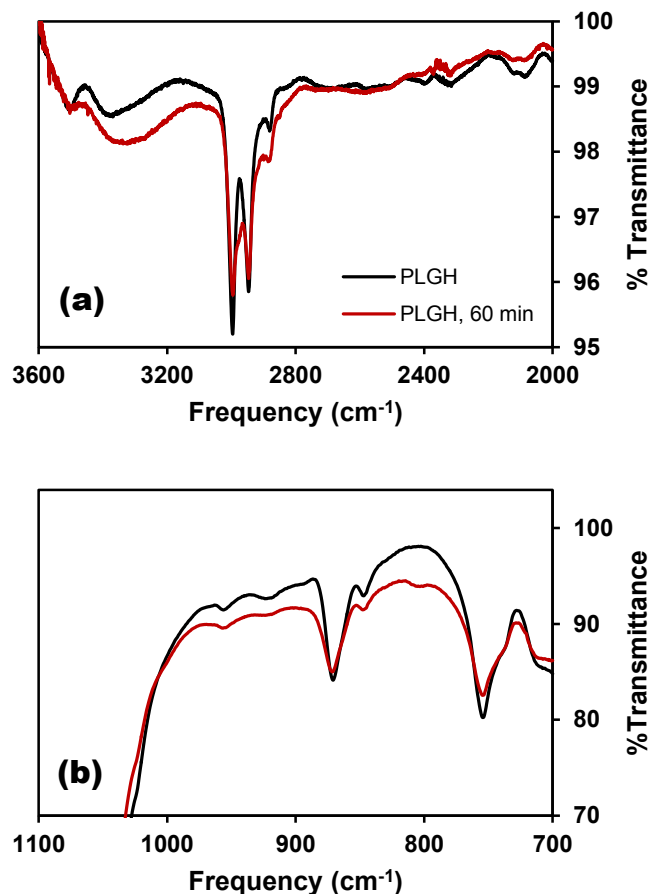


Figure 7.11 Representative IR spectra for the untreated PLGH-cysteine (black) and PLGH-cysteine after a 20 W, 60 min plasma treatment (red) for the (a) 3600-2000 cm^{-1} and (b) 1100-700 cm^{-1} regions.

7.4.5 Effect of plasma treatment on surface morphology. Often, plasma treatment of polymers can result in extensive changes to the film surface.³⁵ Furthermore, changes in surface roughness can affect both surface wettability and interactions of biological components with a material surface.^{9, 42} Thus, evaluating surface morphology is critical not only from the point of view of further biological applications, but also to ensure that the observed changes in surface wettability were not attributable to changes in the surface morphology during plasma treatment. Surface

roughness exists perpendicular to the surface (described as height deviation), and in the plane of the surface (described by spatial parameters and identified as texture).⁴³ Amplitude parameters are critical to characterize surface topography for biological application, and they include the arithmetic average (Ra) and root mean square (Rq).⁴⁴ Table 7.6 summarizes the roughness parameters (Ra and Rq) of the *S*-nitrosated PLGH-cysteine films pre- and post-treatment; Figure 7.12 shows SEM images of the polymer film before and after plasma treatment (20 W, 5 min). No significant changes in the roughness parameters are observed regardless of plasma parameters, demonstrating that the observed changes in surface wettability are not attributable to morphological changes. Further, this illustrates that any etching of the surface that occurs during the 50 W treatment does not significantly affect the overall topography of the films.

Table 7.6 Surface roughness of untreated and plasma treated the *S*-nitrosated PLGH-cysteine films (n=3 for each plasma treatment).

Plasma treatment		Rq (μm)	Ra (μm)
Power (W)	Time (min)		
-	-	18.02 ± 6.92	14.26 ± 6.76
20	1	17.89 ± 4.56	13.73 ± 3.68
20	3	20.45 ± 3.49	16.45 ± 3.08
20	5	15.01 ± 4.84	10.96 ± 3.51
30	5	17.85 ± 3.91	13.63 ± 3.49
50	5	18.57 ± 6.12	13.82 ± 4.48

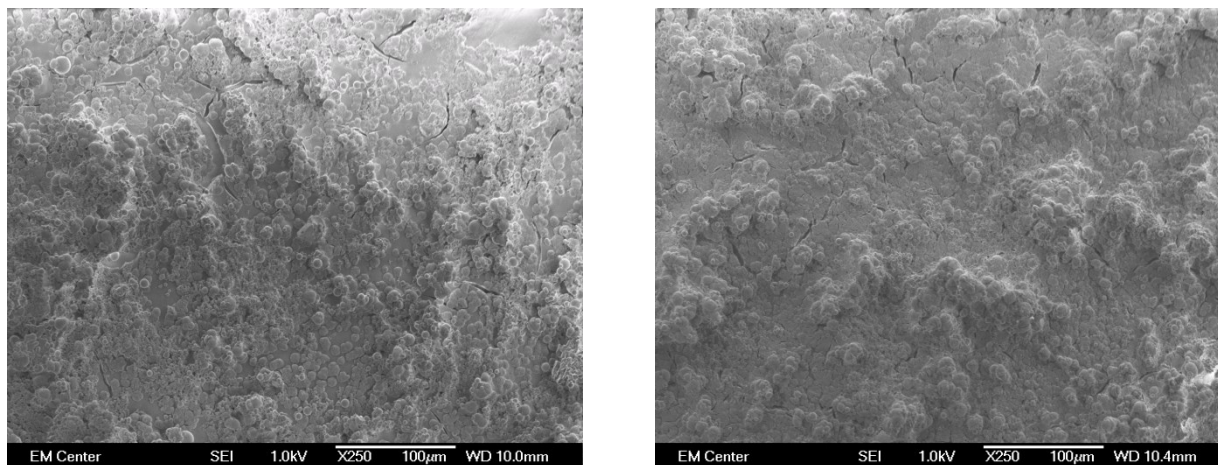


Figure 7.12 Representative SEM images for (left) control *S*-nitrosated PLGH-cysteine films (right) *S*-nitrosated PLGH-cysteine films after 20 W, 5 min H₂O vapor plasma treatment. Images for both samples are shown at 250× magnification.

7.4.6 Stability of the plasma treatment. It has been previously demonstrated that plasma treated surfaces can undergo what is generally referred to as hydrophobic recovery, wherein surfaces that are rendered hydrophilic ultimately revert to their original hydrophobic nature shortly after the treatment.^{34, 39} This is generally thought to occur via polymer rearrangement, chain migration or diffusion, or burial of hydrophilic groups (e.g. O, N) within the bulk of the polymer. Films were treated under 20 W, 5 min plasma conditions and then placed into a freezer at -18 °C under ambient air conditions for a 10-day aging period to examine aging effects on the *S*-nitrosated PLGH-cysteine. Both static water contact angle and XPS analyses were performed to compare surface properties of 20 W, 5 min treated materials stored for 10 days with freshly treated samples. Water spreading time on the material after the 10-day storage period was 249 ± 33 ms, significantly longer than water spreading time on the freshly treated material (43 ± 7 ms).

Despite an increase in the water spreading time, these surfaces are still considered very hydrophilic as the water droplet still spreads rapidly on the surface.

XPS analysis reveals that the 10-day storage resulted in a significant increase in the O/N (17.8 ± 1.4), C/N (27.5 ± 2.3), and C/O (1.54 ± 0.02) ratios compared with the freshly treated samples shown in Table 7.4. These differences in the elemental ratios between freshly treated and aged samples were normalized by the elemental ratio for the untreated samples to yield 32, 34 and 7% for the O/N, C/N and C/O ratios, respectively. This suggests slight hydrophobic recovery may be the result of burial of the N-containing hydrophilic cysteine microdomains accompanied by some burial of surface O-containing moieties. Furthermore, the C/O ratio is larger for the untreated sample than the 10-day aged sample, which suggests that oxygen-containing functional groups implanted via plasma treatment are maintained even after the 10-day storage period.

In addition to the stability and longevity of the plasma treatment effects on the material surface, the stability of the RSNO group will also dictate the lifetime of the material for bioapplications. We found that, after the storage period, the RSNO content was 0.126 ± 0.003 mmol g⁻¹ compared to 0.138 ± 0.004 mmol g⁻¹ for the 20 W, 5 min treated films. The 20 W, 5 min treatment experienced a ~10% decrease in the RSNO content compared to the untreated films, and the storage period results in the loss of an additional 10% of RSNO, where ~80% of the original RSNO content remains after the plasma treatment and storage. Despite an additional decrease in RSNO content, the real-time NO release profile and total NO release over a 12 h period remained the same compared to all other freshly plasma treated films.

We have previously demonstrated that H₂O plasma-treated polymeric materials can exhibit either minor changes in hydrophilicity over extended periods of time or complete

hydrophobic recovery over time due to polymer rearrangement. For example, H₂O plasma treatments have resulted in permanent hydrophilic modifications (lasting months to years) for polymers with rigid, aromatic backbones, such as polysulfone, polycarbonate and polyethylene terephthalate.^{14, 15, 35} The less rigid polyethylene materials however experienced significant hydrophobic recovery after only 48 h to 1 week due to the migration of polymer chains to bury the polar surface groups that were incorporated by H₂O plasma treatment. Comparatively, plasma treated *S*-nitrosated polymer films exhibit a small amount hydrophobic recovery, but still maintain their hydrophilic nature, thus indicating that these materials are relatively stable in terms of wettability and surface functionality after 10 days of storage. The aging studies indicate that these materials are relatively stable in terms of wettability and surface functionality. This result is significant in that other non-aromatic backbone polymers exposed to H₂O plasma treatment exhibited nearly complete immediate hydrophobic recovery in terms of the water contact angle.³⁵ In this work, we present the H₂O plasma treatment of a non-rigid polymer that still retains a hydrophilic surface. Future studies will translate this work to NO-releasing polymer systems with even more rigid backbones with the goal of designing even more stable materials for biological applications.

7.5 CONCLUSIONS

Overall, we report the ability to modify the surface properties of a model NO releasing polymer while still maintaining the NO release parameters associated with the system. H₂O plasma treatments effectively created hydrophilic surfaces for the *S*-nitrosated PLGH-cysteine films, which are naturally hydrophobic. We demonstrate that, for all plasma treatment times (1, 3 and 5 min) for applied powers ≤ 30 W, the films retained 90% of the NO reservoir in the form of

S-nitrosothiol, and the NO release kinetics were not altered. It was not until the applied power was increased to 50 W that an additional loss of RSNO was experienced compared to all other plasma treatments. XPS analysis revealed an increase in N signal relative to O and C, which indicates the rearrangement of the polymer to bring the hydrophilic cysteine residues to the surface of the film. There was no distinguishable change in the C/O ratio, however, which is likely due to conversion of pre-existing carbonyl groups to hydroxyl groups. Additional IR analysis of films with longer plasma treatment times (60 min) demonstrated the appearance of spectral features corresponding to the incorporation of –OH functional groups. Surface roughness analysis indicated no significant changes in the surface morphology after plasma treatment, indicating that the changes in surface wettability are primarily due to compositional changes. Notably, plasma treated surfaces remain hydrophilic after a 10-day storage period in the freezer (-18 °C), which suggests that the films do not experience short-term hydrophobic recovery. Overall, the ability to tune the surface wettability of a polymer film while maintaining the bulk properties, including NO therapeutic releasing parameters, is critical towards creating multi-functional biomaterial systems. The stability of the plasma treatment enhances the consideration of these materials as biomedical polymers since the surface hydrophilicity will persist over the lifetime of the material's NO release. Additionally, the ability of the PLGH materials to withstand processing treatments and maintain the therapeutic reservoirs expands the commercial possibilities for clinical use.

CHAPTER 7 REFERENCES

1. Ratner, B. D., The Blood Compatibility Catastrophe. *J. Biomed. Mater. Res.* **1993**, *27*, 283-287; Ratner, B. D., The Catastrophe Revisited: Blood Compatibility in the 21st Century. *Biomaterials* **2007**, *28*, 5144-5147; Anderson, J. M., Biological Responses to Materials. *Annu. Rev. Mater. Res.* **2001**, *31*, 81-110.
2. Costerton, J. W.; Stewart, P. S.; Greenberg, E. P., Bacterial Biofilms: A Common Cause of Persistent Infections. *Science* **1999**, *284*, 1318-1322; Donlan, R. M., Biofilms and Device-Associated Infections. *Emerging Infect. Dis.* **2001**, *7*, 277-281.
3. Frost, M. C.; Reynolds, M. M.; Meyerhoff, M. E., Polymers Incorporating Nitric Oxide Releasing/Generating Substances for Improved Biocompatibility of Blood-Contacting Medical Devices. *Biomaterials* **2005**, *26*, 1685-1693.
4. Pashkuleva, I.; Marques, A. P.; Vaz, F.; Reis, R. L., Surface Modification of Starch Based Biomaterials by Oxygen Plasma or UV-irradiation. *J. Mater. Sci.: Mater. Med.* **2010**, *21*, 21-32.
5. Arima, Y.; Iwata, H., Effect of Wettability and Surface Functional Groups on Protein Adsorption and Cell Adhesion Using Well-Defined Mixed Self-Assembled Monolayers. *Biomaterials* **2007**, *28*, 3074-3082.
6. Castner, D. G.; Ratner, B. D., Biomedical Surface Science: Foundations to Frontiers. *Surface Science* **2002**, *500* (1-3), 28-60.
7. Van Loosdrecht, M. C.; Lyklema, J.; Norde, W.; Schraa, G.; Zehnder, A., The Role of Bacterial Cell Wall Hydrophobicity in Adhesion. *Appl. Environ. Microbiol.* **1987**, *53*, 1893-1897; Bruinsma, G. M.; van der Mei, H. C.; Busscher, H. J., Bacterial Adhesion to Surface Hydrophilic and Hydrophobic Contact Lenses. *Biomaterials* **2001**, *22*, 3217-3224.

8. Okada, T.; Bark, D. H.; Mayberg, M. R., Local Anticoagulation Without Systems Effect Using a Polymer Heparin Delivery System. *Stroke* **1988**, *19* (1470-1476); Uhrich, K. E.; Cannizzaro, S. M.; Langer, R. S.; Shakesheff, K. M., Polymeric Systems for Controlled Drug Release. *Chem. Rev.* **1999**, *99*, 3181-3198; Hetrick, E. M.; Schoenfisch, M. H., Reducing Implant-Related Infections: Active Release Strategies. *Chem. Soc. Rev.* **2006**, *35*, 780-789; Luscher, T. F.; Steffel, J.; Eberli, F. R.; Joner, M.; Nakazawa, G.; Tanner, F. C.; Virmani, R., Drug-Eluting Stent and Coronary Thrombosis: Biological Mechanisms and Clinical Implications. *Circulation* **2007**, *115*, 1051-1058.
9. Parreira, P.; Magalhães, A.; Gonçalves, I. C.; Gomes, J.; Vidal, R.; Reis, C. A.; Leckband, D. E.; Martins, M. C. L., Effect of Surface Chemistry on Bacterial Adhesion, Viability, and Morphology. *J. Biomed. Mater. Res., Part A* **2011**, *99*, 344-353.
10. Kenawy, E. R.; Worley, S. D.; Broughton, R., The Chemistry and Applications of Antimicrobial Polymers: A State-of-the-Art Review. *Biomacromolecules* **2007**, *8*, 1359-1384; Beck, A. J.; Whittle, J. D.; Bullett, N. A.; Eves, P.; MacNeil, S.; McArthur, S. L.; Shard, A. G., Plasma Co-Polymerisation of Two Strongly Interacting Monomers: Acrylic Acid and Allylamine. *Plasma Processes and Polym.* **2005**, *2*, 641-649.
11. Sohbatzadeh, F.; Hosseinzadeh Colagar, A.; Mirzanejhad, S.; Mahmodi, S., E. coli, P. aeruginosa, and B. cereus Bacteria Sterilization Using Afterglow of Non-thermal Plasma at Atmospheric Pressure. *Appl. Biochem. Biotechnol.* **2010**, *160*, 1978-1984.
12. Griesser, H. J.; Hodgkin, J. H.; Schmidt, R., *Plasma Techniques for the Production of Permanent Hydrophilic Polymers Surface for Biomedical Applications*. Plenum Press: New York, 1990.

13. Lee, J. H.; Park, J. W.; Lee, H. B., Cell-Adhesion and Growth on Polymer Surfaces with Hydroxyl-groups Prepared by Water-vapor Plasma Treatment. *Biomaterials* **1991**, *12*, 443-448.
14. Steen, M. L.; Hymas, L.; Havey, E. D.; Capps, N. E.; Castner, D. G.; Fisher, E. R., Low Temperature Plasma Treatment of Asymmetric Polysulfone Membranes for Permanent Hydrophilic Surface Modification. *J. Membr. Sci.* **2001**, *188*, 97-114.
15. Tompkins, B. D.; Dennison, J. M.; Fisher, E. R., H₂O Plasma Modification of Track-Etched Polymer Membranes for Increased Wettability and Improved Performance. *J. Membr. Sci.* **2013**, *428*, 576-588.
16. Yasuda, H.; Gazicki, M., Biomedical Applications of Plasma Polymerization and Plasma Treatment of Polymer Surfaces. *Biomaterials* **1982**, *3*, 68-77; Yoo, H. S.; Kim, T. G.; Park, T. G., Surface-functionalized Electrospun Nanofibers for Tissue Engineering and Drug Delivery. *Adv. Drug Delivery Rev.* **2009**, *61*, 1033-1042; Osaki, S. G.; Chen, M.; Zamora, P. O., Controlled Drug Release Through a Plasma Polymerized Tetramethylcyclotetrasiloxane Coating Barrier. *J. Biomater. Sci.* **2012**, *23*, 483-496.
17. Carpenter, A. W.; Schoenfisch, M. H., Nitric Oxide Release: Part II. Therapeutic Applications. *Chem. Soc. Rev.* **2012**, *41*, 3742-3752.
18. Radomski, M. W.; Moncada, S., The Biological and Pharmacological Role of Nitric Oxide in Platelet Function. *Adv. Exp. Med. Biol.* **1993**, *344*, 251-265; Reynolds, M. M.; Annich, G. M., The Artificial Endothelium. *Organogenesis* **2011**, *7*, 42-49.
19. Fang, F. C., Mechanisms of Nitric Oxide-Related Antimicrobial Activity. *J. Clin. Invest.* **1997**, *99*, 2818-2825.

20. Schaffer, M. R.; Tantry, U.; Gross, S. S.; Wasserkrug, H. L.; Barbul, A., Nitric oxide Regulates Wound Healing. *J. Surg. Res.* **1996**, *63*, 237-240; Ziche, M.; Morbidelli, L., Nitric Oxide and Angiogenesis. *J. Neuro-Oncol.* **2000**, *50*, 139-148; Rizk, M.; Witte, M. B.; Barbul, A., Nitric Oxide and Wound Healing. *World J. Surg.* **2004**, *28*, 301-306.
21. Varu, V. N.; Tsihlis, N. D.; Kibbe, M. R., Nitric Oxide-Releasing Prosthetic Materials. *Vasc. Endovascular Surg.* **2009**, *43*, 121-131; Seabra, A. B.; Duran, N., Nitric Oxide-Releasing Vehicles for Biomedical Applications. *J. Mater. Chem.* **2010**, *20*, 1624-1637; Jen, M. C.; Serrano, M. C.; van Lith, R.; Ameer, G. A., Polymer-Based Nitric Oxide Therapies: Recent Insights for Biomedical Applications. *Adv. Funct. Mater.* **2012**, *22*, 239-260; Riccio, D. A.; Schoenfisch, M. H., Nitric Oxide Release: Part I. Macromolecular Scaffolds. *Chem. Soc. Rev.* **2012**, *41*, 3731-3741.
22. Kingshott, P.; Andersson, G.; McArthur, S. L.; Griesser, H. J., Surface Modification and Chemical Surface Analysis of Biomaterials. *Curr. Opin. Chem. Biol.* **2011**, *15*, 667-676.
23. Damodaran, V. B.; Joslin, J. M.; Wold, K. A.; Lantvit, S. M.; Reynolds, M. M., S-nitrosated Biodegradable Polymers for Biomedical Applications: Synthesis, Characterization and Impact of Thiol Structure on the Physicochemical Properties. *J. Mater. Chem.* **2012**, *22*, 5990-6001.
24. Djordjevic, I.; Britcher, L. G.; Kumar, S., Morphological and Surface Compositional Changes in Poly(lactide-co-glycolide) Tissue Engineering Scaffolds Upon Radio Frequency Glow Discharge Plasma Treatment. *Appl. Surf. Sci.* **2008**, *254*, 1929-1935.
25. Holy, C. E.; Cheng, C.; Davies, J. E.; Shoichet, M. S., Optimizing the Sterilization of PLGA Scaffolds for use in Tissue Engineering. *Biomaterials* **2001**, *22*, 25-31.

26. Khang, G.; Jeon, J. H.; Lee, J. W.; Cho, S. C.; Lee, H. B., Cell and Platelet Adhesions on Plasma Glow Discharge-Treated Poly(lactide-co-glycolide). *Bio-Med. Mater. Eng.* **1997**, *7*, 357-368; Khang, G.; Choe, J.; Rhee, J. M.; Lee, H. B., Interaction of Different Types of Cell on Physiochemically Treated Poly(lactide-co-glycolide) Surfaces. *J. Appl. Polym. Sci.* **2002**, *85*, 1253-1262.
27. Wan, Y.; Qu, X.; Lu, J.; Zhu, C.; Wan, L.; Yang, J.; Bei, J.; Wang, S., Characterization of Surface Property of Poly(lactide-co-glycolide) After Oxygen Plasma Treatment. *Biomaterials* **2004**, *25*, 4777-4783; Shen, H.; Hu, X.; Yang, F.; Bei, J.; Wang, S., Combining Oxygen Plasma Treatment with Anchorage of Cationized Gelatin for Enhancing Cell Affinity of Poly(lactide-co-glycolide). *Biomaterials* **2007**, *28*, 4219-4230; Khorasani, M. T.; Mirzadeh, H.; Irani, S., Plasma Surface Modification of Poly(lactic acid) and Poly(lactic-co-glycolic acid) Films for Improvement of Nerve Cells Adhesion. *Radiat. Phys. Chem.* **2008**, *77*, 280-287; Fortunati, E.; Mattioli, S.; Visai, L.; Imbriani, M.; Fierro, J. G.; Kenny, J. M.; Armentano, I., Combined Effects of Ag Nanoparticles and Oxygen Plasma Treatment on PLGA Morphological, Chemical, and Antibacterial Properties. *Biomacromolecules* **2013**, *14*, 626-636.
28. Park, H.; Lee, K. Y.; Lee, S. J.; Park, K. E.; Park, W. H., Plasma-Treated Poly(lactic-co-glycolic acid) Nanofibers for Tissue Engineering. *Macromol. Res.* **2007**, *15*, 238-243; Park, K. E.; Lee, K. Y.; Lee, S. J.; Park, W. H., Surface Characteristics of Plasma-Treated PLGA Nanofibers. *Macromol. Symp.* **2007**, *249*, 103-108.
29. Damodaran, V. B.; Reynolds, M. M., Biodegradable S-nitrosothiol Tethered Multiblock Polymer for Nitric Oxide Delivery. *J. Mater. Chem.* **2011**, *21*, 5870-5872.

30. Ellman, G. L., A Colorimetric Method for Determining Low Concentrations of Mercaptans. *Arch. Biochem. Biophys.* **1958**, *74*, 443-450; Ellman, G. L., Tissue Sulfhydryl Groups. *Arch. Biochem. Biophys.* **1959**, *82*, 70-77.
31. Bates, J. N., Nitric Oxide Measurement by Chemiluminescence Detection. *Neuroprotocols* **1992**, *1*, 141-149.
32. Williams, D. L. H., The Chemistry of S-nitrosothiols. *Acc. Chem. Res.* **1999**, *32*, 869-876.
33. Wold, K. A.; Damodaran, V. B.; Suazo, L. A.; Bowen, R. A.; Reynolds, M. M., Fabrication of Biodegradable Polymeric Nanofibers with Covalently Attached NO Donors. *ACS Appl. Mater. Interfaces* **2012**, *4*, 3022-3030.
34. Griesser, H. J.; Da, Y.; Hughes, A. E.; Gengenbach, T. R.; Mau, A. W. H., Shallow Reorientation in the Surface Dynamics of Plasma-Treated Fluorinated Ethylene-Propylene Polymer. *Langmuir* **1991**, *7*, 2484-2491.
35. Steen, M. L.; Jordan, A. C.; Fisher, E. R., Hydrophilic Modification of Polymeric Membranes by Low Temperature H₂O Plasma Treatment. *J. Membr. Sci.* **2002**, *204*, 341-357.
36. Goldstein, J.; Newbury, D.; Joy, D.; Lyman, C.; Echlin, P.; Lifshin, E.; Sawyer, L.; Michael, J., *Scanning Electron Microscopy and X-Ray Microanalysis*. 3 ed.; Kluwer Academic Press: New York, 2007.
37. McArthur, S. L., Applications of XPS in Bioengineering. *Surf. Interface Anal.* **2006**, *38*, 1380-1385.
38. Ershov, S.; Khelifa, F.; Dubois, P.; Snyders, R., Derivatization of Free Radicals in an Isopropanol Plasma Polymer Film: The First Step toward Polymer Grafting. *ACS Appl. Mater. Interfaces* **2013**, *5*, 4216-4223.

39. Gengenbach, T.; Chatelier, R. C.; Griesser, H. J., Characterization of the Ageing of Plasma-Deposited Polymer Films: Global Analysis of X-ray Photoelectron Spectroscopy Data. *Surf. Interface Anal.* **1996**, *24*, 271-281; Tarasova, A.; Hamilton-Brown, P.; Gengengach, T.; Griesser, H. J.; Meagher, L., Colloid Probe AFM and XPS Study of Time-Dependent Aging of Amine Plasma Polymer Coatings in Aqueous Media. *Plasma Process. Polym.* **2008**, *5*, 175-185.
40. Asfardjani, K.; Segui, Y.; Aurelle, Y.; Abidine, N., Effects of Plasma Treatments on Wettability of Polysulfone and Polyetherimide. *J. Appl. Polym. Sci.* **1991**, *43*, 271-281.
41. Croll, T. I.; O'Connor, A. J.; Stevens, G. W.; Cooper-White, J. J., Controllable Surface Modification of Poly(lactic-co-glycolic acid) (PLGA) by Hydrolysis or Aminolysis I: Physical, Chemical, and Theoretical Aspects. *Biomacromolecules* **2004**, *5*, 463-473.
42. Quere, D., Wetting and Roughness. *Ann. Rev. Mater. Res.* **2008**, *38*, 71-99; Thissen, H.; Johnson, G.; McFarland, G.; Verbiest, B. C. H.; Gengenbach, T.; Voelckera, N. H., Microarrays for the Evaluation of Cell-Biomaterial Surface Interactions. In *Smart Materials IV*, Voelcker, N. H., Ed. 2007; Vol. 6413, p B4130; Deligianni, D. D.; Katsala, N. D.; Koutsoukos, P. G.; Missirlis, Y. F., Effect of Surface Roughness of Hydroxyapatite on Human Bone Marrow Cell Adhesion, Proliferation, Differentiation and Detachment Strength. *Biomaterials* **2000**, *22*, 87-96.
43. Thomas, T., *Rough Surfaces*. London, UK, 1999.
44. Carneiro, K.; Jensen, C. P.; Jørgensen, J. F.; Garnoes, J.; McKeown, P. A., Roughness Parameters of Surfaces by Atomic Force Microscopy. *CIRP Ann. Manuf. Technol.* **1995**, *44*, 517-522; Peltonen, J.; Jarn, M.; Areva, S.; Linden, M.; Rosenholm, J. B.,

Topographical Parameters for Specifying a Three-Dimensional Surface. *Langmuir* **2004**, *20*, 9428-9431.

CHAPTER 8:
SUMMARY AND FUTURE DIRECTIONS:
A BRIGHT FUTURE FOR NITRIC OXIDE MATERIALS

8.1 SUMMARY

8.1.1 Controlled preparation and advanced analysis.

This dissertation describes several studies that have been performed to load nitric oxide controllably and efficiently within polymer scaffolds. Additionally, analytical techniques have been developed and modified to enable a thorough characterization of both the NO loading and NO releasing processes for several model systems. More specifically, we have developed methods for monitoring the formation and decomposition of blended or covalently attached *S*-nitrosothiol donor moieties within both biostable and biodegradable polymer systems. A number of model systems have been investigated and the necessary methods were developed to monitor NO processes to understand the NO chemistries. Taken together, the information is used to develop physical models of how properties within the system as well as synthetic conditions can be tuned to acquire the desired NO properties for a given bioapplication.

Harnessing internal and external variables to control NO loading. Current NO materials are severely limited by finite NO reservoirs. Additionally, a lack of complete characterization prevents these materials from being applied in a clinical setting. The first two chapters presented describe efforts toward efficient, controllable and selective *S*-nitrosation within polymer systems. In Chapter 1, the choice of nitrosating agent and the presence of the polymer were found to greatly impact the kinetics of *S*-nitrosation. While nitrous acid was the more efficient nitrosating

agent regardless of polymer presence, the *t*-butyl nitrite allowed for more controllable *S*-nitrosation due to a greater impact on the kinetics due to polymer presence. In Chapter 2, the functional groups present within thiolated polymer derivatives were found to influence the nitrosation products. By tuning the functional groups within a system, undesirable byproducts such as *N*-nitrosamines were eliminated to result in selective *S*-nitrosation; the elimination of competitive byproducts also enhanced NO recoveries. In both Chapters 2 and 3, methods are described that enable characterization and quantification of the *S*-nitrosothiol moiety to describe the extent of *S*-nitrosation. Overall, the methods presented in these chapters are intended to be applied across any number of NO releasing scaffolds to inform the NO loading process in terms of selectivity and efficiency.

Probing NO release kinetics. It is critical toward any biological application that these materials deliver NO in a finely controlled fashion in terms of the release profile and duration of delivery. In Chapters 4 and 5, a biodegradable scaffold is described where differences in the choice of thiol pendant group influenced the loading efficiency, as well as the NO release profiles and percent NO recoveries. The behavior of the *S*-nitrosothiol donor was correlated to direct NO release to ensure that the NO delivered from the system was due to the intended donor. In addition to covalently attached NO donor polymers, donor blended polymers represent an attractive approach due to control over the NO reservoir. To this point, donor blended materials have been plagued by significant donor leaching; however, Chapter 6 describes a system where only surface donor was leached within the first 5 min – 1 h of the soaking period. After this initial leaching period, no more donor was found to leach from the bulk of the material and the system released NO on the order of the natural endothelium. It is therefore of great interest to

continue to investigate different material formulations, both covalently attached and donor blended, that will provide the requisite release profiles in a predictable manner. Again, the methods described in these chapters are presented for model polymer systems, but are intended to be applied across multiple material systems. A final study described in Chapter 7 highlights the ability of these materials to maintain the majority of the *S*-nitrosothiol groups during a water plasma treatment process. The plasma-treated materials still maintained their NO releasing capabilities but surface wettability was significantly enhanced. The ability of these materials to withstand processing conditions makes them more attractive for commercial development.

8.1.2 Summarizing remarks.

The most significant limitation that is recognized by the field is the lack of thorough and consistent characterization of current NO releasing materials. As described throughout this dissertation, there are a host of NO releasing material platforms that are described in the literature. These materials demonstrate great promise as biomaterials due to their ability to modulate biological processes, such as clotting, infection and wound healing. However, these materials are not being applied beyond the laboratory due to their limitations and an unclear understanding of their behavior in different experimental settings. Fundamental studies are required to probe the NO loading and release processes to begin to overcome the major obstacles regarding finite reservoirs and uncontrollable release properties. Systematic studies are critical toward the ability to understand which properties can be tuned to achieve certain therapeutic parameters. By probing the kinetics of NO moiety formation, we can determine how tuning various system components will allow for selective and efficient NO loading. Additionally, by measuring the NO release processes for these systems, we can determine how the material

properties and NO functionalities can be modified to achieve controllable and tailorable drug delivery kinetics. As the library of NO materials expands, it is necessary that researchers within the field apply appropriate characterization methods, such as those described in this work, to probe not only NO release but also to consider the possibility of byproducts that could have significant implications on toxicity. Once these issues are addressed, NO materials can be developed to their fullest capacity to fulfill their intention as biomedical materials and coatings in clinical settings. The advanced methods described in this body of work serve as a starting point for the characterization techniques that need to be performed across current and future NO materials to confirm the physical processes that are occurring in these material systems. The findings from the fundamental studies regarding NO loading and NO release can be applied to many material systems.

APPENDIX 1:
BIOMATERIALS LITERATURE REVIEW

Material classifications and biomedical applications.

A biomaterial is any synthetic or natural material that is used in contact with a biological system.¹ The main function of a biomaterial is to treat, enhance, or replace a tissue, organ, or function of the body. Biomaterials are processed into different forms to satisfy different device requirements for both surgical and pharmacological applications. Materials are tuned to be either biostable or biodegradable to determine the lifetime of the device for permanent implant or temporary treatment applications, respectively. Common examples of biomedical devices include implants, topical treatments, chemical sensors, and drug delivery vehicles. The remainder of this section will highlight biostable and biodegradable implant materials.

Biostable implant materials. Implants are devices that are surgically inserted into a patient and interact with surrounding tissues and fluids to support or replace damaged biological structures. Examples of medical implants include stents, catheters, valves, grafts, meshes, plates, screws, prosthetics and cements ranging from applications in vasculature and soft tissue to cartilage and bone. Implants are typically intended to be a permanent addition to the patient, such as a vascular graft which replaces part of a damaged vein or artery. Due to their permanent nature, implant materials must be biostable such that the device will remain functional over the lifetime of the patient and are typically constructed from polymer, ceramic, metal or composite materials. Common surgical grade metals include stainless steel and cobalt- or titanium-based alloys, while ceramics include glass, hydroxyapatite, and alumina.¹ There are a variety of biostable polymers

that are used for permanent medical devices, which are described in Table A1.1. Generally, polymers are either synthetic or natural, where natural polymers can be composed of proteins (*i.e.* keratin, collagen and actin) or polysaccharides (*i.e.* cellulose, dextran and chitin). Common biostable synthetic polymers include polyvinylchloride, polytetrafluoroethylene, polyurethanes and silicones, among many others. These polymers can be used as homopolymers or copolymers with native or modified backbone compositions, or in conjunction with other material classes to create composite materials.² Other medical devices that require biostable materials include chemical sensors (*i.e.* glucose, pH, blood gases), fluid storage devices (*i.e.* blood and IV bags), extracorporeal circuitry components (*i.e.* blood tubes), and any type of coating that is applied to a device that will contact bodily tissues or fluids.

Biodegradable materials. There are, however, many other applications that require the temporary presence of the device for short-term applications. In such cases, the device is not intended to remain in the patient for their lifetime, such as for sutures, wound fillings and tissue scaffolds. Biodegradable materials that experience chemical breakdown of the polymer backbone over time are used for such applications, where the material is present initially to serve as a scaffold or barrier layer and can break down and be removed from the site as natural cell growth and wound-healing processes take over.³ It is critical that the biodegradation products are non-toxic, and the material is considered bioresorbable if cellular processes act to remove the degradation products from the body. Other short-term biopolymer applications include topical treatments and drug delivery vehicles. Topical materials for dermal applications, such as wound bandages, burn dressings and adhesives, are not necessarily biodegradable, since the material is easily removed from its biological setting. However, advanced wound dressings are of interest where

biodegradable polymers would be placed into an open wound and serve to mimic the extracellular matrix and promote cell growth. As the healing process begins, the polymer can biodegrade and be eliminated from the site without requiring surgical removal of the device. In the case of polymers acting as drug delivery vehicles, it is important that the polymer is bioresorbable such that it is removed once the pharmaceutical is delivered. Common biodegradable polymers include poly(lactic-*co*-glycolic acid), polyesters, and polysaccharides. Modes of degradation include hydrolysis and/or enzyme-induced.

Table A1.1 Common polymers and their biomedical applications.^a

<i>Polymer</i>	<i>Biomedical devices and applications</i>
Silicones	Tubing, oxygenators, plastic surgery implants, catheters, seals and gaskets, adhesives, bandages, transdermal drug delivery, soft tissue reconstruction
Polyurethanes	Catheters, cardiac pumps and valves, tendon/ligament, cartilage replacement, shunts, blood tubing and filters, wound dressings, adhesives, pacemaker insulation
Polytetrafluoroethylene	Vascular clips and grafts, orthopedic implants, cartilage replacement, subcutaneous implants, medical coatings, catheters
Poly(vinyl chloride)	Catheters, blood pushes, intravenous tubing, blood bags, extracorporeal membrane oxygenation, hemodialysis, wound drains, orthodontic retainers, feeding tubes
Poly(methyl methacrylate)	Intra-ocular lens, rigid contact lenses, dental brackets and bridges, bone plates and screws, bone cement
Poly(lactic- <i>co</i> -glycolic acid)	Grafts, sutures, surgical sealants, nanoparticles, drug delivery systems, orthopedic and dental prosthetic devices, guided tissue regeneration, stents, barrier membranes
Polysaccharides	Drug delivery/controlled release systems, sutures, wound dressings and fillings, guided tissue regeneration, mechanical support, blood-plasma expander, cosmetics

^a See references ^{1, 2, 4, 5}

Biopolymers for both permanent and short-term applications can be processed into networks such as elastomers, hydrogels, fibers and biotextiles to create patches, sutures and a wide array of biological structures (*i.e.* arteries, tendons, ligaments, bones and joints). More advanced “smart polymers” are designed to respond to specific chemical (*i.e.* pH, ion or chemical responsive) or physical (*i.e.* temperature, radiation, mechanical stress and pressure) stimuli to result in significant, reversible changes in the material properties. Such materials can be designed to precipitate, adsorb to a surface, or collapse when provoked, which is useful for biomedical applications including drug delivery, toxin removal for wound-healing, or controlling enzymatic processes to regulate physiological responses.

Defining biocompatibility.

The ultimate goal in the field of biomaterials is to create a material that will serve its intended function while integrating appropriately with its biological surroundings to prevent adverse reactions and minimize complications. A material that can perform its intended functions without causing ill effects is considered biocompatible, where this term is variable depending upon the specific application. To satisfy general biocompatibility requirements, a material must be non-toxic, non-allergenic, non-carcinogenic and non-mutagenic. The U.S. Food and Drug Administration (FDA) suggests that biocompatibility assessment of a material proceed according to the guidelines of the International Standard ISO-10993 “Biological Evaluation of Medical Devices Part I: Evaluation and Testing” protocol.⁶ These guidelines include considerations for evaluating cytotoxicity, sensitization, hemocompatibility, pyrogenicity, implantation, genotoxicity, carcinogenicity, reproductive and developmental toxicity, and biodegradation testing. In each of these cases, the guidelines describe that if a representative sample is used for

analysis, the final product itself may not need to be tested directly. Additionally, it is mentioned that relevant animal models must be used for the studies performed. Generally these guidelines are described as suggestions, where rather vague definitions and experimental details are provided, making it difficult to identify a consistent and standardized measure of biocompatibility.

To acknowledge the diversity associated with different biomaterials and the versatility associated with their function, this standard method states that not all tests that are identified are necessary and practical for a particular device. Overall, the relevance of such evaluations is dependent upon the specific device. It is also mentioned that additional tests may be required to fully evaluate biocompatibility of a device for a given application. Finally, it is recommended that scientific justification be provided if a particular suggested test is omitted.

Based on the current view of medical device evaluation, the goal is to create a device that will perform its function with minimal undesirable side effects. For example, the goal would be to develop an implant from a material and in a form that will minimize toxicity, cancer, allergic reaction, fever, thrombosis, infection and genetic mutation. For the purposes of this dissertation, these approaches are considered to be “passive,” wherein a material is simply incorporated into a biological environment with the intention to perform a given function, such as serving as a fluid conduit (*i.e.* stent or catheter) or physically blocking microbes from entering a wound (*i.e.* bandages), with minimal negative effects. This definition does not include the ability to promote certain biological responses that could lead to integration of the device into its biological environment. It has been pointed out that, to truly evaluate material biocompatibility, assessment must be performed “under conditions that are closest to those encountered in a biological system,” where the environment will vary depending upon the specific application and location

of the device in the body.⁴ Overall, current biocompatibility evaluations mostly consider toxicological effects, where a material deemed “biocompatible” essentially exhibits minimal adverse effects while implanted. As discussed later, there is a shift toward developing materials that will not only prevent adverse effects, but will also promote desired processes, such as wound-healing and cell growth.

Biofouling on passive surfaces: Thrombosis and infection.

There are a variety of responses that can occur when a material is interfaced with tissues and bodily fluids: (a) the material is toxic and surrounding tissues die, (b) the material is non-toxic and biologically inactive, rendering the material essentially inert, (c) the material is non-toxic and biologically active such that communication takes place at the interface or (d) the material is non-toxic and dissolves so that the surrounding tissue can replace the material.¹ As mentioned in the previous section, the goal of obtaining a biocompatible material surface is to minimize the toxicity effects, while achieving one of the last three options depending upon the application. For instance, option (b) would be ideal for a biostable implant, whereas (c) would represent a drug delivery system and (d) would represent a biodegradable temporary device. However, materials still exhibit the foreign body response, which complicates the function of the device.

The foreign body response. Upon implantation of a medical device to contact blood and tissue, a multitude of processes are triggered (Figure A1.1).⁷ Within seconds to hours of the initial injury and device implantation, proteins begin to adsorb and microbial action begins at the site of incorporation into the native tissue. Afterwards, a cascade of platelet activation and adhesion,

cell interrogation and attack, and continued microbial action events occur. Within days to weeks of the material introduction, a bacterial biofilm begins to form on the surface of the device accompanied by mature blood clot formation (thrombosis), inflammation due to continued cell interrogation, and infection due to microbial action. The final result is a biofouled surface, which, due to the presence of the biofilm and undesired biological responses, cannot perform its intended function. Commonly implanted blood-contacting devices such as valves, stents and catheters are intended to serve as a conduit for fluid transport or to prop open damaged vessels to allow proper flow. Upon biofouling of the device, the passage will essentially clot shut to prevent flow. Thrombosis related events are a large cause of patient mortality and suffering. A 6-year study monitored 4,500 patients that received a coronary stent implant where, despite dual antiplatelet therapy for all patients, nearly 1% of the patients suffered from stent thrombosis within only the first 30 days after implantation.⁸ Of those who incurred stent thrombosis, nearly 40% suffered a heart attack and almost 50% died, leaving only 10% of the thrombotic patients that did not experience severe complications or death. Further complications arise when antiplatelet treatment is discontinued, with late stage thrombosis being a common complication resulting in heart attack or death.⁹

Infection. In addition to thrombosis compromising device function and patient safety, an equally large problem is the risk of hospital acquired infection during the medical procedure, especially for surgically implanted devices.^{10, 11} Biofilms that form during the foreign body reaction breed chronic bacterial infection, which can lead to sepsis. Hospital-acquired bloodstream infections mark one of the leading causes of patient mortality,¹² where a 7-year study involving nearly 25,000 patients indicated a 27% mortality rate in the United States due to such infections.¹³

A special issue review published in *Emerging Infectious Diseases* highlights that the most common bacteria found within biofilms on implanted devices include *Staphylococcus* and *Streptococcus* strains, as well as *Escherichia coli*.¹¹ These bacteria attach to the medical device surface and begin to form dense networks held together by extracellular polymers (primarily polysaccharides) which are resistant to antimicrobial treatments. Antimicrobial concentrations that are sufficient to eliminate free floating bacteria are typically insufficient to act on bacteria within a biofilm due to inaccessibility and resistance development. Therefore, bacterial biofilms lead to persistent infection at the site of the device, and biofilm detachment from the biomaterial surface leads to severe risk for sepsis, a leading cause of patient mortality.

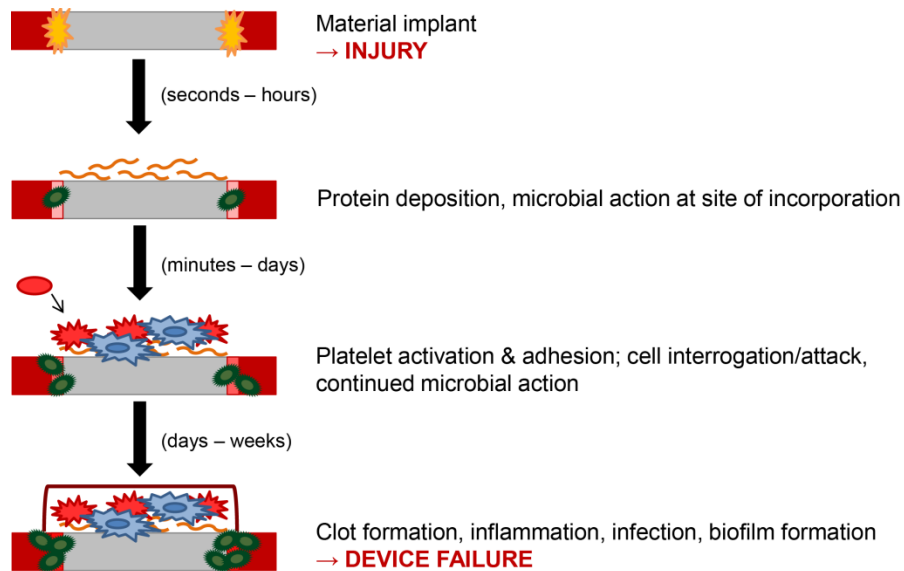


Figure A1.1 Schematic of physiological processes that are involved in the foreign body response.

Systemic approaches to managing biofouling.

Approaches to overcoming biofouling at the site of a material implant can either be categorized as systemic or local. In a systemic approach, a drug is administered to the patient and circulates throughout the entire body, even though the site of the implant is the only site that requires therapeutic action. In a localized approach, the therapeutic action is targeted specifically at the site of the material implant and ideally does not result in downstream effects. Typically, multiple drugs are used to target platelet function, coagulation, and microbial activity individually.

Antithrombogenic therapies. The most popular approach to systemic treatment of thrombosis is to administer antiplatelet or anticoagulant drugs. Popular antiplatelet pharmaceuticals include aspirin, clopidogrel (PlavixTM), prasugrel (EffientTM) and ticagrelor (BrilintaTM), which bind to platelet surface receptors to inhibit platelet activation, a vital stage in thrombus formation.¹⁴ Anticoagulant therapies prevent the conversion of fibrinogen to fibrin, which is a critical part of the fibrous network formation in a blood clot. Commercially available anticoagulants include heparin, warfarin (CoumadinTM), rivaroxaban (XareltoTM) and dabigatran (PradaxaTM).¹⁵ Patients at significant risk for thrombosis are prescribed extended use drugs. For instance, patients that undergo coronary artery stenting are prescribed antiplatelet drugs for up to a year after the initial surgery to prevent acute thrombosis; however, patients that discontinue use of the prescription have an increased risk of late stage thrombosis or death.¹⁶ To prevent instances of mortality due to late stage thrombosis events, patients can extend their use of antiplatelet agents beyond 1 year; however, patients on prolonged therapies are at a high risk of hemorrhage.¹⁷ If the patient requires further surgery at which time they are on antiplatelet therapies, they are at a high risk of

bleeding out.¹⁸ The use of heparin, one of the most popular anticoagulants, has also been shown to result in platelet activation and significant platelet consumption for a Tygon extracorporeal circuit model.¹⁹ Additionally, the use of antithrombogenic drugs requires timely personalized care, where constant blood monitoring is required to assess clotting function and pharmaceutical levels, where there is significant variability in the dosage requirement depending upon the patient.²⁰ Moreover, there are interferences associated with diet that can inhibit drug efficacy, such as vitamin K interfering with warfarin activity, so there may be significant diet restrictions for patients. A recent editorial published in *Drug Development Research* highlights the considerable societal burden associated with thrombosis events and the serious adverse effects due to current antithrombogenic drugs.²¹ Due to the complexity of coagulation and platelet aggregation events, the development of safer and more effective next-generation drugs will require an overwhelming investment. Overall, there are significant costs involved in the use of systemic oral anticoagulants and antiplatelet agents. Additionally, clinical considerations and strategies are of the utmost important for monitoring clotting activity and working toward safe dosages based upon an individual's health and blood chemistry.

Antibiotic therapies. The major mode of combatting hospital acquired infection associated with surgically implanted devices is to implement harsh and stringent sterilization procedures as well as employ the use of systemic antibiotics. Antibiotic drugs can be classified as natural products or synthetic antibiotics, where the major modes of action involve inhibiting the ability of the bacteria to (a) biosynthesize cell walls (*i.e.* penicillins, vancomycin), (b) biosynthesize proteins (*i.e.* erythromycin) or (c) replicate DNA (*i.e.* levofloxacin).²² The natural antibiotic penicillin was discovered in 1929, where the following decades into the 1960s saw the isolation of the

remaining major current classes of natural antibiotics. Much of the research past that point has been focused on synthetically tailoring the chemical structure of different antibiotics to overcome issues with antibiotic-resistant bacteria strains. Antibiotic resistance occurs through one of three pathways; in the first two pathways, the bacteria either destroy or reprogram the function of the antibiotic, and in the third case the bacteria pump the antibiotics from the cell via transmembrane pumps to keep antibiotic levels below a threshold concentration. As a result of increasing drug resistance, next generation antibiotics are tailored based upon the precursors within a given antibiotic class. One major drawback to this high-throughput, combinatorial approach toward the synthesis and discovery of new antibiotics in the pharmaceutical industry is that these screening approaches will not identify drugs that exhibit delayed drug resistance.²³ Several reviews highlight the detrimental impact on human health associated with antibiotic-resistant bacteria,²⁴ including multidrug resistant strains known as “superbugs” which require more complex antibiotic approaches.²⁵ To overcome these issues, a movement toward discovering drugs with alternate modes of action is needed. New approaches include the development of new natural products,²⁶ as well as restructuring the screening process and existing libraries to enable new pharmaceutical platform discoveries.²⁷

Overall, the ability to combat device-associated infection and thrombosis via systemic pharmaceutical approaches has severe limitations. Alternative approaches are therefore required that focus on the ability to mediate and control physiological processes in a localized fashion at the interface between the biomaterial and its surrounding biology.

Functional biomaterials.

Re-evaluating biocompatibility. To this point, biocompatibility has been defined as the ability of a device to serve its intended base function while not provoking adverse reactions. Additionally, it is clear that passive biomaterial surfaces are plagued by biofouling and that the use of systemic drugs is not satisfactory towards preventing infection and thrombosis, which severely compromise patient care. To develop a more successful approach, it is necessary to redefine biocompatibility to include, in addition to preventing thrombosis and infection, the ability to promote cell growth that is necessary to promote wound-healing and integration of the device into its biological surrounding. A review published in *Reactive & Functional Polymers* summarizes this nicely by saying truly biocompatible polymers “should be able to recognize and cooperate in harmony with bio-assemblies and living cells without (promoting) any non-specific interactions,” which represents a distinctly different approach from passive materials.²⁸ Additional functions can include the ability to target specific physiological components, or the development of multi-faceted systems that can target several aspects of the surrounding biology. Most of the common methods for achieving device integration and function are biomimetic because they are inspired by natural systems, such as the function of the endothelium to regulate clotting processes and the ability of the body to combat infection. Approaches that involve imparting these natural functions within a material system to prevent infection and clotting but also promote integration and/or target certain disease states are considered functional. The two main categories of functional biomaterials include the modification of surface properties and the controlled release of drugs. In either case, there is a large emphasis on the ability to either mimic the natural endothelium (“bioactive” strategies) or to minimize the material interaction with

blood components (*i.e.* proteins, platelets) that will initiate a foreign body response (“low fouling” strategies).

Surface modification. There are a variety of surface properties that impact the biological interactions that will occur on the material surface, including surface wettability, composition, charge, and roughness/morphology.²⁹ Several surface modification approaches target one or more of these surface properties and are accomplished via covalent functionalization or adsorption. Some strategies are aimed at incorporating functional groups that will tailor the surface wettability and charge of the film, while other strategies involve the attachment of molecules or macromolecules that will passivate the material surface. The surface wettability³⁰ and surface charge³¹ of a material have been demonstrated to influence protein adsorption events, as well as fibrin proliferation, a critical component to forming the fibrous thrombus network.³² In addition to the surface properties of a material impacting protein and platelet deposition, they are critical factors influencing cell attachment and adhesion processes, which can lead to bacterial biofilm formation.³³ Popular approaches to creating low fouling surface coatings include functionalizing the surface with heparin, polysaccharide, poly(ethylene glycol), and phosphorylcholine.^{34, 35} Bioactive strategies incorporate signaling agents, such as specific integrins and other receptors, onto the material surface to direct cellular behavior in a selective and controlled fashion.³⁴ However, a recent publication in *Organogenesis* points out that these surface-modified materials are still wrought with biofouling issues.^{35, 36}

Drug-releasing materials. In the case of materials that exhibit controlled drug release, there are a variety of therapeutic agents that can be incorporated into a material. The key to achieving a

functional system is to exhibit controlled release of drugs that are anti-proliferative, anti-inflammatory, anti-thrombotic and pro-healing.³⁷ One popular application is the development of drug-eluting biomaterials that release a variety of therapeutic agents to control certain processes, such as the release of heparin to minimize thrombosis or corticosteroids to modulate inflammation.³⁸ Materials that release prostacyclin and heparin have been shown to decrease thrombus formation; however, the flux of antithrombogenic drug being released from the surface is only sufficient over a short-term period, making this an infeasible approach for permanent applications and for preventing late stage thrombosis.³⁹ While heparin-releasing materials have demonstrated a localized ability to prevent smooth muscle cell proliferation to minimize atherosclerosis or restenosis at a material surface,⁴⁰ heparin is notorious for inducing platelet activation,⁴¹ which initiates the coagulation cascade to result in thrombosis. Other agents, such as the anti-proliferative drugs sirolimus and paclitaxel, are of interest for drug-eluting stent applications, where the drugs are intended to minimize the formation of scar tissue and restenosis.⁴² A comparison of the instance of deep vein thrombosis on drug-eluting stents versus bare metal stents was performed; there was no significant difference in the amount of thrombus formed for stents that released sirolimus and paclitaxel as long as the patient was receiving antiplatelet therapy.⁴³ However, another study considering sirolimus- and paclitaxel-eluting stents demonstrated that 60% of the patients experienced early stage thrombosis (87% of these patients were on antiplatelet therapy, thrombus formation occurred within 30 days) while 40% of the remaining patients experienced late stage thrombosis (23% of these patients were on antiplatelet therapy, thrombus formation occurred within 30 days – 3 years after implantation).⁴⁴ Patients on antiplatelet therapies have been demonstrated to experience thrombosis as soon as the antiplatelet therapy is discontinued.⁹ Based on these studies, drug-eluting polymer surfaces are

still significantly plagued by biofouling complications if systemic antithrombogenic agents are not employed.

Other drug-releasing strategies are biomimetic in nature and largely revolve around the use of inhibitors and activators that are naturally released from endothelial cells to regulate hemostasis.³⁵ To accomplish this, different platelet inhibitors (*i.e.* nitric oxide (NO), prostacyclin and matrix metalloproteinases) can be released from the material surface at physiologically relevant concentrations. As described above, the major issue associated with many systemic antiplatelet therapies is that they permanently inactivate platelets, which cause issues in other parts of the body where the therapy is not required. The key to the use of natural platelet inhibitors is that the platelet is only temporarily inhibited and will retain its normal function downstream, making these ideal candidates for therapies that are localized at the biomaterial-biology interface. As highlighted in the following section of Chapter 1, NO is the most popular natural antiplatelet therapeutic that has been investigated for biomaterials applications, and has demonstrated great promise for reducing surface biofouling.

Ideal biomaterial properties.

Many properties have been highlighted that are critical to the performance of materials in biological systems. The ultimate goal is to create a material that will integrate within its biological setting, both in terms of preventing thrombosis and infection, but also in terms of promoting wound-healing and communicating with different biological components effectively to regulate physiological processes. The specific desired material properties will be dependent on the specific application and the location of biomaterial use (*i.e.* dermal, arterial).

Materials for use as biostable implants should exhibit bulk properties, such as solubility, polymer composition and extent of crosslinking, which will render the material inert. Biodegradable materials for temporary applications must have the appropriate biodegradation profiles with non-toxic, bioresorbable degradation products. The polymer must withstand processing considerations, such as extrusion or casting, while the mechanical properties, such as tensile strength, elasticity, rigidity and flexibility, must be appropriate for the application. The material must withstand general sterilization procedures and still maintain the intended surface and functional properties. For practical usage in clinical and surgical settings, material shelf-life and storage considerations (*i.e.* temperature and light sensitivity) must render the material easy to handle. As addressed earlier, the surface properties are also critical to the biological interactions that occur at the material-biology interface thus they must be tuned accordingly. Material function must be imparted adequately, such that the appropriate therapeutic release profiles are achieved over the timeline necessary for the application. Localized therapy is controlled by the drug distribution and diffusion properties and is critical for maintaining therapeutic effects at the site of the implant, where downstream effects should be minimized. Leachables, such as plasticizers and byproducts, must be eliminated unless they are bioresorbable and non-toxic in nature. Bulk erosion should be avoided, unless it is part of the material function. Appropriate permeability should be imparted; for example, selective gas permeability is necessary for wound dressings/bandages, while the admission of cellular components is critical to initiate angiogenesis for tissue and bone scaffolds. Overall, the choice of material and therapeutic agent(s) must be such that a synergistic effect is produced when the material is implanted, leading to appropriate device integration and function.

APPENDIX 1 REFERENCES

1. *Biomaterials Science: An Introduction to Materials in Medicine*. 2 ed.; Elsevier Academic Press: San Diego, California, USA, 2004.
2. Ramakrishna, S.; Mayer, J.; Wintermantel, E.; Leong, K. W., Biomedical applications of polymer-composite materials: A review. *Compos. Sci. Technol.* **2001**, *61*, 1189-1224.
3. Nair, L. S.; Laurencin, C. T., Biodegradable polymers as biomaterials. *Prog. Polym. Sci.* **2007**, *32*, 762-798.
4. Vert, M., Polymeric biomaterials: Strategies of the past vs. strategies of the future. *Prog. Polym. Sci.* **2007**, *32*, 755-761.
5. Arshady, R., Chemistry, Concepts, Criteria In *Polymeric Biomaterials*, Citus Books: 2003; Zdrahala, R. J.; Zdrahala, I. J., Biomedical Applications of Polyurethanes: A Review of Past Promises, Present Realities, and a Vibrant Future. *J. Biomater. Appl.* **1999**, *14*, 67-90; Opinion on Medical Devices Containing DEHP Plasticized PVC; Neonates and Other Groups Possibly at Risk from DEHP Toxicity, The Scientific Committee on Medicinal Products and Medical Devices (European Commission). 2002; Frazer, R. Q.; Byron, R. T.; Osborne, P. B.; West, K. P., PMMA: An Essential Material in Medicine and Dentistry. *J. Long Term Eff. Med. Implants* **2005**, *15*, 629-639.
6. Use of International Standard ISO-10993 "Biological Evaluation of Medical Devices Part 1: Evaluation and Testing, U.S. Department of Health and Human Services. 2013.
7. Coleman, D. L.; King, R. N.; Andrade, J. D., The Foreign Body Reaction: A Chronic Inflammatory Response. *J. Biomed. Mater. Res.* **1974**, *8*, 199-211; Ratner, B. D.; Bryant, S. J., Biomaterials: Where We Have Been and Where We Are Going. *Annu. Rev. Biomed.*

- Eng.* **2004**, *6*, 41-75; Anderson, J. M., Biological Responses to Materials. *Annu. Rev. Mater. Res.* **2001**, *31*, 81-110; Anderson, J. M.; Rodriguez, A.; Chang, D. T., Foreign Body Reaction to Biomaterials. *Semin. Immunol.* **2008**, *20*, 86-100.
8. Orford, J. L.; Lennon, R.; Melby, S.; Fasseas, P.; Bell, M. R.; Rihal, C. S.; Holmes, D. R.; Berger, P. B., Frequency and Correlates of Coronary Stent Thrombosis in the Modern Era. *J. Am. Coll. Cardiol.* **2002**, *40*, 1567-1572.
 9. McFadden, E. P.; Stabile, E.; Regar, E.; Cheneau, E.; Ong, A. T. L.; Kinnaird, T.; Suddath, W. O.; Weissman, R. T.; Kent, K. M.; Pichard, A. D.; Satler, L. F.; Waksman, R.; Serruys, P. W., Late Thrombosis in Drug-Eluting Coronary Stents After Discontinuation of Antiplatelet Therapy. *Lancet* **2004**, *364*, 23-29.
 10. Costerton, J. W.; Stewart, P. S.; Greenberg, E. P., Bacterial Biofilms: A Common Cause of Persistent Infections. *Science* **1999**, *284*, 1318-1322.
 11. Donlan, R. M., Biofilms and Device-Associated Infections. *Emerging Infect. Dis.* **2001**, *7*, 277-281.
 12. Wenzel, R. P.; Edmond, M. B., The Impact of Hospital-Acquired Bloodstream Infections. *Emerg. Infect. Dis.* **2001**, *7*, 174-177.
 13. Wisplinghoff, H.; Bischoff, T.; Tallent, S. M.; Seifert, H.; Wenzel, R. P.; Edmond, M. B., Nosocomial Bloodstream Infections in US Hospitals: Analysis of 24,179 Cases from a Prospective Nationwide Surveillance Study. *Clin. Infect. Dis.* **2004**, *39*, 309-317.
 14. Badimon, L.; Vilahur, G., 2008, *61*, 501-513 Coronary Atherothrombotic Disease: Progress in Antiplatelet Therapy. *Rev. Esp. Cardiol.* **2008**, *61*, 501-513.
 15. Nutescu, E. A.; Dager, W. E.; Kalus, J. S.; Lewin, J. J.; Cipolle, M. D., Management of bleeding and reversal strategies for oral anticoagulants - Clinical practice considerations.

- Am. J. Health Syst. Pharm.* **2013**, *70*, 1914-1929; Bhimani, A. A.; Hong, M., New Alternative Anticoagulants in Atrial Fibrillation: The Move Beyond Warfarin. *Rev. Recent Clin. Trials* **2013**, *8*, 78-85.
16. Bell, B.; Layland, J.; Poon, K.; Spaulding, C.; Walters, D., Focused Clinical Review: Periprocedural Management of Antiplatelet Therapy in Patients with Coronary Stents. *Heart, Lung Circ.* **2011**, *20*, 438-445.
 17. Galper, B. Z.; Mauri, L., Antiplatelet Therapy After Coronary Stenting. *Curr. Treat. Options Cardiovasc. Med.* **2013**, *15*, 1-10.
 18. Vaclavik, J.; Taborsky, M., Antiplatelet Therapy in the Perioperative Period. *Eur. J. Intern. Med.* **2011**, *22*, 26-31.
 19. Annich, G. M.; Meinhardt, J. P.; Mowery, K. A.; Ashton, B. A.; Merz, S. I.; Hirschl, R. B.; Meyerhoff, M. E.; Bartlett, R. H., Reduced Platelet Activation and Thrombosis in Extracorporeal Circuits Coated with Nitric Oxide Release Polymers. *Crit. Care Med.* **2000**, *28*, 915-920.
 20. Bloemen, S.; De Laat, M.; De Laat, B.; Hemker, H. C.; Al Dieri, R., Will One Size of Anticoagulant Dosage Fit All? *Drug Dev. Res.* **2013**, *74*, 406-412.
 21. Gurwitz, D., Personalizing Anticoagulant and Antiplatelet Therapeutics: A Timely Task. *Drug Dev. Res.* **2013**, *74*, 403-405.
 22. Walsh, C. T.; Wright, G., Introduction: Antibiotic Resistance. *Chem. Rev.* **2005**, *105*, 391-393; Kohanski, M. A.; Dwyer, D. J.; Collins, J. J., How Antibiotics Kill Bacteria: From Targets to Networks. *Nat. Rev. Microbiol.* **2010**, *8*, 423-435.
 23. Altman, S., Antibiotics Present and Future. *FEBS Lett.* **2014**, *588*, 1-2.

24. Guillemot, D., Antibiotic Use in Humans and Bacterial Resistance. *Curr. Opin. Microbiol.* **1999**, *2*, 494-498.
25. Alanis, A. J., Resistance to Antibiotics: Are We in the Post-Antibiotic Era? *Arch. Med. Res.* **2005**, *36*, 697-705.
26. Clardy, J.; Fischbach, M. A.; Walsh, C. T., New Antibiotics From Bacterial Natural Products. *Nat. Biotechnol.* **2006**, *24*, 1541-1550.
27. Fischbach, M. A.; Walsh, C. T., Antibiotics for Emerging Pathogens. *Science* **2009**, *325*, 1089-1093.
28. Jagur-Grodzinski, J., Biomedical application of functional polymers. *React. Funct. Polym.* **1999**, *39*, 99-138.
29. Wang, Y.; Robertson, J. L.; Spillman, W. B.; Claus, R. O., Effects of the Chemical Structure and the Surface Properties of Polymeric Biomaterials on Their Biocompatibility. **2004**, *21*, 1362-1373; Ma, Z.; Mao, Z.; Gao, C., Surface Modification and Property Analysis of Biomedical Polymers Used for Tissue Engineering. *Colloids Surf., B* **2007**, *60*, 137-157.
30. Xu, L. C.; Siedlecki, C. A., Effects of Surface Wettability and Contact Time on Protein Adhesion to Biomaterial Surfaces. *Biomaterials* **2007**, *28*, 3273-3283.
31. Hartvig, R. A.; van de Weert, M.; Ostergaard, J.; Jorgensen, L.; Jensen, H., Protein Adsorption at Charged Surfaces: The Role of Electrostatic Interactions and Interfacial Charge Regulation. *Langmuir* **2011**, *27*, 2634-2643.
32. Evans-Nguyen, K. M.; Schoenfish, M. H., Fibrin Proliferation at Model Surfaces: Influence of Surface Properties. *Langmuir* **2005**, *21*, 1691-1694; Evans-Nguyen, K. M.; Tolles, L. R.; Gorkun, O. V.; Lord, S. T.; Schoenfish, M. H., Interactions of Thrombin

- with Fibrinogen Adsorbed on Methyl-, Hydroxyl-, Amine-, and Carboxyl-Terminated Self-Assembled Monolayers. *Biochemistry* **2005**, *44*, 15561-15568.
33. Arima, Y.; Iwata, H., Effect of Wettability and Surface Functional Groups on Protein Adsorption and Cell Adhesion Using Well-Defined Mixed Self-Assembled Monolayers. *Biomaterials* **2007**, *28*, 3074-3082.
 34. Meyers, S. R.; Grinstaff, M. W., Biocompatible and Bioactive Surface Modifications for Prolonged In Vivo Efficacy. *Chem. Rev.* **2012**, *112*, 1615-1632.
 35. Reynolds, M. M.; Annich, G. M., The Artificial Endothelium. *Organogenesis* **2011**, *7*, 42-49.
 36. Bhattacharyya, D.; Xu, H.; Deshmukh, R. R.; Timmons, R. B.; Nguyen, K. T., Surface Chemistry and Polymer Film Thickness Effects on Endothelial Cell Adhesion and Proliferation. *J. Biomed. Mater. Res., Part A* **2010**, *94A*, 640-648.
 37. Raval, A.; Parikh, J.; Engineer, C., Mechanism of Controlled Release Kinetics from Medical Devices. *Braz. J. Chem. Eng.* **2010**, *27*, 211-225.
 38. Babapulle, M. N.; Eisenberg, M. J., Coated Stents for the Prevention of Restenosis: Part I. *Circulation* **2002**, *106*, 2734-2740.
 39. Jozefowicz, M.; Jozefowicz, J., Antithrombogenic Polymers. *Pure & Appl. Chem.* **1984**, *56*, 1335-1344.
 40. Edelman, E. R.; Adams, D. H.; Karnovsky, M. J., Effect of Controlled Adventitial Heparin Delivery on Smooth Muscle Cell Proliferation Following Endothelial Injury. *Proc. Natl. Acad. Sci. USA* **1990**, *87*, 3773-3777.
 41. Greinacher, A., Platelet Activation by Heparin. *Blood* **2011**, *117*, 4686-4687; Lefkowitz, J. B., Heparin Induced Thrombocytopenia. In *An Algorithmic Approach to Hemostasis*

- Testing*, Kottke-Marchant, K., Ed. CAP Press: Northfield, IL, 2008; pp 287–294; Kelton, J. G.; Warkentin, T. E., Heparin-Induced Thrombocytopenia: A Historical Perspective. *Blood* **2008**, *112*, 2607-2616; Otis, S. A.; Zehnder, J. L., Heparin-Induced Thrombocytopenia: Current Status and Diagnostic Challenges. *Am. J. Hematol.* **2010**, *85*, 700-706.
42. Woods, T. C.; Marks, A. R., Drug-Eluting Stents. *Annu. Rev. Med.* **2004**, *55*, 169-178.
43. Moreno, R.; Fernandez, C.; Hernandez, R.; Alfonso, F.; Angiolillo, D. J.; Sabate, M.; Escaned, J.; Banuelos, C.; Fernandez-Ortiz, A.; Macaya, C., Drug-Eluting Stent Thrombosis: Results From a Pooled Analysis Including 10 Randomized Studies. *J. Am. Coll. Cardiol.* **2005**, *45*, 954-959.
44. Daemen, J.; Wenaweser, P.; Tsuchida, K.; Abrecht, L.; Vaina, S.; Morger, C.; Kukreja, N.; Juni, P.; Sianos, G.; Hellige, G.; van Domburg, R.; Hess, O. M.; Boersma, E.; Meier, B.; Windecker, S.; Serruys, P., Early and Late Coronary Stent Thrombosis of Sirolimus-Eluting and Paclitaxel-Eluting Stents in Routine Clinical Practice Data From a Large Two-Institutional Cohort Study *Lancet* **2007**, *369*, 667-678.